The Control of Protein Crystallisation

A thesis submitted to the University of London
for the degree of Doctor of Philosophy

by

Carsten Jacobsen

The Advanced Centre for Biochemical Engineering
Department of Biochemical Engineering
University College London
Torrington Place
London WC1E 7JE

March 1998

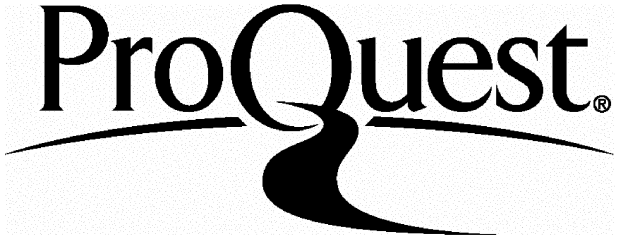

Abstract

The objective of the studies was to learn how to control protein crystallisation to ease the separation of crystals from the mother liquor. The significance of the work is that bulk protein crystallisation could become a cheap alternative to chromatography in obtaining high purity proteins while not compromising the product yield.

Simultaneous product capture and purification are achieved using protein crystallisation and that often with yields as high as 80-90 %. The process is cheap both in operational and fixed cost and is reported to be easily scaleable. Typically, the crystals produced are small (max. 100 μm) and some crystal habit are fragile. Recovering the crystals can hence be difficult. Compared to for example protein precipitation, crystallisation is a slow process allowing time for manipulation during the process and can potentially be based on on-line measurements.

The first part of the study focuses on the characterisation of the crystallisation process in terms of nucleation and growth rates, crystal size distribution and filterability of the final crystal suspension. The aim was to produce large crystals of a narrow size distribution with a view of improving their filterability. Different approaches to achieve this are described in the second part of the thesis. These include addition of surfactant, coating of the impeller, and control of the rate of supersaturation generation combined with seeding. All the approaches proved to have good potentials in the control of the crystal size distribution.

Bulk protein crystallisation for product capture and purification has proven successful. The present method of bulk crystallisation of proteins can however be improved. For example, the seeding technique should be further developed. An understanding of the reason behind the observed high dependency of the growth rate on the degree of supersaturation could also guide the design of a better process. Finally, a better grasp of the interplay between the two observed crystals habits could lead to large reduction in the filtration time combined with a high yield.

Acknowledgments

I wish to thank:

My supervisor Prof. Mike Hoare, for his patience, support, direction and encouragement,

Prof. John Garside of UMIST for his very helpful guidance and criticism,

Prof. Peter Dunnill for providing the benefit of his experience and knowledge,

Novo Nordisk for financial support and Birgitte Mahler Nilsson and Mads Aage Laustsen for their very useful practical input to the project,

The Danish Research Academy and the Biotechnology and Biological Science Research Council for financial support.

Table of content

Table of Figures:

Tables of Tables

Symbols

A	filtration or crystal surface area (m^2)
C	impeller clearance (cm) or protein concentration (g protein/L suspension)
C_S	phase equilibrium concentration of protein (g protein/L suspension)
d	impeller diameter (m)
d_p	filterability (mL/m^2)
b	nucleation rate order
B	nucleation rate (no./(s·μL)) or filterability constant (eq. 38)
F	protein fraction of crystal (g protein/g crystal)
g	growth rate order
G	crystal growth rate (nm/s)
h	filter cake height (m)
H	liquid height in reactor
k	weighting parameter for the Laplace transformation
k_B	nucleation rate constant ($no.\cdot L^m/(s\cdot\mu L\cdot g^m)$)
k_G	growth rate constant (nm/s)
M	mass concentration of crystals (g/L suspension)
m	exponent of mass concentration of crystals
N	impeller speed (1/s) or crystal number
n	number density (no./(nm·μL))
$\bar{\mathbf{n}}$	Laplace transformed number density (no./μL suspension)
S	degree of supersaturation (for definition see equation 6)
s	Laplace transform variable with respect to size (1/nm)
s_f	upper interval end for s (1/nm)
R	size of crystal (μm)

t	time (s)
T	reactor diameter
V	volume concentration of crystals (L crystal/L suspension) or filtrate volume (m^3)
V_S	phase equilibrium volume concentration of crystals (L crystals/ L suspension)
w	dry weight of filter cake (kg)
Q	volumetric flow rate (m^3/h)
ε	filter cake porosity
ρ	solution density prior to crystallisation (g/L)
ρ_c	density of crystals (g/L)
ρ_L	density of permeate (g/L)
Δp	transmembrane pressure (Pa)
μ	solution viscosity prior to crystallisation (kg/(m·s))
μ_k	the k'th moment of the crystal size distribution

Abbreviations

CSD	crystal size distribution
ESZM	electrical sensing zone measurement
FBRM	focused beam reflectance measurement
OD	optical density

Chapter 1. Appraisal of the state of the art.

1.1 General introduction.

1.1.1 Fermentation products and downstream processing.

Recovery of a microbial product from a fermentation broth is the task of downstream processing in many biotechnology industries. Because of the very diverse nature of microbial products the biotechnological downstream processing includes a wide range of methods based on different physical phenomena. Decision on which of these unit operations, how many of them and in which order they should be used, is the challenge to the biochemical engineer. The decisions are taken to favour the demands of optimal yield and purity as well as the constraints of cost, ease of operation and ease of validation.

Before selecting the unit operations it is appropriate to describe the fermentation broth. In Figure 1 is depicted a very general guideline for the approximate composition of a fermentation broth (Taksen, 1984). The broth is often unstable, because of the possible contamination and enzymatic, chemical, thermal or stress related degradation of the product. Hence the broth should go directly to the downstream processing plant or be kept at low temperature (5°C).

Water 80-100 %			
Product 0-20 %	By-products (isomers, precursors, etc.)	Residual substrate/ additives (sugar, salt, vitamines)	Microorganism (bacteria, yeast, fungi)

Figure 1. Typical composition of a fermentation broth (Taksen, 1984).

A characteristic of the broth that complicates downstream processing is the batch to batch variability. Hence monitoring and control is an important skill in this area.

The product of interest is most often a water soluble component of the fermentation broth. The high lability of the products puts several constraints on the selection of temperature, pH, additives and the way of mixing and pumping when designing a plant. Examples of fermentation products are outlined below, emphasizing the diversity of products.

1) pharmaceuticals such as antibiotics and recombinant proteins etc.
2) industrial catalysts such as enzymes for washing detergents, enzymes for the paper industry, etc.
3) chemicals such as citric acid, acetone, 6-aminopenicillanic acid, amino acids etc.
4) beverage such as beer, wine or spirits,
5) whole cells for feed, catalysts or inocula.

Knowing the nature of the broth and the product to recover, one can start to consider how to design the downstream process in the most profitable way. Generally the first steps are non-specific and technically simple. These are followed by more specific, subtle and more expensive steps. If the product is intracellular the microorganisms have to be disrupted first to release the product. This is done with homogenizers, in bead mills or by enzymatic or chemically induced cell lysis. Then, when the product is in solution, the first step is generally removal of cells/cell debris by either centrifugation or filtration. The next step is concentration, by removing water usually by ultrafiltration, extraction, precipitation or, in the rare case of thermally stable products, evaporation can be used. Reducing the overall volume is done early in the downstream process, since it is preferable in order to reduce the scale and thereby the required investments of the following often more expensive part of the downstream processing. It is almost impossible to say more in general about the remaining steps in the downstream processing of fermentation products. Here the decision is to focus on processes relevant for pharmaceuticals and industrial catalysts (1 and 2 above). For these precipitation of the product or the impurities is a commonly used way to concentrate and crudely purify the product. Precipitants can be salts (most often $(NH_4)_2SO_4$), organic solvents or polymers. The resulting purification factor is approximately three fold (Aires-Barros *et al.,* 1994). The subsequent more specific steps are generally: ion-exchange chromatography, gel filtration, affinity chromatography,

adsorption chromatography, and dialysis. Which of these, how many and in what order they should be arranged depends on the actual application and relevant literature has to be consulted. For industrial enzymes, for example, chromatography is probably too expensive while for most pharmaceuticals several (and different) chromatography steps will be used to ensure the absence of pathogens in the product (Bailey and Ollis, 1986).

The classical dilemma of downstream process engineering is the balance between high yield and high purity. High purity means many process steps, which will lower the overall yield and vice versa. The purification factor for each unit operation depends on the number and the type of the foregoing purification steps. For example in the case of lipase a purification factor of 320 was achived in four or five steps (not including cell disintegration and broth clarification) yielding a highly homogenous product but at an overall yield of only 30 %. Normally three or four steps are used in purification of lipase (Aires-Barros *et al.*, 1994).

Until recently it was believed, that successful crystallisation was only possible from almost pure solutions of the product. The pre-purification steps necessary will lower the overall yield and as a result the crystallisation process is generally not favoured as process option. Recent evidence however suggests that high purity prior to the crystallisation might not always be crucial (Judge et al. 1995). If not, crystallisation will be one of the few downstream process where one can achieve both high yield and product purity.

1.1.2 Role of protein crystallisation.

The task of this thesis is to examine the role of protein crystallisation and to assess the circumstances, under which it may become an accepted method for recovery of proteins from crude mixtures.

At presence the role of protein crystallisation is to provide crystals for determination of protein structure by X-ray analysis. The experience from this area of research is that crystallising proteins is time-consuming. Firstly the protein has to be purified to a high degree of purity before conducting a long series of experiments to find conditions (pH, temperature, ionic strength, additives, etc.) under which crystals suitable for X-ray analysis can grow. The general belief that high purity of the protein solutions is crucial to the success of crystallisation, seems to have reduced interest in recovering protein from crude solutions by crystallisation even though there is some prior experience of the technology. For example the first protein crystallised was haemoglobin, by Hünefeld in 1840. This crystallisation must have taken place in

presence of many impurities. The first enzyme to be crystallised was urease from jackbean meal, that also is a complex mixture. This was done by Summer in 1925. Many more crystallisations from crude mixtures have been carried out since (Judge *et al.,* 1995; Hirsch *et al.*, 1989; Visuri, 1989). These have been performed at laboratory scale but also industrial scale protein crystallisations from complex mixtures have been undertaken for years, though only for small proteins such as insulin (M_V = 5700 g/mol) (Brange, 1987).

Advances in fermentation technology in the recent years are believed to have aided the protein crystallisation. For example, there has been a move towards the use of more simple complex media. This will leave the final fermentation broth less impure and therefore improve the likelihood that crystallisation can take place. Also the benefit from the use of recombinant-DNA has lowered the amount of impurities. This was achieved by allowing specific secretion of the product from the cell whereby cell rupture can be avoided. Recombinant-DNA has also be used to improve the stability of the product, which is important because crystallisation often involves long processing times. Reduced levels of protease can also be achieved using recombinant-DNA technology. It seems that protein, produced by over-expression in genetically manipulated microorganisms, crystallises with greater ease than the wild type protein probably because of the increased product concentration and homogeneity (McPherson, 1990). The conclusion is that protein recovery, from complex mixtures as fermentation broth by crystallisation, now should be considered as an optional method in downstream processing. Specially taking into account the very favorable quality of crystallisation, providing both high yield and purity.

Crystallisation in general is an old science mostly dealing with inorganic and small organic components (such as citric acid and some vitamins, antibiotics and amino acids) which can be crystallised at an industrial scale. How much of the experience collected for crystallisation of small components can be transferred to crystallisation of macromolecules as proteins? Below an attempt to answer this question will be made, while also describing the general features of protein crystallisation.

An important characteristic of proteins is that they are very sensitive to their environment. This is because of their dynamic structure, labile nature and microheterogeneous surface (McPherson, 1990). Hence in order to achieve crystallisation one must at least avoid protein denaturation by always keeping the protein fully hydrated and near their physiological pH and temperature. Even in this

limited range of the parameters the protein can attain numerous different conformations of which only one probably can be expected to fit into the crystal lattice. The task is to influence the equilibrium between such different conformation in the direction that provides the highest number of the crystallisable conformation(s) while the protein solubility is slowly reduced. If lowered quickly or lowered too much this will force the crystallisable units to make nonspecific hydrophobic interactions resulting in precipitation. Recent results indicate that light scattering techniques applied to precrystallisation solutions can detect if a solution eventually will produce crystals or precipitates by determining the protein-protein and protein-water interactions in the solution (George and Wilson, 1994).

Comparing protein crystals with crystals of low molecular weight compounds, the protein crystals are much more open in structure with channels and voids, allowing water contents of in the range of 25-90 % of the crystal mass (McPherson, 1990). Since a part of this water is un-bound, the protein crystals can contain relatively large amounts of dissolved low molecular weight impurities. The protein crystals are generally smaller (1-1000 μm, though most often 1-100 μm) than traditional crystals and also more brittle and hence easier to crush, when handling in a process plant. This is explained by the low number of bonds (hydrogen bonds, hydrophobic interactions and salt bridges) in proportion to molecular mass compared with crystals of small molecules.

The physical parameter considered to control the crystallisation is the degree of supersaturation. For protein crystallisations the supersaturation (C/C_S) is in the range of 1.2-10, which is much larger than the (C/C_S) $\cong$ 1.1 used in traditional crystallisation (Durbin and Feher, 1986). The phase diagram in Figure 2 gives an idea of the possibility of controlling the degree of supersaturation and hence the crystallisation. Phase diagrams as in Figure 2 unfortunately only exist for a few of the most investigated proteins such as lysozyme. The basic features of the phase diagram is the division between two regions; undersaturated and supersaturated by the saturation line. Crystal growth can take place anywhere in the supersaturated region, while nucleation only takes place in the region above the metastable region.

Clearly there are common features between small molecule and protein crystallisations but also a number of differences. Further investigations in the so far small field of protein crystallisation will hopefully shed light on exactly what these differences are.

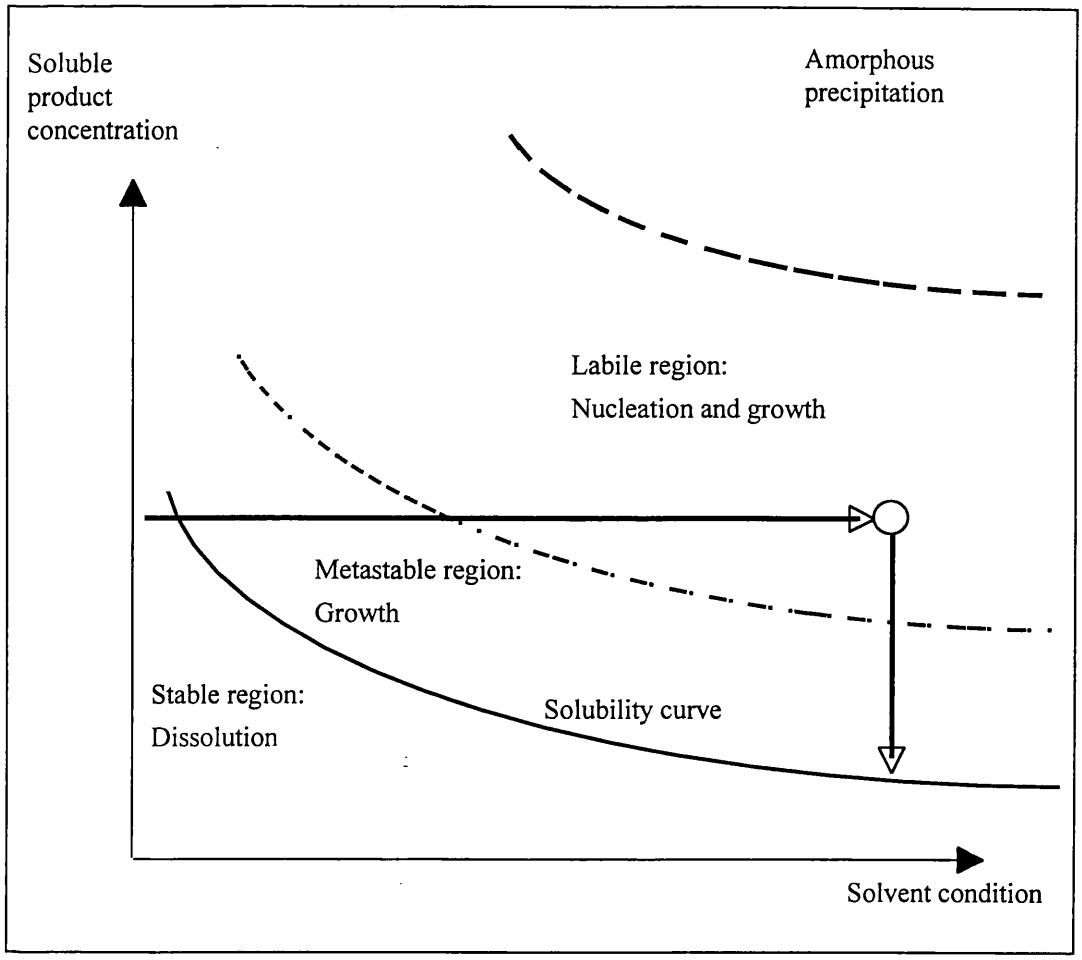

Figure 2. Schematic phase equilibrium diagram for protein crystallisation. The bold straight lines indicate a possible route for crystallisation.

1.2 Process design of crystallisation stage.

1.2.1 Process characterisation.

For process design fundamental understanding of the process, in particular knowledge of the phase equilibrium and kinetics is required. Slow nucleation and fast growth kinetics are important early in the crystallisation and will favour the formation of large crystals. A maximum yield is important and therefore towards the end of the process the phase equilibrium becomes critical.

The determination and use of crystallisation phase equilibrium.

For proteins the parameters affecting solubility are typically; reagent concentration, pH and temperature (McPherson, 1990; Howard *et al.*, 1988; Rosenberger and Meehan, 1988). The phase diagram can be subdivided into a number of regions (Figure 2). The region below the solubility curve is undersaturated and here no crystallisation can take place; above the solubility curve crystallisation can occur. Operation in extreme parts of the labile region (e.g. high product protein concentration

and/or solvent condition) will lead to protein aggregation, probably as an amorphous precipitate (Ducruix *et al.,* 1990; McPherson, 1990). Crystallisation consists of two basic processes: nucleation and growth. In the metastable region nucleation rates are very small and can generally be neglected so only growth is considered; in the labile region both nucleation and growth will occur. Before carrying out crystallisation, the component to be crystallised has to be in solution, the latter being undersaturated. The task is to adjust the system in such a way that the operating point is moved across the solubility limit into the supersaturated region (strictly speaking the labile region) as indicated in Figure 2. Even then crystallisation may not happen immediately because there is an induction time which, particularly for proteins, can be substantial . Furthermore it has been reported to depend strongly on the degree of supersaturation (Ataka and Tanaka, 1986). When growing crystals for X-ray analysis it is often necessary to have induction periods of the order of weeks to minimise the extent of nucleation and thereby obtain the few large crystals needed. For an industrial application it is necessary that the induction times are kept short typically no more than a few hours.

When the crystallisation starts, soluble material is incorporated onto the solid crystals and the operating point will move downwards until it reaches equilibrium at the solubility curve. The first part of the crystallisation will exhibit simultaneous nucleation and growth while the later part will show growth only.

To meet the requirement of optimal product yield mentioned above it is important to know the location of the product solubility minimum. Methods for determination of the solubility curves have been given in various publications (Moré and Saenger, 1995; Mullin, 1993; Boistelle *et al.,* 1992; Howard *et al.,* 1988). Either the crystals are left to grow or an excess of crystalline material is added and allowed partially to dissolve. In both cases the system is left until equilibrium is obtained and measurement of the supernatant product concentration gives the product solubility. Reports on the width of the metastable zone for protein systems are scarce (see for example Judge *et al.* (1995) or Dematteі and Feigelson (1991)). This is probably due to the fact that the metastable zone limit is dependent not only on pH, temperature and reagent concentration but also for example on the impeller speed, the presence of crystalline material and the way the system is operated (Tavare, 1995; Mullin, 1993).

Estimation of crystallisation kinetics.

The crystallisation kinetics account for the rate of processes which are thermodynamically favorable. Determining the kinetic parameters involves estimation

of the growth and nucleation rates. The most widely used expressions for nucleation (**B**) and growth (**G**) rates in conventional crystallisation are (Tavare, 1995; Mullin, 1993; Randolph and Larson, 1988):

$$B = k_B \cdot M_T^m \cdot S^b \qquad \textbf{eq. 1}$$

$$G = k_G \cdot S^g \qquad \textbf{eq. 2}$$

where **S** is the degree of supersaturation, $\mathbf{M_T}$ is the mass concentration of crystalline material and the remaining parameters are kinetic constants which can be estimated from knowledge of the degree of supersaturation, growth and the nucleations rates. Incorporation of the crystal mass concentration, M_T, in the expression for the nucleation rate is to account for secondary nucleation ($m = 0$ for primary nucleation). This is the mechanism of nucleation which only occurs in the presence of crystalline material. Some typical values of the kinetic constants are given in chapter 2 alongside a discussion of the fundamental mechanisms for nucleation and growth.

The degree of supersaturation accounts for the amount of protein which will come out of solution under the given conditions and can be expressed in a number of ways:

1) $C\text{-}C_S$

2) C/C_S (Kam *et al.*, 1985)

3) $\ln(C/C_S)$ (Malkin and McPherson, 1993a)

4) $(C\text{-}C_S)/C_S$ (Randolph and Larson, 1988)

where C is the protein concentration and C_S is the protein saturation concentration at otherwise fixed conditions. The relative degree of supersaturation (2) is the most commonly used.

A number of reports have been published where crystal growth kinetics are estimated on the basis of studies of crystals in static cells (Moré and Saenger, 1995; DeMattei and Feigelson, 1989) or flow cells (Durbin and Feher, 1986). In such cases the advance of the crystal surface is followed by microscopy. However, kinetic data obtained in this way may not be valid for bulk crystallisation where the crystals are suspended.

Suspended protein crystals are typically from a few micrometres to perhaps two

hundred micrometres in size. Relevant methods for measuring crystal size and number in this size range include: electrical sensing zone detection, image analysis and laser light diffraction as will be discussed in section section 1.3.

Once the crystal size distribution and crystal numbers have been determined, nucleation and growth rates can be estimated and in this thesis non-steady state systems will be a particular focus. The nucleation rate is generally determined by assuming that it is constant between two consecutive samples. The difference in overall number of crystals divided by the time elapsed will then give the rate of nucleation. One way of estimating the growth rate is on the basis of how far certain characteristic parts of the crystal size distribution, for example the mode size, shift between two samples. An assumption of constant growth rate between the two samples is necessary and all crystals are assumed to grow with the same rate with no crystal breakage occurring. A disadvantage of the method is that only one data point of the whole size distribution is used for the estimation and information is therefore wasted. Also for crystallisations with long periods of nucleation it can be very difficult to identify the characteristic points. An advantage of this method for estimation of the growth rate is that it is insensitive to sample dilution.

Another method for estimation of nucleation and growth is the so called s-plane analysis (Tavare and Garside, 1986). This method is based on population balances for discrete parts of the crystal size distribution. The change in number of crystals in discrete parts of the particle size distribution for consecutive samples can give an estimate of the growth rate of the crystals in this size range. The method is based on the population balance which can be written as (Randolph and Larson, 1988):

$$\frac{\partial n(t,R)}{\partial t} + G\frac{\partial n(t,R)}{\partial R} = 0$$

eq. 3

where **n (t, R)** is the number density function which is the number concentration of crystals present of a certain size range divided by the width of this size interval, **t** is time, **R** is crystal size and **G** is the crystal growth rate, here assumed independent of crystal size. Assuming that no crystal breakage or agglomeration occurs, we have, using a Laplace transform with respect to size (Randolph and Larson, 1988):

$$\frac{d\bar{n}(t,s)}{dt} + G\left(s \cdot \bar{n}(t,s) - n(t,0)\right) = 0$$

eq. 4

where $\bar{n}$ is the Laplace transformed number density function and s is the Laplace transformed variable with respect to size. The nucleation rate, B, is the rate at which crystals grow into the first discrete part of the crystal size distribution, i.e. $B = G \cdot n(t,0)$. Assuming that the growth rate is constant between time t_1 and t_2 and making the differential discrete:

$$\frac{\Delta\bar{n}(t_1,t_2,s)}{\Delta t} = -\bar{G} \cdot s \cdot \overline{\bar{n}(t_1,t_2,s)} + \overline{B(t_1,t_2,0)}$$

eq. 5

where $\overline{\bar{n}(t_1,t_2,s)}$ is the average change of the Laplace transformed number density function between the two samples taken at t_1 and t_2. A plot of the left-hand side of the equation versus $s \cdot \overline{\bar{n}(t_1,t_2,s)}$ should yield a straight line with slope, –G and intercept B.

Calculating the average size of the crystals present and using the change from one sample to the next can also give crystal growth rates. This method is often encountered as the "methods of moments" based on a moment transformation of the population balance (eq. 3) with respect to size (Tavare, 1995):

$$\mu_k = \int_0^\infty nR^k dR$$

eq. 6

Where **k** is the order of the moment μ_k.

For k = 0 the moment represents the overall number of particles present. From the zero'th moment of two consecutive samples the nucleation rate can be estimated, assuming that the nucleation rate is constant in the period between the two samples times and that no crystal breakage or agglomeration occurs. The difference in the zero'th moments divided by the time between the sampling then gives the average nucleation rate:

$$\bar{B} = \frac{\Delta\mu_0}{\Delta t}$$

eq. 7

Similarly from the first moment the average crystal growth rate can be estimated for the period Δt:

$$\overline{G} = \frac{\Delta\mu_1}{\mu_0 \cdot \Delta t}$$

eq. 8

Constant growth rate between samples, crystal size independent growth and no crystal breakage are assumed. The pitfall with this method is that if the nucleation rate increases significantly over several consecutive samples then the average size of the crystals present will decrease and a negative growth rate will be estimated even though every crystal present does actually grow. Also this method is insensitive to inaccurate sample dilution

Mahajan *et al.* (1991) and Randolph and Larson (1988, p54) used the method of constant oversize population density:

$$G = \frac{dn_o}{dt}\frac{dR}{dn} = \left.\frac{dR}{dt}\right|_n$$

eq. 9

Where n_o is defined as the cumulative oversize of the population density function. In practice this means that from a plot of the n_o as a function of size and where time is the discrete variable, the growth rate can be calculated from the distance (ΔR) between the curves for different times at constant n_o. The weakness of this method is that the growth rate is determined on the basis of only two data points and not from the entire crystal sizes distribution. Moreover a value of n_o has to be chosen. In cases of size dependent growth the choice will affect the estimated growth rate.

The estimation of the growth rate can also be based on changes in the solution. The changes could be the concentration of the crystallising protein, latent heat from the crystallisation or perhaps the rise in concentration of some non-crystallising component. Attempts have been made to estimate the temperature change at protein crystallisation, based on data given by Howard *et al.* (1988). Taking the large heat capacity of water into consideration, only very small changes in temperature can be expected. Tavare (1991) reports a method from which kinetic data can be obtained from the "desupersaturation" curve i.e. the depletion of the crystallising specimen from the solution. The growth rate for such is given as:

$$G_M(t) = -\frac{1}{A_T}\frac{d(\Delta C)}{dt}$$

eq. 10

Where ΔC is the supersaturation and can be in units such as LU/time (lipase activity unit/time), kg/time, etc. The resulting growth rate will include both nucleation and growth contributions, however the contribution from nucleation can often be neglected. Tavare (1991) described how the desupersaturation curve can be fitted with a second order polynomial. The zero time derivative of this polynomial can then be converted to give the order g and kinetic constant k_G (eq. 2) neglecting the contribution from nucleation.

Coupling the information obtained from crystal population balances and the supersaturation data provides the possibility of consistency checks (Tavare, 1991) and the possibility of investigating complex crystallisation kinetics.

Having estimated the nucleation and growth rates the kinetic parameters in equation 1 and 2 can be found by doing double-log plots. The kinetic data can then be used for making decisions for the reactor operation and design and for better understanding of the process.

1.2.2 Reactor operation.

The reactor should be operated such that a maximum yield is obtained quickly. The speed of the process has to be seen in the context of the subsequent solid-liquid separation stage. Long filtration times will result if the crystals are small and of a wide size distribution.

The crystallisation can in terms of operation be broken down into three phases: generation of supersaturation, crystallisation and crystal recovery. Depending on how the crystallisation is operated (batch, metastable or fill and draw) generation of supersaturation and crystallisation may take place simultaneously .

1.2.2.1 Generation of supersaturation.

To allow crystallisation to take place, it is necessary to change one or more parameters to make the solution supersaturated with respect to dissolved protein. This can either be done by decreasing the solubility of the protein or by increasing the concentration of the protein. To decrease the solubility, changing pH, temperature, and concentration of precipitants such as salts, organic solvents, detergents and polymers may be effective.

The ways to create supersaturation can roughly be categorised as rapid and slow response changes. A rapid change in supersaturation can be induced by a pH change, which is almost instantaneous. Temperature adjustments give a slow variation in supersaturation. Solvent evaporation is a slow process as would be changes in salt concentration by the addition of solid, since a finite time is required to dissolve the solid. In terms of control, a rapid change in supersaturation is generally preferred. Processes which induce slow changes in supersaturation are harder to control because of the time lag, but they tend to fluctuate less, which can be advantageous in providing homogeneous environments for crystallisation. Indeed, for protein systems, gentle changes have been recommended (Ducruix and Ries-Kautt 1990; McPherson, 1990) in order to prevent amorphous aggregation.

Unfortunately, in protein crystallisation, it is seldom possible to choose the parameter for induction of crystallisation. Often only one or maybe two parameters possess features which make them suitable. In section 1.4, a review of the effects of the various parameters on crystallisation is outlined. Generation of supersaturation by adding a precipitant is probably most common for proteins (McPherson, 1990). In contrast, for inorganic crystallisation adding a precipitant is considered as a last resource. This is because of poor supersaturation control, long adjustment times and precipitants being a source for defects in crystals (Rosenberger, 1986). For example during growth, the precipitant is rejected from the crystallising units. This increases the precipitant concentration, which in some cases results in showers of unwanted new nuclei.

1.2.2.2 Batch operation.

The term "batch operation" will be used here for crystallisations where the independent parameters are set from the beginning of the crystallisation and kept constant, typically at the value giving the maximum yield. This is probably the most widely used scheme for the operation of crystallisations because it is simple. In Figure 3 such an operation is outlined. Line 1 (the generation of supersaturation) represents the adjustment of the control parameter to the value giving the maximum yield.

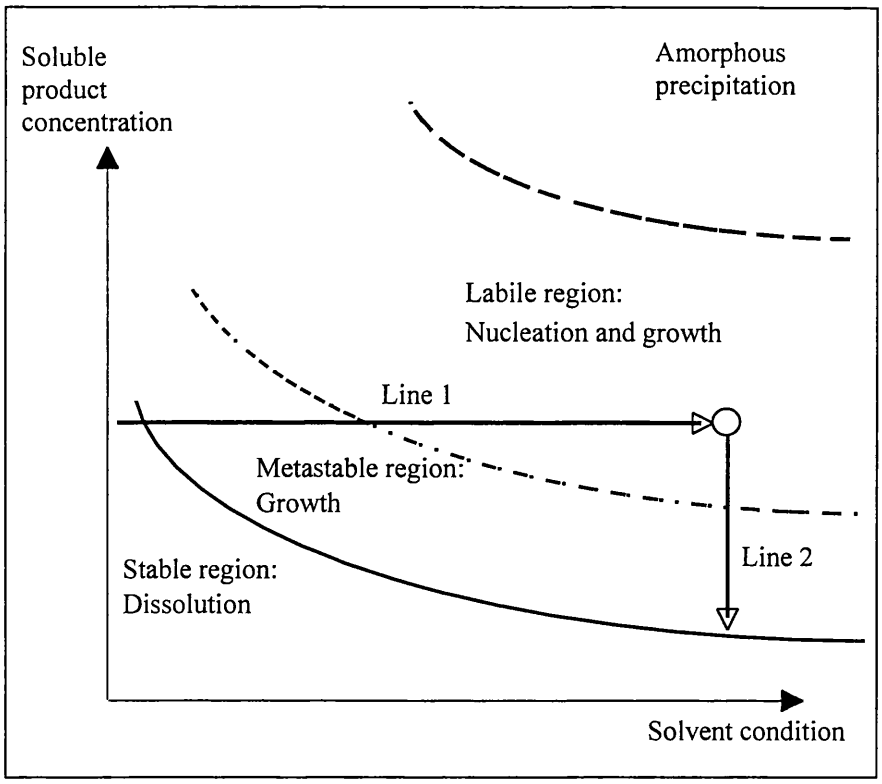

Figure 3. Schematic phase diagram for crystallisation. Operating line for batch crystallisation is added.

The circle at the end of line 1 represents the state in which the system is held till the induction time has passed or if seeding technology is used this could be the time for adding the seeds. Line 2 then represents the actual crystallisation where the first part will be simultaneous nucleation and growth and the later would be growth only. The batch operation will be a relatively fast process because there is a maximum driving force (= supersaturation) for both the nucleation and growth processes. Since the nucleation rate usually increases faster with supersaturation than with the growth rate, the resulting crystal product often consists of mainly small crystals. Due to the large number of crystals present, the protein solution will quickly be depleted, leaving the crystals small. Though the batch operation may be the fastest way of operating the crystallisation, it is likely to produce a crystalline suspension that is difficult to filter and a crystal cake which is difficult to dewater, wash, redissolve and handle.

1.2.2.3 Metastable operation.

During a metastable operation, the operating point is kept within the metastable zone throughout the crystallisation (Figure 4), thereby minimising nucleation. After adding seed crystals the control parameter is slowly changed during the crystallisation. More knowledge about the phase diagram is required to perform such a crystallisation

successfully than for batch operated crystallisation. Not only is the entire course of the solubility curve important but also the width of the metastable zone. If the metastable zone is narrow, this type of operation might be impractical. The process will be expected to be slow compared to the batch mode because the operating point is closer to the solubility curve. The process can however be accelerated by increasing the seed volume. Operating in the metastable zone should in theory mean that no nucleation takes place and only seed crystals grow. However, low levels of nucleation and some crystal breakage will be expected. The filterability of the crystalline material is expected to be significantly improved compared to the batch operation.

Gernert *et al.,* (1988) used a method similar to this to grow crystals for X-ray crystallography though without seeding. To obtain nucleation, they slowly allowed the operating point to move into the labile region. Compared to the batch operated experiment, reduced nucleation and hence increased crystal size was achieved.

Similar operation schemes have been thoroughly investigated for small molecule crystallisations, benefiting from greater availability of crystallisable material and more extensive records of solubility data. Extensive studies have for example been conducted for seeded crystallisation of potassium sulphate, comparing different time profiles for the generation of the supersaturation and evaluated in terms of crystal mean size and filter cake permeability of the final crystal product (Jones *et al.,* 1987; Jones *et al.,* 1986; Mullin and Nyvlt, 1971). These early works were all based on open loop control, i.e. finding the optimal time profile of the control variable which gave crystals of a desired quality. "Natural" (= uncontrolled) cooling was found to produce the smallest crystals because the large initial temperature difference between the reactor and the surroundings gives a high rate of cooling (i.e. a high rate of generation of supersaturation) at a stage of the crystallisation where the crystal surface area available to absorb the supersaturation is still small. Hence, the operating point may move into the labile region resulting in the production of many small new crystals. Based on crystallisation kinetics and mass balances, a theoretical optimal cooling curve was derived which allowed crystal growth rather than nucleation to take place. Experimental results showed a 40 % or more increase in crystal size compared to the uncontrolled crystallisation (Jones *et al.,* 1986; Mullin and Nyvlt, 1971) followed by a 60 % reduction in the specific filter cake resistance. Linear cooling curve was found to give a similar mean crystal size and even lower specific cake resistance indicating a wide metastable zone. Further work showed that lowering the rate of cooling could result in up to 80 % of the material being

deposited on the seed crystals. As expected, the largest crystals were grown at the lowest cooling rates. By comparing filter cake permeabilities, the anticipated improvements were not found. Unseeded crystallisations of the same cooling rate as well as experiments with shorter cooling rates were found to give higher cake permeability (Jones *et al.*, 1987). This was suggested to be a result of closer crystal packing in the filter cake stemming (at least for the seeded experiments) from the bimodal shape of the crystal size distribution.

Work has also been done to determine the optimal addition time profile for potassium sulphate crystallisation by addition of acetone (Jones and Teodossiev, 1988). Constant, instantaneous, linear, parabolic and exponential addition rate policies were tested. A higher recoverability of the resulting crystals was found if the acetone was diluted with water while no difference was found between the different addition profiles except for the instantaneous method.

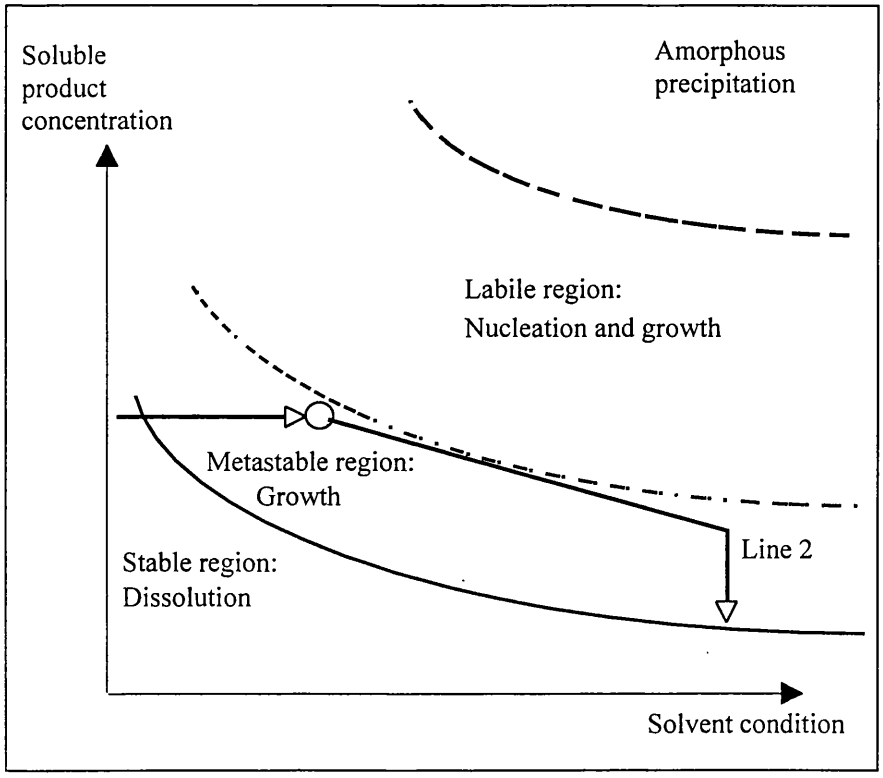

Figure 4. Schematic phase diagram. Operating lines for metastable crystallisation are added. The circle indicates the point of seeding.

1.2.2.4 Fill and draw operation.

With a fill and draw operation, fresh crystallisation material is slowly added to a large excess of crystals suspended in a saturated solution in which they originally grew. The degree of supersaturation can easily be controlled by selecting the speed of

crystallisation substrate addition. An advantage of this mode of operation is that the feed stock of protein can be kept cooled and at a safe pH till the moment of addition. Shortly after introduction into the crystal suspension, the protein will be incorporated into the large excess of crystal lattice present. This tend to reduce the loss of activity compared to the batch operation and even more so compared to the metastable operated crystallisation. Also, the inevitable generation of impurities will be reduced, probably leading to better crystal growth. A potential problem is a carry-over of microbial contamination.

An advantage of the operation scheme is that little information is needed about the system. As was the case for batch operation, the parameters should be maintained at the values which give maximum yield. It is important to know the lower limit of supersaturation where nucleation takes place (i.e. the metastable zone width). The challenge lies in controlling the feed rate since two simultaneous processes take place. The feed being pumped in is both diluted and incorporated onto the crystal surfaces. Thus, the rate of protein uptake will increase as the crystals grow. The feed rate profile required to maintain a certain degree of supersaturation can be found from a mass balance for the product protein in solution. In Appendix 3, it is shown that increasing the addition rate linearly with time would be expected to be a good approximation of the optimal feed addition rate. However, the full feed rate profile will consist of two sections. In the first period, the feed rate should be relatively high so the protein concentration reaches a level of supersaturation where the growth process has a reasonable speed (line 1). When that level has been reached, the feed rate should be dropped to a value which corresponds to the protein taken up by the crystals and then increased linearly with time. The calculation of the optimal feed rate requires a measurement of the crystal size distribution to give the total crystal surface area.

If the total crystal surface area is not available, the degree of supersaturation could be maintained by on-line measurement and control of the feed rate as discussed in Appendix 3.

When the reactor is full, the addition is stopped and the operating point will drop to the solubility limit (line 2). The fill and draw operation is slower than the batch operation, again because the operating point is closer to the solubility curve but an improved filterability of the crystal suspension is expected.

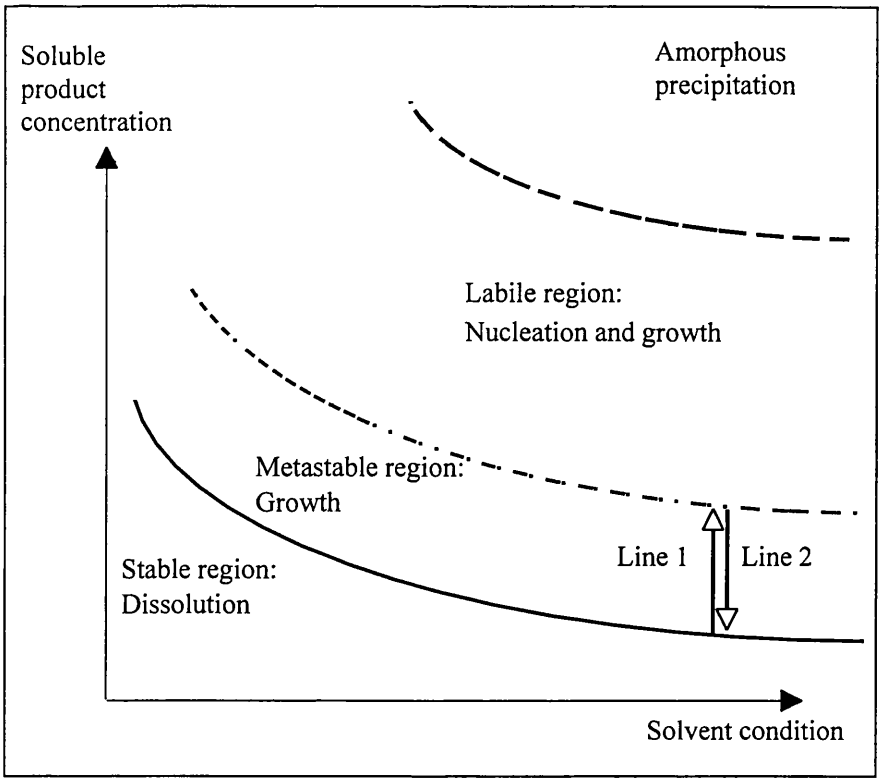

Figure 5. Phase diagram for crystallisation with operating lines for fill and draw operating added.

1.2.2.5 Seeding techniques.

Good control of nucleation is essential for the production of large crystals of a narrow size distribution. By far the easiest way to control nucleation is by using seeding techniques because nucleation and growth then can be optimised separately. Most literature on seeding in protein crystallisation is based on the attempts to grow large crystals for X-ray analysis (Weber 1991; Stura and Wilson, 1990; Thaller *et al.,* 1985; Thaller *et al.,* 1981), although there are also reports on bulk crystal seeding (Judge *et al.,* 1995; Schlichtkrull, 1957a). The guidelines in the X-ray crystallography literature can be applied only with caution to the area of bulk seeding in industrial protein crystallisation. Often the seeds are categorized in one of two groups (Stura and Wilson, 1990):

1) microscopic seeds

2) macroscopic seeds

The drawback of microscopic seeding is that it is difficult to control the number of seeds added. However, microscopic seeds should not need any pretreatment such as washing, etching and/or crushing as might be the case with macroscopic seeds. Macroscopic seeds are often a part of the final product from an earlier crystallisation. The success of

macroscopic seeding is therefore closely related to an understanding of the phenomenon of growth cessation. Macroscopic crystals can be fractionated according to size, counted and sized before addition which allows good control of the final crystal size distribution of the seeded experiment. Washing might be necessary to remove contaminant protein material that is likely to stop further growth on the surface. Etching (= slight dissolution of the crystal) may also be needed if the reason for growth cessation is incorporated defects in the crystal lattice. Finally, the macrocrystals may also be crushed (Thaller *et al.,* 1981). A concern is that crushing could distort the crystal lattice and hence prevent growth of the crystal debris. A requirement for successful use of seeding is that at least a part of the phase diagram is known since the degree of supersaturation should be kept low in seeded crystallisation to avoid rapid initial nucleation and to reduce the extent of secondary nucleation.

Schlichtkrull (1957a) successfully used freeze-dried crystalline insulin as micron-sized seeding material in the bulk crystallisation of insulin. Smaller crystals (25 μm) were obtained compared to the broad crystal size distribution resulting from the unseeded experiment, having an approximately average size of 55 μm. Smaller seed volumes were however found to increase the average size to approximately 40 μm. Judge *et al.* (1995) also produced small seeds (2-3 μm) by using high speed stirring of a crystal suspension of ovalbumin crystals.

If a large seed volume is used and small crystals form anyway, the filtration of the resulting bimodal crystal suspension can be more difficult than for unseeded experiments (Jones *et al.,* 1987). An alternative use of seeding is to add a small volume of seeds to start the crystallisation and thereby avoid the long induction times. Doing this, the seed crystal will make up an insignificant proportion of the final crystal product, thus not affect the filterability of the resulting crystal suspension.

1.2.3 Reactor design.

Here only the mechanically agitated reactor has been considered though other designs such as fluidized bed could be of interest. Low cost and simplicity being the main reason for the choice of this type of reactor.

The reactor design should favour a fast overall process with a maximum yield. The tools available are: **Impeller-:** type, geometry, position in the vessel, material, speed and impeller power. **Reactor- :** shape, geometry, material and baffles. **Monitoring:** pH, temperature and conductivity regulation.

The reason for examining reactor design is that when investigating a process a good design will strengthen the conclusions drawn on the basis of experiments. Also, protein crystals are very fragile particles and a careful design is needed to provide a gentle environment for crystal growth without fragmentation.

Considering optimal reactor design for crystallisation it has to be emphasized that we are handling two quite distinct phases; nucleation and growth, which have different requirements for optimal design. An important problem to address is whether the two phases should take place in the same reactor or in separate ones.

1.2.3.1 Optimal design for nucleation phase.

The major task when designing a reactor for nucleation is believed to be liquid homogeneity, since the reproducibility of nucleation depends critically on the degree of environmental uniformity. To obtain pH, temperature and protein concentration uniformity, the solution needs to be well mixed, preferably in the turbulent flow region (Re > 10000), where the solution can be assumed homogeneous (Edwards *et al.*, 1992). One aspect of homogeneity is how to obtain it and another is how to maintain maximal homogeneity, when a parameter is changed. The time required to return to a predefined level of homogeneity after for example addition of acid, is termed the mixing time (Nienow, 1992, p150). In some cases this parameter is more important than others. Changing the temperature is for example most often a slow process compared to reactor mixing times. On the other hand a pH change is a fast process and sub-regions with either higher or lower pH will exist for a finite time. Such sub-environments might have a large and irreproducible impact on the nucleation. So an improved reactor design should favour reduced mixing time, especially where parameters such as pH are changed. Comparing the impeller rotation needed to obtain a certain degree of homogeneity, Bourne (1992) concluded that the turbine impeller required the lowest speed followed by pitched blade 45° impeller. The hydrofoil impeller required the highest speed (for descriptions of impeller types see Figures 7-8). The mixing time also depends on the degree of turbulence, overall flow pattern and way of changing the parameter. In the case of pH change the mixing time will depend on the position and rate of addition of acid or alkali as well as the characteristics of both the added liquid and the liquid already in the reactor.

The induction and growth time add up to a considerable period. One might be concerned that the soluble protein could be damaged/denatured by effects of shear caused by the agitation. This potential problem has been investigated by Virkar *et al.*

(1981) and Narendranathan and Dunnill (1982) for yeast alcohol dehydrogenase and by Lee and Choo (1989) on lipase from a *Candida* strain. They concluded that hydrodynamic shear is probably far less responsible for the observed loss in enzyme activity in agitated systems, than surface shear related denaturation. Proteins do adsorb on gas-liquid (and also solid-liquid) interfaces and partially unfold because they possess both hydrophilic and hydrophobic parts. In well-agitated systems air bubbles vanish and appear all the time. If the unfolding/denaturation is irreversible, agitation will therefore cause progressive denaturation of the soluble protein. Support for this hypothesis is that, in systems with absolutely no air-liquid interfaces even at very high shear rates, very little loss in enzyme activity is observed (Virkar *et al.,* 1981). So, avoidance of protein denaturation can be achieved by operating the reactor with little or no headspace or having less violent mixing that can create air bubbles. Adding surfactant (polypropylenenglycol) has also been proven to be effective. The resulting reduction in the surface tension protected a lipase from inactivation by interface tension. Inactivation of enzyme is reported to decrease 97 %, 61 % and 93 % as a result of no air-liquid interface, less mixing and addition of surfactant, respectively (Lee and Choo, 1989). Concerns about the air-liquid interfaces are of course true for the whole process, from the moment where the enzyme has left the microorganism and through the downstream processes to the final product. When dealing with a fermentation broth the denaturation may be less extensive because of the presence of stabilising components such as sugars and antifoam agents.

The type of reactor construction material may also affect the nucleation, suggested by work of McPherson and Schlichta (1987). They found that the presence of a solid matter causes crystallisation to start at a reduced level of supersaturation and/or at a reduced induction time for a range of materials in a study of four proteins.

1.2.3.2 Optimal design for growth phase.

The task of designing a reactor for the growth phase is somewhat different from design for the nucleation phase. In the growth phase the task is to keep the crystals suspended to assure optimal surface available to growth. Poor suspension leads to some classification of the crystals in the reactor, with higher concentration of larger crystals near the bottom. In all other aspects such as pH, temperature and protein concentration the reactor might be expected to be homogeneous.

To limit the extent of crystal breakage agitation should be kept at a minimum. A gentle environment for crystallisation involves the design of a reactor that promotes

solid suspension and finding the minimum impeller speed and/or power necessary for just suspending the solids.

Impeller:

The impeller is most often situated in the horizontal centre of the tank. If one chooses off-centre stirring, better mixing will be obtained, but few investigations have studied quantitatively the effects of off-centre stirring.

In protein crystallisation two basic types of impellers are generally used: the axial flow impeller and the radial flow impeller, providing two different flow pattern (see Figure 6). Unfortunately there is no commonly accepted nomenclature for further describing the impellers. Included in the group of axial flow impeller (by some called propellers) are: 1) the pitch blade turbines (Figure 7a) with various numbers of blades and pitch angles (but not 90°). 2) the hydrofoil propellers (Figure 7b). Included in the group of radial flow impellers are a variety of vertical blade impellers, some shown in Figure 8. According to Edwards *et al.* (1992) the axial flow impellers are by far the most effective in solid suspension. In addition the axial impellers, and among these especially the hydrofoil impellers, are reported to have the lowest energy demand for solid suspension (Nienow, 1992; Bates *et al.,* 1963). By careful design, the 45° pitched blade impeller could be as effective as the hydrofoil impeller. Comparative studies of pitched axial flow impellers and radial flow impellers have been carried out with a 4 blade 45° pitched impeller, a hydrofoil impeller and a backcurved vertical blade impeller

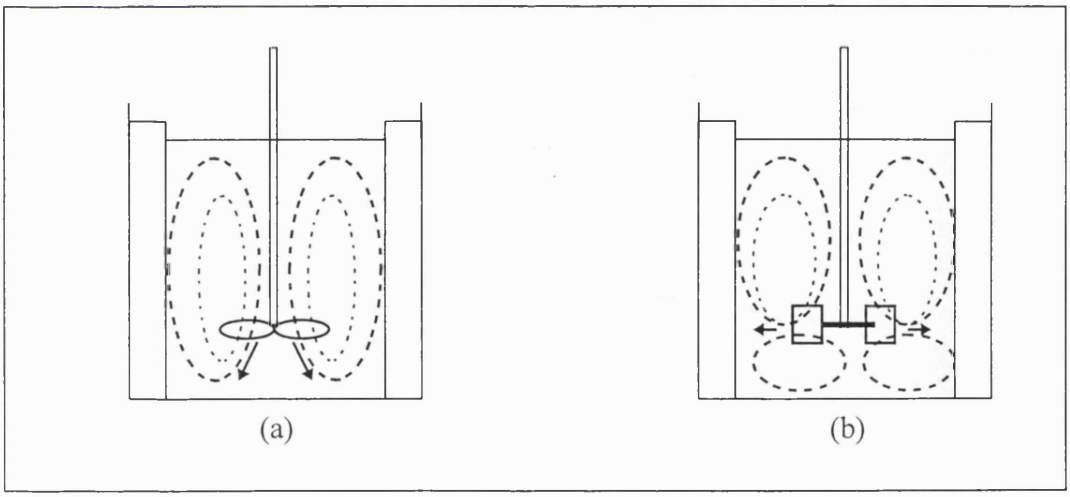

Figure 6. Flow pattern for axial flow impellers: (a) axial and (b) radial flow impeller.

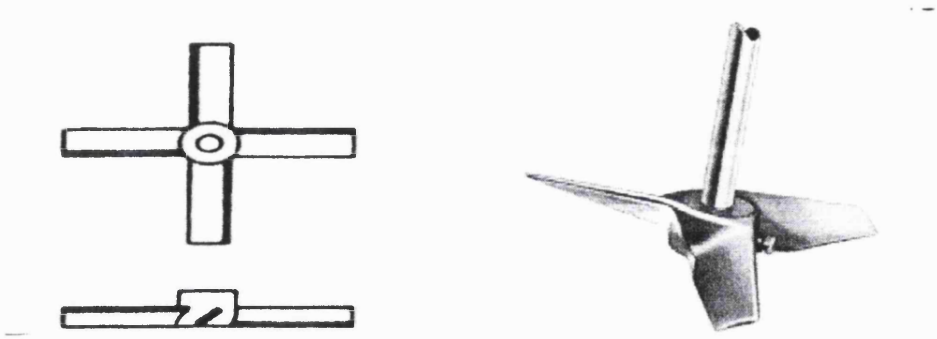

Figure 7. (a) Pitched blade impeller and (b) hydrofoil impeller.

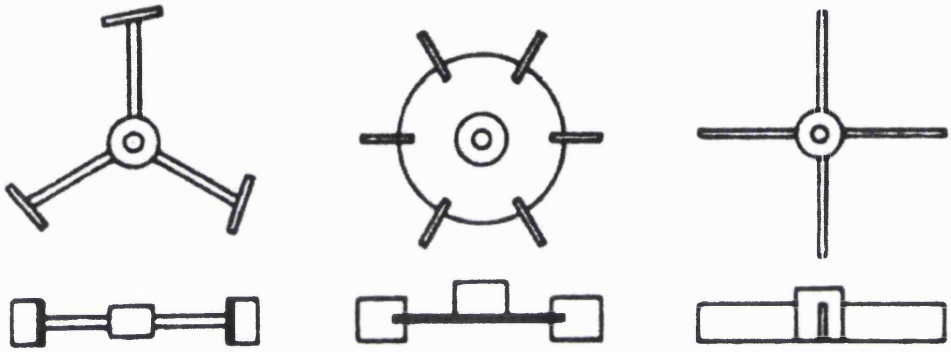

Figure 8. Radial flow impellers (Bates *et al.*, 1963).

This revealed that the radial flow impeller requires nearly twice the amount of energy compared with axial flow impellers for a particular degree of particle suspension, (Gray *et al.*, 1986, p26). Thus, the focus in this study will be on axial impellers; pitched blade and hydrofoil impellers.

The impeller size, given as impeller diameter to tank diameter (d/T) is reported to be optimal at d/T = 1/3-1/2 for high particle concentration suspensions with an axial flow impeller (Chudacek, 1986). Nienow (1992) states that with increasing d/T the speed required to suspend particles decreases. However this is only true in the range d/T = 1/3-1/2. At higher ratios, particles get trapped in the dead volume under the impeller and increased impeller speed is needed.

Tank geometry:

Firstly, it is best to choose a cylindrical vessel to have easy and well-defined mixing. The diameter of the vessel (T) is nearly always used as a key geometrical parameter and all other dimensions are given as ratios of this. The liquid height in the reactor is usually chosen as the same value as the diameter (H/T = 1), since the liquid depth has little influence on particle suspension (Nienow, 1992). Where damage at an

air-liquid is of concern, it could be advantageous to operate with higher H/T ratios to minimise the surface/volume ratio.

The disadvantage of the conventional flat bottomed tank is that it has several dead zones. One is a cone just under the impeller and the other is where the tank base meets the tank wall. To suspend particles in these regions, more than the minimal agitation is needed in the rest of the tank (Rieger and Ditl, 1994; Chudacek, 1986). By having tank with dished base (Figure 9a) the dead volume next to the wall is avoided. In the cone and fillet reactor (Figure 9b) both dead volumes are avoided and finally in the fully profiled reactor (Figure 9c) the bottom is completely streamlined. A way to further direct the flow is to equip the reactor with draft tube (Figure 9d).

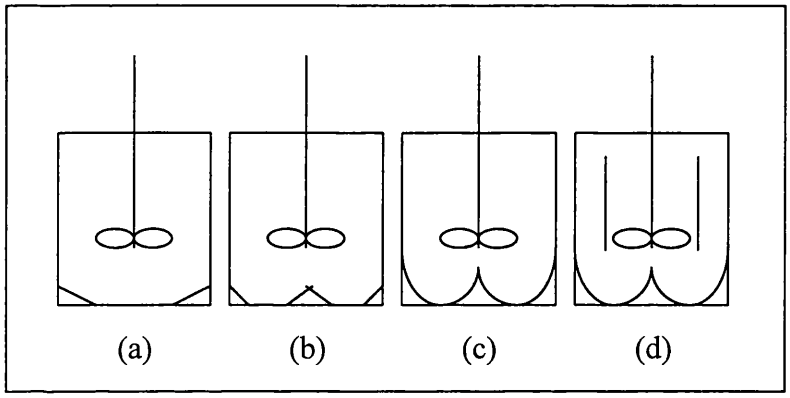

Figure 9. (a) Dished bottom tank, (b) fillet and cone tank, (c) fully profiled tank and (d) tank equipped with draft tube.

A comparison of the flat bottomed, cone and fillet and fully profiled reactor all equipped with a 3 or 6 blade 45° pitched impeller was made by Chudacek (1985). His conclusion is that both the cone and fillet and the fully profiled reactors are highly efficiently in solid suspension. But in case of the 6 blade impeller in a fully profiled reactor the advantage is very small compared to the flat bottomed. Gray *et al.* (1986) (p27) reports that in a dish bottomed tank with a 4 blade 45° pitched impeller 30 % more energy was required to suspend the particles than in a flat bottomed tank. This is in contrast to the observation of Nienow (1992) where the dish bottomed reactor exceeded the flat bottomed in particle suspension efficiency. The cone and fillet tank becomes increasingly more efficient than the flat bottomed as the scale of the tank increases, based on the complete off bottom criteria (see below) (Chudacek, 1986). The bottoms of batch tanks used for production of a solid product are often conical shaped to promote emptying the tank at the end of a run. During a run the apex will act as a dead volume,

where the particles are easily caught, why this shape is not recommended in cases where suspension is crucial.

Almost all reactors for solid suspension are equipped with baffles to prevent gross votexing behavior in cylindrical tanks. Baffles improve mixing significantly, but will impose extra stress on both crystals as well as on the soluble protein (Lee and Choo, 1989). The width of the baffles is often chosen to be 1/10 or 1/12 of the tank diameter and the number is usually 4 equally spaced and normal to the vessel wall (Leedom and Parker, 1967).

Impeller clearance:

The distance from the tank base to the impeller is termed the impeller clearance and is often given as a ratio of the tank diameter (C/T). Reduction in clearance leads to a lower agitator speed necessary to suspend particles but also increases the power consumption (Bates *et al.,* 1963). Normally the clearance is chosen in the range C/T = 1/3 to 1/2. Nienow (1992) states that for hydrofoil impellers the efficiency is insensitive to the impeller clearance, as long as $d/T < 0.5$. Minimum energy requirements for 6 blade 45° pitched impeller in flat bottomed tank are observed for d/T = 1/2 and C/T = 1/4.

Implicit in the above discussion is that it is possible to decide if a given reactor system is sufficiently agitated. In the following section, criteria for sufficient suspension as well as methods for determination of the degree of suspension will be described.

Minimum agitation:

In evaluating and interpreting solid suspension experiments one has to be aware of the several criteria for minimum suspension:

1) the most generally used is the that particles remain on the tank base for no more that 1-2 seconds (Nienow, 1992),

2) the 100 % suspension criterion, where no particles rest on the tank base even for a short period (Chudacek, 1986), This is also called the complete off bottom criterion (Chudacek 1986) or the 1-s criterion,

3) homogenous suspension throughout the vessel,

4) slurry height of 90 % of the liquid height (Rieger and Ditl, 1994).

The most relevant in industry is expected to be 1) and 4), but on a bench scale the complete off bottom criterion is best since more homogeneity is required to be able to investigate the system.

The challenge is how to find the optimal degree of agitation in a batch crystallisation. Basically we are dealing with a dynamic system, starting out as a low viscosity, Newtonian liquid and an essentially one phase system. The end point is a high(er) viscosity (because of the presence of crystals), with maybe pseudo plastic rheology and two phases (Gray, 1986). Therefore, the optimal degree of agitation should be adjusted dynamically. It is then necessary to decide the required degree of agitation. Several on-line methods for measurement of degree of suspension have been described (Nienow 1992, p.369). The most simple method is to construct a transparent tank and illuminate it. Visual inspection of the amount of particles left on the bottom will serve as a guideline for how much impeller speed and power is needed. Since this method suffers from some degree of subjectivity, instrumental methods have been developed as well. With these methods the local solid concentration is estimated near to the tank base. As the impeller speed is increased the solid concentration will also increase, but only up to an upper limit after which no further increase occurs. The break in solid concentration curve can be used as an indication of sufficient suspension (Rieger and Ditl 1994; Nienow, 1992; Shamlou and Kautsakos 1989). The solid concentration can either be determined by direct sampling (Buurmann *et al.*, 1986) or by measuring the light absorbed while passing the suspension (Shamlou and Kautsakos, 1989) or by conductivity measurement (Nienow, 1992).

Along with these experimental methods, theoretical considerations are available to describe the system (Nienow, 1992).

Protein crystals are generally small (< 100 μm) and of a density near to that of the mother liquor. Consequently they require relatively low impeller speeds to stay suspended. Additionally, the literature indicates that the growth kinetics are independent of the impeller speed (see chapter 2). The required impeller speed in protein crystallisation is therfore low, determined by the need to maintain a homogenous mixture allowing uniform crystallisation.

In practise, the above considerations may be difficult because many large scale impeller motors are capable of running at only two speeds: high and low. Moreover, the energy cost of agitation will, in the production of pharmaceutical, make up an insignificant proportion of the overall cost. Only for very brittle and fragile materials, for which a mechanical gentle environment is crucial, will design efforts be spent on minimising agitation.

1.2.4 Process control.

Downstream processing of fermentation broths is bound to vary from batch to batch. The operational criteria are maximum yield, maximum speed and a final crystal product with high filterability. Process on-line measurements are therefore expected to help fulfill the operational criteria and improve the reproducibility of crystallisation significantly.

An important aspect in maximising the yield is to decide whether more product can be extracted from the fermentation broth. The crystallisation could be allowed to proceed until a target amount of crystalline material had been produced. The target value (percentage sludge for example) is normally based on experience from earlier batches. However, the titers vary from batch to batch and so does the quantity of crystallisable product, thus risk discarding valuable product. A similar problem would be encountered if spectrophotometrical measurements on the supernatant were to be used to determine process completion by attaining a certain OD reading. The best result will undoubtedly be achieved if a lipase activity measurement could be done on-line or at-line on the factory floor. The reference assay for lipase is a pH-stat rate assay which could be automated, but easy and quick color assays would be preferable.

Deciding when the process has been completed is another challenge. Due to logistical limitations, a fixed processing time is often chosen. In this case, the process is either left for too long, which means that production capacity is wasted, or the crystallisation is prematurely terminated and valuable product lost. Measuring changes in OD(280 nm) on the supernatant or OD(680 nm) on the crystal suspension may show if protein is still being recovered.

Measuring the crystal size in a process environment can have several adventages (some measuring methods are discussed in Appendix 1.). One reason is process confidence. Another is that the way the crystallisation develops can be used as a basis for decisions during later steps in the process. Moreover, if accurate crystal number and size distributions can be measured, process control based on nucleation and growth rates can be done.

A simple batch operation needs no control. An "Open-loop" metastable operation can be improved by using on-line measurements to indicate whether the operating point has reached the solubility curve, indicating that faster reduction in the product solubility is needed. Changes in OD for the crystal suspension and changes in OD of the supernatant may be used for this purpose.

Similarly, a fill and draw operation can be controlled at a fixed OD for the suspension or for the supernatant, both of which can be related to degrees of supersaturation.

1.2.5 Crystal shape.

Many examples exist where proteins form crystals of different shapes (for lipases: Ransac *et al.,* 1994; Kordel *et al.,* 1991; Schrag *et al.,* 1991). The shape has to be taken into account when designing the industrial process.

The crystal shape, which can also be termed the crystal habit or the crystal morphology, is determined by three main factors: the internal structure of the crystal, the relative growth rate of the different crystal faces, and the extent of crystal breakage and attrition. Crystals that appear similar on visual inspection might not be identical since they could possess different internal structure (see for example Schrag *et al.* (1991)). If several different internal crystal structures of a protein are possible, the group of crystals is said to be polymorphs.

The objective of crystal shape control is primarily to obtain a crystal that is easy to dewater. Dewatering is necessary to remove the mother liquid and later the wash water. Generally, spherical particles are easier to dewater than for example needles or plate shapes. Increasing solvent retention can also be caused by crystal breakage, since a larger spread of the size distribution allows the crystals to pack more densely.

Which of several polymorphs will be dominant is a result of an interplay between kinetics and thermodynamics. The more stable polymorph will have a lower solubility. It may however not be the first of the polymorphs to form, since the kinetics of its formation might be slower than that of other polymorphs. If such a crystal suspension is left long enough, eventually a transformation to the more thermodynamically stable form will occur. Such temporary formation of a metastable polymorphs followed by transformation into a more thermodynamically stable form was first observed by Ostwald (Tavare, 1995). His understanding was that a system will often prefer a series of small energy transformations rather than a direct transformation to the most stable form. Any of the crystal forms can be the preferred one in an industrial process. However in high product value industries, the high yield that results from the formation of the most stable polymorph can supersede the demand for a polymorph that is easy to handle in the process steps which follow.

The relative growth rate of different faces of a crystal can result in a change in the appearance of the crystal, the so-called habit modification (Monaco and

Rosenberger, 1993). Some crystal faces may allow more bonds to be formed and are thus energetically more favorable and will grow faster. Impurities might specifically contaminate the growth sites on some types of face and cause these to grow more slowly or not at all. A method for predicting the relative growth rate of the different crystal faces and thereby the final shape based on thermodynamics and simulation of molecular dynamics was successfully tested for urea (Liu *et al.,* 1995). At present, the amount of thermodynamic data available for proteins is too scarce for such predictions. It is worth noting that the faster growing faces will make up a decreasing proportion of the total crystal surface as the crystal grows. For example a cube, for which the sides grow much faster than the top and bottom, will eventually transform into a plate.

There has been no explicit reports on growth of dendrites on protein crystals although both photographs and experimental data published by Azuma *et al.* (1989) seem to indicate such formation. Dendrites form when high gradients in supersaturation radiate from the crystal surface. Generally, however the growth of protein crystal is believed to be attachment controlled (see Chapter 2), for which no gradients in supersaturation are expected and hence no dendrite formation.

1.2.6 Crystal recovery.

After a certain time, further crystallisation is economically unattractive and the crystals have to be harvested. Since most of the impurities are now in the mother liquor, the crystals have to be separated efficiently from the mother liquor. For example, the crystals may be allowed to settle to the base of the tank and then removed as a crystal slurry through the bottom. If the crystals have only a slightly higher density than the solvent (a crystal density of an average of 1.3 ± 0.2 g/cm^3 for 9 proteins was calculated by Matthews (1974)) they will settle very slowly and the crystal suspension can instead be centrifuged or filtered.

Following the separation from the mother liquor, the crystals have to be washed, removing as much of the adhered impurities and resudial mother liquor as possible. The more irregularly shaped crystals tend to retain more mother liquor which is why much effort should put into avoiding these (Mullin, 1993, p423). To enhance the washing operation and to improve the filterability of the crystals, it is necessary to control the crystallisation in a way in which the final product has a narrow crystal size distribution and a high average crystal size. A narrow size distribution is the most important of the two (Mullin, 1993, p366) because such crystals will form a more open filter cake with a low specific cake resistance and thereby higher filtrate flow. The more open structure of

the dewatered crystals also retains less mother liquor and prevents crystal caking. Crystal caking can give problems in the washing step because impurities are trapped in the interior of the cake from where they are difficult to remove by washing (Mullin, 1993, p366). The wash water should not dissolve the crystals. Redispersion and washing should mean less loss than may occur during a recrystallisation. This statement applies to inorganic crystals that generally are low in water content. It might not be true for protein crystals since these contain 25-90 % water (McPherson, 1990). In the un-bound part of this water small impurities can be retained (Rosenberger, 1986). If redispersion increases the spread of the crystal size distribution because of crystal breakage and attrition, redispersion can be avoided by washing the filter cake when it is still on the filter cloth.

A requirement for the success of recrystallisation is that the impurities are more (best: much more) soluble in the solvent than the product. Moreover the equilibrium concentration of product over the product crystals should be low so as to reduce the loss of product. The main impurities in protein crystallisation are:
1) low molecular weight components such as salts, sugars and metabolites from the fermentation step.
2) protein material such as other proteins, product degradation material etc.
The former impurities are more easily removed by diafiltration prior to the crystallisation step. The latter impurity is likely to be absorped onto the crystal surface. They are thus probably more successfully removed by a thorough wash of the crystals. Therefore recrystallisation for protein purification does not offer any particular advantages. Additional Ewing *et al.* (1996) pointing out the similarity between ion-exchange material and the surface of protein crystals. The often small crystals may bind the charged impurities.

Since enzymes are manufactured both as solutions and as dry product, the crystals are either redissolved or dried before standardisation.

1.3 Monitoring of crystallisation.

1.3.1 Characterisation of prenucleation solutions.

To be able to control the crystallisation process, one first has to be able to monitor it and then understand the underlying physical mechanism. This would help to predict optimal process operation. This section deals with monitoring, which requires the measurement of particle sizes in the range 5 nm to 1200 μm. The whole range

cannot be covered with just one size measuring technique. Dynamic light scattering covers the range from few nanometers to 1 μm. The electrical sensing zone method covers sizes from 0.6 to 1200 μm, while image analysis via optical microscopy and laser light diffraction cover 0.5 μm and upwards and 2-1200 μm respectively (Allen, 1997). Basic principles of the above size measuring techniques are outlined in this section.

1.3.1.1 Dynamic light scattering.

Size distribution measurements of macromolecules in solution by light scattering intensity measurements were developed by Debye and Zimm in the 1940s (Berne and Bercora, 1976). Substantial investigation of protein kinetics has only recently been undertaken. Light scattering techniques allow us to follow the nucleation down to the molecular level and on that basis might enable us to predict the direction that the process will go (crystallisation or amorphous precipitate).

The way the scattered light is processed determines the kind of experiment e.g. intensity spectroscopy, photon correlation spectroscopy, laser light diffraction, static light scattering etc. Dynamic light scattering is based on analysis of scattered light fluctuations frequency rather than the absolute intensity or photon counts.

A dynamic light scattering (DLS) measurement is performed by illuminating a sample of suspended particles and detecting the light scattered via a pinhole to a sensitive detector. The intensity of the scattered light will fluctuate because of continual translation, rotation and vibration due to Brownian motion of the particles. Detection of the fluctuation of the scattered light can reveal the particle size distribution of the particles.

A particle in suspension will move as a result of gravity and Brownian (thermal) motion. For small particles the Brownian motion far exceeds the gravitational motion and therefore characterises the overall motion of the particle. The Brownian motion depend on various physical parameters and all these effects can be lumped in the entity called the diffusion coefficient of the particle. The physical parameters are: 1) size, 2) shape, 3) surface characteristics, 4) temperature, 5) particle concentration, 6) solvent and 7) solvent viscosity. In designing the experiment the aim is, if possible, to eliminate the effect of 2-7 to provide reliable particle size distributions.

The detected light signal is used to produce the autocorrelation function (self-similarity as a function of time). For mondisperse particle suspensions this function is a single exponential decaying function from which the particle diffusion coefficient can be estimated. Stoke-Einstein's equation further allow to estimate the equivalent

hydrospherical radius of the diffusing specie. For polydisperse particle suspensions the correlation function will be the sum of exponential decays, one for each particle size (or, more correctly one for each diffusion coefficient). Several methods are available to decompose the autocorrelation function into the different particles present. The most important are the cumulant moment method and the inverse Laplace transformation method (Thibault *et al.,* 1992).

When a size distribution based on radii are obtained from the Stokes-Einstein equation, the volume, mass or number distributions can easily be obtained by appropriate assumptions.

A crucial point for successful DLS analysis is that the sample is 100 % free of dust and air bubbles and special attention should be given to use only filtered and degassed water. Also the solution most be free of any foreign scatters such as non-specific aggregates formed between other proteins present. This could limit the use of the technique on industrial relevant solutions (Skouri *et al.,* 1995).

The advantages of DLS is 1) it is non-invasive, 2) requires only small sample volumes (10 µl), 3) possibility of on-line measurement since the results are obtained essentially in real time, 4) no calibration is needed and 5) it is not concentration dependent, when diluted to about 2 %w/v or lower.

1.3.1.2 Other methods.

Other methods for observation of nucleation are mainly derivatives of light scattering. This means that other data are collected or other data processing schemes applied for essentially the same experimental set-up as described in section 4.1.1. **Relative light scattering** (Bishop *et al.,* 1991; Pusey 1991). The equilibrium constants in the formation of lysozyme aggregates have been estimated by collecting the scattered light intensity at 90° and at the incident light frequency. The Raleigh theory predicts that the scattered intensity is proportional to the weight of the scatterer. Two conditions of a protein solution of the same overall protein concentration are known. One where only monomers are present and one where a mixture of (small) aggregates is known to be present. Taking the ratio of the scattered intensity from the two will give a measure of the degree of aggregation. This has been theoretically quantified by Pusey (1991) and he was in this way able to identify the most probable route of aggregation (monomer→ dimer→ tetramer→ crystal or monomer→ dimer→ trimer→ crystal or monomer→ dimer→crystal) which is important information in the examination of nucleation and crystal growth kinetics. The conclusion was that lysozyme crystals grow by addition of

clusters larger than tetramers. The weakness of the method is that a condition, where monomers exist in solution has to be known to evaluate the collected data.

Scatterers of the same magnitude and larger than the wavelength of the incident light are called Mie scatterers. For these scatterers the electric field across the particle is not constant at a given moment and therefore tends to scatter non-uniform angular distribution of light. This is in contrast to the smaller Raleigh scatterers which experience a constant electric field across the particle and therefore tend to scatter light uniformly in all directions (Bishop *et al.*, 1991). As a crystal grows it will pass from being a Raleigh scatterer to be a Mie scatterer. Detecting the ratio $I_{30°}/I_{90°}$ as a function of time has been used by Bishop (1991) as a measure of growth. The same qualitative picture of the crystal growth rate was recorded as when using static light scattering.
Static light scattering. The scattered light intensity in this method is integrated over times much longer than the vibration and rotation periods of the particle motion.
Interferometry. Scattered light will be frequency shifted and/or spread compared to the incident light and accompanied by a change in polarisation (Berne and Pecora, 1976). The frequency spectrum of the scattered light can help to determine translational and rotational diffusion coefficients whereby an indication of particle shape can be obtained (Michielsen and Pecora, 1981).

1.3.2 Characterisation of crystal nucleation and growth.

Four methods for particle characterisation have been considered. Microscopy which is based on static images, two are stream scanning methods and one is a field scanning method. The electrical sensing zone method counts and size particles flowing through an electrical field while focused reflectance measurements are based on the chord length observed by moving laser optics. Finally the field scanning method is the low angle laser light scattering based on larger particles scattering more in the forward directions. The mentioned laser methods suffer from the limited ability in giving physical particle number concentrations.

Sieving and sedimentation methods are also available but not considered here due to low size resolution and difficulty in data interpretation.

1.3.2.1 Microscopy

Observation of crystallisation by microscopy is useful in some respects. It is very easy and the best way to identify crystal shape, while assessment of crystal size distribution and concentration is quite labor-intensive.

Three classes of microscopy exist: 1) optical microscopy covering 3 -150 μm large objects, 2) transmission electron microscopy (TEM) covering 0.001-5 μm and scanning microscopy (SEM) having a resolution of 15-20 nm. So the whole size range of crystallisation can be observed, though the two last methods are less straightforward to apply, requiring more complex sample preparation. Manual or semi-automatic techniques for sizing and counting helped by use of graticules have been described (Allen, 1997).

1.3.2.2 Electrical sensing zone.

Determination of crystal size distribution in the size range 400 nm to 1200 μm can be achieved by a method called electrical sensing zone, the Coulter principle (Lines, 1992). In practise however the lower limit is near 1 μm.

The principle of electrical sensing zone is outlined in Figure 10. The crystal sample is suspended in an electrolytic solution in a beaker. A controlled low pressure inside the vial draws the electrolytic suspension of crystals through the small orifice at a fixed velocity. A current path is established between two immersed electrodes across the orifice. When a particle passes the orifice, the resistance increases and a voltage pulse can be detected. The height of the voltage drop is proportional to the crystal volume. Hence with electrical sensing zone it is possible to count the crystals as well as size them, giving the number or volume distributions as well as particle concentration. Knowing the density of the crystals, a mass distribution can easily be obtained, assuming a size independent crystal density. This assumption is reasonable for crystals, because of their structural uniformity. The experimental set-up is shown in Figure 10. A vacuum pump is used to create an imbalance in a mercury column. The vacuum pump is then turn off. The system will now equilibrate by drawing the crystal suspension through the orifice. The amount of suspension is accurately metered by the position of start and stop probes detecting the mercury surface passing. The voltage pulses are amplified before counting and sizing and the crystal size distribution and number concentration can be calculated. A minimum threshold value of voltage pulses to be counted has to be selected, ensuring that noise will not be detected as crystals.

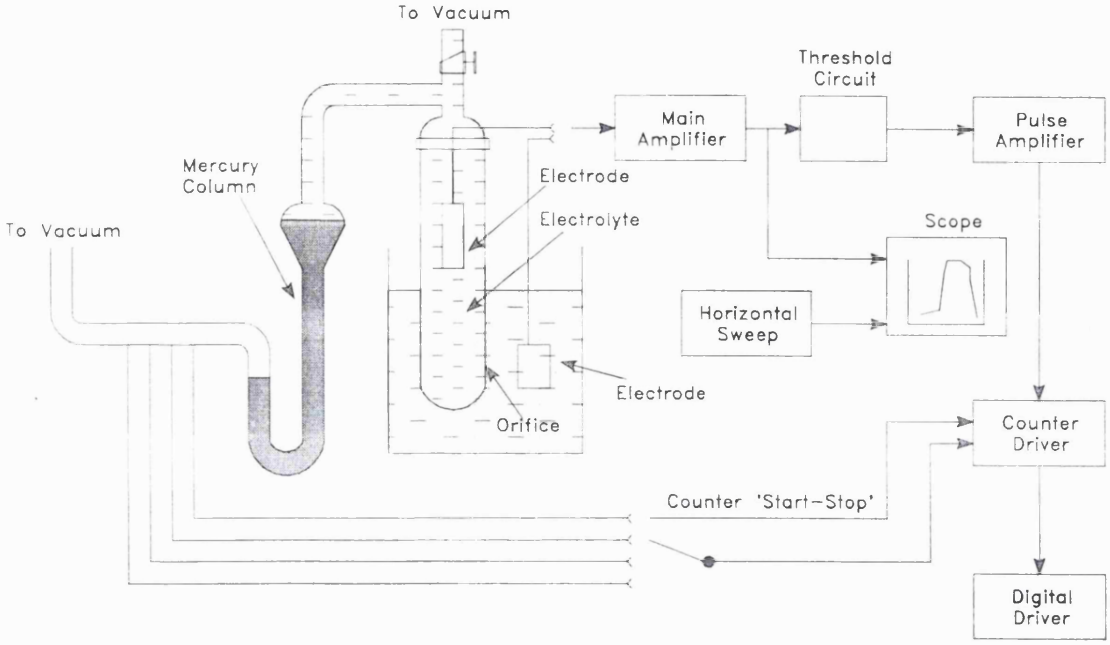

Figure 10. Schematic drawing of an electrical sensing zone instrument.

The upper size limit of this method is given by the lack of ability to keep big particles in uniform suspension. Because of the generally low density of crystals protein ($\rho \approx 1.3$ g/mL) this is not expected to cause problems in the indicated size range.

The problems involved in this method are 1) two crystals passing the orifice at the same moment will be counted and sized as one 2) if two under threshold size particles passes at the same moment and their sizes add up to an over threshold size, they will be counted anyway, 3) the determined sizes do depend on particle shape and surface characteristics, 4) porous particles or particles with conductivity close to that of the electrolyte will be undersized or ignored, because the current can flow through them. A sizing error can therefore occur when calibrating with material of very different conductivity. The first two problems can to a large extent be resolved by increasing the dilution, but correction formulae have also been developed and most interface software does the correction automatically. The third reservation is a problem when non-spherical particles are counted, though it is reported that the shape effect is constant over the whole size range (Lines, 1994). There could be a problem for rod-shaped crystals if the whole of the crystal cannot be accommodated in the electrical sensing zone. An approximate length of the sensing zone has been given to 70 % of the orifice diameter (Allen, 1997). In addition it has been observed that the length of the voltage pulse can give information on the particle length (Lines, 1992).

The electrolyte should have a conductivity equivalent to 0.2-20 % NaCl in water and can be increased if measuring very small particles (1 μm). Calibration is needed for every combination of buffer and electrolyte temperature. The crystal concentration must be low, so situations 1) and 2) above are avoided. However the concentration should be high enough to achieve sufficient statistical confidence in the results (Lines, 1992).

1.3.2.3 Image analysis.

Computer automation of for example the manually counting and sizing of particles in an ordinary light microscope is called image analysis. Direct processing of the image from the microscope in a computer can greatly speed-up the job. A grid of points called pixels is overlaid the image and the light intensity is measured in each point. These values are then compared to a scale of for example 0-255 and the operator decides below which light intensity particles should not be detected (Vecht-Lifshitz and Ison, 1992). The number of pixels and the type and magnification power of the microscope determines the resolution of the technique. Generally particles in the range from 1 μm and up to macroscopic size can be detected with a light microscope.

For image analysis as for the electrical sensing zone method the particles have to be diluted to such extend that no particle is very close together or overlapping each other since this would result in just one large particle detected. If the sample on the other hand is too dilute difficulties would be meet in getting a statistically significant result and large areas of the microscope slide would have to be analysed. A limitation in the image analysis technique is the lack of ability of focusing on both small and large particle at the same time. Particles out of focus would be seen blurred and their size will therefore be slightly overestimated. The is a problem if the particle size distribution is wider than say 50 μm.

There are some problems which can be expected particular with image analysis of protein crystal populations. One is that the protein crystal often appear at least partly translucent meaning that the crystal may not be detected. Staining techniques could be used to solve this problem though the technique is likely to have an effect on the crystals. Another problem could be that protein crystals are fragile and therefore easily crush under the weight of the cover slip and that mostly for the largest crystal because they would carry the cover slip. Special object glass with a small well on can solve this problem.

Currently image analysis is being developed to become an on-line method but it has not reached the commercial stage yet.

1.3.2.4 Focused beam reflectance measurement.

Lasentec® is the name of the company producing particle characterisation equipment based on the focused beam reflectance measurement (FBRM®) technology. The FBRM® technology measures particle chord lengths by detecting the duration of the reflected light while particles pass a focused laser light beam.

A stationary laser beam passes a small optical window that rotates rapidly perpendicular to the laser beam. This window focuses the laser beam in some distance out in the fluid and moves the focus point in a circular path with a speed of 2 m/s. Such high speed justifies the assumption that the particle movement due to the fluid flow, is much slower. This allows for the estimation of the particle chord length directly from the duration of the reflected light signal.

The advantages of the FBRM are that the probe is very robust and can endure even tough chemical environments. Moreover the technique is on-line and able to operate in high solids concentrations. The wide particle size range (0.8-1000 μm) covered in one measurement is also useful but at the expense of resolution. It has got only 38 channels cover the 1000 μm size range compared to commonly 128 channels for the electrical sensing zone method. As for most laser based techniques for particle characterisation in the size range above say 3 μm the conversion of the reflected light signal to a particle size distribution involved a number of assumptions which can be difficult to evaluate. Finally physical crystal number concentration cannot be determined with the equipment.

1.3.2.5 Low angle laser light scattering.

Also called laser light diffraction and it measures the scattered light intensity over time spans much longer than the time typically for molecular translation and rotation, at several different angles, reveals the particle size distribution using the Fraunhofer theory.

The upper limit of this method is determined by the ability to measure scattered light at very small angles, close to the unscattered laser light. The lower limit is determined by the transition of particles to become Raleigh scatterers. Raleigh scatters cannot be measured since they scatter light uniformly in all directions.

The size resolution and span is reasonable. For example in 32 channels Malvern Particle and Droplet Sizer can measure sizes of 2-197 μm, 5.7-560 μm and 12-1182 μm, depending on the detector/lens system (Allen, 1981).

1.3.3 Process yield.

In the evaluation of an industrial process yield, and purity are key parameters. So, reliable assays have to be established. In focus here is the determination the specific activity of lipase. What makes lipase assays more complicated, is that the lipase molecules are both hydrophilic and hydrophobic and only active at the interface between the hydrophilic and hydrophobic regions. The assay has to provide sufficient interface to ensure that the enzyme activity is not restricted by the availability of surface. A common method for providing interface is to create reverse micelles by the use of emulsifiers and powerful agitation (Martinelle and Hult, 1994). The choice of surfactant is important since different results are obtained with different surfactants and the same lipase sample. Because of these complications and since this is not a study in lipase kinetics, the standard lipase assay from Novo Nordisk A/S was adopted (see Appendix 4). In this method the surfactant is glycerol and gum arabic and the lipase substrate is tributyrin. The activity is determined by titration of the liberated butyric acid with NaOH. This is the most generally accepted assay for lipase (Brockerhoff and Jensen 1974, p30-32).

Since enzyme assays are often labour intensive, simpler but less accurate method have been suggested. In most work done on protein crystallisation, the progress has been measured by the loss of soluble protein using optical absorption at 280 nm (Bishop *et al.,* 1992; Kadima *et al.,* 1990; Mikol *et al.,*1990; Durbin and Feher, 1986). This is a good method when dealing with fairly pure single protein solutions. A review by Peterson (1983) warns about the risk using UV-absorption at 280 nm since in addition to proteins nucleic acid also absorbs at this wavelength. Moreover the absorption of protein is caused by only two amino acids (tyrosine and tryptophan), hence the absorption might vary considerably with different proteins. Dealing with protein mixtures, removing one of the proteins, can result in inconsistencies. Peterson (1983) concludes that subtracting absorption at 224 nm from the absorption at 236 nm, is better since at this wavelength several amino acids absorb (Trp, Tyr, Phe, His, Met and Cyt) as well as the peptide bond. The method is called the isoabsorbance wavelength method, because nucleic acids have an absorption maximum at 230 nm and by measuring in the same distance on either side of the optimum, the effect of nucleic acid can be eliminated.

Another way of quantifying crystallisation progress is by summing the volume of all the crystals detected, for example by the electrical sensing zone method. In the

absence of any other types of particles such as aggregates, this would be expected to be rather accurate.

1.4 Protein crystallisation: effects of environment on nucleation and growth.

This section should be viewed as an outline of the various effects on protein crystallisation as reported by other researchers. They provide ideas of how to manipulate the crystallisation in general. It has to be emphasized that the reported data can only be taken as rough guidelines, because of the great diversity of proteins. This review is not exhaustive and further information can be obtained from the Biological Macromolecule Crystallization Database (http://ibm4.carb.nist.gov:4400/). Unfortunately it has been impossible to make any generalisations even on the basis of this large database. It therefore still serves just as a bank of crystallisation experience.

Lysozyme is the most studied protein and is in several aspects different from the enzyme to be studied in this project. For example the isoelectric point (pI) is 4.3 and 11.1 respectively for the lipase in this project and for lysozyme. Also the lipase is expected to have a far more hydrophobic surface than lysozyme and lipase has a molecular weights of 35 kDa while lysozyme weights 14 kDa. Thus the behavior of the two enzymes cannot be expected to be similar.

Ideally this section should present phase diagrams for protein solubility as a function of various parameters such as pH, temperature, protein and salt concentration and absence/presence of other components. At the moment such phase diagrams have only been constructed for few proteins such as lysozyme (Feigelson, 1988; Howard *et al.,* 1988; Ataka and Tanaka, 1986), glucose isomerase (Visuri, 1989) and insulin (Brange, 1987). Furthermore the effect on the kinetic parameters (p22) would be useful for process design. However such data are still scarce (Judge *et al.,* 1995; Durbin and Feher, 1986).

1.4.1 pH.

That pH is one of the most important parameters in crystallisation has been stated by various researchers (Larson *et al.,* 1991; Carter, 1990; McPherson, 1990). In crystallising lipase from *Pseudomonas fluorescens* Larson (1991) revealed that pH is a crucial parameter and it should be kept the range pH = 8.45-8.6 for growth of large crystals.

A preliminary estimate of the optimal pH for crystallisation is given by the pI of the protein (Gilliland and Bickhan, 1990). At their pI molecules have a minimum net-

charge, and hence the crystallisation units more easily make contacts. Proteins tend to crystallise over a pH range of 1.5-2.5 units (Weber, 1990). So, finding the optimal pH will in most cases be an easy job.

In a study of the crystallisation of canavalin pH was used to promote the formation of trimers which appeared necessary for crystallisation (Kadima *et al.*, 1990). This suggests that pH changes may lead to conformational changes both for the single molecules and in the way the molecules interact allowing crystallisation to happen.

It has to be kept in mind when evaluating the effect of pH that inherently the ionic strength will change when changing the pH, so interpretation can be somewhat ambiguous.

The advantage of pH as a control variable it is easy to measure and has short adjustment times.

1.4.2 Temperature.

Temperature change for induction of crystallisation is often used in combination with some other methods of reducing the solubility (pH change, for example) (for glucose isomerase by Visuri (1989) and for insulin by Baker and Dodson (1970)). Higher protein stability at lower temperatures being the main reason. Crystals of alpha-amylase, glucagon excelsin and others have been grown by raising the temperature of the solution above the solubility limit and then allowing the solution to cool slowly until crystals appear (McPherson, 1985c). Raising the temperature, Rosenberger *et al.* (1993) achieved crystal growth for lysozyme, pointing out that proteins are not always more soluble at higher temperatures.

An increased temperature will result in more Brownian motion in the solution and therefore more protein molecule-crystal impacts, which may increase the rate of protein incorporation in the crystal. Also higher temperature allows the protein to attain high energy conformations that could be both advantageous or disadvantageous (Ries-Kautt and Ducruix, 1992)

Temperature is a "slow" control variable limited by the ability of transferring energy to/from the solution. This provides steady changes and uniform distribution of temperatures in the reactor due to rapid temperature equilibration in the liquid. Moreover if a set-point is exceeded, the temperature controlled crystallisation is the only crystallisation method which can easily by contra-adjusted without affecting the solution.

1.4.3 Ionic strength.

Increasing the ionic strength is probably the approach that has yielded most varieties of protein crystals (McPherson, 1990). This is not surprising, since it is well known that precipitation, which in many ways resembles crystallisation, is largely induced by increasing ionic strength (salting-out) or decreasing ionic strength (salting-in). Both in precipitation and crystallisation changing ionic strength is used to decrease the solubility of the protein and thereby at a certain salt concentration induce either precipitation or crystallisation. The mechanism for decreasing protein solubility at high salt concentration is as follows. Protein is kept in solution by a hydration sphere. The added salt ions are more easily hydrated than protein, so at a certain salt concentration the salt ions will disrupt the protein hydration sphere causing the protein to aggregate and eventually to precipitate or crystallise. The classical salt used for increasing the ionic strength is ammonium sulphate, but also phosphates and citrates have traditionally been employed with success (McPherson, 1990). Direct crystallisation achieved by reducing the ionic strength through dialysis have proven successful in numerous cases (McPherson, 1990). A few researchers report protein crystallisation in low ionic strength solutions (Nilsson *et al.,* 1994; Yoshikawa and Shinzawa, 1991; McPherson 1985b). These rely on the principle that the charged protein molecule requires a certain lower level of counter ions for shielding of its charges. When removing these, the protein molecules satisfy the electrostatic requirements through interactions among themselves (McPherson, 1990). The selection of the optimal ionic strength is not just a case of finding a salt concentration providing nucleation. Salt concentration does have an impact on growth kinetics as well. Durbin and Feher (1986) report a 10 fold increase in growth rate at the same supersaturation when going from 3.5 % NaCl to 5.0 % NaCl. Changing the salt concentration has also been suggested to maintain supersaturation during crystallisation (Carter, 1990).

1.4.4 Ion type.

Different ions have different effects on crystallisation which underlines that the ionic strength of solution is insufficient in characterising the solution. Salts generally used in protein crystallisation are $(NH_4)_2SO_4$, Na or NH_4-citrate, Na or K or NH_4-Cl, Na or NH_4 -acetate, $MgSO_4$, NH_4NO_3, Na-formate and LiCl (McPherson, 1985a). That some ions decrease protein solubility more effectively than others was noted by Hofmeister as early as 1889 while doing experiments on egg white lysozyme (Bailey and Ollis, 1986). Recently Ducruix and Ries-Kautt (1990) investigated the effect of

different ions on crystallisation of lysozyme. Their conclusion is that protein solubility is affected more by anions than cations, probably because of the basicity of lysozyme (pI = 11.1) having a positive net-charge at the experimental pH of 4.5. When pH is near to the isoelectrical point, a big difference in effect between anions and cations was not expected. Ducruix and Ries-Kautt (1990) also confirmed that the relative capacity of lowering the protein solubility of the ions corresponds to the order reported by Hofmeister, though the anions were in reverse order. They suggest this discrepancy is due to a difference in the degree of purification of the lysozyme used by Hofmeister and themselves. In addition the pH of Hofmeister's experiments was not either known or kept fixed. McPherson (1985a) states that generally at low ionic strengths the cations seem important. This has been supported by Carter (1990) stating that monovalent cations seem more important for crystallisation. Moreover the presence of Zn^{2+} ions was crucial, when crystallising insulin as rhombohedral crystals, since Zn^{2+} ions take positions in the crystal lattice (Brange, 1987). The most effective ion in crystallisation of lysozyme is thiocyanate anion (SCN^-), which promotes crystallisation at concentrations as low as 0.1 M, although this ion should be used with caution, since it is a helix breaker at higher concentrations (Ducruix and Ries-Kautt, 1990). Generally more polarizable anions such as formate, acetate, benzoate, benzenesulfonate and SCN^-, are effective at a 10-100 fold lower concentration than less polarizable anions such as Cl^-. This may be because these do not bind appreciably to the protein (Conroy and Lovrien, 1992) or because they form a low solubility complex with the protein (Ducruix and Ries-Kautt, 1990).

From the point of view of process control an interesting observation has been made by Ducruix and Ries-Kautt, that it is possible to change the features of the phase diagram by adding specific ions. Taking for example the phase diagram shown in Figure 2, where the undersaturated, metastable and supersaturated region are depicted as a function of a solvent condition and protein concentration. For process control it is preferable to have a broad metastable zone, to avoid parallel nucleation and growth. Ducruix and Ries-Kautt have shown the in the case of KSCN the metastable zone is only 100 mM while it is 1400 mM for NaCl. An interesting thing to investigate is whether it is possible also to broaden the metastable zone in a pH vs. protein concentration phase diagram by for example addition of salts. Experience with lipase from *Pseudomonas fluorescens* is that microcrystals can be obtained from at least 6 different salts over nearly the entire pH range (Larson *et al.*, 1991).

A final important characteristic for an ion is its ability to decrease the protein solubility to low concentrations. Some ions tend to decrease the protein solubility to a certain value, which cannot be lowered even with further addition of the specific ion. If an ion, on the other hand, is able to decrease the protein solubility infinitely, this ion will be suitable for keeping the solution supersaturated even at the very end of the crystallisation.

1.4.5 Protein concentration.

A protein is kept in solution by a primary hydration sphere. As the concentration of the protein is increased, at some point the amount of water available to solvate the protein becomes limiting and the protein will aggregate. At and above the solubility limit, the protein will crystallise or precipitate.

The protein concentration is the most dynamic parameter in protein crystallisation, making it difficult to define an optimal protein concentration. Giegé *et al.* (1986) states that solutions should have protein concentrations higher than 2 mg/ml to provide a successful crystallisation. For crystallisation trials, 10-20 mg/ml is generally sufficient (Gilliland, 1988). Wozniak *et al.* (1990) states that 8-37 mg/ml is appropriate. While McPherson (1990) gives 10-100 mg/ml as an appropriate protein concentration range when crystallising a protein for the first time. But if the aim is to grow large perfect crystals, lower concentrations are recommended (Ataka and Tanaka, 1986). The protein concentration is recommended for control of the growth rate (McPherson, 1990). Also, high protein concentration is reported to promote non-specific hydrophobic aggregation that does not lead to crystallisation (Giegé *et al.*, 1986).

1.4.6 Protein purity.

When crystallising a protein from a complex mixture, such as a processed fermentation broth, a range of impurities would be present. It is important to focus on the nature of these impurities and the mechanisms behind their interference with the crystallisation, e.g. inclusion, co-crystallisation, surface absorption and others. Several of these are likely to affect product solubility and the basic processes of nucleation and growth. Finally, impurities may, even at low concentrations, change the crystal habit.

There are a range of fermentation related impurities. Some originate from the substrate (particularly in cases where non-defined substrates are used) others are secondary metabolites, products of cell lysis and partially formed product. The latter is more common if cell disruption is necessary for product release. Also, reagents added during processing such as antifoam agents, acids and bactericides are considered as

impurities. During processing all these impurities can be denatured or react with other components in the system generating yet other impurities.

The heterogeneous forms (also called related forms) of the crystallising protein are a major source contamination. Ewing *et al.*, (1996) even stated that compared to small molecule impurities and impurities which can be removed by cation exchange chromatography, the heterogeneous forms of the lysozyme crystallised in their experiments apparently had the greatest effect on the crystallisation behaviour. Heterogeneous forms of the crystal protein include partly translated or denatured protein molecules.

A final source of impurities is microbial infections. Microbial contamination either originates from the fermentation step or from poor containment of the crystallisation process. Micro-organisms often secrete proteolytic enzymes which in itself is an impurity but which also can infer substantial damage to the crystal protein (McPherson, 1990) and cause protein aggregation (Skouri *et al.*, 1995; Sazaki *et al.*, 1994; Lorber *et al.*, 1993).

The effect of impurities on the nucleation step is known but not well understood. A general rule is that protein impurities reduce or inhibit the nucleation (Abergel *et al.*, 1991; Hirsch *et al.*, 1988). Combined with a longer induction time (Abergel *et al.*, 1991), the presence of impurities may have a positive effect by increasing the width of the metastable zone (Boistelle and Astier, 1988). The reduction in nucleation could however also be a result of a reduction in supersaturation caused by the presence of the impurity.

The effect of a particular impurity on the crystal growth will depend on the type of impurity-crystal interaction as outlined below.

Co-crystallisation covers the situation where an impurity takes up a position in the crystal lattice similar that of the crystal protein. Macromolecular impurities causing the formation of ill-shaped and twin crystals were however found not to incorporate into the crystal lattice (Skouri *et al.*, 1995).

Impurities that are structurally related to the crystallising protein would be expected to be incorporated into the lattice. They can then either be overgrown or simply inhibit further growth because they do not provide the right binding sites to allow continued growth. Eventually crystal growth may stop if many of such imperfect molecules are incorporated into the crystal lattice.

Protein crystals are very porous entities with solvent contents typically ranging 25-90 % (McPherson, 1990). Dissolved in this non-bond intracrystalline water will be smaller impurities and in rare cases small protein contaminants. Little or no effect on crystallisation is expected from these impurities though a final product of low overall purity can result.

Absorption of impurities to the crystal surface can also reduce the crystal growth rate significantly. For small molecule crystallisation, elaborate models exist to predict the degree of supersaturation required for crystal growth step to pass a row of adsorbed impurities (Mullin 1993). The growth of protein crystals is at present not investigated to the same extend. Reversible and competitive binding of impurities leads to a larger effect of the impurities at low supersaturation. In particular, this is the case if the kinetics of impurity binding is slower than the time between passing growth steps (Simon and Boistelle, 1981). For irreversible binding of the impurities, the crystal growth is poisoned, which in some cases can be overcome by increasing the supersaturation above a certain limit (Monaco and Rosenberger, 1993; Vekilov *et al.*, 1993; Boistelle and Astier, 1988).

Quantitative measures for the effects of impurities on crystallisation kinetics are rare. Judge *et al.* (1995) found that adding lysozyme and conalbumin to the crystallisation of ovalbumin had no effect on the growth kinetics. Unusually high growth rate dependencies on the degree of supersaturation were found for lovastatin and asparagine at high supersaturation by Mahajan and Kirwan (1994) and this was tentatively suggested to be due to impurities.

The presence of impurities will in many cases affect the solubility of the product and hence the process yield. Generally the presence of impurities is said to increase the protein solubility. This was found by mixing lysozyme with other proteins (Skouri *et al.* 1995) and by Visuri (1989) adding lysine and glucose to glucose isomerase. An increase in solubility of 50 % was found upon adding glucose and lysine up to concentrations of 120 g/L. However the salts used for "salting-out crystallisations" reduce the product solubility, so if they are considered as an impurity that is an exception from the rule. To achieve maximum single step yield from the crystallisation process, the impurities should therefore be removed prior to crystallisation. In doing this, the overall process yield can drop below the yield of the original single step process.

A complete change in crystal shape as well as more moderate habit modifications have been observed as a result of the presence of related protein

impurities (Abergel *et al.*, 1991). A gradual change from tetrahedral to orthorhombic shape was observed for haemoglobin C crystals formed when adding haemoglobin A (Hirsch *et al.*, 1988). Similarly, the c-axis shortened upon addition of hen and Japanese quail egg white lysozyme to the crystallisation of turkey egg white lysozyme while crystals formed when adding pheasant egg white lysozyme (Abergel *et al.*, 1991). Ewing *et al.* (1996) also obtained bundles of chicken egg white lysozyme crystals when crystallising from an extensively dialysed commercial solution. If the solution was further purified using cation exchange chromatography, the expected tetragonal crystal formed. Finally, increased crystal twinning was suggested to be linked to the presence of impurities (Lorber *et al.*, 1993).

1.4.7 Surfactants.

Lipases are known to be active on the interface between hydrophobic and hydrophilic regions and therefore have such regions on their surface too. That surfactants do affect the crystallisation of lipases is hence not surprising.

The surfactants used by X-ray crystallographers is mostly mild neutral (= non-ionic) detergents at low concentration. Examples are α-octyl glycoside (Garavito and Rosenbusch, 1980), β-octyl glycoside (Garavito and Picot, 1990; McPherson *et al.*, 1986), octylthioglucoside (Kouyama *et al.*, 1994), n-octyl-β-D-glycopyranoside (Lang *et al.*, 1994), Triton X-100 (Paetzel *et al.*, 1995), Tween 20 (Bohach *et al.*, 1992) and Brij-35 (Yoshikawa *et al.*, 1991). The concentration used is generally below 2 % but up to 10 % (w/w) has been reported (Bohach *et al.*, 1992). In some of these cases, surfactants were an essential additive to obtain crystals (Paetzel *et al.*, 1995) while in other cases the surfactant merely improved the quality of the crystals produced (McPherson *et al.*, 1986). This improved quality could both be in terms of increased crystal size, better diffraction and/or better crystal habit (i.e. more bulky habit). An advantageous change in crystal habit was observed for enterotoxin (Bohach *et al.*, 1992), membrane proteins (Kouyama *et al.*, 1994) and glutamic acid (Garti and Zour, 1997).

In the crystallisation of small molecules, the effects of surface-active agents have also been observed (Mullin, 1993). Concentrations as low as a few parts per million of certain surfactants are reported to have strong effects on the crystallisation and often as so-called habit-modifiers. Here mainly cationic and anionic surfactants are used.

Surfactants affect crystal nucleation and growth in several ways. For example, crystal growth has been observed to slow down in the presence of surfactants (Bohach *et al.*, 1992). This is expected because the surfactant is believed to bind to crystal surfaces

(i.e. the name "surfactant") and hence become a physical barrier to crystal growth (Garavito and Picot, 1990). Lower observed growth rates could also be a result of the lower degree of supersaturation expected when adding a solubilising additive such as surfactants. Contrarily, there are arguments that the growth rate should increase in the presence of surfactants due to a decrease in the interfacial tension (Mullin, 1993). Surfactants are also expected to bind to the surface of the protein in solution (Garavito and Picot, 1990). This is particular useful for the crystallisation of membrane proteins because the surfactants are suggested to bind to hydrophobic areas on the surface of the protein molecule, helping to carry the protein into solution. This shielding of hydrophobic areas is also thought to limit the amount of unspecific interaction between protein molecules and thereby promote the specific interactions leading to successful nucleation (McPherson *et al.,* 1986). The increased concentration of surfactant has been reported to reduce nucleation resulting in larger single crystals (McPherson *et al.,* 1986; Garavito and Rosenbusch 1980; Bohach *et al.,* 1992).

Generalisation of the effects of surfactants is impossible at this stage of the art because several of the authors state that out of a number of surfactants tested only few have been efficient (Kouyama *et al.,* 1994; Yoshikawa *et al.,* 1991). Better understanding of the fundamental interactions between surfactants, proteins in solution and the crystals would be required before a more general use can be suggested.

A concern is that the detergent is contained in the crystals (Yoshikawa *et al.,* 1991; Garavito and Picot, 1990) at levels of up to 25 % of the molecular weight, which then have to be removed after dissolution of the crystals. The advantage of an addition of detergent is a higher degree of reproducibility and a shower of microcrystals is largely avoided (McPherson, 1986).

1.4.8 Other parameters.

Besides the parameters mentioned above, a number of other parameters have been investigated. Pressure (Takano *et al.,* 1997; Visuri *et al.,* 1990), solution age (Ewing *et al.,* 1996; Hirschler *et al.,* 1995), co-solvents, surfaces and additional precipitants have been shown to affect crystallisation.

For example, glycerol is considered as a co-solvent and this and other polyalcohols, such as sugar, are reported to stabilise proteins in solution (Sousa and Lafer, 1990). Sugars will often be present in the fermentation broth and they can be left in the crystallising solution with beneficial effects. But if left, extra caution is necessary to avoid contamination. The mechanism of this stabilisation is that the polyalcohols

force the dissolved protein into a more compact configuration. In water/glycerol mixtures for example, when decreasing the relative amount of water, the glycerol will partly act as a solvent for the proteins. Because of steric hindrance, the glycerol cannot solvate clefts in the protein molecule, which contracts and is left in a more stable state. The compact configuration fits easier into the crystal lattice since they are expected to be a more homogeneous.

If the presence of a solid matter causes crystallisation to start at a reduced level of supersaturation and/or at a reduced induction time, the nucleation is termed heterogeneous. Most of the crystals will grow from the solid surface. A range of mechanisms can be responsible. Epitaxy for example is the formation of crystals that have a lattice which approximately matches that of the solid surface. The lattice of the solid surface is thought to organise the nucleating molecules on its surface and thereby mediate the nucleation. Mineral surfaces possess lattice unit cells five to ten times smaller than an average protein crystal unit cell, but this may be of no concern since the protein crystal can form over several cell units. In a study of four proteins and 50 minerals by McPherson and Schlichta (1987), they found only one example believed to be truly epitaxic. They found almost 50 cases of reduced induction time and these were thought to be a result of other and less specific heterogeneous mechanisms. These could include adsorption of the protein on to the mineral surface, creating a higher local supersaturation which promotes nucleation at the interface. Another explanation could be that the crystal-solution interfacial energy is larger than the crystal-solid surface interfacial energy, making the formation of nuclei on the solid surface more energetically favourable. Finally a "chemical" mechanism is suggested where the surface reacts with the protein causing denaturation or precipitation, which may then again act as a nucleant for the protein crystallisation. Other reported examples of heterogeneous nucleation is on cellulose fibres (Stura and Wilson, 1990) and latex microspheres (Malkin *et al.,* 1993).

Precipitants in crystallisation are a large and diverse group. The most important of these are the salts and they are treated in a separate section. Precipitants also include polyethyleneglycol (PEG) and organic solvents. The role of PEG in crystallisation is not completely clear. At least a part of its precipitating effect on protein relies on preferential hydration as is the case with salts. PEG with a molecular weight of 1000-4000 are normally applied and no general criteria exists for which one to choose. Since the effect of PEG molecular weight is significant, one has to investigate which is the

optimal (McPherson, 1985b). The effects of PEG are most pronounced at minimal ionic strength (McPherson, 1985b). PEG concentration is considered as a good control parameter because protein tends to crystallise over a fairly narrow concentration range, but within this range, it seems quite insensitive to exact PEG concentration. In addition to this crystals grow slower when PEG is the precipitating agent compared to $(NH_4)_2SO_4$, but the induction time is shortened and therefore often leaves the overall crystallisation time shorter (McPherson, 1985b).

Organic solvents are also precipitants, which as with salt and PEG, lower the water concentration of the solution, thereby forcing the protein out of solution. The organic solvents will not be treated in this introduction since application of organic solvents are irrelevant in industrial scale because of the safety and environmental considerations.

Chapter 2. Theoretical considerations.

2.1 Crystal formation.

2.1.1 Pre-nucleation.

2.1.1.1 Mechanism of processes leading to nucleation.

This section will treat nucleation, not only as an isolated event, but also as a result of properties of the solution (that is undersaturated and supersaturated), which lead to crystallisation.

A definition of nucleation is presented by Kam *et al.* (1978). Nuclei are formed by an aggregation process:

$$A_j + A_1 \Leftrightarrow A_{j+1}$$

eq. 11

$$K_j = \frac{k_j^f}{k_j^b}$$

eq. 12

assuming that the aggregation proceeds through the addition of monomers.
$\mathbf{K_j}$ is the equilibrium constant for the j'th aggregation process, **j** being the number of monomers, $\mathbf{k^b_j}$ and $\mathbf{k^f_j}$ are the backward and forward reaction rates respectively, and

$$K_j = \exp\left(-\frac{d(\Delta G_j^0)}{d(j)} \Big/ kT\right)$$

eq. 13

Where **k** is Boltzmann's constant and $\Delta\mathbf{G_j^0}$ is the standard Gibb's free energy for the formation process of an aggregate of j monomers. The dependence of G_j on j is shown in Figure 11. During pre-nucleation aggregates grow and dissolve in a statistically random way. After a period of time called the induction time, some of the pre-nuclei aggregates will reach the size, called the critical size, after which they will grow rapidly and spontaneously. The reason for this free energy barrier to nucleation is as follows. The ΔG for the process is the sum of two contributions. ΔG_V is the free energy difference between a protein unit in solution and one incorporated into the interior of the crystal. This entity is a function of the protein solubility and is negative for all supersaturated solutions.

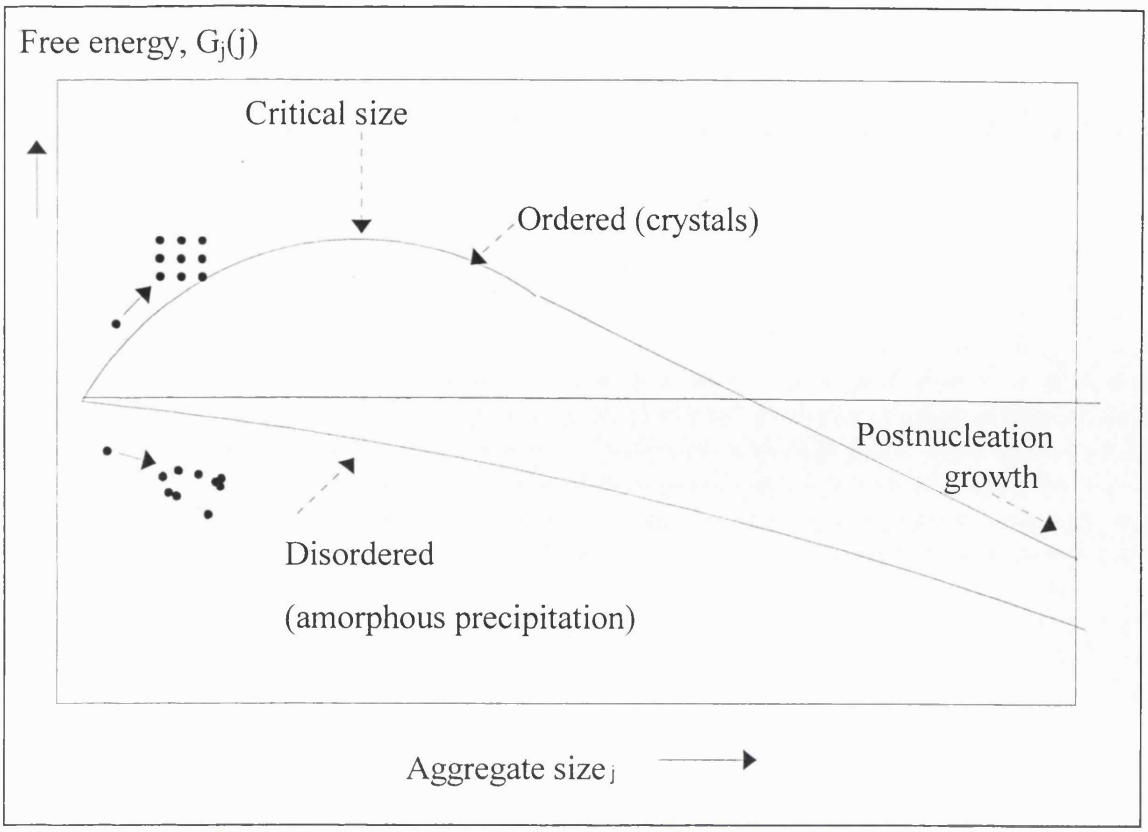

Figure 11. Energetics of nucleation (Kam *et al.,* 1978).

Some of the incorporated units will make up the crystal surface and these positions are less energetically favourable since fewer bonds are formed. Calculating ΔG for the aggregating process as ΔG_V for all the incorporated units and then taking into account the missing change in free energy originating from the surface, the following expression is obtained.

$$\Delta G(r) = 4\pi r^2\sigma + \frac{4}{3}\pi r^3 \Delta G_V$$

eq. 14

$\Delta \mathbf{G}$ **(r)** being the change in Gibb's free energy in the formation of a crystal nucleus of radius **r** (spherical shape assumed) and σ is the specific surface energy.

For small radii, the first term will be dominant, while for larger radii the second term will be dominant. This explains the features in the crystallisation phase diagram. In an undersaturated solution, both terms in eq. 14 are positive, making the crystallisation process thermodynamically impossible. In the metastable region the second term is negative, but not enough to balance the positive free energy from surface creation. Hence no nucleation occurs, but for existing crystals, for which the second term exceeds the first, growth can takes place. On the edge of the metastable region facing the labile-

supersaturated region, the two terms are equal. In the labile-supersaturated region, the sum is always negative making the crystallisation process thermodynamically possible.

The critical size of an aggregate is reported to decline as the supersaturation increases. Malkin and McPherson (1993b) found a linear relationship between the reciprocal supersaturation (supersaturation defined as $\ln(C/C_S)$) and the size of the critical nuclei. They also showed that the induction time increases with increasing size of the critical nuclei, as expected from the theory described above. This has been quantitatively supported by Ataka and Tanaka (1986) stating that the induction time appears to be proportional to $(C/C_S)^{-n}$, n = 5 for lysozyme.

The thermodynamic difference between crystallisation and precipitation can be expressed in terms of K_1/K_∞ ratios, where the K's are defined in eq. 12. The process of incorporation of a unit into the crystal lattice becomes more and more energetically favourable as the crystal grows, i.e. $K_1/K_\infty >> 1$. Precipitates are believed to grow by addition to a one-dimensional polymer like structure, where only one bond is formed upon incorporation. Thus for precipitation $K_1/K_\infty \approx 1$ (Kam *et al.*, 1978).

A model similar to the one presented above was used to computer simulate the events leading to nucleation and hereby successfully predict the frequency at which certain space groups occur (Pellegrini *et al.*, 1997).

2.1.1.2 Probing pre-nucleation solutions.

Attention has been turned to the characterisation of the precrystallisation solution to study if it is possible to predict the fate (e.g. precipitation or crystallisation, of a solution). Recent dynamic light scattering investigations indicate some possibilities. Changing for example pH, ionic strength or temperature of a batch might turn the batch into a crystallising batch (Wilson, 1990). This type of dynamic control will be a big advantage in fermentation downstream processing, due to batch to batch variability. The future prospects could also be to change the morphological fate of the crystallisation into a crystal shape which is easier to handle in the following processes.

The suggested methods can be categorised: 1) methods of measuring the undersaturated solution and 2) methods of measuring the supersaturated prenucleation solution. The latter suffers from the fact that, for some systems, the induction time is short, leaving little time to make a measurement and hence change the system before nucleation has taken place. Most work is now done with intensity fluctuation spectroscopy, while early work was done by light scattering spectrum analysis (Kam *et al.*, 1978).

George and Wilson (1994) used static light scattering measurements to estimate the osmotic second virial coefficient, B_{22}. Crystals resulted from solutions that had values B_{22} falling in a narrow range named "the crystallisation slot". Conditions not leading to crystallisation were found to have values of B_{22} well outside this range. That B_{22} for the crystallisation slot is slightly negative was suggested to indicate weak protein-protein attractive forces promoting crystallisation but too weak to lead to amorphous precipitation.

Alternatively, if the diffusion coefficient is independent of concentration the system will crystallise when supersaturation is reached. If the diffusion coefficient is concentration dependent then precipitation will result. Conditions which favour the free state of macromolecules in undersaturated solution favour crystallisation (Mikol *et al.*, 1990). Later work on other proteins reveals exceptions from the rule (Mikol *et al.*, 1991). It seems that a non-constant diffusion coefficient near supersaturation is an indication of hindrance to crystallisation, while constant diffusion coefficient only indicates the possibility of crystallisation. Kadima *et al.* (1990) showed that in cases where for example a trimer is precursor for crystallisation, discontinuities in the diffusion coefficient are likely to be observed during solution transformation from monomer to trimer form. Such would appear not to obey the constant diffusion coefficient theory. Experimental results of Veesler *et al.* (1994) do however not support the constant diffusion coefficient theory but rather suggest that monodispersity could predict crystal formation. Thibault *et al.* (1992) also found that the solution was monodisperse in the undersaturated state. When making the solution supersaturated, two effects could be observed. Firstly, a new peak appeared, a factor of ten smaller in diffusion coefficient than the original peak. Secondly, a shift in position of the original peak toward a smaller diffusion coefficient was observed. If one or both of these effects was observed, no crystals were formed. The absence of the two effects indicated that crystallisation was very likely.

Doubts about the validity of the constant diffusion coefficient theory have been raised, mainly because the diffusion coefficient is a function of the protein concentration itself (Skouri *et al.*, 1992; Wilson, 1990). Concentration dependence of the diffusion coefficient has been taken into account by Eberstein *et al.* (1994). They however conclude that laser light scattering techniques may still be used as a primary tool for obtaining information about the future of the solution.

A last method with which the future of a supersaturated solution can be predicted is by finding "n" in the following equation

$$G = G_0 t^n \qquad \textbf{eq. 15}$$

where **G** is the rate of aggregation and **n** is a constant. Evaluating n for a entire crystallisation run gave $n \cong 0.2$ for aggregation and n = 0.33-1.0 for crystallising systems (Malkin and McPherson, 1993a).

Rather than setting up simple qualitative criteria such as constant diffusion coefficient more fundamental work is required before laser light scattering techniques can be used in a robust manner for prediction of crystallisability. The limitation of the methods discussed above is that they have been applied to very pure solutions, i.e. dust free solutions of a single protein. For industrial solutions, this could be difficult to achieve.

2.1.2 Nucleation.

2.1.2.1 Categories of nucleation.

The general accepted way of categorising the different types of nucleation is shown in the diagram (Larson and Randolph, 1988):

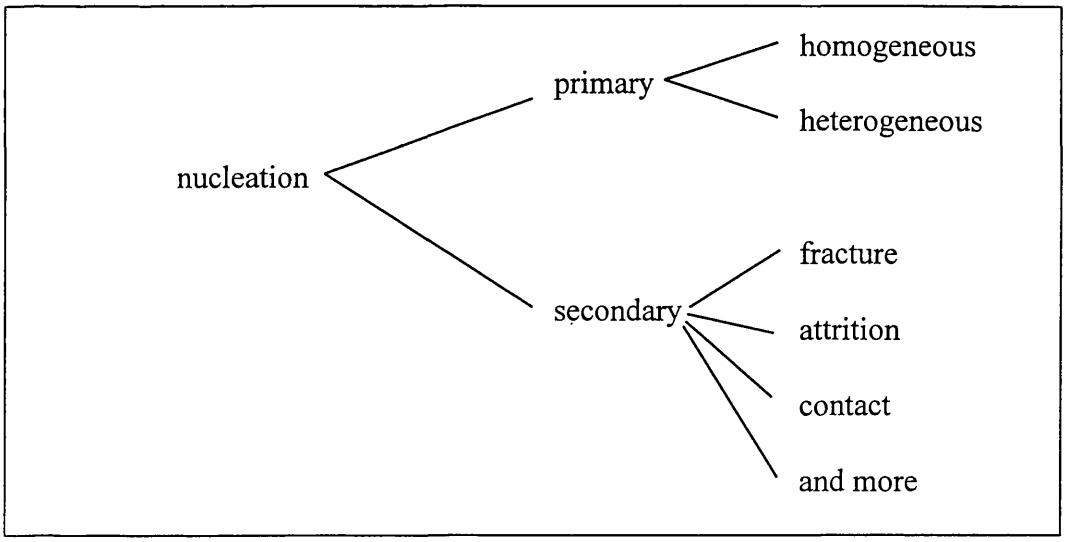

Primary nucleation (often termed spontaneous nucleation) takes place independent of the presence of its own crystalline material. This is mostly encountered at the beginning of an un-seeded batch operated crystallisation. Homogeneous nucleation is independent of solid phases, such as dust or the reactor surfaces. Heterogeneous nucleation is facilitated by such solid phases. As mentioned in Chapter 1 this has been observed for protein crystallisation with a range of minerals (McPherson

and Schlichta, 1987), latex microsphere (Malkin *et al.,* 1993), protein aggregates (Skouri *et al.,* 1995) and cellulose fibres (Stura and Wilson, 1990).

Secondary nucleation is dependent of the presence of crystalline material. It is thought to be dominant in industrial crystallisers. Secondary nucleation takes place in the labile region of the phase diagram and in at least a part of the metastable region (Mullin 1993, p185). The secondary nucleation is suggested to arise in one of the following ways (Randolph and Larson, 1988):

Fracmentation- which is most likely for fragile crystals larger than the turbulent eddies (Synowiec *et al.,* 1993) or in violently agitated systems leading to collisional fragmentation and/or break-up induced by fluid stresses. The size of the resulting fragments are of the same order of magnitude as was the parent crystal.

Attrition- due to both crystal-crystal and crystal-apparatus impacts, especially in high concentration crystal suspensions for crystals larger than the turbulent eddies (Synowiec *et al.,* 1993). The final crystal product may appear rounded and the produced fragments are much smaller than the parent crystals.

Contact nucleation only takes place on growing crystals. This suggests that partly crystallised material might be displaced from the crystal surface at the contact. This mechanism is easy to imagine for crystal growth by the surface nucleation mechanism (see later in this chapter). Also contact nucleation only occurs for crystals above a certain size, since smaller crystals will just follow the flow pattern. Important parameters for the secondary nucleation is crystal size, impeller speed, degree of supersaturation, impeller power input and material (Synowiec *et al.,* 1993).

2.1.2.2 Models describing nucleation.

Theoretical models for primary homogeneous nucleation rates exist, but their ability to describe real systems is very poor (Randolph and Larson, 1988). This is thought to be due to the large extent of heterogeneous nucleation, where dust particles and surfaces of the apparatus act as a nucleation mediator. Added to this the induction time depends on agitation speed and surface character of the apparatus, making it hard to model the system (Rosenberger and Meehan, 1988).

Instead, empirical models have been used with success (Randolph and Larson, 1988).

$$B = K(C - C_M)^n$$

eq. 16

where **B** is the nucleation rate (number of nuclei produced per unit volume and per unit time), **C** is the concentration, $\mathbf{C_M}$ is the concentration of the limit of metastable region and **K** and **n** are constants and n typically having values larger than 1 (according to Tavre (1991) up to approximately 10).

For inorganic systems, the metastable zone is often very narrow i.e.:

$$B = K(C - C_S)^n$$

eq. 17

where $\mathbf{C_S}$ is the saturation concentration.

Considering nucleation by attrition and defining the nucleation rate as the increase per time in number of fines, Synowiec *et al.* (1993) have published some useful theoretical based relations. For crystal-impeller impact attrition, for example, the nucleation rate has been observed to have a first order dependence on both impeller power input and crystal concentration and a fifth order dependence on particle size. For crystal-crystal attrition, the nucleation is 1.5th, 2nd and 8th order dependent on power input, crystal concentration and crystal size respectively. Generally secondary nucleation is far less dependent on the degree of supersaturation than primary nucleation. Typical values of "n" in eq. 17 is 0.7-2.6 (Crystallisation Course, UCL April 1995).

An empirical relationship for nucleation rate was found by Schlichtkrull (1957b) for insulin. He found the nucleation rate to be proportional to the product of the growth rate and either the number of crystals or their surface area. This indicates that secondary nucleation is significant. A quite surprising report suggests that nucleation rate (or the resulting number of nuclei) might not depend on the degree of supersaturation, but rather on the absolute protein concentration (Howard *et al.*, 1988).

2.1.3 Crystal growth.

Immediately after the nuclei have formed, their growth phase starts. The characteristics of this phase are to some degree determined by the foregoing nucleation. For example, the internal structure of the crystal is determined by the nuclei while the crystal habit can be modified during the growth phase. The number and therefore the size of the final crystals is determined by the nucleation step. The actual growth rate is

on the other hand almost solely (see below) dependent on the present physical conditions.

2.1.3.1 Crystal growth rate.

The crystal growth rate is defined quantitatively by the crystal sizing method used. If the measurement is based on sieve size analysis, the growth is measured as the change in the second longest dimension with time. On the other hand, if dynamic light scattering is used, growth is the change of the equivalent hydrodynamic diameter with time. Given a crystal size distribution, growth can be expressed as the change in, for example, geometric or arithmetic mean size per unit time. This is simple when the crystals are spherical or cubical, while for irregular shaped crystals the crystal growth rate may have to be evaluated as change in the equivalent spherical diameter. Finally the single crystal surface displacement velocity (distance per time) observed microscopically can be a measure of the crystal growth. These different growth rates are not directly comparable, but all can be used to quantify crystal growth.

These definitions of growth are easy to apply if only growth occurs. When growing crystals in stirred reactors however, crystal breakage and attrition as well as secondary nucleation occur, which will obscure the true growth rates defined above. At a certain stage of the crystallisation, the attrition might even exceed the growth rate resulting in decreasing crystal size. In such cases, population balancing can be helpful in determining a growth rate (Randolph and Larson, 1988).

Often it is stated that crystals of macromolecules grow slowly compared to crystals of small molecules. This is not entirely true. The rate of attachment is lower for protein crystal growth, but since the growth units are much bigger, the linear growth rate is of the same magnitude (Feigelson, 1988; Rösenberger, 1986). Linear growth rates in orders of 0.1 nm/s have been measured for several protein crystals (Weber, 1991). A growth rate of a single face of 1.9 nm/s for lysozyme has been reported by Miyashita *et al.* (1994) at a supersaturation of 3, while DeMattei and Feigelson (1989) observed growth rates in the range (1.7-6.7) nm/s for canavalin at supersaturations below 2. Likewise, Vekilov *et al.* (1993) found growth rates of 2 nm/s at supersaturations up to 5. Finally, Durbin and Feher (1986) observed lysozyme crystal growth rates of 15-20 nm/s at supersaturations as high as 7-10. All the reported growth rates so far have been for single crystal surfaces while for growth of crystals in suspension, the reported growth rates will often be based on change in crystals diameter. For the growth of rod-shaped ovalbumin crystals in suspension, Judge *et al.* (1995) found growth rates of up to 1.7

nm/s (given as change in volume equivalent spherical diameter) at a supersaturation of 7. The growth rates reported here correspond to an addition of approximately 1-3 layers of protein molecules to the crystal lattice every second (Feigelson, 1988).

In conclusion protein crystals (suspended or fixed) grow with growth rates in orders of nanometers per second, which is comparable to the growth rate of inorganic crystals. However, inorganic crystals grow at supersaturations of 1.0-1.1 while protein crystals grow at supersaturations of 1-20.

2.1.3.2 Crystal growth kinetics.

A major issue in protein crystal growth is whether the growth is diffusion and/or incorporation limited. Most studies (experimental and theoretical) suggest that surface effects are rate limiting in protein crystal growth (Judge *et al.* 1995; Grant and Saville, 1991; Weber, 1991; Feigelson, 1988; Schlichtkrull, 1957c) though diffusion limited systems have also been reported (Malkin and McPherson, 1993b). That both mechanisms should have equal importance at high degree of supersaturation is suggested by Monaco and Rosenberger (1993) and seems to be the understanding of results reported by Azuma *et al.* (1989). Growth by aggregation of small crystals has not been reported for protein crystallisation probably because lattice imperfections would be expected

Diffusion limited growth is characterised by increasing growth rate at higher rates of agitation (thinner boundary layer). It is a result of a higher probability for incorporation of a protein unit than the probability of a protein unit impinging on the crystal surface. A relatively low protein concentration is expected next to the crystal surface. Generally the growth rate is expected to have a linear dependence on the supersaturation (Mullin, 1993).

On the other hand, when the probability of incorporation is low, the system will be insensitive to the rate of agitation because the protein concentration next to the crystal surface will be near that of the bulk solution. Incorporation limited systems are often reported to have a square dependence of the degree upon supersaturation (Pusey and Naumann, 1986), though other kinetic descriptions do exist.

Inorganic components exhibit both of the above patterns of limitation. Because proteins are big, dynamic and loose entities, it would be reasonable to expect the protein crystal growth will be diffusion limited because of the high diffusion coefficient. Protein crystal growth could also be incorporation limited, since protein in solution has far more possible configurations and orientations which do not all fit into the crystal lattice. A

depletion layer, indicating diffusion-limitation, was seen by Kam *et al.* (1978) observing a single lysozyme crystal with UV-light. The relevance of these results has later been questioned, since the channel in which the crystals were grown was only 180 μm wide, may not allow convection to be effective (Pusey and Naumann, 1986). Also trying to find evidence for a depletion zone, Miyashita *et al.* (1994) used a type of Michelson interferometry to observe the growth of lysozyme crystals in a larger growth cell. They found only a slightly lower protein concentration near the crystal surface, concluding the growth to be incorporation limited. On the basis of a convection-diffusion model, work done by Pusey and Naumann (1986) indicates that the lysozyme crystal growth must be limited by the rate of incorporation. Which view is correct concerning the limiting mechanism is still uncertain, but it seems difficult to ignore the UV-observations as visual evidence. An additional complication is that small crystals (<5-10 μm) might not be influenced by the fluid flow field i.e. they are moving around the reactor in a stagnant fluid "box". For these small crystals the growth will be controlled by diffusion, but is unaffected by increased agitation (Nielsen and Toft, 1984). The limit of 5-10 μm was given for the growth of inorganic crystals. For protein crystals, this limit will be expected to be higher because the density difference between the crystals and the aqueous liquor is less than for most inorganic systems.

2.1.3.2.1 Diffusion controlled crystal growth.

Diffusion controlled growth is modelled using Fick's first law:

$$\frac{dM}{dt} = \frac{A}{x}(C - C_s)$$

eq. 18

where **M** is mass incorporated, **A** is a constant, **x** is boundary layer thickness, **C** is protein concentration in bulk suspension, $\mathbf{C_S}$ is protein saturation concentration. Instead of mass, eq. 18 can also be written for changes in average size. The equation suggests that the growth rate is proportional to the supersaturation. Rosenberger (1986) argues that Fick's first law needs to be modified, both when the mass fraction of solute is significant (i.e. no longer much less than one) and when solvent, precipitant and other impurities are (partly) rejected at the growing protein crystal surface, resulting in a flow away from the crystallisation zone. Grant and Saville (1991) on a theoretical basis state that this phenomenon is not expected to have an appreciable effect.

The major effect on the Fick's law description is the boundary layer thickness (x). In the presence of convection, for example in the gravitational field, convection will decrease x, and thereby decrease the resistance to transfer of protein units to the crystal. Attempts have been made to take into account the effect of convection on the thickness of the diffusion layer (Pusey and Naumann, 1986). The conclusion, even though the applied model is crude, was that lysozyme crystal growth will always be limited by the rate of incorporation.

2.1.3.2.2 Incorporation controlled crystal growth.

The kinetics of incorporation controlled protein crystal growth seem far more diverse than for inorganic crystals (Malkin *et al.,* 1995). Some understanding of the underlying mechanisms can be found from the functional dependencies of the crystal growth primarily on the degree of supersaturation presented in this section. Mechanisms have been found and modelled for inorganic crystals and should therefore be used only with caution for protein crystals. However, combined with recently developed high powered microscopic methods rigorous, new understanding of protein crystal growth has been achieved (Malkin *et al.* 1995; Moré and Sanger, 1995; Monaco and Rosenberger, 1993; Sazaki *et al.*, 1993; Vekilov et al., 1993).

The classical mechanism for incorporation controlled growth of inorganic crystals are shown in Figure 12. An additional mechanism observed for the growth of protein crystals is given at the end of the section.

The continuous growth model is shown in Figure 12(a), with a crystal having a rough surface. A crystallising unit will integrate at the position of lowest energy for its orientation, i.e. where the unit can form the highest number of bonds to the crystal. This sort of incorporation gives a growth rate proportional to the supersaturation (Randolph and Larsen, 1988).

$$G = K(C - C_S)$$

eq. 19

This mechanism will lead to rounded crystals and not the perfectly flat faces and sharp corners often found with protein crystals (Durbin and Feher, 1986). A good example of protein crystal growth by this mechanism has been given for concanavalin A crystals (Moré and Sanger, 1995). The continuous growth model has the same rate expression as for diffusion controlled growth but since the continuous growth, is a surface controlled mechanism there will be little dependency on the speed of agitation.

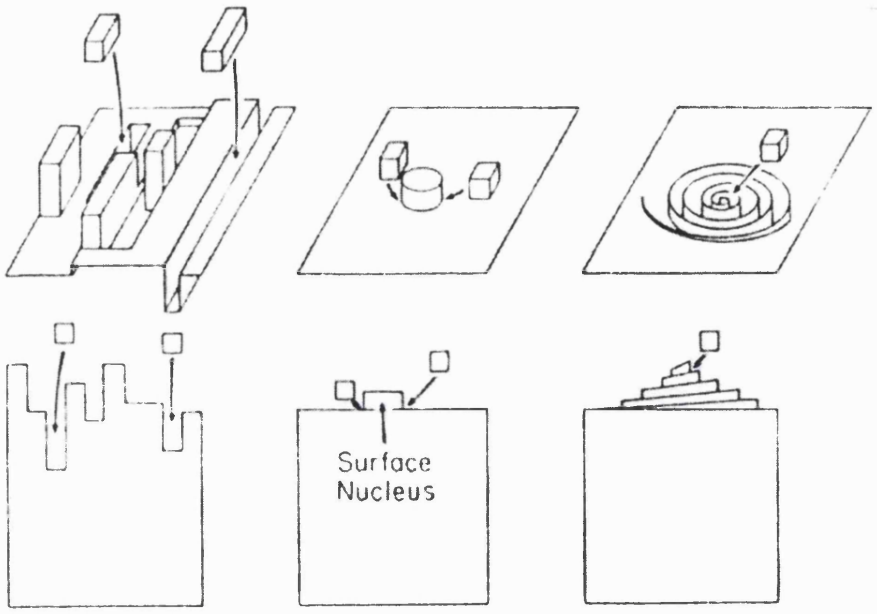

Figure 12. Crystal growth models. (a) continuous growth, (b) surface nucleation growth and (c) screw dislocation growth (Larson and Randolph, 1988).

two dimensional nucleation on the crystal surface, followed by growth spread from the nucleation point. This model is also termed "birth and spread" model, and its overall rate is determined by the rate of nucleation. Theoretical descriptions of Randolph and Larson (1988) have the form:

$$G = A(C - C_S)^p \exp(-\frac{B}{(C - C_S)})$$

eq. 20

where **A** and **B** are constants and **p** is a constant usually between 1 and 2 for inorganic crystallisation,

Durbin and Feher (1986) and Weber (1991) report a very similar growth expression to eq. 20, but they also include as a factor the natural logarithm of the relative supersaturation. DeMattei and Feigelson (1989) also used a similar expression, though $(C\text{-}C_S)$ in the exponential function is replaced with $\ln(C/C_S)$. The above mentioned continuous growth mechanism can take place at lower degrees of supersaturation than mechanisms involving smooth surfaces where the energy required to start new growth layers is higher (Weber, 1991).

Screw dislocation mechanism is shown in **Error! Reference source not found.** (c) (Randolph and Larson, 1988, Durbin and Feher, 1986). The growth units are added to an

levels of supersaturation. At low supersaturation the theory predicts the growth rate as eq. 21:

$$G = K(C - C_S)^2$$

eq. 21

while for high supersaturation systems eq. 22 among others has been suggested.

$$G = A(C - C_S)^2 \tanh\left(\frac{B}{(C - C_S)}\right)$$

eq. 22

DeMattei and Feigelson (1989) successfully fitted a different theoretical model for screw dislocation (eq. 23), with the growth of canavalin crystals in the supersaturation range of 1.05-1.7 (given as $\ln(C/C_S)$), although for only four data points.

$$G = A \cdot C\left[\ln\left(\frac{C}{C_S}\right)\right]^2$$

eq. 23

"Normal" growth mechanism was observed by Malkin *et al.* (1995) for crystal growth of apoferritin and under some conditions tetragonal lysozyme and trigonal catalase. "Normal" growth is characterised by a very rough surface growing by intensive random surface nucleation.

Caution should be taken when trying to fit these kinetic models over wide ranges of supersaturation. Several authors reported different mechanisms for growth at high and low supersaturation basing their understanding on microscopic observations. Malkin *et al.* (1995) for example observed spiral dislocations at low supersaturation and two-dimensional nucleation at high levels for lysozyme crystals using atomic force microscopy. Specifying the transition supersaturation between the two mechanisms to 5, *Vekilov et al.* (1993) got the same result using laser Michelson interferometry. Moreover, at supersaturations below 1.5, growth was observed to proceed by macrosteps. Durbin and Feher (1986) initially only attempted to fit some of these models to the growth of lysozyme crystals. They observed the growth rate of single faces of the crystal in a flow cell with constant supersaturation. They concluded that the responsible growth mechanism at low supersaturation could be screw dislocation. At high supersaturation, growth via the surface nucleation model fitted the data best. This conclusion was supported by the observation of relatively high (10 %) growth rate

dispersion at low supersaturation and less at high supersaturation. This is because the number of screw dislocations on the crystal surface together with the supersaturation will determine the growth rate. In contrast, surface nucleation is a more random process only determined by the supersaturation and causing all crystals to grow with approximately the same rate. In a second paper, Durbin and Feher (1990) substantiated their conclusions with microscopical observations of the crystal surface.

There are of course also empirical correlations for crystal growth in the literature. The most popular is (Durbin and Feher, 1986; Pusey and Naumann, 1986):

$$G = K(C - C_S)^n$$

eq. 24

n and **K** are empirical constants, **C** is the protein concentration and $\mathbf{C_S}$ is the protein concentration at saturation.

Here as in most models the growth rate is given as a function of the supersaturation, K and n depend on the protein and numerous physical parameters where n = 1 corresponds to diffusion controlled growth. Values of $n \cong 2$ are generally assumed to fit growth proceeding by screw dislocation, while $n>2$ is taken to indicate growth by the surface nucleation mechanism (Durbin and Feher. 1986).

For systems of various origins, sub-micron clusters or aggregates of protein have been observed present in crystallisation (Malkin *et al.,* 1993; Sazaki *et al.,* 1993; Pusey, 1991; Azuma *et al.,* 1989; Durbin and Feher, 1986). It is however difficult to tell if these aggregates are crystal growth units.

Azuma *et al.* (1989) claim to have demonstrated that the growth unit was monomolecular for growth of lysozyme crystals while an indication that large particles form the growth unit was obtained using atomic force microscopy observations (Malkin *et al.,* 1995). For satellite tobacco mosaic virus, microcrystals were seen sedimenting and adsorbing to the crystal surface of larger crystals. These microcrystals were reorientated so their lattice was matching the lattice of the big crystal. Such addition of three dimensional nuclei was reported not to cause defects in the resulting fused crystal. Pusey (1991), using relative laser light scattering data of precrystallisation solution, estimated initial equilibrium constants for the formation lysozyme aggregates (dimers, trimers, etc.). From a theoretical evaluation of possible routes to crystallisation addition, monomers was found less likely than addition of aggregates.

The general understanding of the attachment process of growth units is however poor. Even the in case of monomers the attachment process is quite complex. In solution the crystallising units are (nearly) fully hydrated, hence in order to be incorporated in the crystal, the unit has to get rid of at least a part of the hydration water. Moreover one can imagine reorientation and establishment of more bonds in the period after the first contact has been made. Apparent growth via aggregates could be that aggregates are present until shortly before the attachment process, in which rearrangement or dissociation into monomers could occur. Interpretation of growth dependence on protein concentration in the presence of several sizes of aggregates will be blurred, since the effective protein concentration will be overestimated and all the aggregates will exist in equilibrium with each other (Wilson *et al.,* 1993).

2.1.3.3 Growth rate dispersion.

Two types of growth rate dispersion exist. One is size dependent growth and the other is where crystals of comparable size grow at different rates in the same environment. The latter is believed to be a result of characteristics of the surface of individual crystals. For example in the case of growth via screw dislocation, growth rate dispersion is expected since some of the crystals will be born with a slightly higher/lower number of dislocations than the average. Also differences in mechanical induced stress or random extend of absorbed impurities have been suggested to be the reason for otherwise identical crystals growing at a different rate (Mullin, 1993).

In the case of crystals with significantly different sizes growing at different rates, other explanations exist. For diffusion controlled crystals grown in suspension, the thickness of the boundary layer will be smaller for larger crystals, and hence these will grow faster. This is due to the larger momentum of the large crystals making their movement more independent of the general flow in the reactor. The diffusion layer for very small crystals may not be affected by convection at all. The small momentum will mean that the crystal will travel in a stagnant box, a so-called turbulent eddy as mentioned above.

In short the difference between the two types of growth rate dispersion is that either large crystals have become large because they grow faster or they grow faster because they are large (Randolph and Larson, 1988).

Generally growth rates appear to be independent of size, though early work on insulin, indicates that this might not be true for crystals smaller than 10 μm (Weber, 1991). Pusey and Naumann (1986) concludes that, for lysozyme crystals in the size

range from a few microns to 70 μm, no size dependence of the growth rate was seen. Durbin and Feher (1986) working with lysozyme crystals of sizes 50 μm and upwards observed as much as 100 % variation in growth rate between different single crystals grown at low protein concentration.

2.1.3.4 Growth cessation.

That crystals in some case should not grow in supersaturated solutions is called growth cessation. There are many suggestions for this phenomenon.

Kam *et al.* (1978) reported that a partly fragmented lysozyme crystal which had ceased to grow, regrew to approximately its original size upon re-introduction into a supersaturated solution. The authors suggested that this could be a result of accumulation of lattice errors or impurities adsorbed eventually preventing further growth.

Strain imposed on the crystal lattice by agitation or handling has been reported to stop growth for inorganic crystals (Randolph and Larson, 1988, p 122). However for protein crystals often referred to as a "gel", such strain will not be expected to last long after the impact. This is true of course only for non-destructive impacts.

Young *et al.* (1988) have used colloid theory to explain growth cessation. Due to the charge deposition in the crystal while growing, electrolyte partitioning occurs. This could eventually lead to agglomeration at the crystal surface resulting in cessation of growth.

Fluid shear near the crystal surface caused by density driven plumes or convection has also been suggested to promote growth cessation (Pusey *et al.*, 1988). However "an order of magnitude" calculation performed by Grant and Saville (1991) conclude that these forces are probably too small to affect the molecules at the crystal surface.

Speculations that gradual poisoning of the crystal surface by defective product molecule and impurities could cause growth cessation has also been reported (Weber, 1991). Growing lysozyme crystals over long periods (>10 days), non-uniform, "patchy" growth was observed microscopically, indicating inactive parts of the crystals surface. Impurities or denatured crystal surface molecules were tentatively suggested to be the reason (Durbin and Feher, 1986). The issue of the effect of impurities on crystal growth is treated elsewhere (Chapter 1).

Structural defects resulting from too high of a crystal growth rate has also been suggested as a reason for growth cessation (Weber, 1991). There is however little experimental data to confirm this view.

2.2 Dead-end filtration of particulate suspensions.

Three models describing filtration of particulates are described. One model is for standard blocking filtration, two models for cake filtration, followed by a section on the calculation of the important dead-end filtration parameter: the cake porosity.

2.2.1 Standard blocking filtration law.

This model describes situations where the particles enter the filter pores and are deposited on the walls. The pore volume and hence the filtration area will decrease proportionally to the volume of suspension filtered. In deriving the model, the filter is considered to consist of parallel tubes of constant length. Deep filtering is an example where this law will be expected to apply. A mass balance over the solids yields:

$$N^* \cdot \pi(d_0^2 - d^2)L = 4 \cdot C \cdot V$$

eq. 25

where $\mathbf{N^*}$ is the number of pore channels, $\mathbf{d_0}$ is the pore diameter at the start of the experiment, **d** is the pore diameter after a filtrate volume of **V** has passed the filter, **L** is the length of the pores and **C** is the solids volume fraction in the slurry. Expressing **d** using eq. 25 and inserting in Poiseulle's equation (eq. 26) gives eq. 27.

$$Q = N^* \left(\frac{\pi \cdot d^4 \cdot \Delta P}{128 \cdot \mu \cdot L} \right)$$

eq. 26

where **Q** is the volumetric flow rate through the filter, $\Delta\mathbf{P}$ is the filtration pressure and μ is the filtrate viscosity.

$$Q = Q_0 \left(1 - \frac{K_S \cdot V}{2} \right)^2$$

eq. 27

where $K_S = 2C/(LA_0)$.

This equation can be integrated and reorganised to:

$$\frac{t}{V} = \frac{K_s}{2} t + \frac{1}{Q_0}$$

eq. 28

The standard blocking law has here been given in a form that makes it easy to evaluate if a given system can be described by the model doing a simple linear plot (Hermia, 1982).

2.2.2 Cake filtration laws.

The first of the two cake models assumes that the resistance to flow is the sum of a constant filter resistance (**r**) and a linearly increasing resistance with filter cake build up, i.e. the cake is incompressible:

$$r = r_0 + \alpha \frac{w}{A}$$

eq. 29

where **w** is the mass of the cake, **A** is the filter area and α is the specific cake resistance. This equation combined with Darcy's law,

$$Q = \frac{\Delta p \cdot A}{\mu \cdot r}$$

eq. 30

and a simple mass balance on the solids:

$$w = \frac{V \cdot s \cdot \rho}{(1 - m \cdot s)}$$

eq. 31

where **s** is mass fraction of solids in the slurry, ρ is the filtrate density and **m** is the mass ratio of wet to dry cake.

yields:

$$K_C \cdot V = \frac{1}{Q} - \frac{1}{Q_0}$$

eq. 32

where $K_C = \alpha\rho\mu s/(A^2 P(1\text{-}ms))$ and $Q = dV/dt$. Hence we have:

$$\frac{t}{V} = \frac{K_C}{2} V + \frac{1}{Q_0}$$

eq. 33

Again a simple linear plot can evaluate if the model can used to describe a given data set (Hermia, 1982).

A different model for cake filtration law was derived by Doshi and Trettin (1981). They modelled the general case, also allowing back diffusion from the filter cake to the solution. This is relevant when working with macromolecular solutions. However for the filtration of particle and colloidal suspensions the back diffusion term can be ignored. The model is based on a steady-state mass balance for the solution volume immediately above the filter cake.

$$\frac{\partial C}{\partial t} + v\frac{\partial C}{\partial y} = D\frac{\partial^2 C}{\partial y^2}$$

eq. 34

where **C** is the solute concentration, **v** the filtrate flux, **y** the distance from the filter cake and **D** the solute diffusion coefficient. It is assumed that the solute density is near to that of the liquid.

The left-hand side accounts for material leaving as filter cake and material entering by filtration flow. The right-hand side accounts for solute back-diffusion from the surface of the filter cake to the solution. An additional equation accounts for the solids deposition on the membrane surface ($\mathbf{n_s}$):

$$n_s = v \cdot C_w - D\left(\frac{\partial C}{\partial y}\right)_{y=0}$$

eq. 35

The increasing thickness of the filter cake will move the solution volume in consideration away from the filter cloth. Also Darcy's law in the following form is needed:

$$-v_w = \frac{\Delta p}{\mu \cdot \alpha \cdot \rho_S (1-\varepsilon) S}$$

eq. 36

where Δp is the filtration pressure, μ is the filtrate viscosity, α is the specific cake resistance, ρ is the density of solute, ε the filter cake porosity and **S** is the cake thickness.

For no back-diffusion, the above reduces to (Doshi and Trettin, 1981):

$$\frac{2\phi}{K} \rightarrow V_w^2$$

eq. 37

ϕ is the dimensionless solids concentration, $K = \alpha\mu DC_0/\Delta p$ and $V_w = -v_w (4t/D)^{1/2}$, i.e. the dimensionless filtrate flux at the filter cake surface.

Inserting V_w in eq. 37 and integrating for 0 to t and 0 to ΔV gives:

$$\Delta V = B \cdot t^{\frac{1}{2}}$$

eq. 38

$$B = A \cdot d_p \cdot \rho_L \cdot \left(\frac{2 \cdot \Delta p}{\mu}\right)^{0.5} \cdot \left(\frac{\varepsilon^3 \cdot \left[\rho_c - \left(\frac{C_S}{1-\varepsilon}\right)\right]}{150 \cdot (1-\varepsilon) \cdot C_S}\right)^{0.5}$$

eq. 39

where $\mathbf{d_p}$ is the estimated filtration based particle diameter, ρ_L is the density of the permeate and ρ_c is the density of the crystals. The specific cake resistance, α, was determined by Kozeny-Carman's relationship for flow through a porous media applies. Methods for the calculation of filter cake porosity are discussed in the next section.

2.2.3 Estimation of filter cake porosity.

In theory the porosity can also be calculated from a number based crystal size distribution for spherical particles (Diepen *et al.,* 1997). However all particle sizing techniques have a lower detection limit. The high number of particles smaller than this limit is likely to reduce the porosity significantly by filling the gaps between the larger particles.

Since the porosity is the volume fraction of the filter cake not occupied by crystals, basing the estimation on volumes rather than numbers is expected to give better results. The void volume can be found from the difference between the total cake volume and the volume of the particles. The former is given by the thickness and area of the filter cake and the latter can be found using methods as the electrical sensing zone method (see Chapter 1). The fraction of the total particle volume below the lower limit of detection is generally much smaller than for numbers, reducing the impact of undetected particles on the estimate.

$$\varepsilon = \frac{h \cdot A - V_{elzone}}{h \cdot A}$$

eq. 40

where **h** is the cake height and $\mathbf{V_{elzone}}$ is the volume of crystals in the suspension loaded onto the filter.

An empirical way of estimating the cake porosity is by assuming that at the end of a run the pores are full of free water that can be removed by heating. There are two restrictions to this assumption. One is that at the end of a run, the high pressure air will partly remove such free water. Secondly, the water removed by heating may not just be free water in the pores but also water bound within the crystal. The effect of the first restriction can possibly be reduced by soaking the filter cake in the mother liquor weighing and drying.

If both the crystal density (ρ_c) and the protein fraction of the crystals (**F**) are known, the porosity can be estimated from:

$$\varepsilon = 1 - \frac{w_{dry}}{A \cdot h \cdot F \cdot \rho_c}$$

eq. 41

where $\mathbf{w_{dry}}$ is the dry weight of the filter cake. The advantage of this method is that it can be calculated from simple and easy-to-get values and the crystal protein content and density can be determined once for all the filtrations.

In the evaluation of the filterability of inorganic crystal suspensions, Jones *et al.* (1987) estimated the porosity from the suspension settling velocity as described by Selim *et al.* (1983).

2.3 The s-plane analysis.

The s-plane analysis as described by Garside and Tavare (1986) and Tavare (1991) was developed to characterise simultaneous nucleation and growth rates for time-variant systems such as batch crystallisation. This section will give both the theoretical background for the method but also try to explain the method in a more intuitive fashion.

2.3.1 Theoretical derivation of the s-plane analysis.

The s-plane analysis is based on discrete population balances. Before doing the population balance the variable $n(t.\overline{R})$ has to be defined. $n(t.\overline{R})$ is the number concentration of crystals of a size interval ΔR (in which $\overline{R}$ is midpoint) divided by ΔR, at the time t. The liquid volume over which the balance is done is assumed constant. Time zero is the moment when supersaturation is reached. The population balance is made for the period Δt and the size interval ΔR with $\bar{t}$ and $\overline{R}$ respectively as midpoints:

$$\text{in} + \text{net generation} = \text{out} + \text{accumulation}$$

eq. 42

$$v(\bar{t},R-\frac{1}{2}\Delta R)\Delta t = v(\bar{t},R+\frac{1}{2}\Delta R)\cdot\Delta t + \left[n(t_2,\overline{R}) - n(t_1,\overline{R})\right]\Delta R$$

eq. 43

v(t,R) is the number of crystals per unit time that passes the size R. The net generation term is set to zero since it is assumed that no crystal breakage is taking place and that the crystals are born with zero size i.e., v(t,0). Dividing eq. 43 with Δt and ΔR and allowing Δt and ΔR to approach zero the result is:

$$\frac{\partial n(t,R)}{\partial t} + \frac{\partial v(t,R)}{\partial R} = 0$$

eq. 44

Realising that the linear growth rate G(t,R) = v(t,R)/n(t,R) and assuming that the growth rate is size independent:

$$\frac{\partial n(t,R)}{\partial t} + G\frac{\partial n(t,R)}{\partial R} = 0$$

eq. 45

This equation is a non-linear first order partial differential equation. Direct extraction of the nucleation, B (B = G·n(t,0)), and growth rate, G, from this equation is difficult. Hence often the problem is simplified by converting the equation into a form for which simpler parameter estimation techniques exist.

Making a Laplace transformation of eq. 45 with respect to size is one such method:

$$\frac{d\bar{n}(t_1,s)}{dt} + G\left[s\bar{n}(t_1,s) - n(t_1,0)\right] = 0$$

eq. 46

If t_2 is only a short time interval (Δt) after t_1, it can be assumed that the growth rate G and the nucleation rate (B = G·n(t,0)) are constant within this time interval, having values of G and B respectively. For this short time interval the derivatives in eq. 46 can be replaced with differentials yielding:

$$\frac{\Delta\bar{n}(t_1,t_2,s)}{\Delta t} = -\bar{G}\cdot s\cdot\overline{\bar{n}(t_1,t_2,s)} + \overline{B(t_1,t_2,0)}$$

eq. 47

This version of the population balance is particularly convenient since it allows estimation of the nucleation and growth rate by a simple linear regression method, plotting the left hand side of eq. 47 as a function of $s\cdot\overline{\bar{n}(t_1,t_2,s)}$.

2.3.2 Explanation of the s-plane analysis method.

Here the s-plane analysis is explained in a slightly different and probably more intuitive way than in the previous section.

Making a population balance for consecutive pairs of samples for every channel of the above discussed crystal size distribution would give the maximum amount of information that can be extracted from the system. Such population balance is:

$$\Delta N = G\cdot n_{in} - G\cdot n_{out}$$

eq. 48

where ΔN is the change in the overall number of crystals in the size range considered, G is the growth rate of the crystals (assumed independent of crystal size) and n_{in} and n_{out}

are the population densities (number of crystals per channel width) at the entrance and the exit of the channels respectively. The change in the total number of crystals in a channel equals the difference between the number of crystals growing into the size range and those growing out in the time range considered. Of the parameters in eq. 48, ΔN is known from the crystal size distributions of consecutive samples and the aim is to estimate the growth rate, G, while n_{in} and n_{out} are unknown for the channel considered. However n_{out} for the last channel (with a count in) is zero because no crystals have grown out of this channel and n_{in} for the first channel (if no crystal breakage is assumed) must be the nucleation rate ($B = G \cdot n_{in}$) calculated as the overall change in crystal number in the measuring range divided by the time span between the consecutive samples. Overall there are n channels and hence n population balances. Because the growth rate was assumed independent of the crystal size, the unknowns are G and (n-1) n_{in}'s and none n_{out}'s because $n_{in}(i+1) = n_{out}(i)$ and the last n_{out} was zero. That sums up to n equations and n unknowns that are mathematically easy to solve though it would be somewhat tedious.

Instead of solving the n equations, the Laplace transformation method does something similar. The crystal size distribution channels are weighted with a negative exponential function of the product of crystal size and the Laplace variable, s, i.e. exponentially less weighting of the crystals in the upper channels. Every weighting can then be considered as a new type of crystal (Laplace) size. As before the growth rate can be estimated from the change in this Laplace size for a given size interval for two consecutive samples. Significant data smoothing is achieved compared to the method where numbers in single channels are used. However in doing the mathematical weighting, a decision has to be made on the actual range of the weighting parameter. A different emphasis on the fines part of the crystal size distribution can be achieved in this way. This issue will be further discussed in Chapter 5 using real data to guide the decision.

Chapter 3. Materials and Methods.

3.1 Process material.

3.1.1 Feed material.

The proteinaceous material used in this study was a processed fermentation broth (Novo Nordisk A/S, Bagsværd, Denmark). Following the fermentation step the broth had first been subjected to centrifugation to remove cells, then ultrafiltration to increase the total dry weight to more than 20 % and finally diafiltration to lower the conductivity of the solution to approximately 2 mS/cm or lower. The resulting material contained high levels (8-10 % dry weight) of a lipase (EC 3.1.1.3) and lower levels of other microbial proteins as well as other contaminants commonly found in fermentation broths. The lipase was originally found in a *Humicola lanuginoso* and was expressed in a fungal host. The lipase activity of the solution was typically 500-700 KLU/g (defined below) and had a molecular weight of 35 kDa. Several large batches of crystallisation material were prepared (see Table 1), providing enough material for extensive studies on a single batch as well as comparison studies. The material was frozen in 10-25 L lots and kept at -20°C. When necessary a container was thawed and the material split into 250 mL lots and frozen again.

batch	production id.	crystal shape
1	LAZ 13071	rod and diamond
2	LAZ 0643	rod
3	PW 5055	rod and diamond

Table 1. Batches of feed material used in this study.

3.1.2 Crystallisation agents.

The main crystallisation agent was a 20 % (w/w) formic acid (F-0507, Sigma, Poole, UK) solution as recommended by Nilsson *et al.,* (1994) generating the supersaturation driving the crystallisation process.

In some experiments surfactants were used: Brij-35 (56003 4B, BDH Laboratory Supplies, Poole, UK) and 'Tween'80 (Prod 560234H, BDH Laboratory Supplies, Poole, UK) added to give final concentrations in the broth of 0.2 and 1.3 % (w/w) respectively.

3.2 The crystallisation experiment.

3.2.1 Small scale.

3.2.1.1 The experimental set-up.

The first part of the crystallisation experiments were conducted in a 225 mL working volume reactor. The vessel was cylindrical and made of glass except for the perspex lid. The dimensions of the reactor were chosen according to Bates *et al.* (1963): d/T = 1/3, C/T = 1/3 and H/T = 1, where d is the diameter of the impeller, T is the reactor diameter (= 6.6 cm), c is the distance between the impeller and the bottom of the reactor and H is the working height of liquid in the reactor.

The vessel was stirred with a 6-blade, 45° pitched axial flow impeller positioned in the horizontal centre of the vessel. The stirrer was made of stainless steel and driven by a conventional overhead motor. The speed of agitation at a certain motor setting was dependent on the alignment of reactor and motor. Hence it was necessary in each experiment to adjust the stirring speed using a tachometer. Pumping downwards a Reynolds number of 6500 seems fully to suspend the crystals. This corresponds to a speed of 800 rpm and a tip speed of 0.8 m/s. Baffles were not used in the experiments since the probes effectively prevented vortex formation.

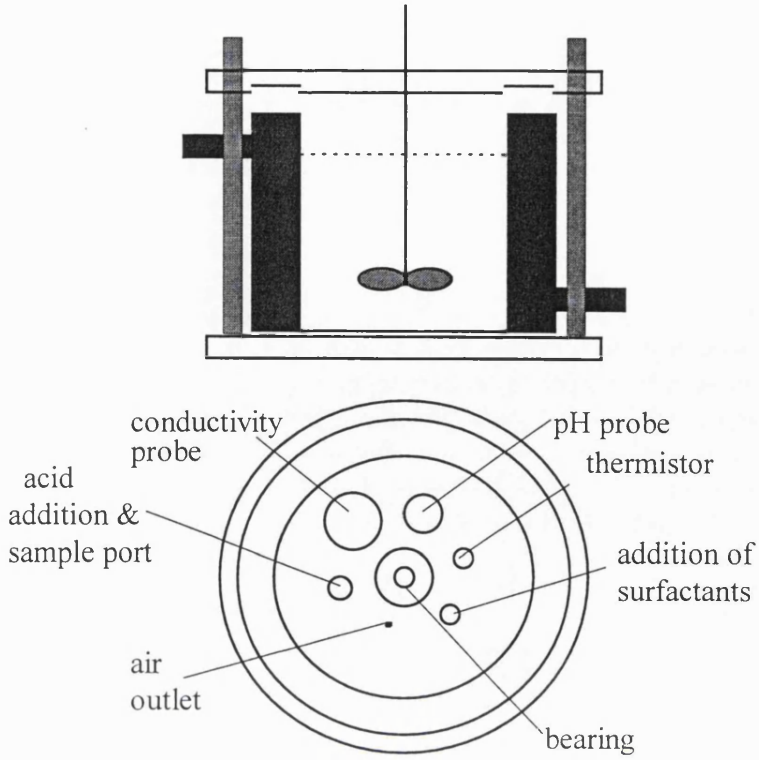

Figure 13. Draft of the reactor design. The upper drawing views the reactor from the side and the lower from the top. The dark areas are the water jacket used for temperature control while the long vertical grey areas are beams used to keep the reactor and the lid firmly together. The liquid working level is indicated with a dashed line.

Changes in the pH of the solution is the only known way to initiate the crystallisation. Accurate pH monitoring of the process was therefore established with a Radiometer titration set-up (Radiometer, Copenhagen, Denmark). This comprised pH meter (PM 82), titrator (TTA 80), an autoburette (ABU 80) and a combined pH electrode (pHC 2406, Radiometer, Copenhagen, Denmark). The titrant, formic acid (20 % w/w), was added via a glass rod. A conductivity meter (CDM 83, Radiometer, Copenhagen, Denmark) and a conductivity probe (CD 364 immersion cell, Radiometer, Copenhagen, Denmark) were also parts of the experimental set-up.

The temperature in the reactor was measured using a thermistor (Digitron Instrumentation, Model 3204 Pt, England) and controlled by a thermostat circulating water in the jacket surrounding the sides of the vessel.

3.2.1.2 The experimental procedure.

The 250 mL lots of crystallisation material were thawed in the container using a circulated water bath (22 ± 2°C) for approximately one hour. The material was then

transferred to the reactor and preheated to 27 ± 0.1°C before commencement of the pH adjustment. An autoburette (2-4 μL/s) gave an overall pH adjustment time of 20 mins. Surfactant was added either as a 50 mg Brij/g RO water solution at a rate of 5.8 μL/s for 30 mins or as 0.2 g 'Tween'80/g RO water at a rate of 21 μL/s for 15 mins. After completion of the adjustments the crystallisation was run at constant pH which required addition of acid (≈ 0.3 mL). Samples, 50 μL, of the crystal suspension were taken with a 200 μL Gilson pipette and diluted 100 times with the sample buffer and then left at room temperature before analysis.

3.2.2 Medium scale.

3.2.2.1 Experimental set-up.

The geometry and construction material of the small and medium scale reactors are not similar. The medium scale reactor was designed to be similar to a typical large scale reactor for protein crystallisation in production.

Reactors of 1 L working volume were made of stainless steel. They were made in-house to be cylindrical (10.9 cm diameter and 12.5 cm high) with a dished bottom. The dished bottom contained 90 mL.

The impeller was located in the axial centre of the reactor, 2.5 cm from the deepest point of the dished bottom. Pumping axially this was a propeller type impeller with two orthogonally positioned curved blades. The impeller diameter was 5 cm and the width of the blades was 1.4 cm at the shaft mounting point while it gradually became more narrow reaching 0.7 cm at the tip. The impellers were pumping downwards with a tip speed of 1.8 m/s.

Four equally spaced baffles (1.2 cm wide by 1.5 mm thick) were located in the cylindrical part of the reactor 0.4 cm from the reactor wall.

The reactors were all equipped with combination pH electrodes (P/N 10 405 4476, TYPE: HA405-DPA-SC-S8/120, S/N: 6506033, Mettler Toledo, Urdorf, Switzerland). The pH probes were connected to pH transmitters (INGOLD pH transmitter 2400, Mettler Toledo, Urdorf, Switzerland) which both display the measured pH and transmit a signal to the process computer. The pH was controlled by pumping in 20 % (w/w) formic acid using Watson Marlow pumps (101U/R, 2rpm, Watson-Marlow Limited, Düsseldorf, Germany).

Although the conductivity probes were fitted they were unable to do measurements in the conductivity range found in these experiments. Nevertheless they were connected to a CR 7300 transmitter (both Mettler Toledo, Urdorf, Switzerland)

because they were capable of measuring the temperature in the reactor and this signal was used instead of a separate temperature probe. The temperature in the reactor was controlled via a thermostat (Hetotherm, type 23 DT-2, Heto, Birkerød, Denmark).

The pH and temperature were adjusted to within ± 0.2 pH units and 0.5°C using proportional control (Paragon TNT, Intec Controls Corporation, Walpole, Mass, USA). However the control gain was increased during the pH adjustment to maintain a reasonable rate of adjustment and keep the overall time to reach pH 4.3 down to one hour.

3.2.2.2 Experimental procedure.

The procedure for the medium scale experiments was designed to mimic the small scale experiments as closely as possible. Problems unique to the medium scale experiments did however dictate some deviance.

It was found much more difficult to attain a clean system at this larger scale. Self-seeding and a high rate of contamination (seen as fungal "hairs" in the crystal filter cake) meant that a more extensive cleaning program had to be employed. Residues of crystals on the reactor wall were removed by soaking the reactor in alkali (pH = 11) between the runs. As a part of the start-up procedure the reactor was scrubbed with a 2 % P3-Ultrasil® 91 (Henkel-Ecolab, Valby, Denmark), rinsed with RO water and then left for at least 15 mins in 0.15 % Divosan Forte (Diversey A/S, Herlev, Denmark). Any solidified crystallisation material inside the acid addition tube was removed manually.

While the reactors were being cleaned the 1 L lots of the crystallising material were defrosted on a circulated water bath. To complete this within the one hour used on the small scale a temperature of 30°C was used. Due to limitation in pumping capacity the acid addition time had to be longer than the 20 mins spent in the small scale experiments. Simultaneous temperature and pH adjustments were therefore used giving an overall adjustment time of similar length to that of the small scale. In cases where 'Tween'80 was added this was done in parallel with the pH and temperature adjustments at a rate of 1 g 'Tween'80 per min and as a 17 % solution.

3.3 Analysis.

3.3.1 The electrical sensing zone method (ESZM).

Particle size analysis in the range of 5 μm to 120 μm was achieved using the electrical sensing zone method described in the section "The electrical sensing zone method" (Chapter 1.3).

3.1.1.1 Sampling.

Samples were taken from the stirred reactor using a 200 μL pipette, rinsed twice upon discharge into low conductivity water (0.05 μS/cm, Prod 10292 3C, BDH, Poole, UK) to achieve 100 fold dilution of the sample. The samples were stable as such at room temperature up to 7 h; size analysis was completed within 2 hours.

There was no evidence of crystal classification in the reactor during sampling.

3.1.1.2 The particle sizing buffer.

The buffer was a 0.13 % (w/w) lithium chloride (LiCl) buffer with $1 \cdot 10^{-4}$ % (w/w) sodium azide (NaN_3) adjusted to pH = 4.0 ± 0.1 with acetic acid and finally filtered through a 0.2 μm cellulose nitrate membrane (Whatman, Kent, UK). During the later part of the this work (Chapter 8) the blank count of the unfiltered buffer was found to be sufficiently low and similar to that of the filtered buffer. The filtration step was therefore omitted.

Usually the conductivity of the particle sizing buffer is given by the orifice diameter used according to the approximate formula: the conductivity of the buffer (mS/cm) = 3000/orifice diameter (μm). However for ease of comparison only the one particle sizing buffer was used for all the orifices.

3.1.1.3 The ESZM measurements.

The equipment used was an Elzone® (280 PC, Particle Data, Consdorf, Luxembourg). Analysis was done on a fixed volume of 5000 μL using one of three orifices: 300 μm orifice to detect particles in the range between 9 μm to 120 μm, 210 μm orifice for 8 μm to 113 μm and a 120 μm orifice for 5 μm to 63 μm.

All glassware was rinsed thoroughly before every run. At the start of the day three blank runs were done on the buffer and the data stored. Reduced levels of noise were found if the particle sizing buffer was left stirred in the sample beaker for around a minute before the start of a measurement. After leaving the toggle on "vacuum" the equipment was normalised once. This was repeated as soon as a volume of typically 50 μL-5 mL of crystal containing sample buffer had been added to 60 mL of the particle sizing buffer. The volume of particle buffer was 60 mL in every run while the added volume of sample buffer was chosen such that a maximum of 1 % coincidence was achieved. Normally one repeat was done but for samples of low particle concentration and/or wide crystal size distributions several were done.

3.3.2 Low angle laser light scattering.

Low angle laser light scattering measurements were performed on a Malvern Particle Sizer (3600 E Type, Worcestershire, UK, 63 mm lens). The equilibrium crystal suspension was kept at room temperature for no longer than 5 h before the analysis. The mother liquor needed for dilution was prepared by centrifugation of a part of the crystal suspension for 10 mins at 20°C and 3930g (Beckman, CA, USA) and filtered (Nitrocellulose, 0.2 μm, Whatman, Maidstone, UK).

3.3.3 Focused beam reflectance measurement.

The Lasentec system Model A 100 (Lasentec, Redmond, WA, USA) was used in this work for focused beam reflectance measurements. Before use the laser beam had to be focused. This was done by covering the laser window with a special purpose black marker pen and then the micrometer was adjusted. When the maximum count rate in the differential signal strength window had been found, the micrometer nut was then set 0.5 units higher to move the focus point out into the liquid passing the window. After a thorough cleaning of the window with alcohol the probe could be positioned in the reactor. Five measuring cycles of 1 s were averaged to give an output every 8 s.

The speed at which the particles pass the probe must not be higher than that of the laser optics. The fastest moving particles will be found near the tip of the impeller which in these experiments was moving at a speed of 1.8 m/s and this is acceptable for this set-up.

3.3.4 Filtration test.

A dead-end, feed pressure filtration test was developed to evaluate the recoverability of the final crystal product.

A pressure filter (Laboratory Filter "60", Schenk Laboratory Systems Limited, Oxton, Wirral, UK) fitted with filter cloth (Propex-23, Scapa Filtration LTD, Lancashire, UK) had a filter area of $2 \cdot 10^{-3}$ m^2, feed pressure 1 bar g was used to process 60-100 mL crystal suspension. The mass of the filtrate was recorded every 1-40 s using a balance. The experiment was left running till air penetrated the cake releasing the filtrate retained on the back side of the filter. The filter was then opened and the height of the filter cake measured before samples were taken to determine the dry weight of the filter cake.

3.3.5 Lipase activity assays.

Determination of the lipase activity in solution is done using two methods: a pH-stat method on a tributyrin substrate and a sequential injection analysis (SIA) method based on the yellow colour reaction of p-nitrophenol.

In the first method the lipase/esterase activity is measured as described by Novo Nordisk A/S (AF 95/6-GB see Appendix 4). The amount of enzyme present which liberates 1 μmol titratable butyric acid per minute is equivalent to one Lipase Unit (LU). The lipase is thought to be active at the interface between an aqueous and polymer containing phase. It is therefore of great importance to be able to reproduce the characteristics of this interface, i.e. to create a homogeneous series of emulsions. Factors that might effect the emulsification are: the batch to batch variability of the gum arabic used to create the polymer phase and variability between tributyrin batches. These variabilities are eliminated by running a lipase standard of known activity.

The lipase incorporated into the crystal lattice is likely to exhibit some activity especially if the lipase molecule is situated near the crystal surface (McPherson, 1992b). Hence the crystals were separated from the mother liquor by centrifugation at 3250g for 3.5 minutes (Microfuge, Beckman, CA, USA).

The procedure described by Novo Nordisk A/S (AF 95/6-GB) was followed as closely as possible. Different suppliers of chemicals were however used: sodium chloride (Prod 10241, BDH, Poole, UK) potassium di-hydrogen phosphate (P-5379, Sigma, Poole, UK), glycerol (G-6279, Sigma, Poole, UK), gum arabic (G-9752, Sigma, Poole, UK), tributyrin (T-8626, Sigma, Poole, UK) and benzoic acid (B-3250, Sigma, Poole, UK). The stirrer used in this work was from Gallenkamp (model: SWT-310-010U, Middelsex, UK) set at maximum speed during substrate preparation otherwise setting 5. The dilution range was 2500-3500 and obtained using volumetric flasks. To insure accuracy of the method a lipase standard in two different dilutions in the relevant range was run at the beginning of the day.

The SIA method for determination of the lipase activity was carried out on a in-house made equipment (see Appendix 4) and the assay was based on a photometric reaction where the lipase converts p-nitrophenylbutyrate to the yellow p-nitrophenol which is then detected and quantified at a wavelength of 405 nm (Novo Nordisk A/S, Denmark, AF-6491 see appendix 4). The samples were supernatant from the crystallisation clarified by filtration. These were stored frozen (-20°C) till analysis. After defrosting the samples were diluted in volumetric flasks 500 000-2 500 000 fold. Following the first dilution step the sample/buffer mixture was left stirred for at least 10 mins to ensure proper dissolution after which the diluted samples were kept in the fridge for no more than an hour. A standard curve was produced daily to ensure correct function of the equipment.

3.3.6 SDS-polyacrylamide gel electrophoresis.

The purity of the resulting crystals was assessed using SDS-polyacrylamide gel electrophoresis. It has proven suitable to use a dissociating discontinuous buffer system in a 12.5 % acrylamide gel. The procedure used was as described by Hames and Rickwood (1990) though 20 μL TEMED and 30 mg of ammonium persulphate were used instead of the prescribed amounts.

3.3.7 Protein analysis.

Crystals were recovered (Microfuge, Beckman, CA, USA, 3 mins at 3250g) and the supernatant diluted 1000-2000 fold in RO water prior to absorbance measurements at 280 nm wavelength (1.0 cm path length).

3.3.8 Crystal suspension turbidity.

The crystal suspension was diluted using clarified mother liquor from a previous crystallisation and absorbance read at 680 nm.

3.3.9 Crystal density.

The crystal density was determined using a kit from Nycodenz® (Nycomed Pharma, Oslo, Norway). Nycodenz® powder and water were mixed in different ratios. Crystals were layered on top of low density and high density mixtures and gently spun for 30 s. The density difference between the layers was decreased until a density of the required accuracy was achieved. It is assumed that the experiment is shorter than the time it takes for salts and other components present to diffuse in or out of the solvent channels in the crystal since this will change the overall density of the crystals (Matthews, 1974).

3.3.10 Sludge height.

Measured as the height of solid phase obtained after spinning 2 mL crystal suspension at 3000g for 10 mins (Heraeus, Megafuge, 1.0R, Holmby & Halby, Denmark).

Chapter 4 Experimental development.

4.1 The electrical sensing zone method.

To determine crystal size distributions (CSD) during crystallisation by the electrical sensing zone method (ESZM) two buffers were needed. The first was the sample buffer which "freezes" the crystal size distribution until it could be analysed. The second was the particle sizing buffer in which the analysis was performed. The following sections validate the stability of the crystals in these two buffers.

4.1.1 The sample buffer.

The specification of the sample buffer requires that the crystals do not grow, dissolve or aggregate either on dilution or during storage prior to analysis. A reasonable stability of the crystals has been found in low conductivity water (0.05 μS/cm, PROD 10292 3C, BDH, Poole, UK).

To evaluate the effect of the dilution step crystals were diluted both in the equilibrium supernatant from the crystallisation (eq. assumed after 24 h) and low conductivity water. This was done for rod-shaped crystals (Figure 14) and diamond-shaped crystals (Figure 15). Dilution in the supernatant from the crystallisation is assumed not to affect the crystals because they have equilibrated against this solution. The CSD were measured using low angle laser light scattering because this method does not have any special requirements for the suspending medium other than it has to be clear. From Figure 14 it can be seen that the two CSD for the rod-shaped crystals are almost identical. The crystals seems a little smaller when measured in the supernatant than in the low conductivity water. This is probably a result of the large difference in transparency of the two liquors rather than any crystal aggregation. Diamond-shaped crystals are also unchanged by dilution in the low conductivity water (Figure 15). The very tall peak at 3 μm represents tiny aggregates produced upon addition of the surfactant. These could be protein-protein or protein-surfactant aggregates but not surfactant micelles because even though the critical micelle concentration probably was exceeded (Porter, 1994), micelles are only a few nanometers large. Although the height of this peak is smaller in the low conductivity buffer, this part of the CSD is outside the ESZM size range studied. The particles of interest in this work are larger than 5 μm which in Figure 15 shows no clear signs of dissolution.

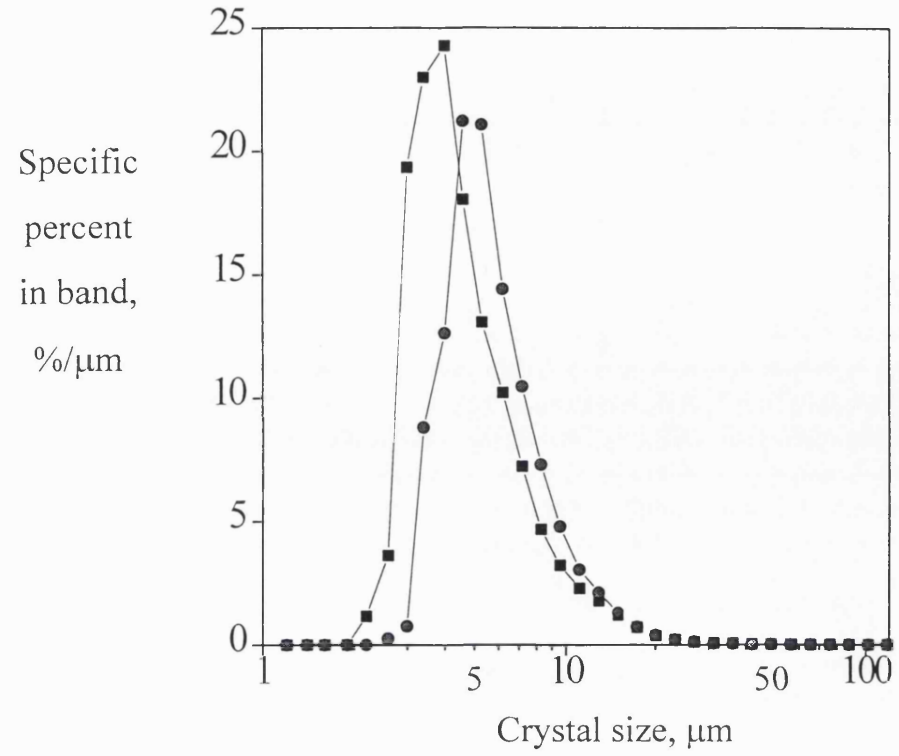

Figure 14. The effect of dilution on rod-shaped crystals in the sample buffer. Crystals were measured in the equilibrium supernatant (●) and low conductivity buffer (■) using the low angle laser light scattering technique.

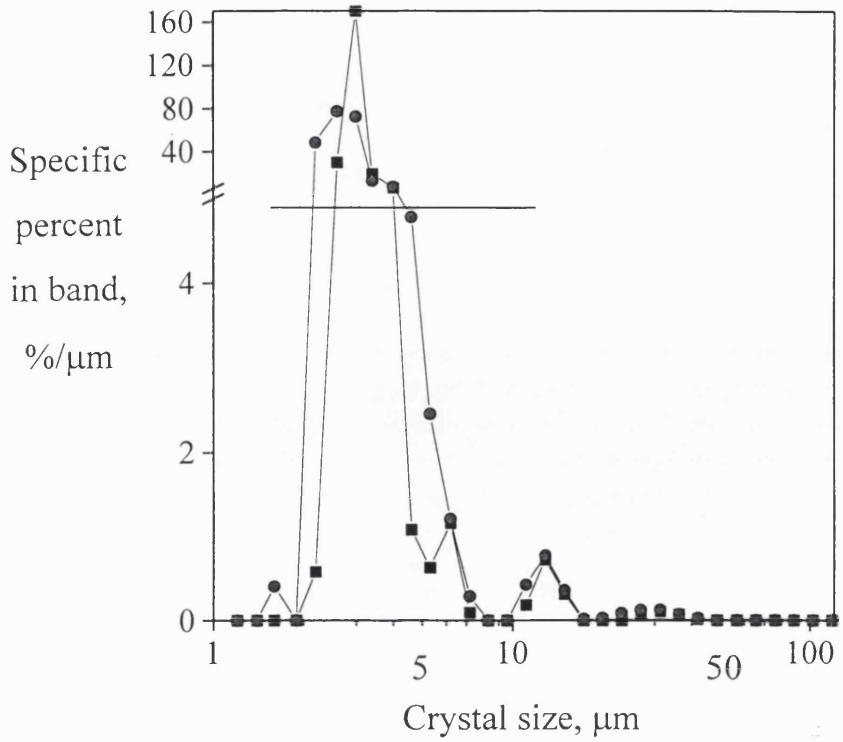

Figure 15. The effect of dilution of diamond-shaped crystals in the sample buffer. Crystals were measured in the equilibrium supernatant (●) and in the sample buffer (■) using the low angle laser light scatting technique.

To test if any slow changes happen while the crystals are stored in the sample buffer the ESZM was preferred. This method offers accurate measurements of *both* the crystal number and size which neither low angle laser light scattering nor microscopy provide.

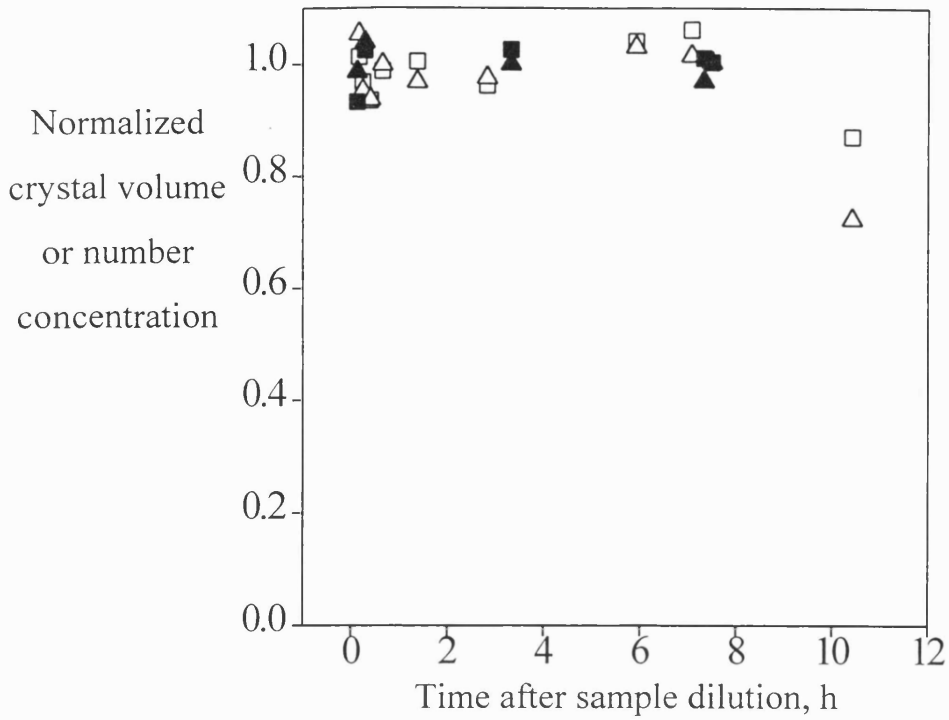

Figure 16. Long term stability of crystals in sample buffer. Several samples were diluted at time zero and analysed between 0-10 h using the ESZM. Both the data points for the total crystal volume concentration (diamond: ■, rod: □) and the total crystal number concentration (diamond:▲, rod:Δ) have been normalised to the average of the first few samples.

From Figure 16 it is clear that both rod and diamond-shaped crystals can safely be stored up to 7 h.

Poor stability (microbial and enzymatic) of the equilibrium supernatant from the crystallisation is one reason for not using it as sample buffer. Moreover, slow crystal growth is more likely in such a solution than in low conductivity buffer.

4.1.2 The particle sizing buffer.

The particle sizing buffer needs to have a certain conductivity as given by the following approximate formula: the conductivity of the buffer (mS/cm) = 3000/(D(μm)) where D is the orifice diameter. The buffer used was a 0.13 % (w/w) lithium chloride (LiCl) with $1 \cdot 10^{-4}$ % (w/w) sodium azide (NaN_3) adjusted to pH = 4.0 ± 0.1 with acetic acid and finally filtered through a 0.2 μm cellulose nitrate membrane (Whatman, Kent, UK). LiCl was chosen among a range of common salts (NaCl, KCl, $CaCl \cdot 2H_2O$, $MgSO_4 \cdot 7H_2O$, $ZnSO_4 \cdot 7H_2O$, $Fe(NO_3)_3 \cdot 9H_2O$, acetates and formates) because judging from microscopically observations the crystals dissolved to a significantly lesser extent.

Moreover crystallographers are familiar with this salt (McPherson, 1990). The conductivity of the resulting buffer was approximately 3 mS/cm which represented a compromise between the required conductivities for size analysis while avoiding crystal dissolution.

The results of stability tests of the rod and diamond-shaped crystals in this buffer is shown in Figures 5 to 8.

The comments made on the effect of dilution on the crystals in the sample buffer also applies for the particle sizing buffer as is clear from Figures 17 and 18. The CSD obtained in the sample and particle sizing buffers are essentially identical (compare Figure 14 and Figure 17, ■), suggesting that a higher background count of the supernatant is the reason for the slightly smaller size measured in this.

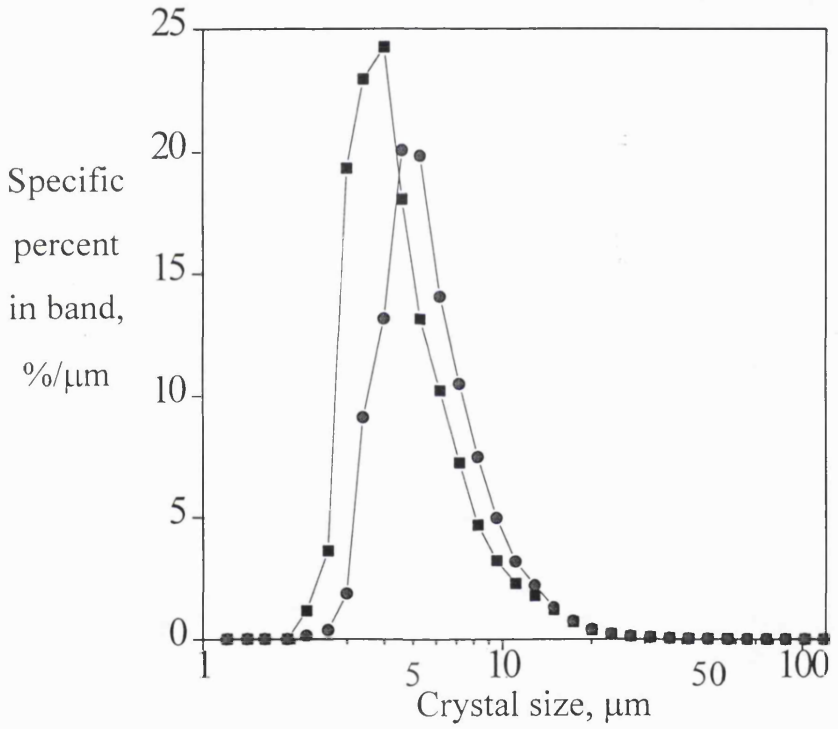

Figure 17. The effect of dilution on rod-shaped crystals in the particle sizing buffer. Crystals were measured in the supernatant (●) and in the particle sizing buffer (■) using the low angle laser light scattering technique.

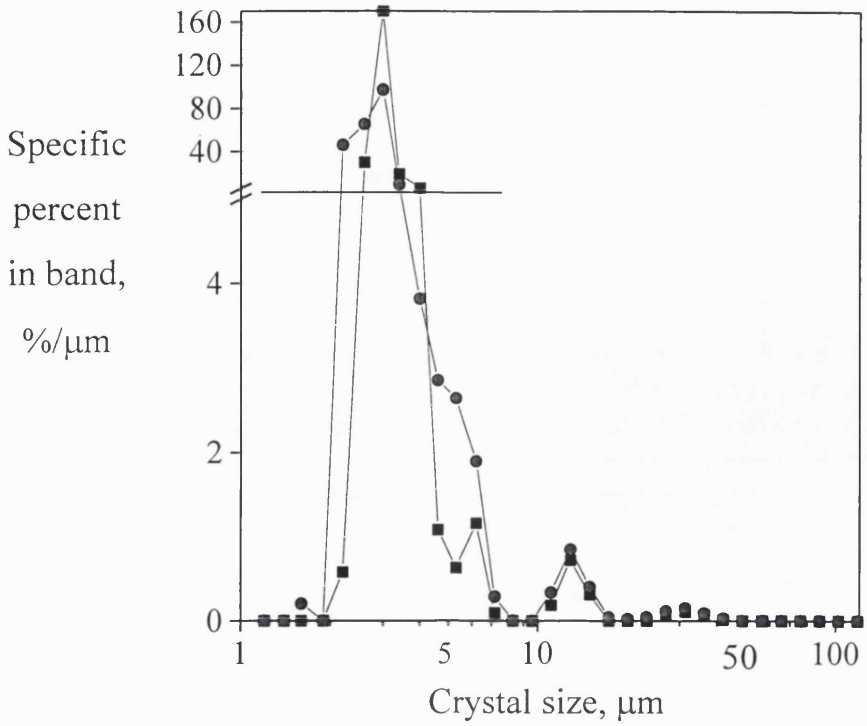

Figure 18. The effect of dilution on diamond-shaped crystals in the particle sizing buffer. Crystals were measured in the equilibrium supernatant (●) and the particle sizing buffer (■) using the low angle laser light scattering technique.

Some dissolution of the crystals was expected in the particle sizing buffer during the measurement. The degree of dissolution has been estimated by quickly re-running the measurement on the same sample dilution in the particle sizing buffer (around 2 mins per run). Simple linear back-extrapolation can give some idea of the degree of dissolution. This is shown for the rod-shaped crystals in Figure 19 suggesting that approximately 8 % of the crystals may have dissolved at the end of the measurement leaving the volume some 4 % underestimated for the sample run. A similar plot of the stability of the diamond-shaped crystals in the particle sizing buffer is shown in Figure 20. Here a maximum of 1 or 2 percentage dissolution during measurement was estimated.

Although not perfect for the rod-shaped crystals the particle sizing buffer was deemed acceptable for this study.

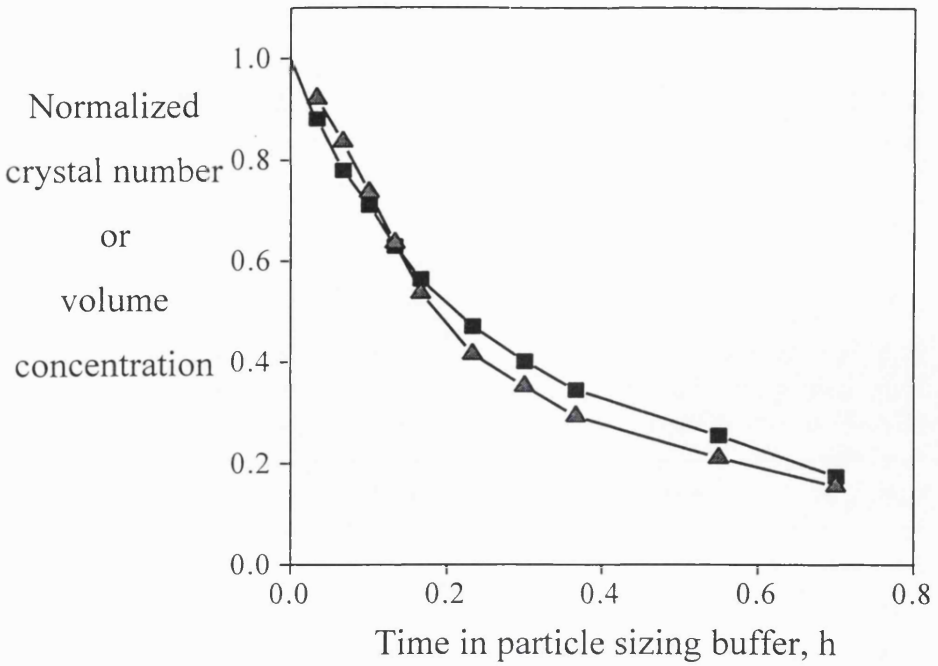

Figure 19. Long term stability of rod-shaped crystals in the particle sizing buffer. One sample of rod-shaped crystals was diluted once in the particle sizing buffer and then analysed repeatedly over 0.7 h using the ESZM. Both the data points for the crystal volume concentration (■) and the crystal number concentration (▲) have been normalised using the extrapolated value for time zero, i.e. when the sample was diluted in the particle sizing buffer.

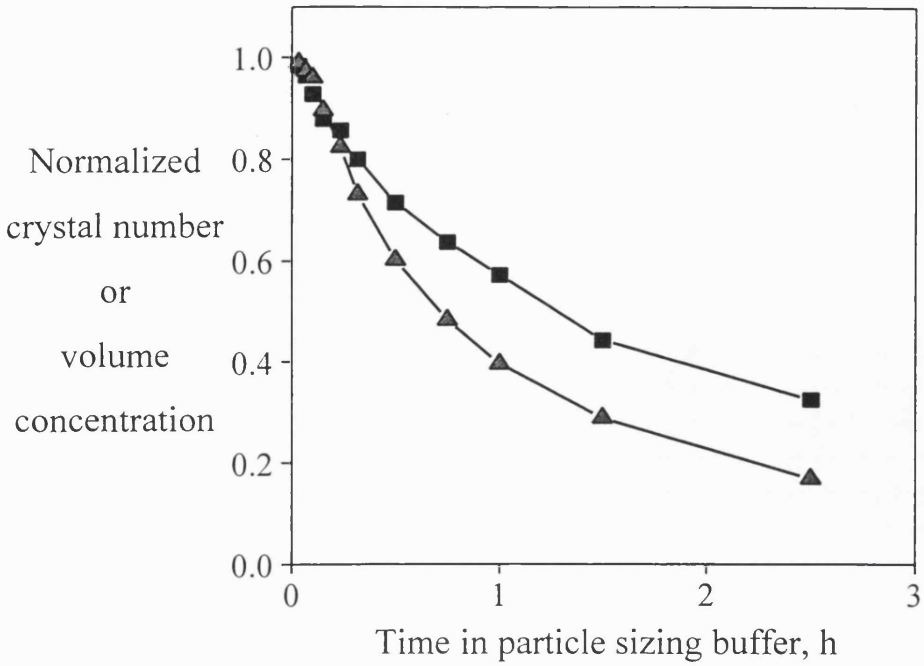

Figure 20. Long term stability of diamond-shaped crystals in the particle sizing buffer. One sample of diamond-shaped crystals was diluted once in the particle sizing buffer and then analysed repeatedly over 3 h using the ESZM. Both data points for the crystal volume concentration (■) and the crystal number concentration (▲) have been normalised using the extrapolated value for time zero, i.e. when the sample was diluted in the particle sizing buffer.

4.1.3 The crystal size distribution data.

The CSD obtained should be critically evaluated. The question to ask is if they are a true representation of the physical size of the crystals. Sections of the crystal size distribution may for example have to be omitted due to high levels of noise. In Figure 21 the result of the ESZM is compared to light microscope (400 times magnification) for a given crystal size distribution. Clearly the actual size of the crystals is well estimated. The shape of the two size distributions is the same except around 8-9 μm, where the EZSM shows a small peak. This is however near its lower detection limit and probably a result of measuring noise. Before the data is subject to further analysis the first 8 channels should therefore be omitted. A similar trend is seen in Figure 22 where measurements obtained with different orifices are compared.

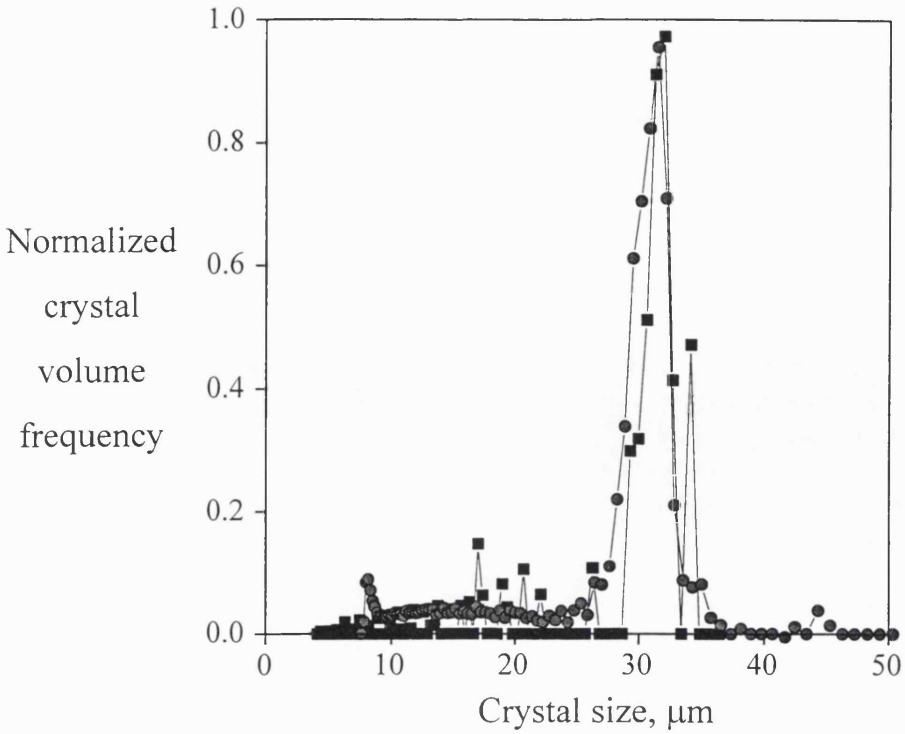

Figure 21. Comparison of CSD measured using light microscopy (400 times magnification) (■) and the ESZM (●). Some 150 crystals where manually sized from 6 microscope images and plotted using the 210 μm axis (ESZM) and normalised for comparison. A 210 μm orifice was fitted to the ESZM.

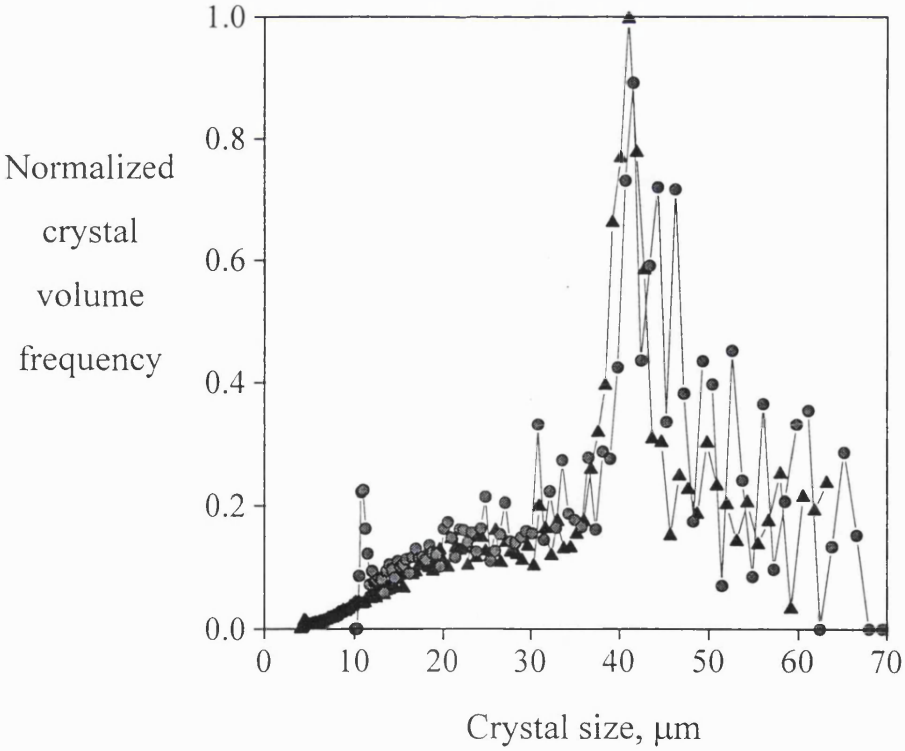

Figure 22. Comparison of crystal size distributions measured with a 120 (●) and 300 (▲) μm orifice using the EZSM.

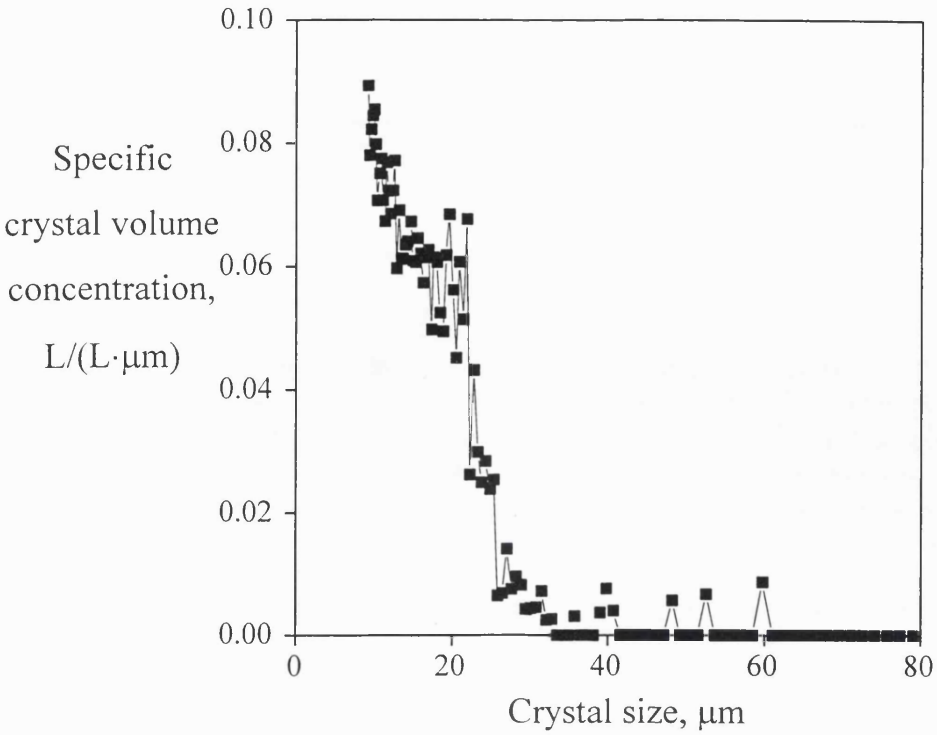

Figure 23. A CSD for rod-shaped crystals grown at standard conditions (pH 4.3, 28.0°C). The data was obtained with a 210 μm orifice.

A limitation in using the ESZM for determination of the total crystal volume and thereby the process yield, is that some crystals are smaller than the lower limit of detection. This is a particular problem when measuring small particles such as the rod-shaped crystals because a part (up to roughly a 1/3) of the volume would remain undetected. However for a system crystallising as the diamond system almost all the volume is detected. It should be stressed here that the shown example is a worse-case because the detection limit was 10 μm and not the 5 μm for the experiments described in Chapter 6 and 7. Moreover there is a limited effect on the estimated kinetic parameters as will be discussed in Chapter 5.

4.2 Choice of filtration model describing the system of study.

Three of the filtration laws explained in Chapter 2 have been tested in this section for the filtration of both the rod and diamond-shaped crystals produced in this study. The aim is to gain a better understanding of the filtration of the two crystal forms and to select a model which describes the data well. The estimated parameters from this model will be used to compare the filterability of the crystals obtained under different experimental conditions.

From Figure 24 it can be seen that the standard blocking law describes the filtration of rod-shaped crystals better than the cake filtration law. The rod-shaped crystals are small and therefore likely to block the pores in the filter. Due to their fragile nature they may moreover compress with time giving rise to a long filtration time. That crystal cake compression could be happening after 15 h is most clearly seen from the plot using the cake filtration law.

From Figure 25 it can be seen that the filtration of diamond-shaped crystals is better described with the cake filtration law than with the standard blocking law. This was expected because the diamond-shaped crystals are big and hence not expected to block the filter. The kink in the curves is a result of filtrate retained inside the filtration rig being released by air penetrating the filter cake. The part of the curve after the kink describes the dewatering of the filter cake. In the evaluation of the filtration models these data point are obviously not included.

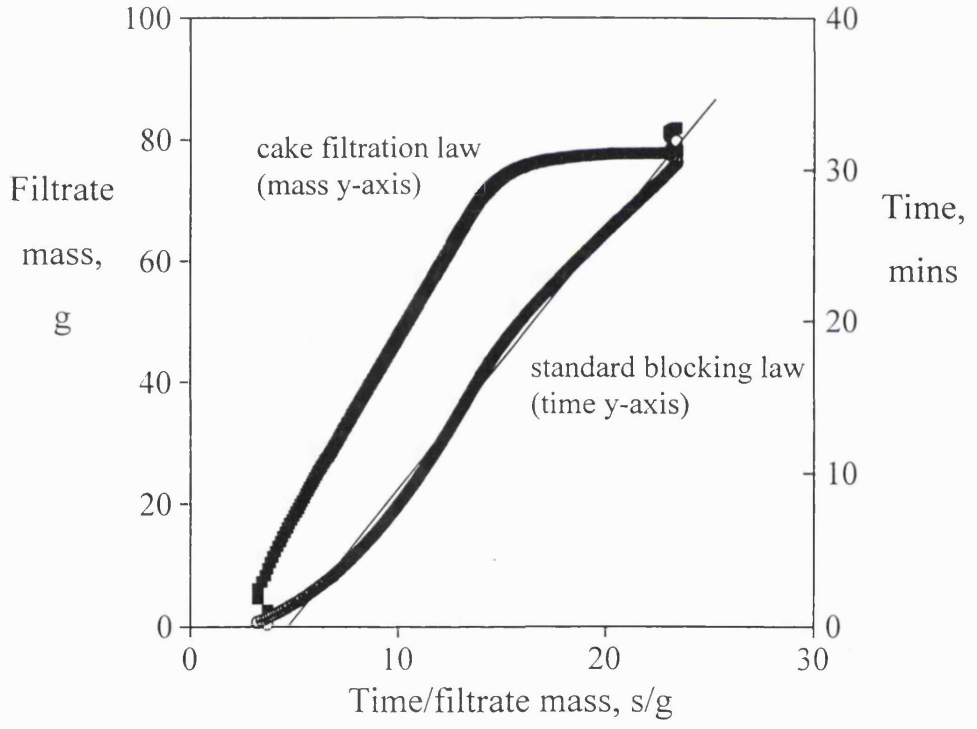

Figure 24. The filtration of a suspension of rod-shaped crystals is analysed by comparing the cake filtration law (eq.33) to the standard blocking law (eq. 28). The experimental data was the mass of filtrate recorded as a function of time for a dead-end filtration of crystal suspension. The linear regression line (thin and straight) gave $R^2 =$ 0.9912 for the standard blocking law. Only the data points before the kink (marked with black dot) are included in the linear regression.

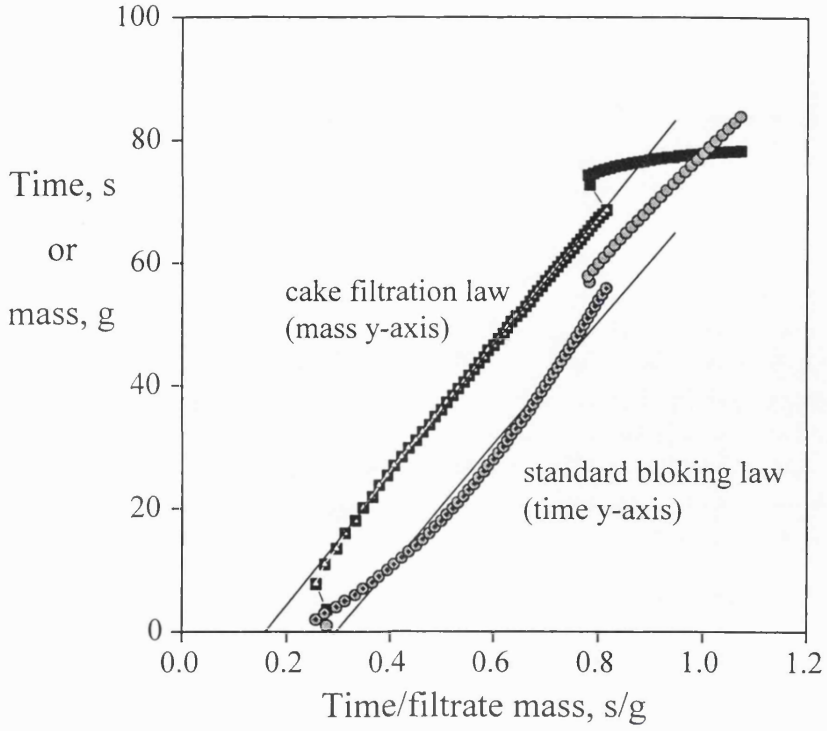

Figure 25. The filtration of a suspension of diamond-shaped crystals is analysed comparing the cake filtration law (eq. 33) to the standard blocking law (eq. 28). The experimental data was the mass of filtrate recorded as a function of time for a dead-end filtration of crystal suspension. The linear regression line (thin and straight) gave $R^2 = 0.9992$ for the cake filtration law and $R^2 = 0.9783$ for the standard blocking law. Only the data points before the kink (marked with a dot) are included in the linear regression.

Finally in Figure 26 an evaluation of the filtration law given by Doshi and Trettin (1981) is plotted for the two crystal forms. The fit is very good for the diamond-shaped crystals while the filtration of rod-shaped crystals is less well described by this model. The filtration probably does not obey Darcy's law due to compression of the fragile rod-shaped crystals. The two curves are according to the model expected to go through (0,0). This is not the case in Figure 26 due to filtrate retained inside the set-up. The estimated model parameters are however unaffected by this.

The conclusion of the filtration experiments is that the diamond-shaped crystals are filtering according to the cake filtration law but is even better described by the cake filtration law given by Doshi and Trettin (1981). The filtration of the rod-shaped crystals is best described by the standard pore blocking model. Crystal cake compression may however cause some deviation from the model.

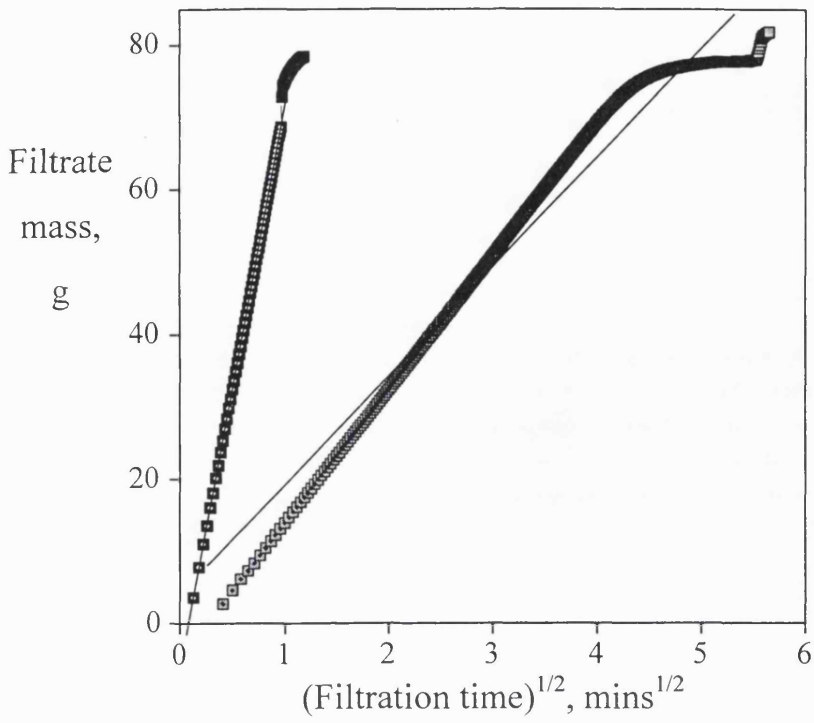

Figure 26. The data shown in Figures 24 and 25 are plotted according to the filtration law given by Doshi and Trettin (1981) (eq. 39). Linear regression gave $R^2 = 0.99998$ for the filtration of diamond-shaped crystals and $R^2 = 0.9594$ for the filtration of rod-shaped crystals. The experimental data was the mass of filtrate recorded as a function of time for a dead-end filtration of crystal suspension. Only the data points marked with a dot are included in the linear regression.

4.3 Protein UV-absorption.

The extent of crystallisation was also estimated by measuring the remaining protein concentration in solution. Two absorption curves are shown in Figure 27 of which OD(280 nm) was chosen due to the larger linear range. In the appendix this method is compared to other techniques for measuring the rate of crystallisation.

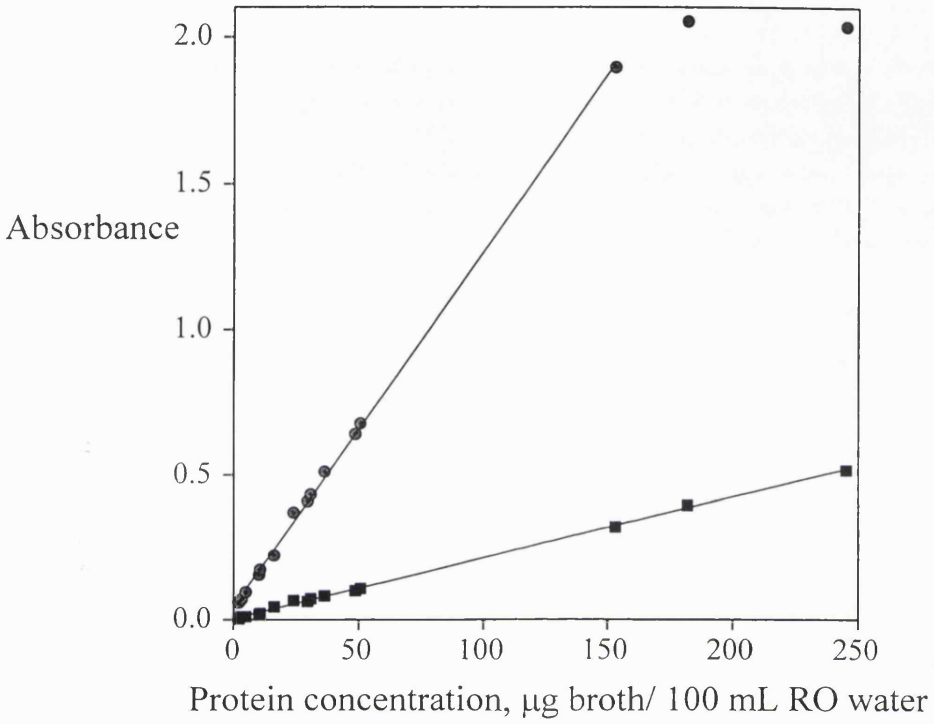

Figure 27. Dilution curve for crystallisation starting material. (●) represents (OD(224 nm)-OD(236 nm)) and (■) represents OD(280 nm) measured in a quartz cell of 1.0 cm light path length. $R^2 = 0.99943$ for (OD(224 nm)-OD(236 nm)) and $R^2 = 0.99931$ for OD(280nm) for linear regression curve based on data points below an absorbance of 1.

4.4 Crystal suspension turbidity.

A fast but empirical method for quantifying the progress of crystallisation could be by measuring the turbidity of the crystal suspension (OD(680 nm)). To keep the reading below one dilution was required. Aggregation will result if RO water was used so mother liquor from a similar experiment was used. The turbidity of neither rod nor diamond-shaped crystal suspensions is a linear function of the crystal concentration. For dilutions less than 100 fold for rod-shaped crystals and 50 for diamond-shaped crystals the slope drops (Figure 28). If however the diamond-shaped crystals are diluted in the 30-200 fold range and the rod-shaped crystals 150-4000 fold, the output is reasonably linear.

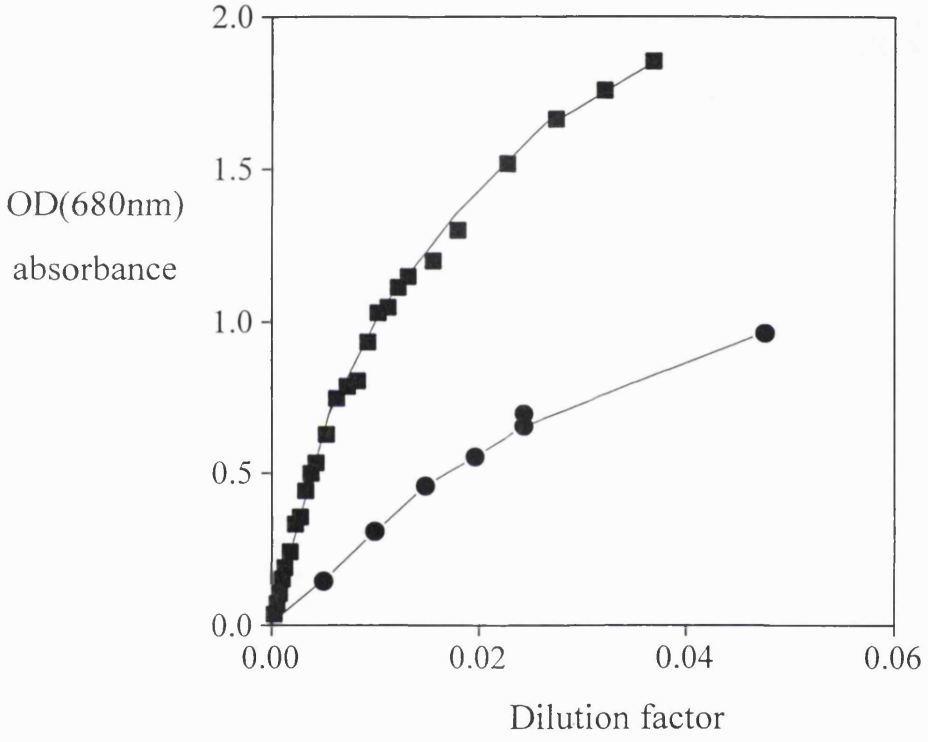

Figure 28. Dilution curves for the rod-shaped crystals (■) and the diamond-shaped crystals (●). The crystal suspensions were diluted with clarified equilibrium supernatant from a crystallisation conducted under the same conditions.

Chapter 5. Analytical development.

5.1 The s-plane analysis.

The s-plane analysis was developed for the simultaneous estimation of nucleation and crystal growth rates from series of size distributions measured during crystallisation. As was described earlier (Chapter 2), simple sub-population balances for consecutive samples can yield nucleation and growth rates similar to those estimated by the s-plane analysis. The advantage of s-plane analysis is that instead of using the change in the actual number of crystals in specific size ranges between two samples, it uses the change in total number after exponential weightings of the entire crystal size distributions and compares these for consecutive samples. This makes the estimates less sensitive to experimental noise. A criterion for success is however that a suitable range of the weighting parameter has been found. If the range of this parameter (which is preceded by a minus) chosen is too small, the larger crystals will be heavily weighted, the number of which is often less statistical secure. Whereas if the value of the weighting parameter chosen is too high, the emphasis will be on the fines (and signal noise).

Usually the range of this weighting parameter starts at $s = 0\ (\mu m)^{-1}$, which correspond no exponential weighting ($N \cdot \exp(-s \cdot R)$, with R being crystal size) and ends at some value, s_f. The weighting is often discussed in terms of k, given as $s_f = k \cdot \mu_0/\mu_1$ where μ_x is the x'th moment of the size distribution. Values of k reported in the literature are 1 (Tavare 1991) and 3-5 (Tavare and Garside 1986).

The approach to finding a suitable range of k will be to compare the estimated nucleation and growth rates to those obtained by other methods. The nucleation will be compared with the change in total number divided by the time span between the samples. Growth rates estimated from the shift of characteristic points from one sample to the next will also be compared to the growth rate estimated by the s-plane analysis.

In Figure 29, a crystal size distribution has been subjected to the exponential weighting, the range starting at $s = 0\ (\mu m)^{-1}$ and ending at $s_f = 1(\mu m)^{-1}$. For increasing values of s, smaller and smaller parts of the crystal size distribution is included in the population balance, ending with only the first few channels. Indeed, for s higher than 1 a significant part of the weight will be put on the empty channels between 0-5 μm which was found to distort the results. A simple trick to avoid this is to redefine the crystal size

scale such that the smallest detected crystals are given the size of zero. This practically eliminates the dependence of the estimates on the weighting parameter, k, (Figure 30).

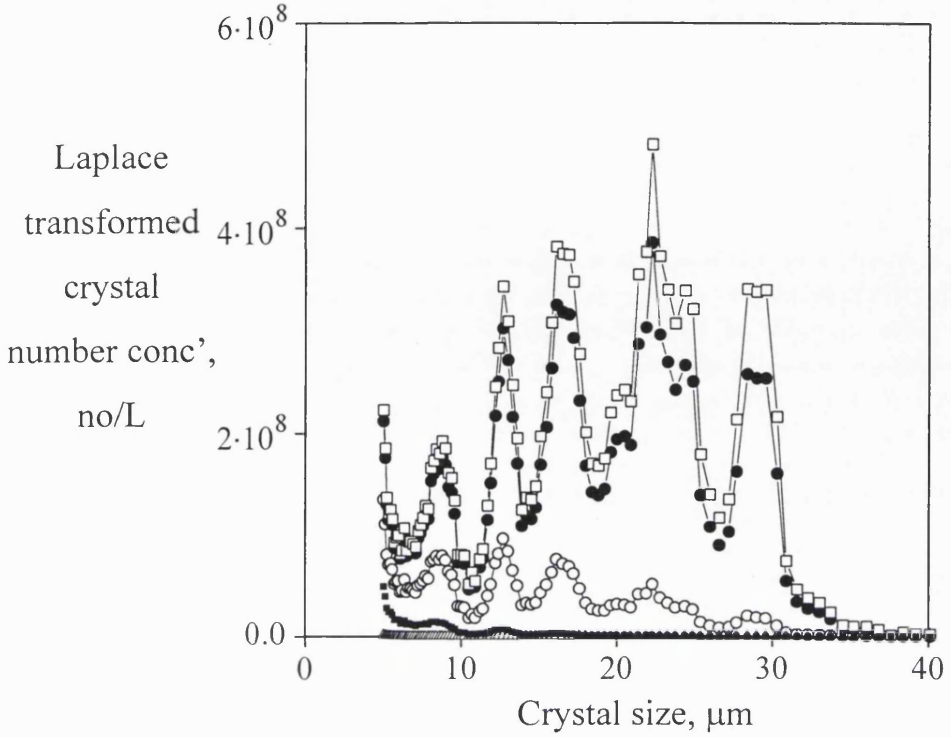

Figure 29. Example of the exponential weighting of the crystal size distribution being a part of the Laplace transformation: N·exp(-s·crystal size). The example is for s = 0 (□) (raw data), 0.01 (●), 0.1 (O), 0.3 (■) and s_f = 1 (Δ). The unit being $(\mu m)^{-1}$

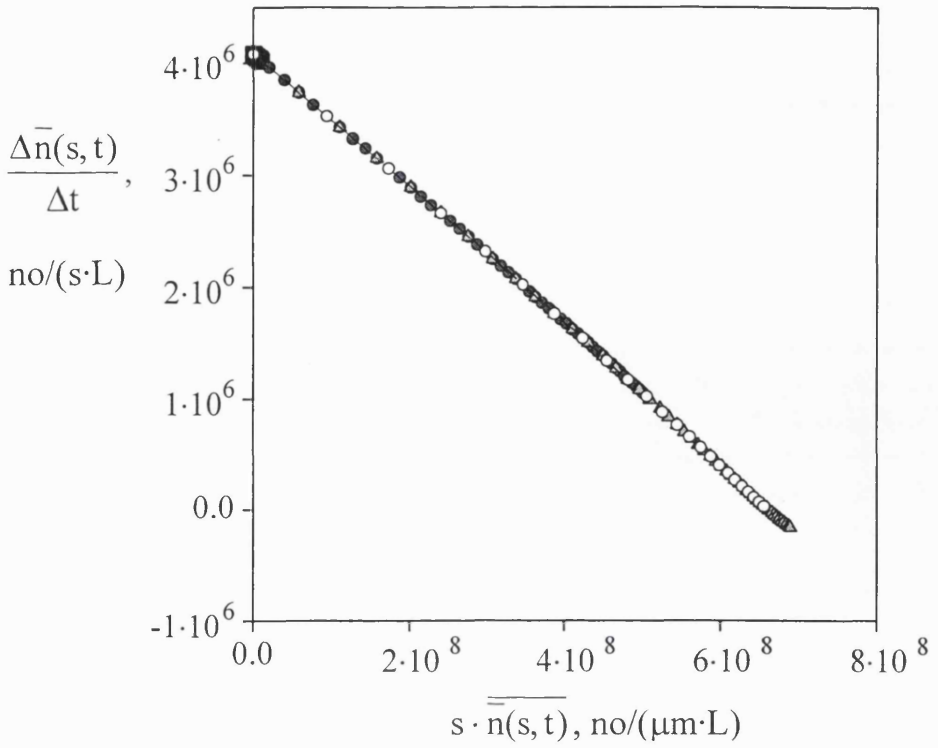

Figure 30. Curves for s-plane analysis estimation of nucleation and growth rates for different values of k = 0.01 (■), 1 (●),3 (o) and 5 (▲) for the redefined size scale (see text). Linear regression gave R^2 = 1.0000, 0.9998, 0.9995 and 0.9979 respectively. For comparison to Figures 31 and 32, the data presented was measured 3.2 h into the crystallisation.

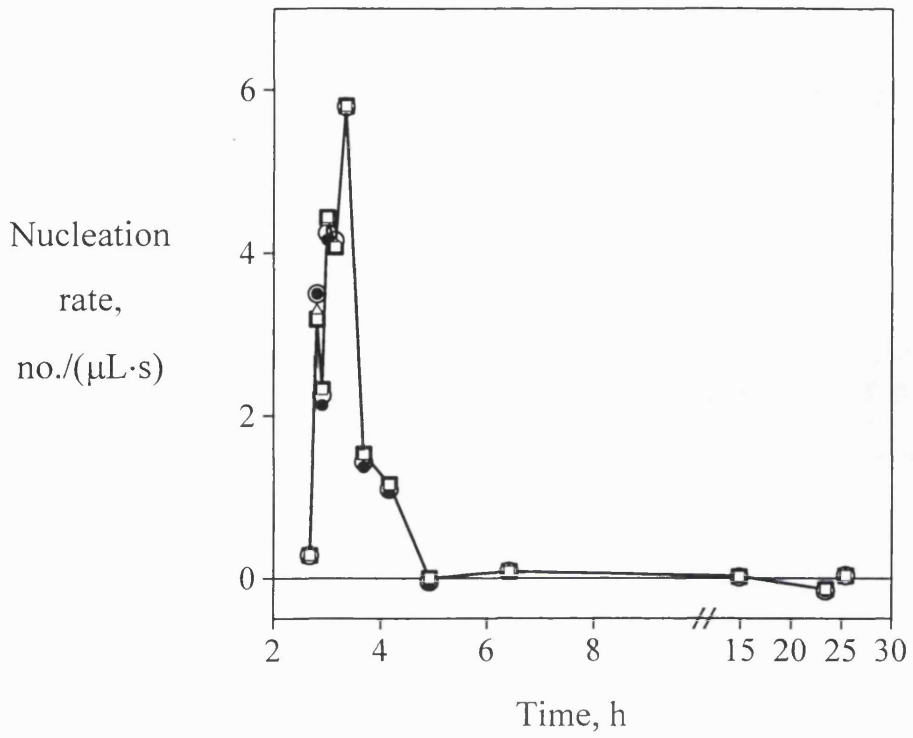

Figure 31. Comparison of the s-plane analysis method to simple nucleation rate (Δno./Δt) for k = 0.01 (■), k = 1.0 (Δ), k = 3.0 (○) and k = 5.0 (●). The data points for simple nucleation rate (-□-) have been connected with a line to guide the eye.

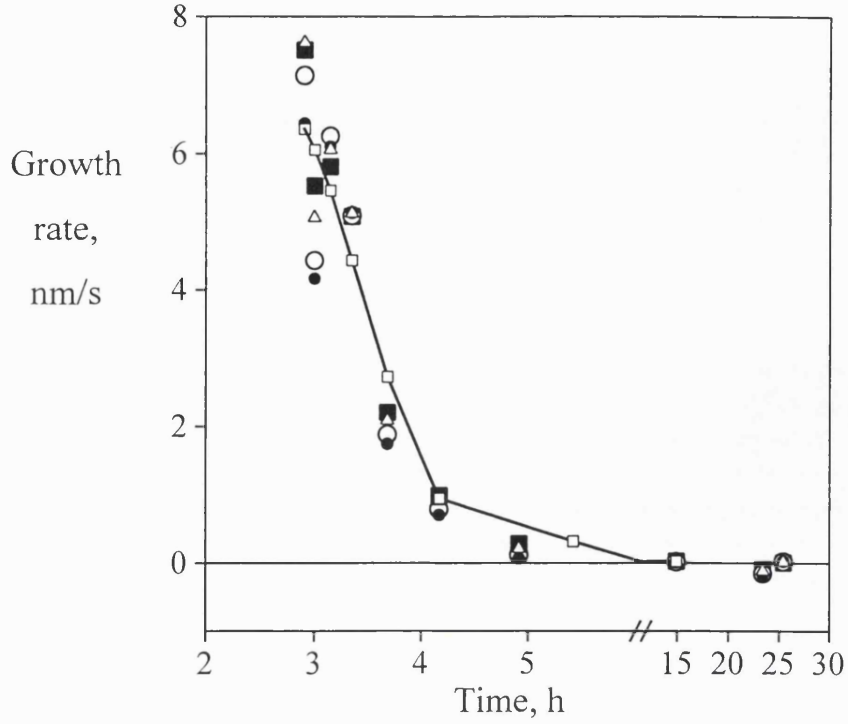

Figure 32. Comparison of the s-plane analysis method and peak growth rates (-□-) for k = 0.01 (■), k = 1.0 (Δ) k = 3.0 (○) and k = 5.0 (●). The data points for peak growth rate have been connected with a line to guide the eye.

Furthermore in Figures 31 and 32 for different values of k, the nucleation and growth rates obtained by the s-plane analysis are compared to the simple nucleation rate and growth rate of characteristic points respectively. Good correspondence was found independent of the value of k.

In conclusion, the value of k has little effect on the estimated nucleation and growth rates. The estimates correspond well with those obtained from crystal size distributions with other analytical methods. For this study, k = 0.01 has been chosen, for which nucleation rates were identical. For growth, the best match was achieved for k = 0.01 for all but the first data point. In the next section, the effect of the value of k on the estimated kinetic parameters will be discussed.

Every point on the curves in Figure 30 corresponds to a sub-population balance mentioned earlier but are presented here in the Laplace domain. As can be seen, little extra information is obtained if the number of sub-population balances is high, so 50 sub-population balances was chosen to reduce data processing time. Tavare (1991) used

10 sub-population balances for the analysis of a system with size distributions consisting of 15 channels with crystals in all but the last channel.

5.2 Estimation of kinetic parameters.

Rather than describing a batch crystallisation with time-dependent nucleation and growth rate profiles, these are often reduced to a few kinetic parameters that characterises the experiment. Usually these are found by linking nucleation and growth to the degree of supersaturation (S) shown below. The aim of this section is to design the algorithm for the estimation of these kinetic parameters, particular focusing on the effect of the range of S. The effect of experimental scatter of the data as well as deviation form the models are considered. Moreover, the effect of data smoothing will be discussed as a way of reducing the effect of the former.

$$B = k_B \cdot M_T^m \cdot S^b$$

eq. 49

$$G = k_G \cdot S^g$$

eq. 50

where $\mathbf{k_X}$ are rate constants, $\mathbf{M_T}$ is the mass concentration of crystalline material, **m**, **b** and **g** are kinetics constants while the supersaturation, **S**, is given by:

$$S(t) = 1 + \frac{(V_S - V(t)) \cdot \rho_C \cdot F}{C_S}$$

eq. 51

where $\mathbf{V_S}$ and **V(t)** are the crystal volume concentration at equilibrium (assumed after 24 h) or at time, **t**, respectively. ρ_C is crystal density and **F** is the protein mass fraction of the crystals.

The value of m, the power dependency on the crystal mass concentration for nucleation, is obtained by maximisation of the linear correlation coefficient between the specific nucleation rate (B/M^m) and the degree of supersaturation. Using this value of m, a linear least squares fit will give the nucleation rate constant, k_B, and the power dependency, b, on the degree of supersaturation. Similarly, a linear least squares fit was used to obtain the growth rate constant, k_G, and the power dependency, g, on the degree of supersaturation. Crystal volume is used as a measure of the progress rather than lipase activity or protein concentration due to concerns over long term stability of the lipase and the difficulty of distinguishing crystallising and non-crystallising proteins.

The kinetic parameters should be estimated for the phase of rapid nucleation and growth since this period of the crystallisation will have the largest effect on the resulting crystal size distribution. Since different models or model parameters may describe the rest of the crystallisation experiment, the range of supersaturation was selected with caution. The quality of the data obtained would probably not allow reliable estimation of more parameters, such as for the early and late parts of the crystallisation using the above model.

The maximum range of supersaturation in which the estimation of the kinetic parameters can be carried out is from the first positive estimated growth or nucleation rate (i.e. at high S-values), to the last data point before the estimates again become negative (i.e. at low S-values) because the power law model cannot handle negative estimates. When the changes in the system from one sample to the next become smaller than the background noise and dilution errors, small negative and positive nucleation and growth rates are estimated. Smoothing can extend the supersaturation range in which the estimates are positive, usually more than 30 %.

The algorithm for the smoothing was to correct the dilution factor such that the total number and volume profiles as a function of time became monotone and smoothly increasing functions of time since neither were expected to fluctuate. In most cases, a few percentage increase/decrease in the dilution factor were sufficient to bring a particular point in line but in rare cases up to 10 % correction was used. If no correction factor could give a reasonably smooth curve for both the number and volume profiles then the sample was eliminated although this was rarely necessary. If correction of more than one point was needed, a best fit was achieved by obtaining an average correction factors of one. The relative standard deviation of dilution of samples taken near the end of the crystallisation run was found larger than for the early samples, leading to corrections almost exclusively being carried out for the later samples.

The nucleation and growth rate data points towards the ends (at S_{max} and S_{min}) are more uncertain than those collected during rapid nucleation and growth. In the beginning of the experiment, the measurement noise (non-crystalline particle in the solution and noise detected by the sizing equipment) would be significant. Thus for slowly starting crystallisations it can appear that the growth rate is increasing with decreasing supersaturation. This is due to larger and larger fractions of the detected particles becoming crystals. Such data points are omitted in the estimation. The later data points are more affected by dilution errors. For example, if there are three

consecutive samples of which the second has a too large dilution factor, the samples allow the calculation of two sets of nucleation and growth rates. In this case, the first will be over-estimated and the second under-estimated. Hence, the effect of dilution errors on the estimated kinetic parameters is not expected to be large. However, at low S-values an effect may be seen because the second estimates may become negative, leaving only the highest values of nucleation and growth rate in the range of S used for the estimation of the kinetic parameters.

The range for the estimation of the kinetic parameters was chosen as S_{max}-1.3, where S_{max} generally was the first positive estimate. Although if the early growth rate was found to increase significantly with decreasing supersaturation, these data points were omitted. The lower value of S = 1.3 was chosen as a compromise. A slight extension of the S range below that of the raw data which allows the inclusion of a larger part of the data in the estimation is desirable. However below a supersaturation of 1.3 changes were small and the data points seem to affect the overall kinetics estimated. If any nucleation and growth rate data points within this range were negative, the smoothing procedure was applied.

Now having selected a suitable range of supersaturation for the estimation, the s-plane estimated kinetic parameters can be compared to those estimated from the alternative methods mentioned above. For growth, some difference was found but deemed acceptable. For nucleation, exactly the same kinetic parameters were estimated, which is not surprising from the data shown in Figures 30 and 31.

	g (-)	k_G (nm/s)	b (-)	k_B[(a)]	m (-)
s-plane	7.22	0.0171	11.6	203	0.55
peak growth rate	7.94	0.0098			
simple nucleation rate			11.6	203	0.55
percentage difference	9 %	12 %*	0 %	0 %[(b)]	0 %

Table 2. Comparison of estimates of the kinetic parameters based on data shown in Figures 31 and 32. (a) the units of k_B was $(no./(s \cdot L)) \cdot (g_c/L)^{-m}$), (b) the percentage difference is calculated for the logarithmic values.

The effect of the weighting parameter, k, on the estimated kinetic parameters is shown in Table 3, which indicates that the choice of the value of k does not strongly effect the estimated kinetic parameters. A k-value near 3 gives growth kinetics almost

identical to those obtained from the growth rate of peaks. However, the nucleation kinetics for k = 3 are significantly different from those obtained from simple nucleation rate data. Elimination of the first growth data point in Figure 32 will make k = 0.01 fit the data best, also for the growth process. Hence k = 0.01, is chosen for this study.

k	g (-)	k_G (nm/s)	b (-)	k_B[(a)]	m (-)
0.01	7.2	0.017	11.6	203	0.55
0.1	7.3	0.016	11.7	188	0.56
1	7.5	0.013	12.0	145	0.58
3	7.8	0.011	14.3	19	0.78

Table 3. Kinetic parameters estimated for different values of k based on data shown in Figures 31 and 32. (a) the units of k_B was $(no./(s \cdot L)) \cdot (g_c/L)^{-m}$).

One concern is whether the volume of crystals smaller than the lower detection limit for the electrical sensing zone method could have an effect on both the calculated degree of supersaturation and more seriously on the estimated kinetic parameters. Judging from the shaped of the crystal size distribution, this problem is expected to be more evident for the crystallisation of rod-shaped crystals. Therefore an extrapolation to crystal size zero and that of the crystal size distribution based on specific crystal volume was attempted. A Gausian model was used (Origin, version 3.5, Microcal Software, Inc., USA) and ten data pairs of (0,0) were added to the size distribution, because theoretically the curve should go through this point. By including the extrapolated crystal volume below the size of 5 μm resulted in approximately a 10 % larger total crystal volume throughout the crystallisation. Using a 10 % higher degree of supersaturation with growth and nucleation rates, new kinetic parameters were estimated (Table 4). The changes resulting from the extrapolation are all below 10 %, which is acceptable. That the kinetic parameters g, b and m are probably unaffected by the extrapolation can be predicted by the fact that throughout the crystallisation, the fraction of undetected crystal volume remains constant ((11 ± 2) %). Hence, including the extra volume merely shifts the regression curve horizontally and only changes its slope marginally. A similar exercise has not been repeated for the crystallisation of diamond-shaped crystals because even less of an effect is expected to be even less and moreover extrapolation of the multimodal crystal size distributions is difficult.

	g (-)	k_G(nm/s)	b (-)	k_B[(a)]	m (-)
raw data	3.0	0.190	4.8	8600	1.27
extrapolated data	2.9	0.161	4.6	6600	1.26
percentage difference	3 %	10 %*	4 %	3 %[(b)]	1 %

Table 4. Worse-case-scenario for the effect of volume of fines on the estimated kinetic parameters. A Gausian model was used for the extrapolation of crystal size distributions based on specific volume. (a) the units of k_B was $(no./(s \cdot L)) \cdot (g_c/L)^{-m}$), (b) indicates that the percentage difference is calculated for the logarithmic values.

5.3 Porosity estimation.

In Table 5, the filter cake porosity calculated using models described in Chapter 2 is compared. As expected, volume extrapolation did not significantly change the porosity for the diamond-shaped crystals while the effect was significant for the rod-shaped crystals because they are generally smaller. The mass balance method underestimates the porosities for both crystal forms. This may be because the crystals have been compressed during filtration. Surprisingly, the calculating the porosity from the weight loss upon drying gives an estimate similar to that determined by the electrical sensing zone method.

	volume extrapolation	mass balance	loss on drying
rod-shaped	105	70	105
diamond-shaped	100	83	94

Table 5. Comparison of methods for estimating the filter cake porosity for two crystal forms. The porosity calculated using the volume detected by the electrical sensing zone method (lower limit 5 μm) has been given an index of 100 and the other methods are give relative to this. The extrapolation to zero crystal size was done using a Gausian model. A crystal solvent content of 43 % (Appendix 6) was used together with a crystal density of 1.25 g/mL.

Chapter 6. Characterisation of batch protein crystallisation.

6.1 Introduction.

Bulk crystallisation is emerging as a new industrial operation for protein recovery. Characterisation of bulk protein crystallisation is more complex than protein crystallisation for structural study where single crystals are grown in flow cells. This is because both nucleation and crystal growth processes are taking place while the supersaturation falls. An algorithm is presented to characterise crystallisation using the rates of the two kinetic processes, nucleation and growth. The values of these rates allow ready comparison of the crystallisation process under different operating conditions.

6.2 Results.

A solubility diagram for the protein crystallised in this study is shown in Figure 33. Formic acid is added to reduce the pH from 6.6 and the solubility curve is defined as the concentration of product left in solution after 24 h. A minimum solubility was recorded at pH = 4.3- 4.5 where just over 60 % of the protein was recovered in the form of crystals. This is comparable to the average of 65-75 % calculated for a range of protein separation techniques (Bonnerjea *et al.*, 1986). The crystallisation studied in this chapter follows the operating line shown in Figure 33, starting the crystallisation by changing the pH from 6.6 to 4.3 and then maintaining pH 4.3 during the rest of the crystallisation. In the pH range of 4.25-4.65 the protein crystallises in a diamond habit (hexagonal bipyramidal, see Figure 34). At higher pH, crystals of a rod-shaped habit are formed after which the diamond-shaped crystals appear. At pH 4.25 small stable aggregates of amorphous precipitate are formed which remain throughout the crystallisation process. These are followed after several hours by the formation of diamond-shaped crystals which comprise the majority of material brought out of solution. Crystallisation at these higher and lower pH values was not studied in detail.

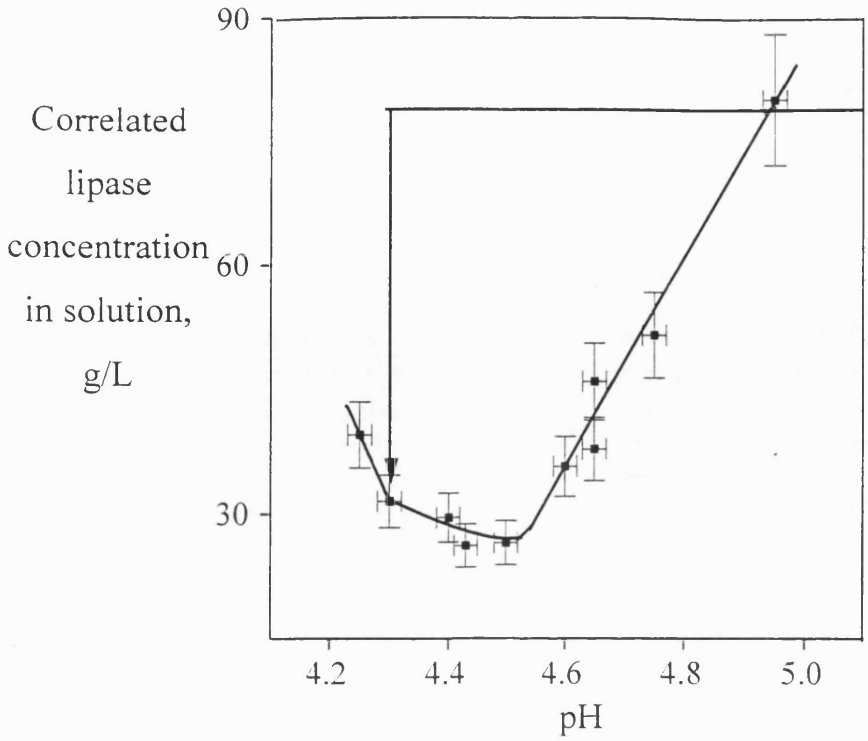

Figure 33. Solubility diagram for lipase protein crystallisation at 28.0± 0.1°C as a function of pH based on crystal volume formed and lipase activity remaining in solution after 24 h. The point of minimum solubility is in the range pH 4.3-4.5 where a yield of (57±4) % based on the activity assay was found. A linear correlation between the volume of crystals formed and the amount of lipase activity removed from the lipase solution was found (data not shown). The error bars indicate a 90 % confidence interval.

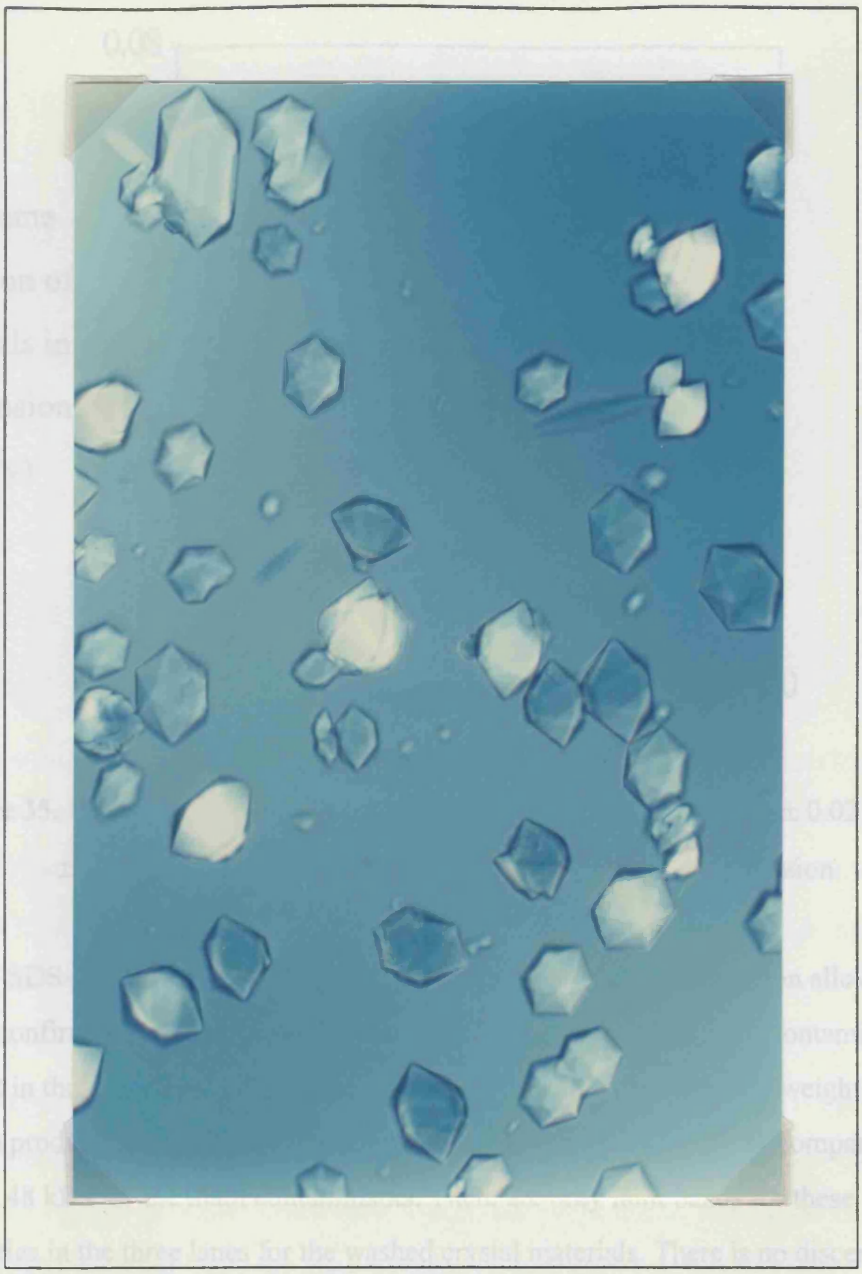

Figure 34. Photo of the crystals formed in the experiments. The crystal are up to 40 μm in size and are hexagonal bipyramids.

Figure 35 shows the change in crystal volume within 24 h and thereby how the process yield changes with time. Some further increase in volume may still be occurring after 24 h but this is considered to be the process limit due to possible long-term instability of the solution used.

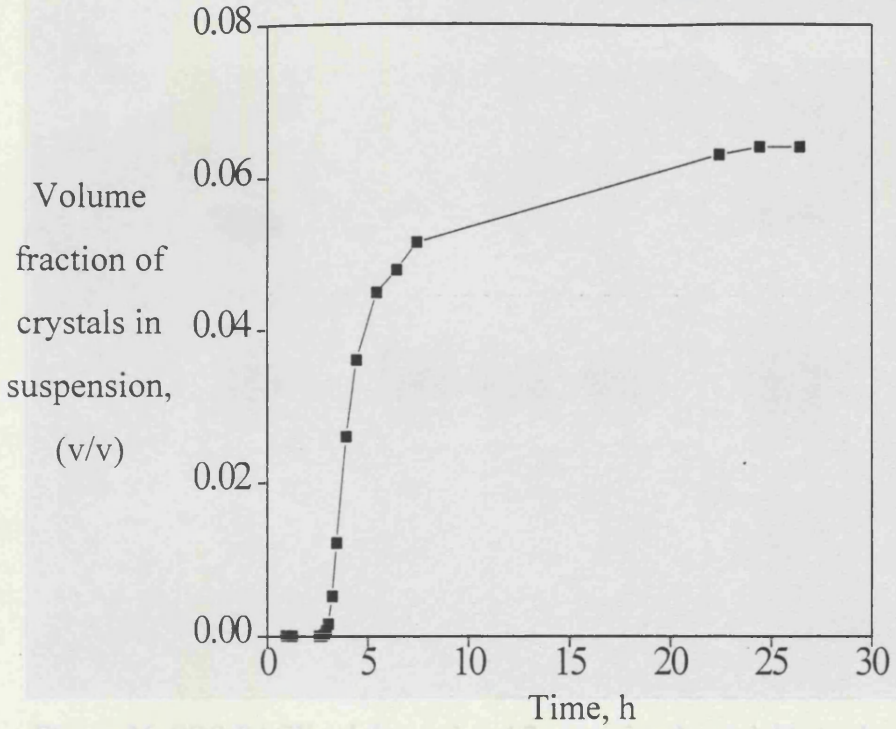

Figure 35. Volume of crystals formed as a function of time at pH 4.30 ± 0.02 and 28.0 ± 0.1°C, calculated by summing over the crystal size distribution.

SDS-PAGE analysis of the feed and products of the crystallisation allowed visual confirmation of the purification process (Figure 36). Two major contaminants are present in the starting material, one larger and one smaller in molecular weight than the protein product. The molecular weight of the product protein is 35 kDa compared with 25 and 48 kDa for the main contaminants. There are only faint bands for these impurities in the three lanes for the washed crystal materials. There is no discernible difference in gel patterns for crystals produced with (lane 4) or without (lane 3 and 5) surfactant present. The loading of the supernatant on the gel is 15 % higher than the loading of the processed fermentation broth so there is a significant decrease in the amount of product in the supernatant while the contaminants are present at the same level.

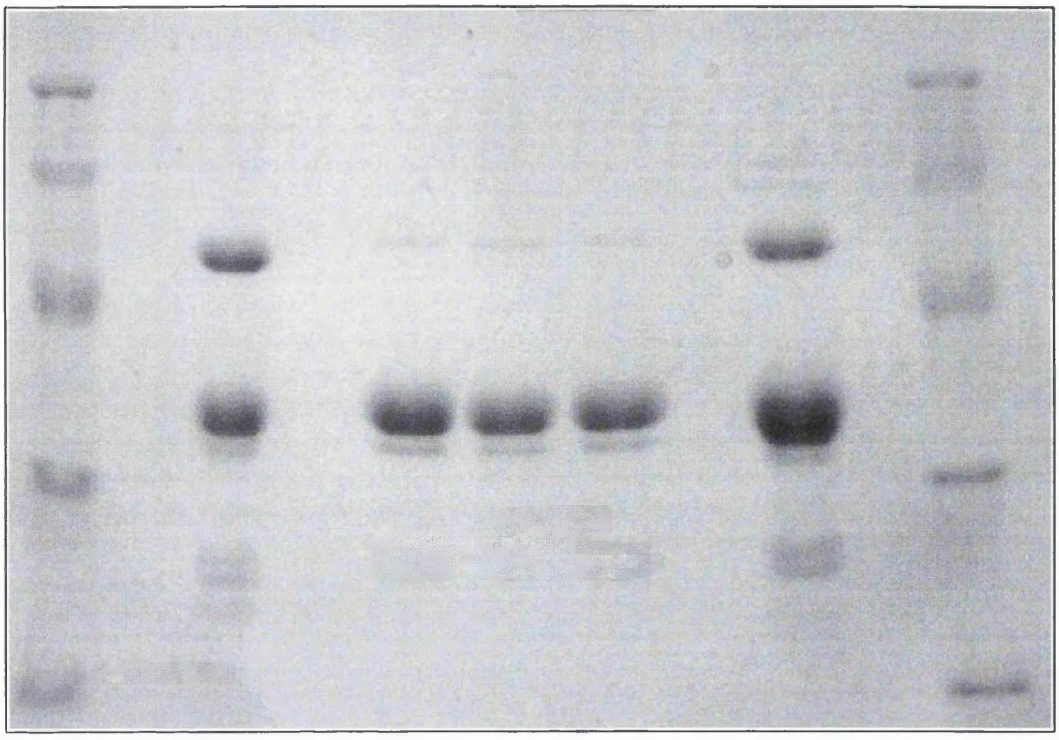

Figure 36. SDS-PAGE gel. Lanes 1 and 7 are molecular weight standards (from top: 97.4, 66.2, 45.0, 31.0 and 21.5 kDa), lane 2 is the supernatant from the end of crystallisation at pH 4.30 ± 0.02 and 28.0 ± 0.1°C, lane 3 is from crystals produced at pH 4.90 ± 0.02, without surfactant and 28.0 ± 0.1°C, lane 4 is from crystals produced at pH 4.30 ± 0.02 and 28.0 ± 0.1°C with surfactant (see materials and methods), lane 5 is from crystals produced at pH 4.30 ± 0.02 and 28.0 ± 0.1°C without surfactant and lane 6 is the processed fermentation broth (feed). All the crystalline material was been washed three times in RO water, each volume of the wash water being the same as that of the original sample of crystal suspension. The crystal preparations were all loaded in the same total volumes while the mass of supernatant loaded was a factor of 1.15 higher than that of the processed fermentation broth. The gel was a 12.5 % SDS-PAGE.

The extent of crystallisation was measured by determining crystal size distributions and number concentrations. A series of crystal size frequency distributions covering the entire process is shown in Figure 37 with the area under the curves being proportional to the volume of crystals. The multiple peaks seen particularly in the late size distributions could be mistaken for measurement noise or statistically insignificant results. They are however an array of narrow sub-populations of crystals the existence of which is confirmed by microscopic examination.

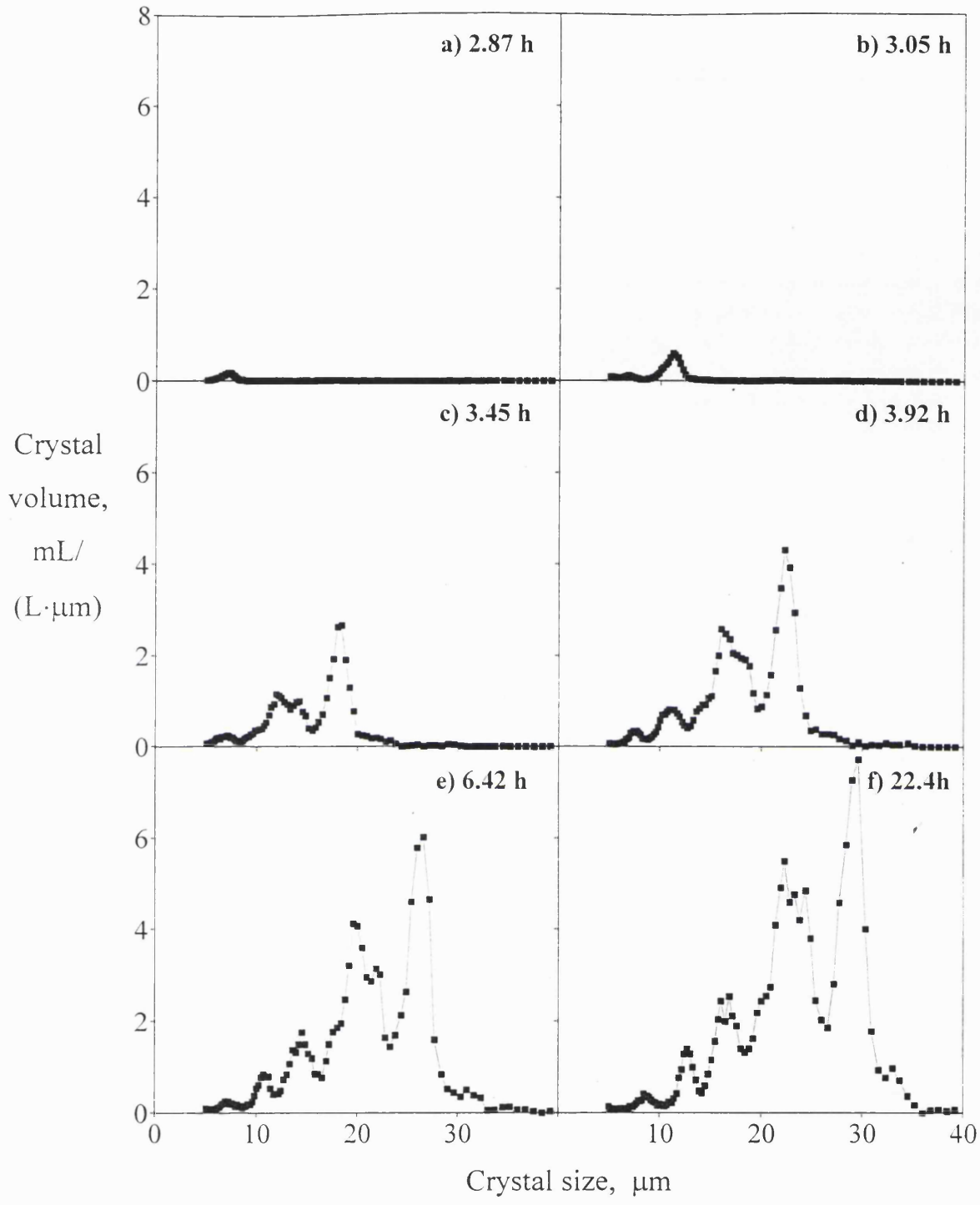

Figure 37. Particle size distributions measured using the electrical sensing zone method for various stages of the crystallisation process. Crystallisation at pH 4.30 ± 0.02 and 28.0 ± 0.1°C. Specific volume concentration plots are such that the area under the curve corresponds to the volume of crystals found in the relevant size range. The unit of the specific volume is mL of crystal volume per L of crystal suspension per μm crystal size.

From the final crystal size distribution it is clear that there are some obstacles to be overcome before the process is attractive for industrial scale operation. The crystal size distribution is wide and of a low average size of 16.2 μm (arithmetic number mean size of crystals in the measuring range: 5-65 μm). The presence of particles smaller than 5 μm was confirmed using laser light diffraction. The crystal size distributions contain a large amount of information and indicates how complex is the crystallisation process. It was decided to quantify the formation and growth of the crystals in terms of nucleation and growth rate and then reduce these to the kinetic parameters as a function of the degree of supersaturation. The results of this analysis are presented in the next section.

6.3 Discussion.

Each set of consecutive crystal size distributions can be reduced to two parameters, nucleation and growth rate using the s-plane analysis discussed earlier (Chapters 1, 2 and 5). The nucleation and growth rates were determined for discrete periods of time (= the time between two samples) and discrete parts of the crystal size range. The estimated values are the average for the time interval between the two samples analysed. Each point in Figure 38 represents such a population balance for a small crystal size range between two samples in the Laplace domain. The growth rate is obtained from the slope of the linear regression line while the ordinate intercept gives the nucleation rate (see Chapter 2). The changes in the growth rate with time are clearly seen in Figure 39. The plots are sufficiently linear to suggest that the assumptions of no crystal breakage and size independent growth are probably valid.

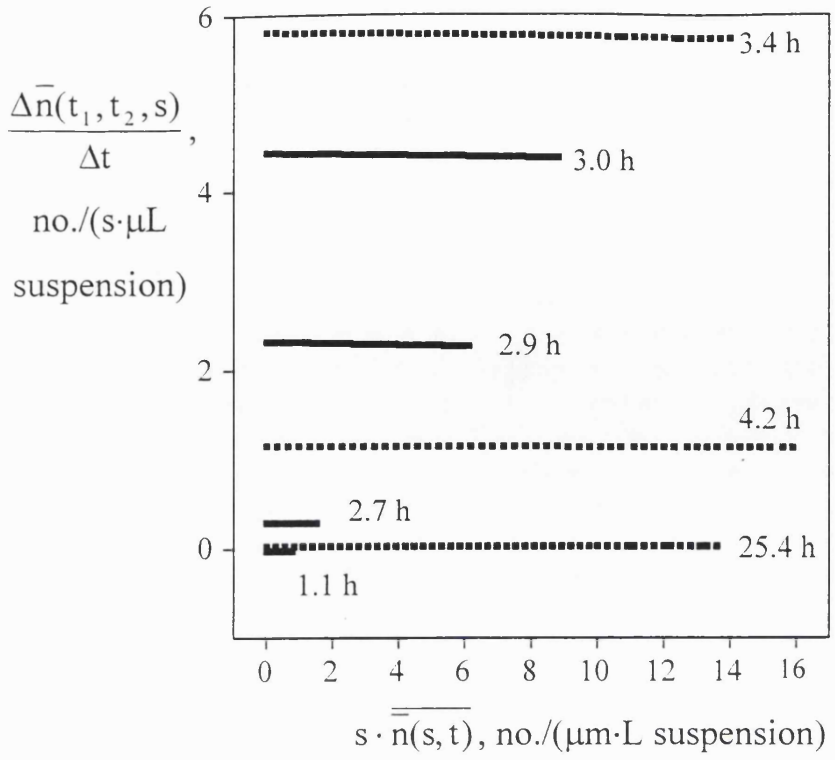

Figure 38. Estimation of nucleation and growth rates using s-plane analysis. Each line is the result of analysis on two consecutive samples. The times shown are the midpoint of the time interval between the two consecutive samples. The slope of the lines gives minus the growth rate while the ordinate intercept gives the nucleation rate.

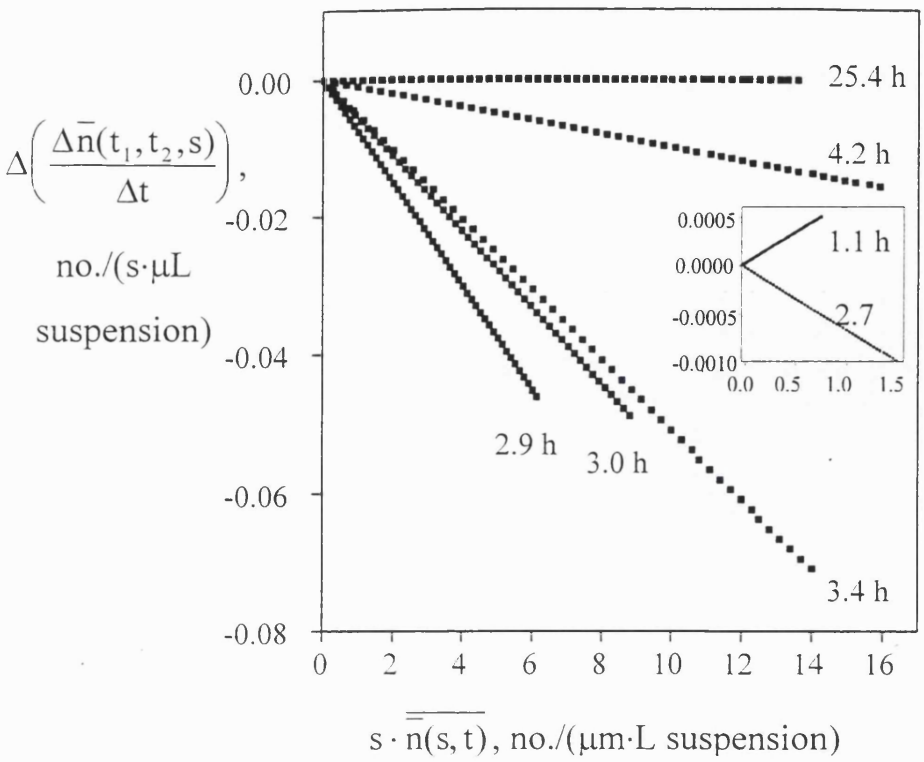

Figure 39. Change in rate for evaluation of growth rates during the crystallisation. A maximum growth rate is observed after about 3 hours.

The resultant nucleation and growth profiles are shown in Figures 40 and 41. The profile of the nucleation rate shows a steep increase and peaks after about 3 h, with a value of 5-6 crystals formed per second per μL suspension, before dropping sharply. The growth rate exhibits almost a step increase when crystallisation starts to a maximum value of 6-8 nm/s. Growth rates of this magnitude are typical for crystallisation of proteins (Pusey and Naumann, 1986; Weber, 1991) and for growth of small molecule crystals (Mullin, 1993; Tavare, 1995). The subsequent simultaneous decrease in nucleation and growth rates is in part the reason for the low average size of the crystals. The time course of the degree of supersaturation is also displayed in Figures 40 and 41 with the nucleation and growth profiles.

As was described in Chapter 5, the kinetic parameters can be estimated from linear least squares fits of the specific nucleation rate and growth rate both as a function of the degree of supersaturation (Figures 42 and 43).

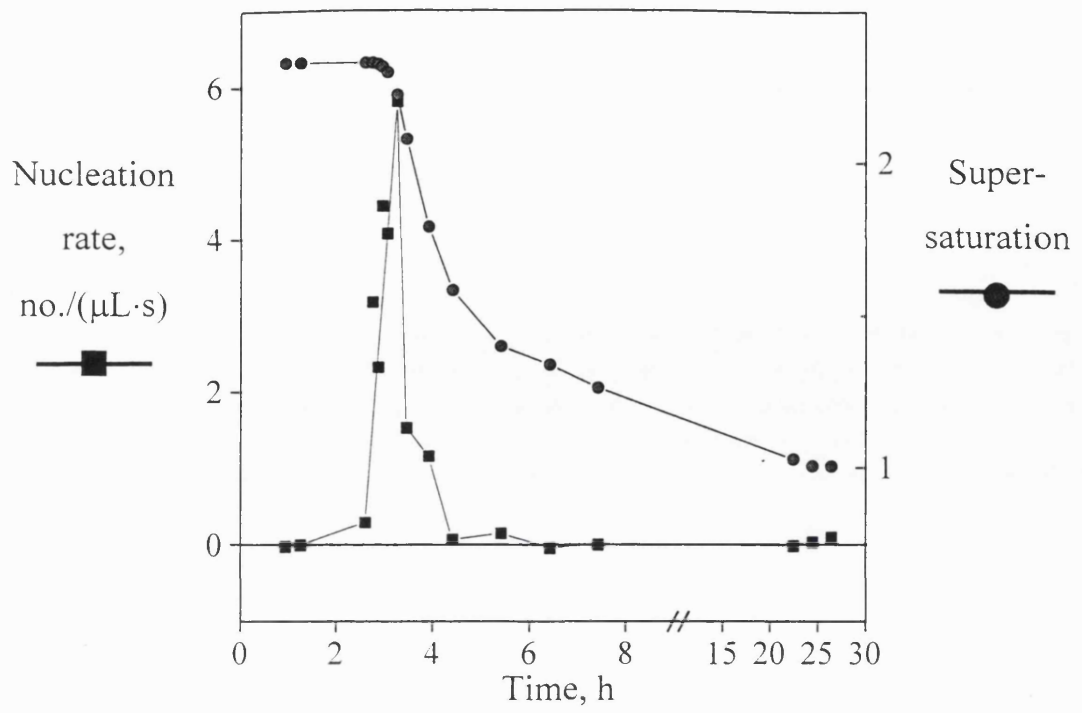

Figure 40. The nucleation rate plotted as a function of the crystallisation time (squares) at pH 4.30 ± 0.02 and 28.0 ± 0.1°C. The nucleation rate is given as number of crystals formed per second per microliter of suspension, and becomes indistinguishable from zero after 6 h. Also shown is the time course of the degree of supersaturation (circles).

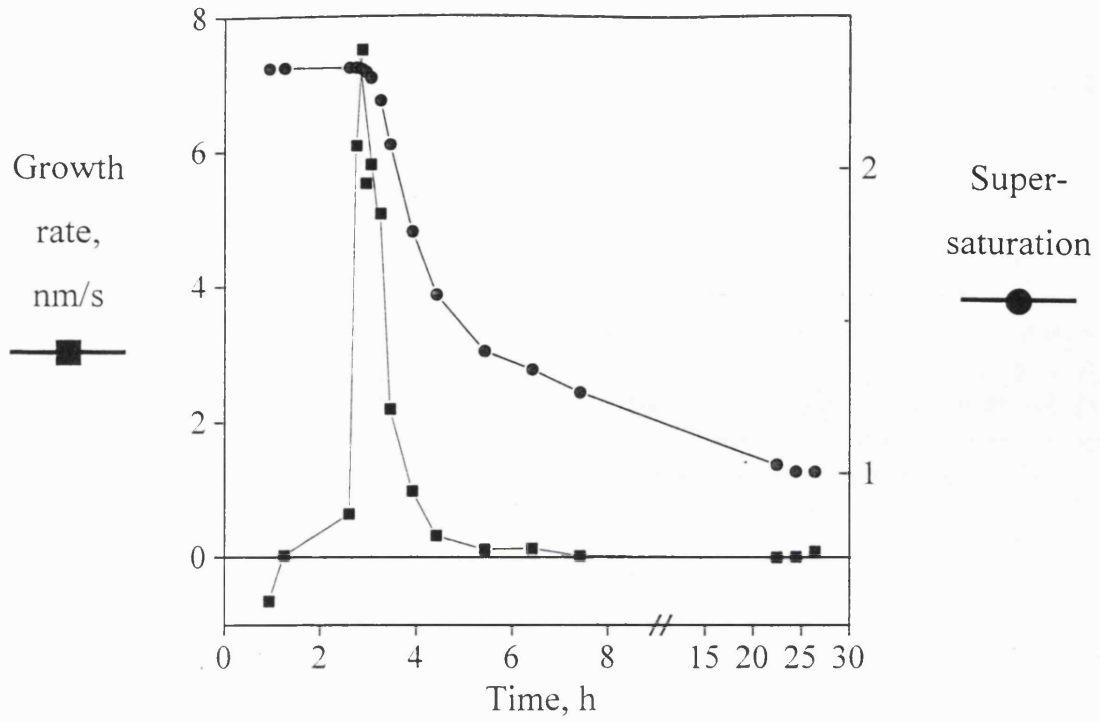

Figure 41. The growth rate plotted as a function of the crystallisation time (squares) at pH 4.30 ± 0.02 and 28.0 ± 0.1°C. The growth rate becomes indistinguishable from zero after 5 h. The early negative estimates of the growth rate are believed to be due to deaggregation of non-crystal particles. The number of these is low and does therefore not affect the later estimates of the crystal growth rate. Also shown is the time course of the degree of supersaturation (circles).

One value only of m has been used to describe the entire crystallisation run. It is however likely that primary nucleation is dominant in the early part of the crystallisation ($m \rightarrow 0$) and secondary nucleation is dominant in the later part ($m \rightarrow 1$). The observed nucleation rate power dependency on the crystal mass concentration of 0.8 ± 0.3 is lower than values often found for industrial inorganic crystallisations where values often approach one (Tavare, 1995). Lower values indicate that a large proportion of the nucleation is primary and is indicative of little crystal breakage; this is confirmed by microscope examination showing little evidence of breakage in the reactor. The power dependency of the nucleation rate on the degree of supersaturation, of 14.5 ± 4.0, is higher than the values of 3-4 often found for inorganic crystallisations. This difference can only be partially explained by the degree of supersaturation possibly being an underestimate of the true value due to the need to limit the experiments to 24 h.

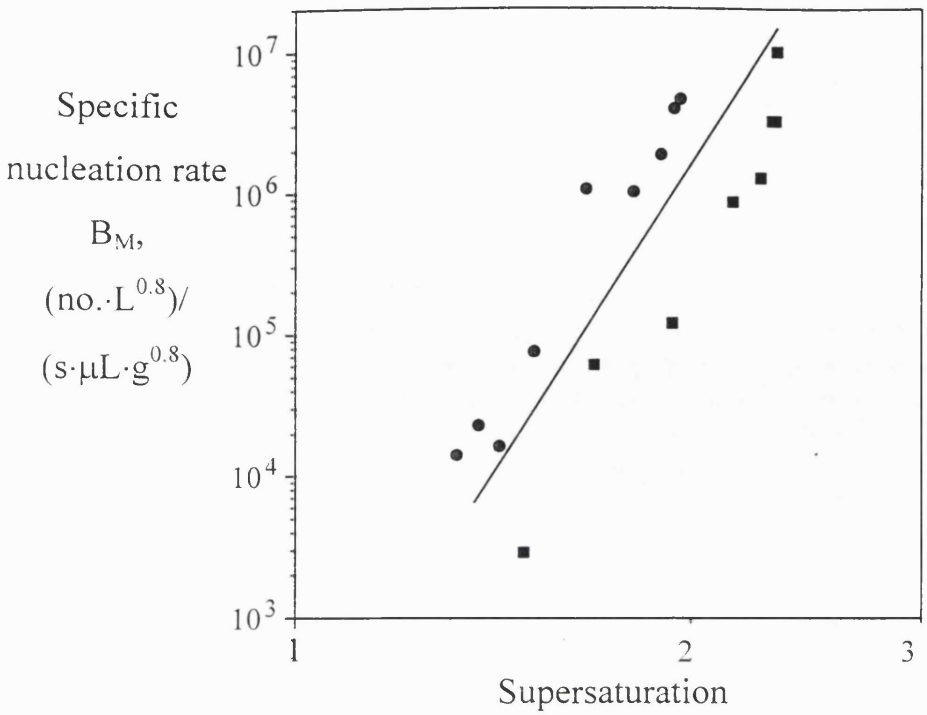

Figure 42. The mass specific nucleation rate plotted as a function of the degree of supersaturation for crystallisation at pH 4.30 ± 0.02 and 28.0 ± 0.1°C. Data points for degrees of supersaturation lower than 1.3 are not plotted because the nucleation has become indistinguishable from zero. Each nucleation rate estimate is plotted at the degree of supersaturation corresponding to the average of the two samples the estimation is based on. The linear regression line shows how well the data fit the chosen kinetic expression and this line can be given by $B = 10^{(1.8\pm1.9)} \cdot M^{(0.8\pm0.3)} \cdot S^{(14.5\pm4.0)}$. Data points; ■, data derived from analysis of Figures 40, ● derived from a duplicate crystallisation experiment.

The growth rate shows a much higher dependency than usual on the degree of supersaturation; this parameter is generally found in the range 1-2 for inorganic crystallisation (Tavare, 1995), while Durbin and Feher (1986) found a value of 2 for the surface of single fixed crystals to be in agreement with that estimated for the growth of suspended ovalbumin crystals (Judge *et al.*, 1995) compared to 8.4 observed in this paper. Such high power dependencies have been found for growth starting at high degrees of supersaturation (Forsythe *et al.*, 1994; Mahajan and Kirwan, 1994; DeMattei and Feigelson, 1989; Durbin and Feher, 1986; Fiddis *et al.*, 1979; Schlichtkrull, 1957d). Again underestimation of the degree of supersaturation only partly explains these high

values and it may be that the growth process is gradually poisoned by contaminating proteins rather than controlled by surface kinetics or the diffusion of the protein to the crystal surface (Weber, 1991). Increases in contaminating proteins has been shown elsewhere not to affect the growth kinetics (Judge *et al.*, 1995). However the system studied here does contain high levels of contaminants compared with most systems reported in the literature. Another possible explanation for the high power dependency is that the growth process proceeds by addition of growth units consisting of several monomers (Pusey, 1991).

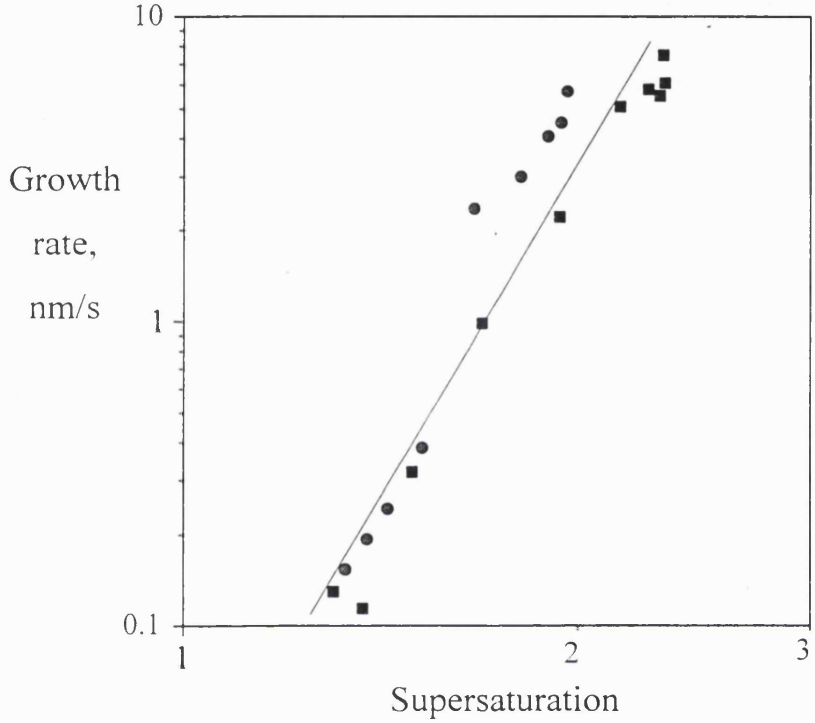

Figure 43. The growth rate plotted as a function of the degree of supersaturation for a crystallisation at pH 4.30 ± 0.02 and 28.0 ± 0.1°C. Data points for degrees of supersaturation lower than 1.3 are not plotted because the growth rate has become indistinguishable from zero. The linear regression line for all the shown data points can be given by: $G = 10^{(-1.9\pm0.5)} \cdot S^{(8.4\pm1.3)}$. Data points; ■, data derived from analysis of Figures 41, ● derived from a duplicate crystallisation experiment.

The nucleation and growth rates observed in this paper are characteristic of a final crystal product with a large number of fines, i.e. the growth and nucleation approaching zero simultaneously. It is the control of this high concentration of fines which will affect the recovery of the crystals and this is the subject of Chapter 8. The

nucleation and growth rates determined may be used to help predict the final size distribution but only based on an actual measure of an early crystal size distribution.

6.4 Conclusion.

Bulk purification of proteins by crystallisation in the presence of impurities has been demonstrated for a fungal lipase enzyme. The nucleation and growth of the lipase crystals have been characterised. A nucleation rate of 5-6 crystals formed in each μL suspension every second and a growth rate of 6-8 nm/s were found under a degree of supersaturation of 2-3. The growth rate power dependency on the degree of supersaturation was around 8.4 ± 1.3 indicating that the growth is probably blocked by contaminating proteins binding to the crystal surface or that crystal growth proceeds via addition of large growth units.

Chapter 7. Micro-environment induced changes in crystal morphology .

7.1 Introduction.

As described earlier, at least two forms of the lipase crystals have been found: diamond and rod. Observations of the effect of surfactants and the coating of the impeller were that they could determine the morphology. This chapter explores these effects trying to gain some understanding of the environmental influences the crystal morphology.

7.2 Results.

Three different batches of clarified fermentation broth were used and Table 6 summarises the results of the experiments.

batch	repeats	exp. no.	coated	'Tween'80	Brij-35	habit
1	3	1	no	no	no	rod
1	3	2	yes	no	no	rod
1	3	3	no	yes	no	diamond
1	4	4	yes	yes	no	diamond
1	2	5	no	no	yes	rod
2	7	6	no	no	no	dia.+rod
2	1	7	yes	no	no	diamond
2	1	8	yes	no	yes	diamond
2	2	9	no	no	yes	diamond
2	1	10	no	yes	no	diamond
3	1	11	no	no	no	dia.+ rod
3	1	12	no	no	no	rod + dia.

Table 6. Experimental outline. All experiments were run as un-seeded batch crystallisations, except exp 12 which was seeded with a small volume of diamond and rod-shaped crystals and conducted with a pH ramp from 5.1 to 4.3 over 1000 mins.

As outlined in Table 6, five types of experiments were conducted with the first batch. Crystallisation with no added surfactant and using an uncoated impeller (exp 1) yielded thin rod-shaped crystals with a crystal size distribution as shown in Figure 44.1. Coating the impeller (made of stainless steel and the only non-glass material in contact

with the crystallisation) with a polymeric material also resulted in rod-shaped crystals but of a broader crystal size distribution (Figure 44.2). Addition of surfactant caused the formation of diamond-shape crystals whether using coated or uncoated impeller, although quite different crystal size distributions resulted (Figure 44.3 and Figure 44.4, respectively).

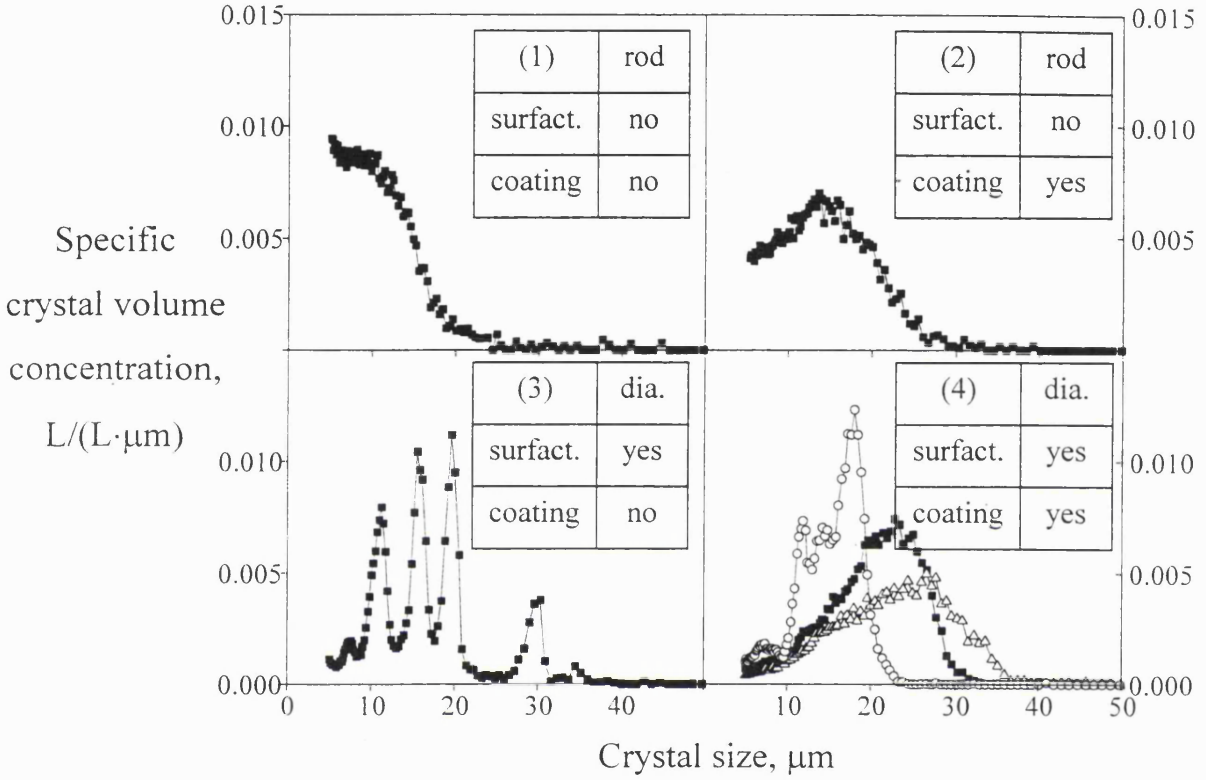

Figure 44. Size distributions measured after 22 h crystallisation for exp 1-4, Table 6. Several repetitive experiments are shown in sub-plot 4 because of problems in reproducing the experiment. Exp 1 and 2 yielded rod-shaped crystal while exp 3 and 4 gave diamond-shaped crystals (dia.).

Figures 45-46 give the corresponding nucleation and growth rate profiles plotted as a function of the crystallisation time. Comparing Figures 45.1 and 45.2, and Figures 46.1 and 46.2 strongly suggests that coating of the impeller had a significant effect on the nucleation and growth rate of the rod-shaped crystals. The time required for the crystallisation to be noticeable was doubled and the maximum nucleation rate was decreased.

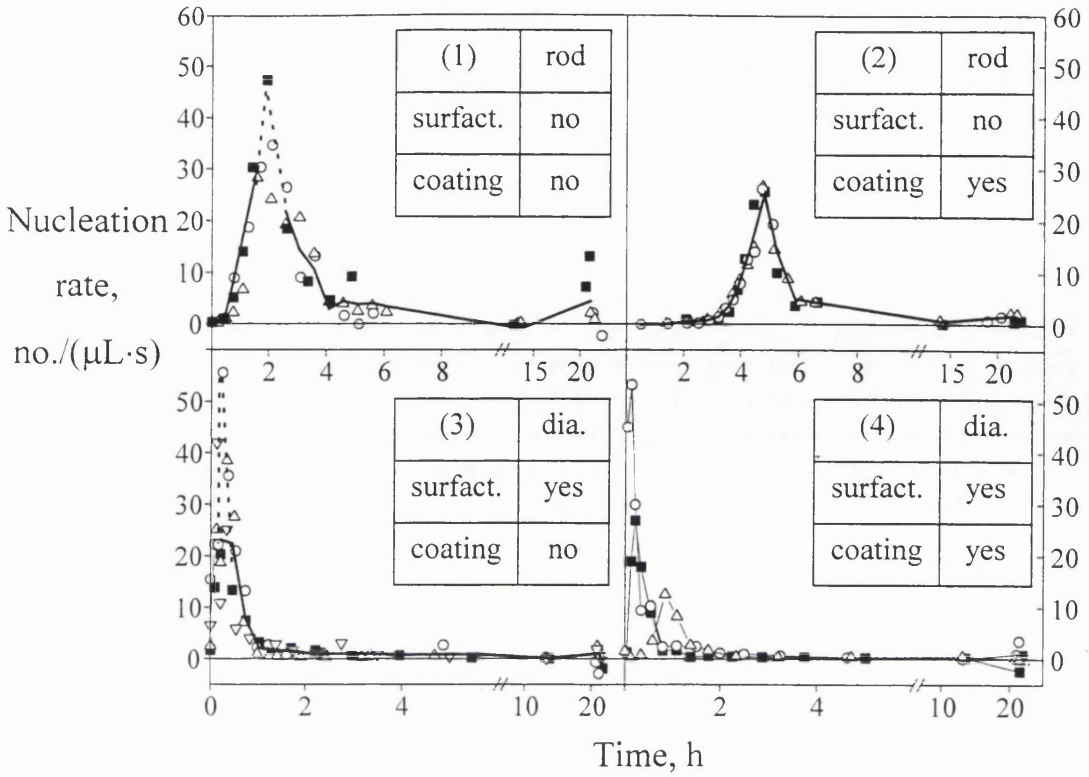

Figure 45. Nucleation rate profiles for experiments 1-4, Table 6. Note that the time axis is different between the first and second row. The thick line in sub-plots 1-3 represents an average of the repeats. The symbols links to repeats of the experiments and is the same as in Figure 46. A dashed line indicates less confidence.

The presence of a surfactant ('Tween'80) changed the morphology of the resulting crystals from rod to diamond-shaped. The mode of nucleation for the two crystal forms is different. The nucleation of rod-shaped crystals lasted more than 4 hours while for the diamond-shaped crystals the nucleation finished within 1 h. The growth rate of the diamond-shaped crystals was initially much faster than for the rod-shaped crystals, 15-20 nm/s and 2 nm/s respectively. After only 1 hour, the diamond-shaped crystals appear to have almost completely stopped growing, while the rod-shaped crystals grew for 4 h. The rod-shaped crystals grew almost exclusively at the two ends giving a relatively small area for growth. The changes in the volume equivalent spherical diameters (as estimated by the electrical sensing zone method) may therefore not change very quickly. This can at least partly explain the much lower growth rate observed for the rod-shaped crystals.

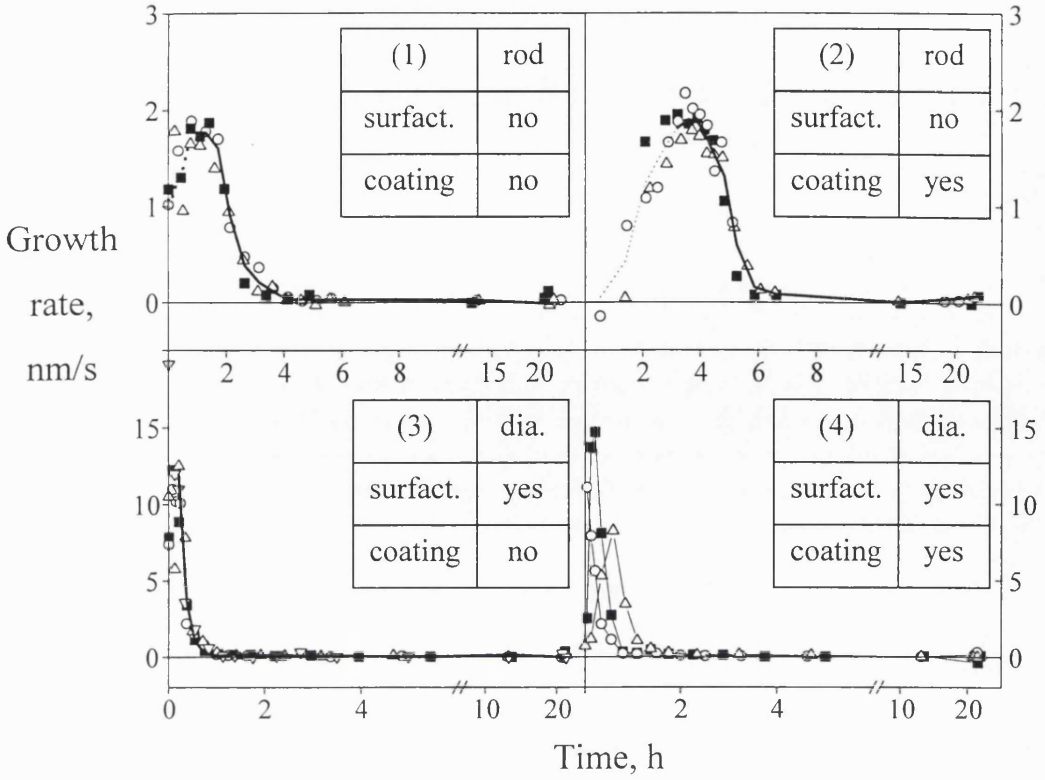

Figure 46. Growth rate profiles for experiments 1-4, Table 6. Note that the time axis is different between the first and second row. The thick line in sub-plots 1-3 represents an average of the repeats. The symbols links to repeats of the experiments and is the same as in Figure 45. A dashed line indicates less confidence.

For diamond-shaped crystals the only significant trend observed in coating the impeller is a slightly longer growth time. It is interesting to match the nucleation and growth curves with the resulting crystal size distributions. As can be seen, high initial nucleation and growth rates give a narrow distribution of small crystals, while low nucleation and growth rates link to a wide crystal size distribution of large crystals.

To verify the observed effects of surfactant or the coating of the impeller, a few experiments were conducted on the second batch of crystallising material. Though produced in the same way, this second batch yielded a mixture of the two crystal forms. The diamond-shaped crystals formed first, followed by the rod-shaped crystals a few hours later. Coating the impeller (exp 7) delayed the formation of the rod-shaped crystals. Addition of surfactant caused a morphological change to diamond-shaped crystals. Again the characteristic multimodal crystal size distribution was found (Figure 47).

Finally two experiments were done on the third batch. An unmodified crystallisation (exp 11) gave results similar to the second batch, i.e. first the formation of the diamond-shaped crystals, followed by the formation of rod-shaped crystals. The opposite occurred when seeding was done at high pH, followed by slow generation of supersaturation. Rod-shaped crystals formed first, followed by diamond-shaped crystals after 19 h. In Figures 48 and 49, the crystal number and volume concentration as a function of crystallisation time are compared for the two experiments. It is noticed that the nucleation of diamond-shaped crystals stopped between 4 and 8 h and is then followed by the nucleation of rod-shaped crystals. The same was not seen in the volume concentration plot indicating that nucleation stopped at 4 h but growth continued. Photographic evidence for the observations in exp 11 and 12 are shown in Figure 50.

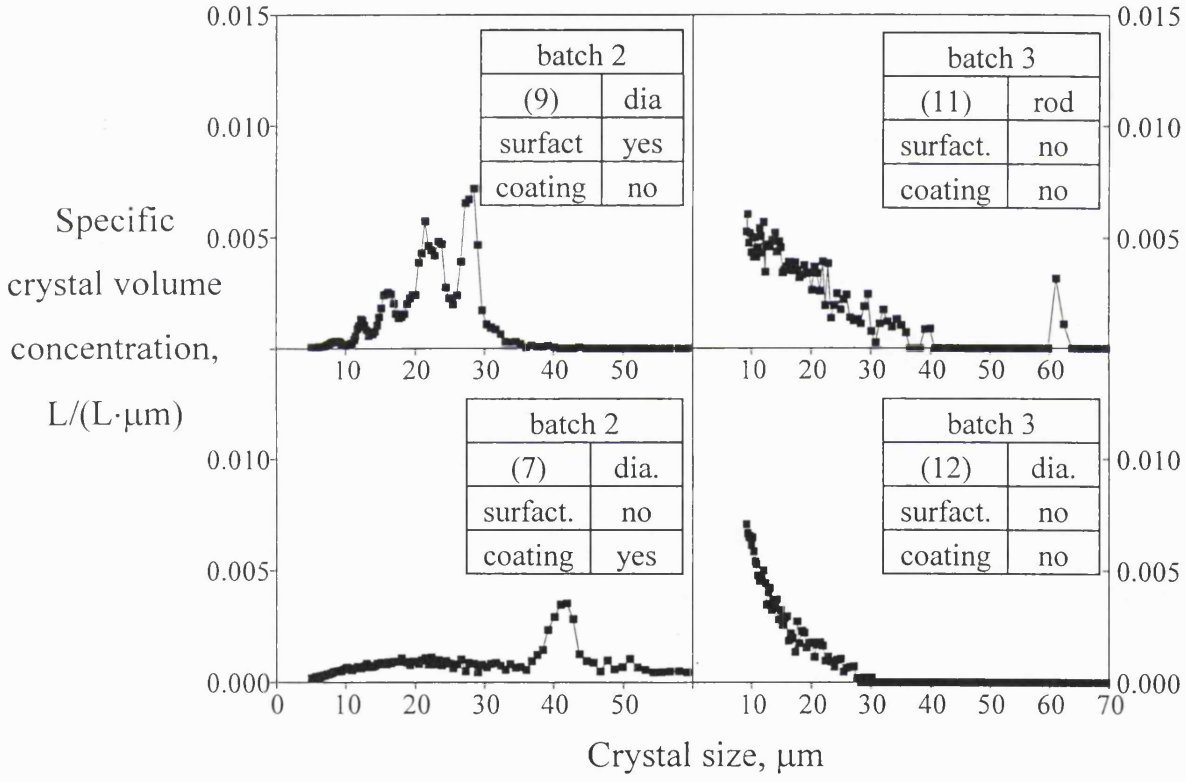

Figure 47. Size distributions measured after 22 h crystallisation. Note that the size axis is different in the two columns. The number given in brackets is the experiment number.

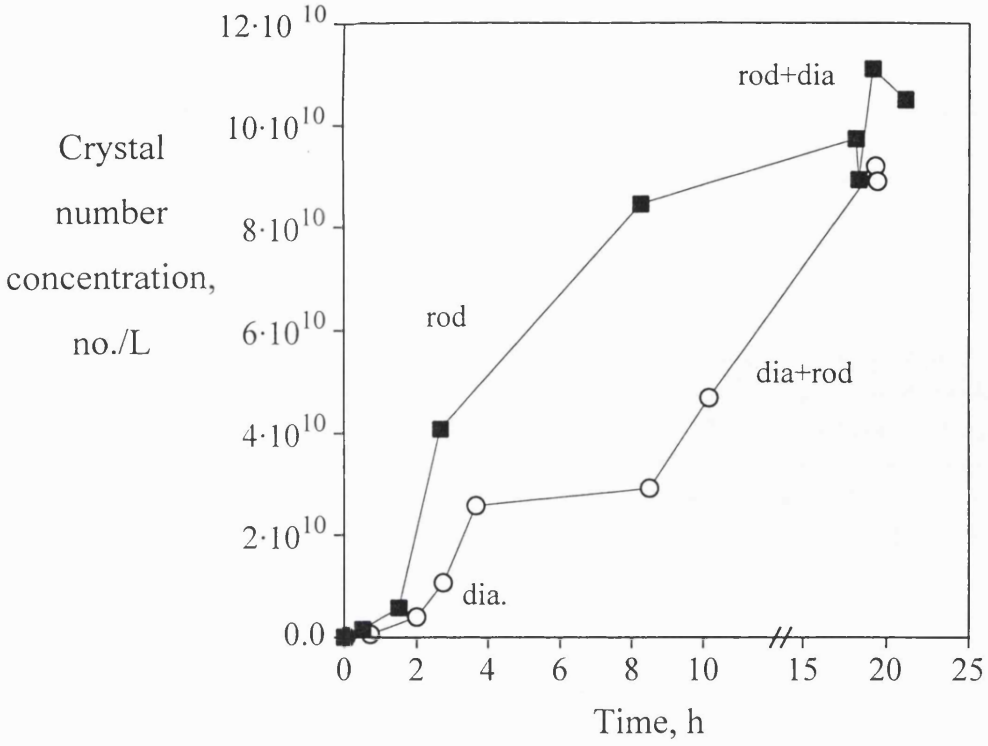

Figure 48. Crystal number concentration plotted as a function of time for batch 3, uncoated with no added surfactant. Constant pH crystallisation (exp 11, O) and pH ramping (exp 12, ■).

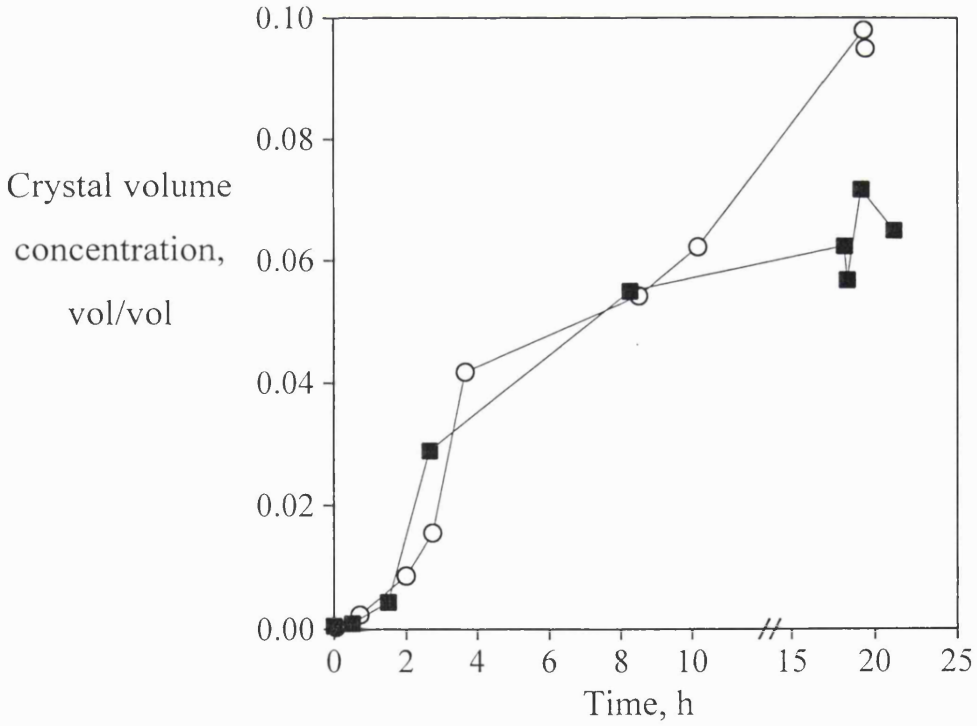

Figure 49. Crystal volume concentration plotted as a function of time for batch 3, uncoated and no added surfactant. Constant pH crystallisation (exp 11, O) and pH ramping (exp 12, ■).

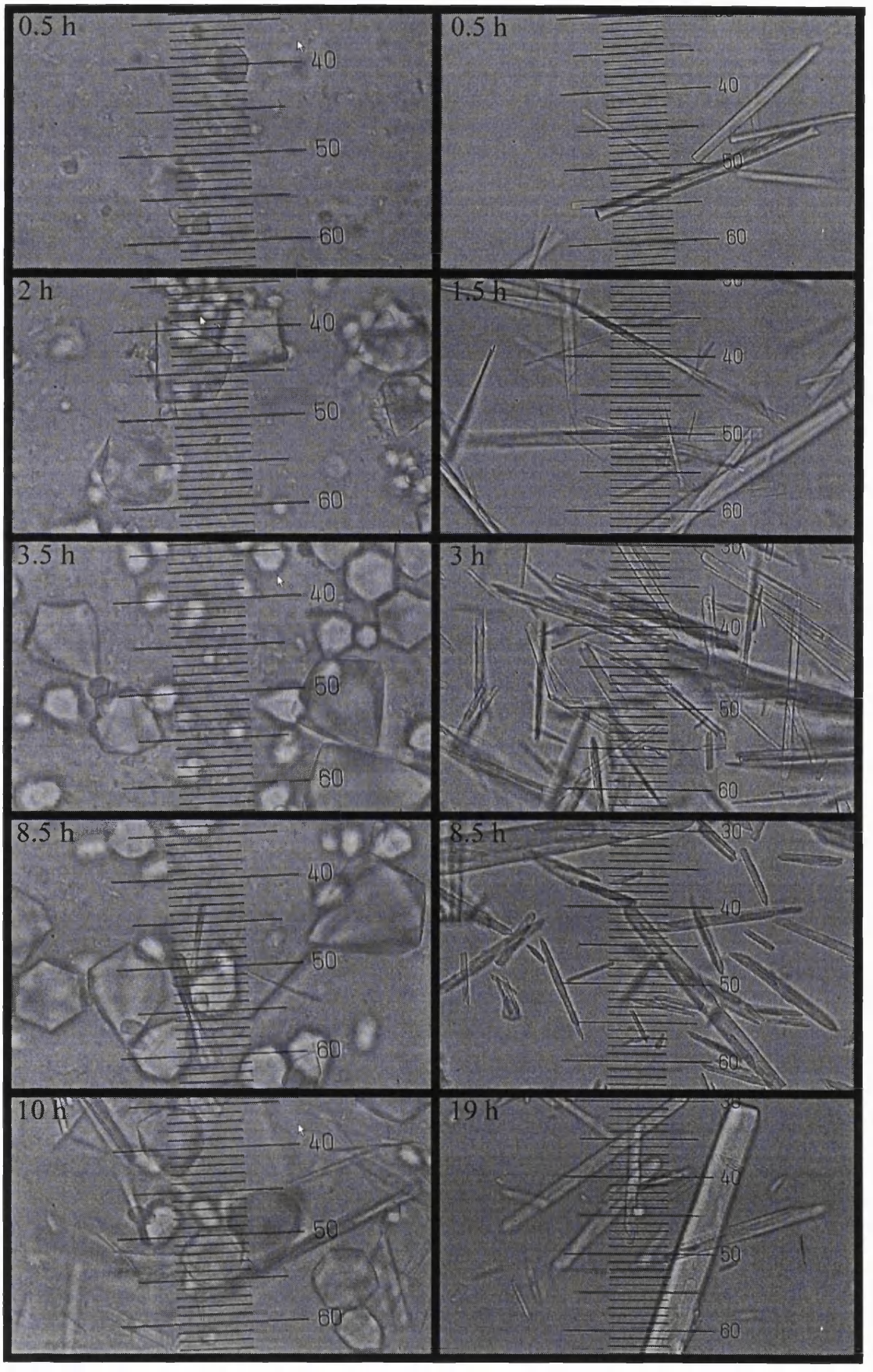
0.5 h
40
50
60
0.5 h
40
50
60
2 h
40
50
60
1.5 h
40
50
60
3.5 h
40
50
60
3 h
40
50
60
8.5 h
40
50
60
8.5 h
40
50
60
10 h
40
50
60
19 h
40
50
60

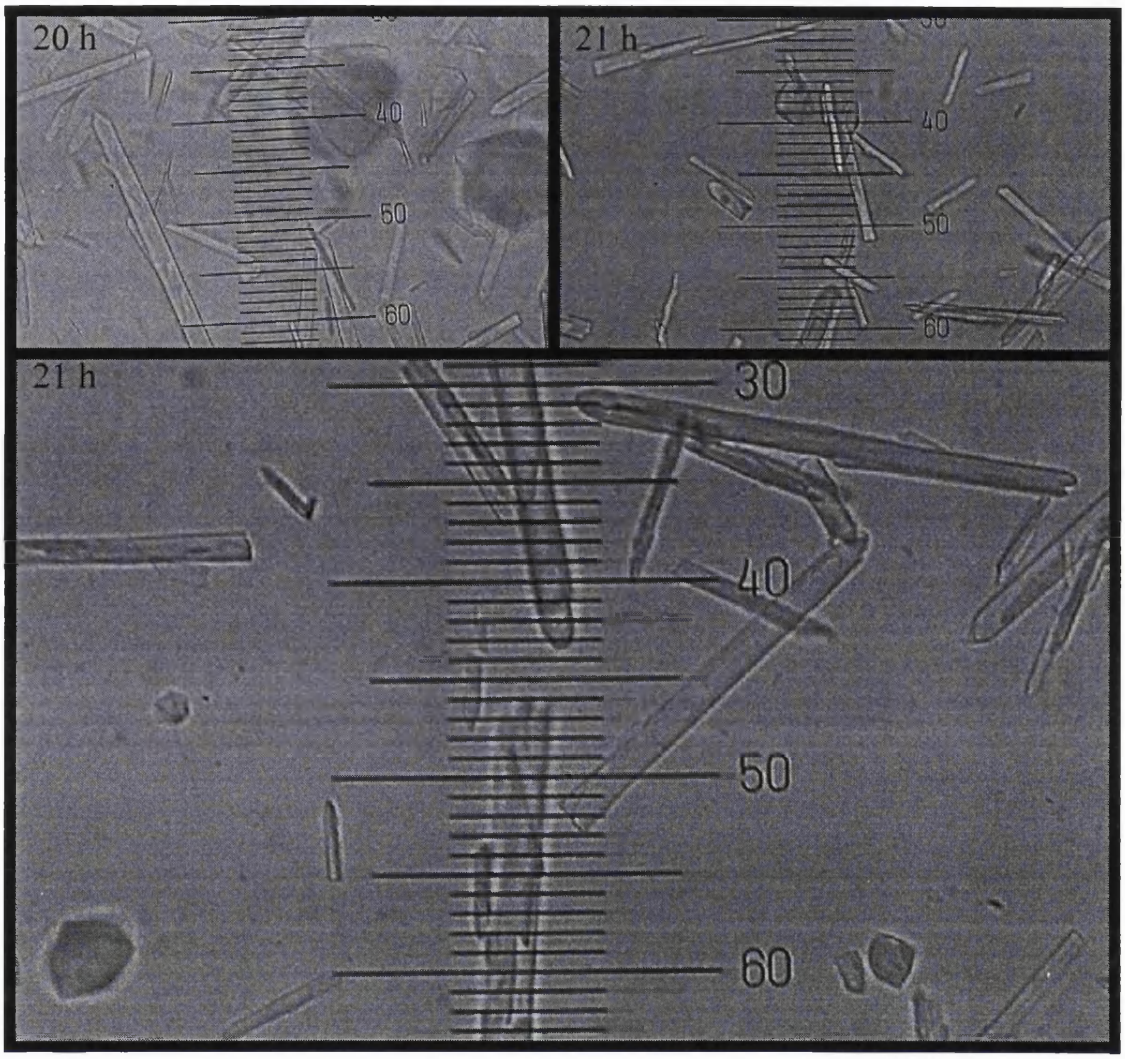

Figure 50. Changes in crystal form during a batch (exp 11, left column) and pH ramping (exp 12, right column) experiment (400 times magnification). Samples of rod-shaped crystals taken after 9 h have been diluted in supernatant. The distance between the small bars is 2.5 μm. The large image at the end is taken at the end of the pH ramping experiment.

Further characterisation of the experiments was achieved by combining the nucleation and growth rate profiles with the corresponding degree of supersaturation (see Chapter 5). The resulting kinetic parameters are given in Table 7.

Exp. no.	d_v (μm)	m (-)	b (-)	k_b[(a)]	g (-)	k_g (nm/s)
1	11±1	1.1±0.3	3.1±0.7	$10^{4.2 \pm 3.7}$	2.6±0.3	$10^{-1.5 \pm 0.3}$
2[(b)]	15±2	1.8±0.6	6.6±1.5	$10^{2.1 \pm 1.8}$	3.7±0.3	$10^{-1.6 \pm 0.3}$
3	20±2	1.3±0.4	8.5±1.7	$10^{1.0 \pm 0.8}$	6.1±0.7	$10^{-2.8 \pm 0.6}$
4[(c)] (○/■/▲)	15/20/23	0.7/0.9/0.8	9/8/8	$10^{2.6/0.5/1.1}$	8/6/6	$10^{-3.0/-3.4/-2.5}$
6	19±2					
7	36±11	0.9±0.3	10±4	$10^{2.5+/-3.8}$	5±1	$10^{-1.5+/-0.6}$
9	21±3	0.8±0.3	15±4	$10^{1.8+/-1.9}$	8±1	$10^{-1.9+/-0.5}$

Table 7. Estimated kinetic parameters according to the procedure described in Chapter 5. The experimental conditions are given in Table 6. d_V is the average volumetric size of the crystals larger than 5 μm. The results are given with a 95 % interval of confidence. (a) the unit of k_B is $(\text{no.}/L_{suspension})\cdot(L_{suspension}/g_{crystal})^m$), (b) for exp 2 only data points from 3 hours crystallisation time and onwards were used for the estimation. (c) for exp 4 the estimated kinetics parameters are given for each of the repeats.

7.3 Discussion.

It is necessary to understand the interplay between the two observed morphologies before discussing the kinetic data estimated in this work. Therefore first the batches producing a mixture of the two crystals forms will be discussed, followed by an examination of the effect of surfactants and impeller coating. The interplay between the two crystals forms was explored using two common ways of understanding crystallisation; Ostwald's rule of stages and growth cessation. It is argued that none of these can explain the lipase system. Size dependent growth and dendrite formation lead to the suggestion that the crystal growth was diffusion controlled. With the use of acid addition profiles, nucleation pulsing and solubility diagrams for the two crystal forms, a diffusion model was developed which can fully explain the observations made.

7.3.1 Ostwald's rule of stages.

Systems forming mixtures of crystal forms are often explained using Ostwald's rule of stages, that is metastable crystal morphologies forming first followed by a

transition to a more stable crystal form (Garti and Zour, 1997; Kabasci et al., 1996; Tavare, 1995). For glutamic acid crystallisation, Garti and Zour (1997) observed a change in morphology from a bulky to needle-like crystal form. This transition could be delayed by the addition of a surfactant. The bulky habit had the higher solubility. The effect of the surfactant was explained as being a specific binding to the crystal surface of the metastable (bulky) form. This delays the induction of the more stable (needle) crystal form and was thought to be due to nucleation becoming more homogeneous rather than heterogeneous in character.

This would suggest that for the lipase, the diamond morphology is the metastable form and the effect of surfactant is to delay the formation of the rod-shaped crystals due to its binding to the diamond-shaped crystals. This explanation is not thought to describe the data presented in this work for two reasons. Firstly, the ramping experiment yielded diamond-shaped crystals after the rod-shaped crystals (exp 12). Secondly, when rod-shaped crystals form after diamond-shaped crystals, the diamond-shaped-crystals are not reduced in size and there is no evidence of dissolution (when viewed in the microscope). It seems that the diamond-shaped crystals had the same or lower solubility than the rod-shaped crystals, but almost stopped growing in supersaturated solution.

7.3.2 Grow cessation.

Growth cessation in supersaturated solution has been observed previously (Kam *et al.,* 1978) and has been explained in a number of ways. One is that the crystals will only grow to a certain size at which the number of incorporated mistakes in the crystal lattice is so high that further growth is impossible. This cannot explain the data shown here, because when the crystals are seeded to a fresh solution (as the one they originally grew from) then the growth kinetics for the seed crystals have been observed to be even faster than for the newly nucleated crystals (see Figure 51). A strong and irreversible binding of impurities (growth poisoning) seems necessary for explaining the sharp drop in crystal growth rate in highly supersaturated solution. However this would be in contradiction to the fact that seed crystals continue to grow after being seeded to a fresh solution. Since the state of the crystal surface itself does not seem to provide an explanation for the observed kinetics and neither do the traditional models for incorporation controlled crystal growth, it may be useful to focus on properties of the solution near the crystal surface.

7.3.2 The existence of a diffusion layer.

Diffusion layers have been experimentally observed using light techniques to measure the protein concentration near the growing crystal surface (Miyashita *et al.*, 1994; Azuma *et al.*, 1989; Boistelle and Astier, 1988; Kam *et al.*, 1978).

The experimental data supporting the existence of the diffusion layer are shown in Figure 51 where it is demonstrated that larger crystals grew faster than smaller ones in the same bulk solution, i.e. the size gap between them will widen during crystallisation. Size dependent solubility (the Gibbs-Thomson's effects) could be the reason, but it is more commonly linked to diffusion controlled crystal growth. Larger crystals grow faster because convection will reduce the thickness of their diffusion layer due to larger momentum of the crystals.

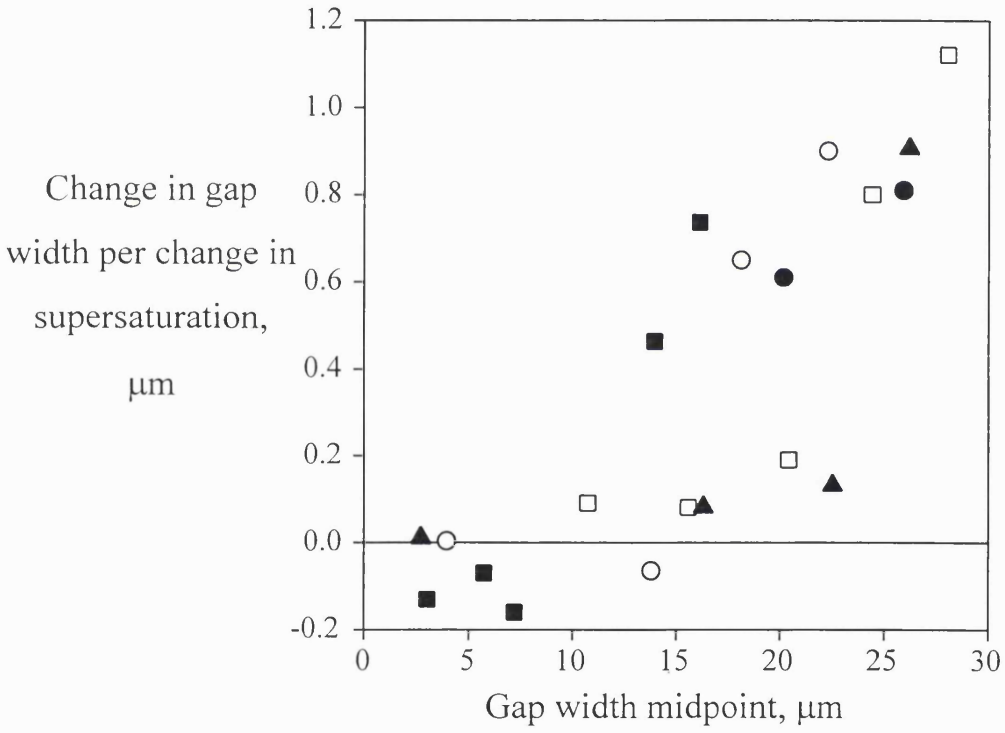

Figure 51. The change in the width of the gap between peaks per change in supersaturation plotted as a function of the gap width. The change in gap width has been divided with the change in supersaturation rather than time since growth links closer to supersaturation. All the gap widths given are between the first peak formed and later peaks. Every symbol links to one of the repeats of exp 3, except the experiment marked with (●) which was started with 2 % (vol./vol.) seeds allowing comparison of seed crystal growth to that of newly formed crystals.

One question is why the rod crystal form at all in the presence of a large excess of a more stable (i.e. lower solubility) crystal form. The most obvious suggestion is dendrite crystal growth due to the shape. Dendrites only form in the presence of (strong) supersaturation gradients radiating out from the crystal surface as observed by Azuma *et al.* (1898) and Boistelle and Astier (1988). The existence of a diffusion layer cannot be explained by Fick's law of diffusion (Grant and Saville, 1991). So the diffusion layer must have another nature.

7.3.3 Nernst-Planck diffusion.

When charged molecules migrate, the zero-current constraint will cause coupled diffusion of other charge molecules present in solution. The effects of this phenomenon is significant at low salt concentration (Hu *et al.*, 1992). In this section, it is first argued that hydrogen ions are released during crystal growth, inducing a pH instability near the crystal surface resulting in the generation of a micro-environment.

In the present study, the crystallisation is conducted at low conductivity at the isoelectric pH, i.e. the crystallising protein is not expected to carry any net-charge at bulk conditions. This may however not be the case near the crystal surface. The incorporation of the molecules in the crystal lattice is expected to liberate some hydrogen ions (Monaco and Rosenberger, 1993). Experimental confirmation was given by DeMattei and Feigelson (1991). This is also suggested in Figure 52, where acid was observed to be liberated during rapid crystallisation making it unnecessary to add acid to maintain a constant pH.

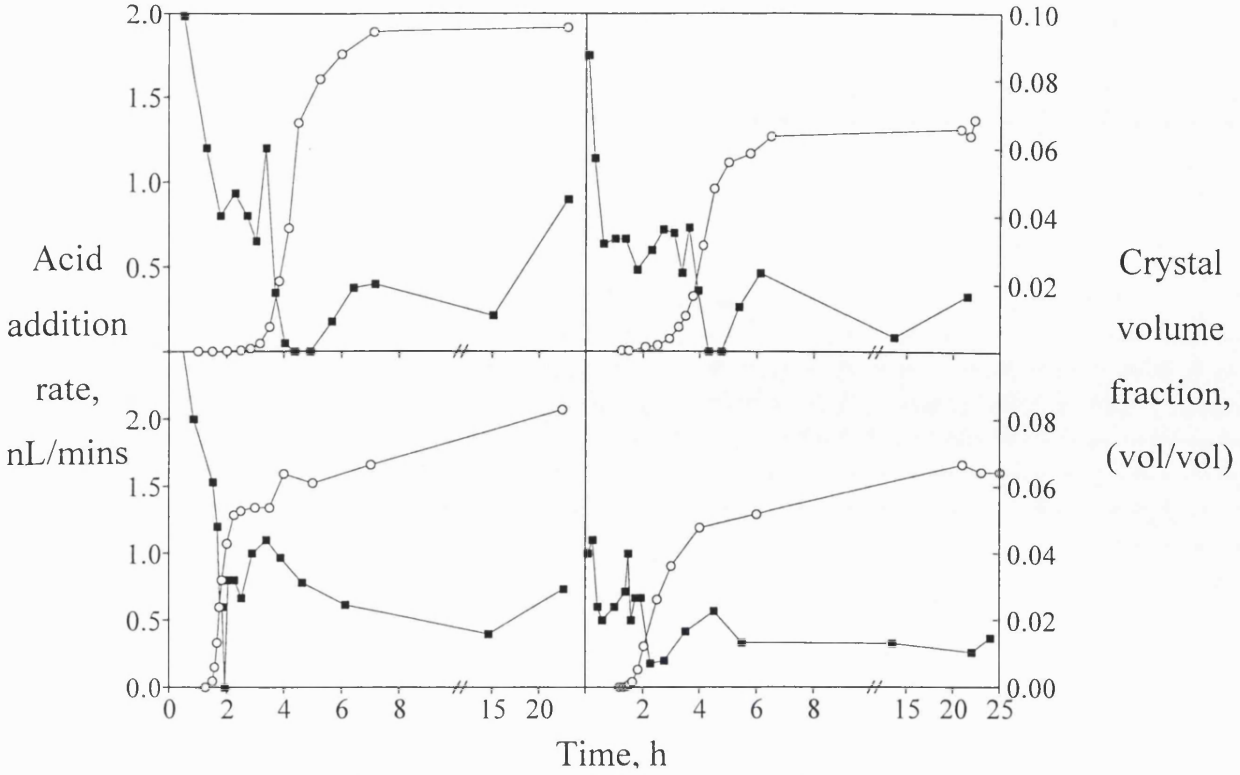

Figure 52. Acid addition rate profiles (■) for exp 1, 2, 3 and 9. Also shown are the curves for the total crystal volume concentration (O). The acid consumption was believed to be due to the liberation of carbon dioxide to the air and/or a result of protease activity. During rapid growth, liberation of hydrogen ions causes the required acid addition rate for pH control to drop (often to zero for 1/2 -1 h).

In the micro-environment near the crystal surface, pH may therefore be lower than in the bulk of the solution, making the crystallising protein molecules carry a net positive charge. Such diffusion in a low conductivity media will couple to a counter-diffusion of positive charges to satisfy the zero current constraint. Since the system has low pH and salt concentration, hydrogen ions are likely to be forced to counter-diffuse. The resulting pH at the interface will therefore depend on the balance between generation and removal of hydrogen ions. There two are indications that pH in this system goes above pI of the crystallising protein. The rod-shaped crystals form much more readily at higher pH (Figure 53). So either the observed rod-shaped crystals are formed as dendrites or because the higher pH at the interface promotes the formation of rod-shaped crystals. Both understandings support the idea of a micro-environment near the growing crystal surface with conditions different to those of the bulk solution. Further support for a pH increase after the initial decrease is the pulsing nucleation pattern. The solubility curve

for the diamond-shaped crystal displays a narrow minimum at pH 4.3-5.0 (Figure 53), so during the pH increase, the condition near the crystal surface will for a short period be highly supersaturated and a pulse in the nucleation will result. The same type of pulses can be generated by seeding a highly supersaturated solution with non-growing crystals. For tight size distributions, this pulse will occur at a certain size resulting in a second narrow peak of crystals.

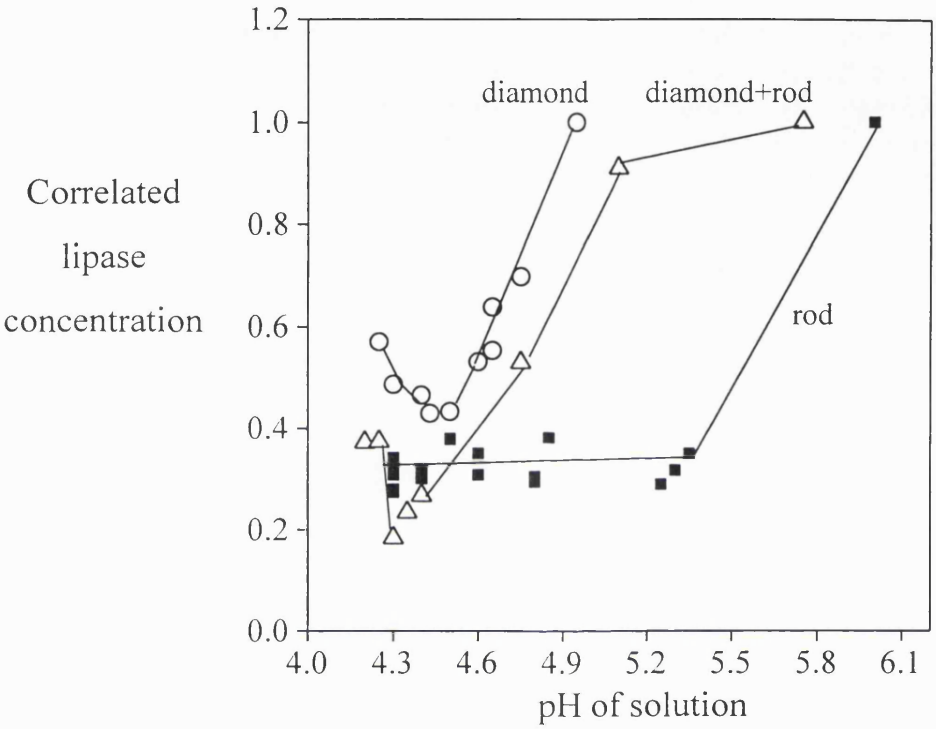

Figure 53. Apparent solubility diagram. (O) exp 9 - just diamond-shaped crystals, (Δ) exp 7 - both rod and diamond-shaped crystals and (■) exp 11 - just rod-shaped crystals.

It could be argued that the suggested pH increase will stop the coupled diffusion of hydrogen ions. This is probably true for the zone very near to the crystal surface but the produced hydrogen ions will have to diffuse to the bulk of the solution. A second layer outside the layer of high pH will therefore have a lower pH than the pI and hence still drive the coupled diffusion of hydrogen ions.

The above hypothesis is somewhat speculative and other ways of explaining the results may exist. For example, the two crystal forms may grow by the addition of different types of precursors in equilibrium with each other (e.g. monomers, dimers, etc. (Wilson *et al.*, 1993; Kadima *et al.*, 1990). The precursors for rod-shaped crystals may be favoured by conditions of high pH (4.5-6.0) and diamond-shaped crystals by the

presence of surfactants and perhaps lower pH. The nucleation and growth kinetics could then be explained by a slow conversion of inactive to active precursors. It is however difficult to explain the size dependent growth observed and the pulsing nature of the nucleation.

In summary, the results presented indicate that the crystallisation is controlled by a Nernst-Planck diffusion layer. Rapid crystal growth generates a micro-environment near the crystal surface which promotes the formation of the diffusion layer. The interplay between the crystal forms, growth cessation and the pulsing mode of nucleation were hereby explained.

7.3.3 Effect of coating and surfactant.

This understanding can be used to explain the observations in exp 1-4 (Table 6). The observed boundary between the regions of diamond and rod-shaped crystals has been observed to move to a higher pH by the addition of surfactant in all batches. The binding of surfactant to the surface of the diamond-shaped crystals during slow growth could be a sterical hindrance to the formation of the rod-shaped crystals in the mixed habit batches (2 and 3). The binding may also prevent instability of the supersaturation gradient caused by convection. Such instabilities are important for the formation of dendrites.

Coating of the impeller had a significant effect on the nucleation of the rod-shaped crystals. For the second batch, the formation of the rod-shaped crystals was delayed 10-15 hours while for the first batch the rod-shaped crystals grew larger. The estimated kinetics suggest that the nucleation rate drops faster with decreasing supersaturation and probably to a lower level. It could be that metal surfaces promote the nucleation. Another suggestion could be that the rod-shaped crystals form mostly by breakage allowing then to grow larger in the gentle environment of the coated impeller (Synowiec *et al.*, 1993). The growth rate was found to drop faster with decreasing supersaturation when a coated impeller was used. This could be due to lesser breakage and hence less rod-ends on which fast growth can take place.

The effect of coating on the crystallisation of diamond-shaped crystals was limited to a change in the shape of the crystal size distribution. Perhaps the coated impeller provides a less efficient agitation, increasing the thickness of the diffusion layer and hereby decreasing the degree of supersaturation near the crystal surface. This was high enough to produced showers of nuclei while in exp 4, the lower supersaturation

meant a lower and more secondary type of nucleation. A similar trend was seen for the second batch when stirred with coated impeller at low levels of surfactant (exp 7).

Comparing exp 4 (coated and surfactant, batch 1) with exp 7 (coated, batch 2) could indicate that higher levels of surfactant not only is a hindrance to the formation of rod-shaped crystals but also slows down the growth of diamond-shaped crystals. This was further confirmed by comparing the size of the largest diamond-shaped crystals obtained in exp 6 (no coating, no surfactant, batch 2) with exp 9 (no coating, surfactant, batch 2).

7.4 Conclusion.

A crystallisation producing two crystals forms was studied. Significant effects were observed with the addition of surfactant and coating of the impeller. Both variations affected the crystallisation kinetics and in some cases also a change in crystal habit. Addition of surfactant favoured the growth of diamond-shaped crystals to rod-shaped crystals while coating of the impeller reduced the number over rod-shaped crystals formed.

In order to explain this and a series of experimental observations it was suggested that the crystallisation could be controlled by Nernst-Planck diffusion.

Chapter 8. Controlled protein crystal growth by seeding and manipulation of supersaturation.

8.1 Introduction.

A key bioprocess dimension of protein crystallisation operation is the integration of the reactor and the subsequent recovery and dewatering of protein crystals. The objective of this section was to examine the control of the reactor to maximise crystal size by reducing the extend of nucleation.

8.2 Results.

The effect of seeding and slow generation of supersaturation were tested for process solutions where the resulting crystals were diamond-shaped.

Four ways of operating the crystallisation stage were tested and compared (Figure 54). In the first experiment (A) the crystallisation was left to start unaided, that is non-seeded. After approximately one hour at pH 4.3 and 28.0°C the crystallisation started and a wide crystal size distribution resulted (Figure 54A). In experiment B, a 0.5 % volume of seed crystals was added when pH 4.3 and 28.0°C had been reached, resulting in the formation of crystals of the same size range and morphology as the seed crystals. The seed crystals were of a narrow crystal size distribution near 30 μm. In experiment C the pH, at which the seeds were added, was 5.0-5.1. This has earlier been found to be near the solubility curve (see Chapter 6). Following the seeding, the solution pH was slowly lowered to 4.3 staying near the solubility curve. The crystals which formed were of a similar size to those found in experiment B. Experiment D closely followed experiment C but with a larger seed volume of 12.5 % combined with a faster lowering of the pH to 4.3. By following the entire crystallisation run, it was revealed, that the crystals in the peak at 42 μm had grown from the initial 30 μm of the added seed crystals.

Figure 54 illustrates how seeding and manipulation of the degree of supersaturation can be used to control the balance between the simultaneous processes of nucleation and growth leading to very different crystal size distributions. Experiment A is characterised by slow nucleation in parallel with crystal growth, while in experiment B the use of seeding gave fast nucleation followed by growth. The growth of the seeds in experiment B could not be observed due to dilution. Experiment C is dominated by rapid nucleation followed by growth and experiment D exhibits simultaneous growth of the seed crystals and nucleation and growth of the new crystals were seen.

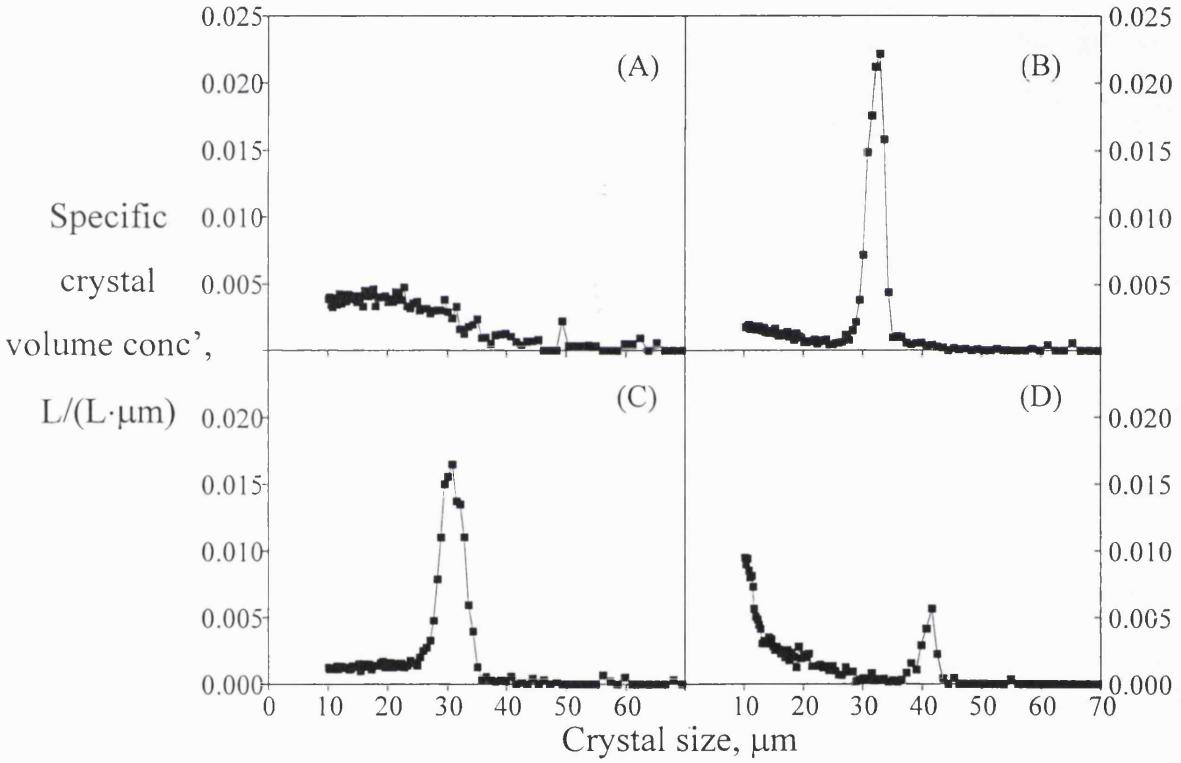

Figure 54. Final crystal size distributions after 22 h for experiments A-D. A: unseeded pH 4.3, B: 0.5 % seeds added at pH 4.3, C: 0.5 % seeds added at pH 5.1 followed by a 1000 mins pH ramp to 4.3 and D: 12.5 % seed added at pH 5.1 followed by a 60 mins ramp to pH 4.3.

In experiments E, F and G (Figure 55) the same large seed volume was used while the ramping time was increased to 300, 700 and 1000 mins respectively. For longer ramping times the growth of the seed crystals becomes dominant, to such extent, that at ramping times for 700 and 1000 mins no nucleation could be observed.

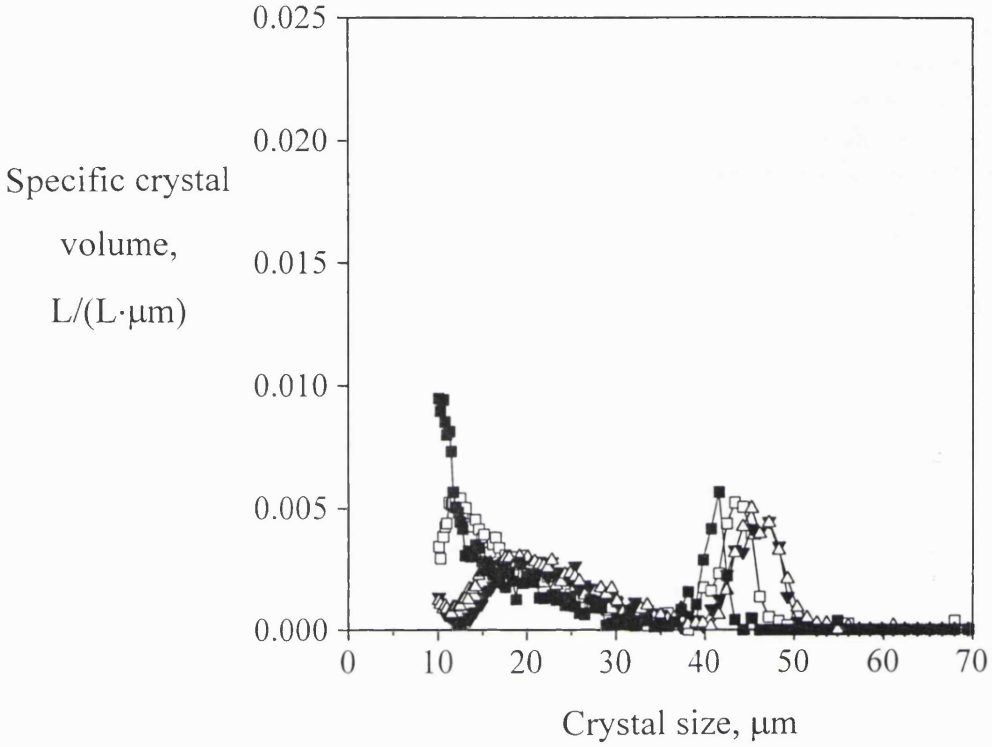

Figure 55. Final crystal size distribution for a series of experiments (D-G) where the length of the pH ramp is varied. A volume of 12.5 % seed stock was added at pH 5.30 to give starting pH 5.10 for the mixture before pH was lowered to 4.3 as a linear function of time over the next 60 (D, ■), 300 (E, □), 700 (F, ▼) and 1000 (G, Δ) mins.

Finally in experiment H (Figure 56) the 1000 mins ramping time experiment (G) was repeated but the pH, at which the seeds were added, was 5.5. A narrow peak of seed crystals can be observed at 52 μm and another peak can be seen at 15 μm. As in experiments D and E, simultaneous growth of the seed crystals and nucleation followed by growth of new crystals were observed. Partial dissolution of the seed crystals has removed the "tail" of the seed crystal peak observed in experiments D to G.

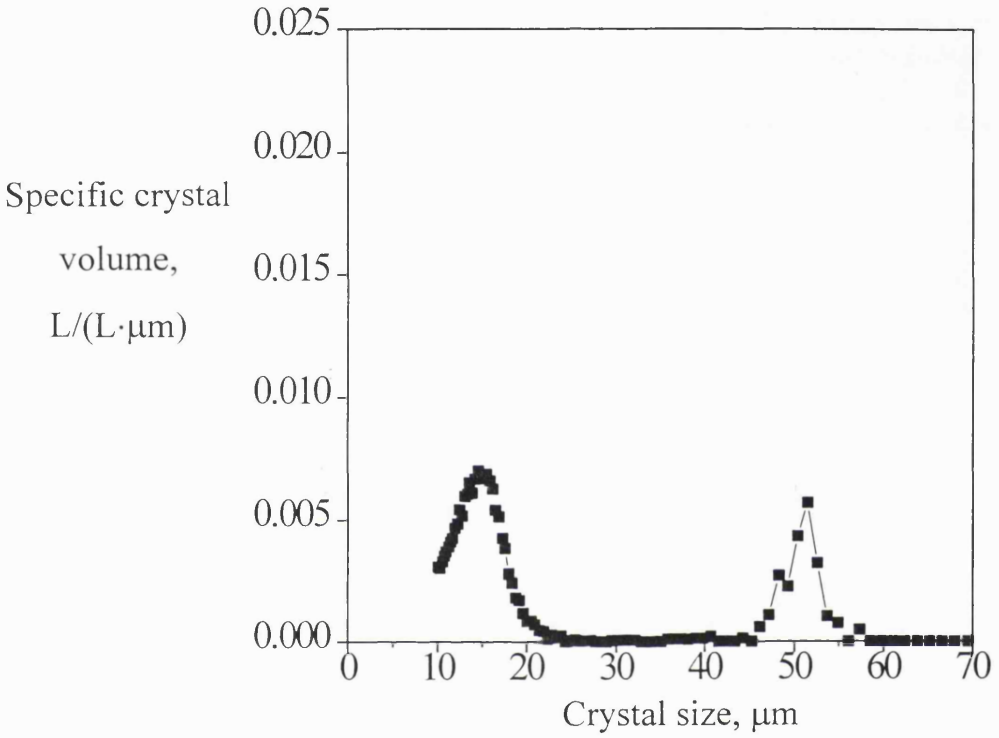

Figure 56. Final crystal size distribution for experiment H, where a volume of 12.5 % seed stock was added at pH 5.5 after which pH was lowered to 4.3 as a linear function of time over the next 1000 mins. Significant seed dissolution was microscopically observed down to pH 5.11 at which the crystal resumed their sharp features.

8.3 Discussion.

To understand fully the experiments presented here it should also be realised that crystals can have at least five different sources. They can: 1) be seed crystals, 2) be crystal fines and debris carried with the seed crystals, 3) originate from surface dust, 4) be formed by nucleation or 5) be produced by crystal breakage. Little or no crystal breakage is believed to happen in these experiments because the crystals looked perfectly diamond-shaped upon microscopic observation.

Exp.	Operation	Size distribution	Processes
A	unseeded, pH 4.3	broad	slow nucleation + growth
B	low seed at low pH	narrow	fast nucleation + growth
C	low seed, high pH, 1000 mins ramp	narrow	fast nucleation + growth
D	high seed, high pH, 60 mins ramp	bimodal with tail	seed growth, nucleation + growth
E	high seed, high pH, 300 mins ramp	bimodal with tail	seed growth, nucleation + growth
F	high seed, high pH, 700 mins ramp	monomodal with tail	seed growth
G	high seed, high pH, 1000 mins ramp	monomodal with tail	seed growth
H	high seed, high pH, diss., 1000 mins ramp	bimodal	seed growth, nucleation + growth

Table 8. Interpretation of experiment in terms of the processes leading to various types of crystal size distributions. The seed crystal preparation was of a monomodal size distribution with tail.

Seed crystals were generally easy to identify by measuring crystal size distributions throughout the crystallisation experiment. The peak in the range of 40-52 μm in experiments D to H (Figures 55-56) was identified as seed crystals in such way.

Crystal fines and debris (<10 μm) carried with the seeds will, after the introduction in the supersaturated solution, grow into the measuring range. Since the seed crystals grew 15 μm during the run, no crystals originating from fines can be

smaller than 15 μm and equally no new crystal can be larger than 15 μm. The crystal population between 15 and 40 μm in experiment G is therefore probably due to crystals grown from fines. This is strongly supported by the result of experiment H where the seed crystal suspension was allowed partly to dissolve before pH was lowered.

Crystals originating from crystal surface dust could explain the very short duration of the nucleation found in experiment B. The lack of effect when changing the seeding pH between experiments B and C could support this view. The number of crystals originating from surface dust would be expected to be proportional to the volume of seeds used. Hence in experiments D to G, the number of dust related crystals should be 25 times larger than in experiment C meaning that these would barely grow into the measuring range during a run. However, if such a large number of small crystals were present in experiment D to G, no effect of changing the ramping time would be expected.

Nucleation is therefore understood to be the major source of crystal formation in all the experiments. Nucleation takes place at high degrees of supersaturation as was demonstrated in experiment B. A high degree of supersaturation causing nucleation was also achieved in experiments D, E and H where supersaturation was generated faster than it could be consumed by crystal growth. In Chapter 7 nucleation was suggested to happen at the surface of growing crystals due to a temporary pH instability during the establishment of a Nernst-Planck diffusion layer (further explained in Chapter 9). The narrow peak found in experiment B could therefore have been produced by nucleation at the surface of the seed crystals.

The result of experiment C is at first surprising because of its similarity to experiment B, although they were operated very differently. Rapid crystallisation did not occur until 5-6 hours after the beginning of the pH ramp and the seeds had been added. Due to the slow approach to the metastable limit, nucleation was expected to produce a broad crystal size distribution. The fact that a very narrow peak resulted could mean that the metastable limit is very sharp leading to a shower of crystals once it has been exceeded. Another possible explanation is that the surface pH instability for slowly growing seed crystals did not occur before well out in the labile region. In such a case, the similarity to the seeded experiment at pH 4.3 (B) would be expected.

Experiment D uses a larger seed volume and seeks to adjust pH slowly enough to keep the operating point below the metastable limit. The seed crystals successfully grew from the initial 30 μm to 42 μm. However, a second peak can be seen below 15

μm. This is thought to result from of operation above the metastable region leading to rapid nucleation. The longer the pH ramping time, the less into the labile region the operating point will be, hence fewer small crystals will be expected than for the longer ramping times. Increasing the pH ramping time to 300 mins the number of small crystals was sufficiently reduced allowing the peak to grow fully into the measuring range. For even longer pH ramping times no sign of such new crystals could be seen, indicating that the speed at which the supersaturation was generated matched the rate at which it was consumed by crystal growth.

The last experiment (H) was conducted to test if the crystals in the size range between 15 and 37 μm were crystal fines and debris carried with the seeds. This was done by adding the seeds at the higher pH of 5.25 at which extensive dissolution happened. Only the large seed crystals were expected to survive this, starting to regrow when the operating point crosses the solubility curve at pH 5.1. As can be seen in Figure 56 the crystals in the size range between 15 and 37 μm did disappear suggesting that they did indeed originate from fines carried with the seeds.

These experiments indicate that if crystals fines are removed, using a slight dissolution of the seed crystals combined with a sufficiently long ramping time, then the optimal size increase of 28 μm (for 12.5 % seed volume) could be achieved. The seed volume dictates the minimum allowable ramping time to achieve the maximum size increase.

In summary seeding combined with slow generation was used to increase the average size of the crystals (up to 32 %) as well as the size of the added seed crystals (50 %). Careful control of the degree of supersaturation have allowed preferential growth of the seed crystals and prevented simultaneous nucleation. An improved seed preparation method was shown to remove crystal fines allowing the seed crystals to grow larger.

In Table 9 some key results are compiled from the experiments. Increased ramping times were clearly successful in growing larger seed crystals and in making more of the material crystallise on them. If however crystals of 30 μm are acceptable, then it is easier and quicker just doing the seeded experiment at low pH. In the bulk production of enzymes the filterability of the produced crystals is more important and is given here as a filtration based particle diameter d_p (volume/area). The filterability is generally thought to relate to the crystal number rather than crystal volume. Since a large number of crystals (but not necessary a large fraction of the volume) is expected in

the size range below 10 μm, it is important to conduct these filterability tests to verify the improvement of the process.

As can be seen from Table 9, the increased seed crystal size by pH ramping did not result in an improved filterability, an increased percentage of fines seems to be the cause (Figure 57). Doing pH ramps means the average protein molecule will spend longer time in solution and that may cause protein aggregation (of both impurities and product). Another possibility is that small and non-growing particles are carried with the seeds since the reduced filterability could be linked to the experiments using a large seed volume. In some of the experiments there are also expected to be crystals smaller than 10 μm (experiment D, E and H) which seem to have a positive effect on the filtration.

		d_p mL/m^2	$d_{V,\ seed\ peak}$ μm	% on seed w/w	% fines (<10 μm)
A:	non-seeded, constant pH	1.8 ± 0.2		0	14
B:	seeded, constant pH 0.5 % seed volume at pH 4.3	1.6 ± 0.1	(32)	(65)	19
C:	pH profile, 1000 mins, 0.5 % seed volume at pH 5.0	1.9 ± 0.2	(32)	(63)	25
D:	pH profile, 60 mins, 12.5 % seed volume at pH 5.10	1.3 ± 0.2	41	15	33
E:	pH profile, 300 mins otherwise as for D	1.3 ± 0.2	44	21	29
F	pH profile, 700 mins otherwise as for D	0.9 ± 0.2	46	26	31
G	pH profile, 1000 mins otherwise as for D	0.9 ± 0.2	47	29	36
H	pH profile, 1000 mins, 12.5 % seed volume at pH 5.5	1.2 ± 0.2	51	27	39

Table 9. Results of crystallisation and filtration trials. d_p measures the filterability of the crystals, $d_{v\ seed\ peak}$ is the volumetric average size of the seed crystals at the end of the run, "% on seeds" is an estimate of the percentage of the total crystal dry weight that the seeds comprise. "% fines" is the percentage of the total crystal dry weight that the fines (<10 μm) comprise. The d_p results are given with a 95 % level of confidence for repeated crystallisations. Brackets indicate that the estimate is for a population of crystals which are not seed crystals.

The growth of larger crystals at reduced rate of generation of supersaturation was also reported by Jones *et al.* (1987) for potassium sulphate crystallisation. As with data presented above, Jones *et al.* found no improvement of the filterability of these larger crystals. They suggested that the more bimodal crystal size distributions of the ramping experiments reduced the filterability due to a closer crystal packing in the filter cake.

The conclusion on the filtration trials is that the attention should be focused on particles smaller than 10 μm because these, rather than crystals in the size range of 10-60 μm, determine the filterability.

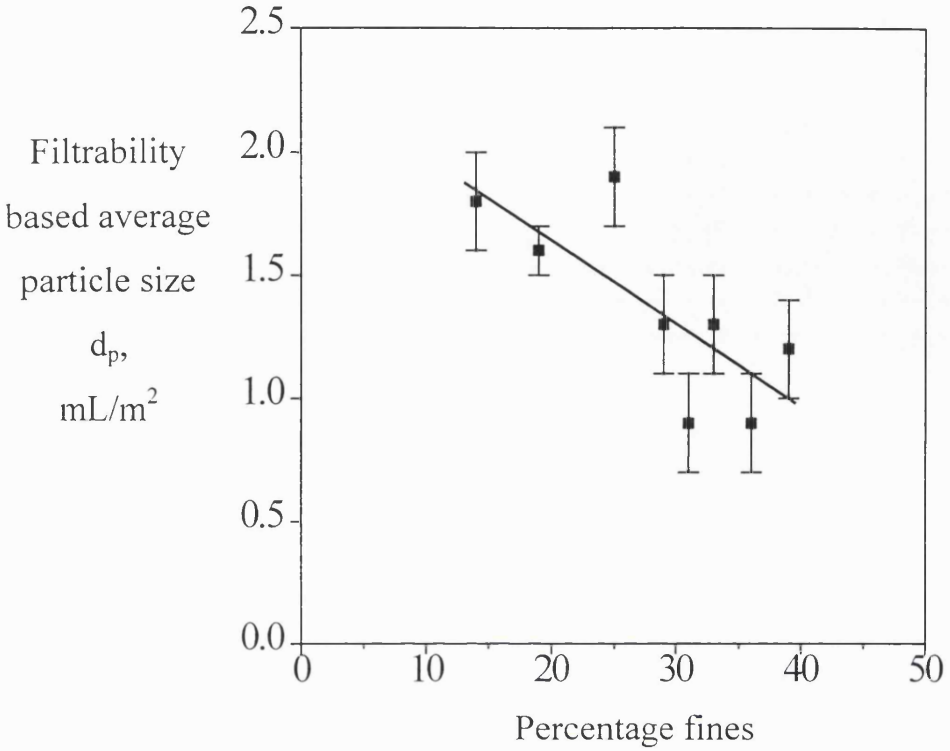

Figure 57. Filterability (d_p) plotted as a function of the percentage of fines (mass fraction of particles smaller than 10 μm). As expected, a higher percentage of fines results in a more difficult filtration.

8.4 Conclusion.

The method of seeding at low supersaturation followed by slow generation of supersaturation has proven successful in growing seed crystals up to 50 % larger. This was a result of shifting the balance towards the growth of the seed crystals rather than nucleation and growth of new crystals.

Filtration of the crystal suspensions produced suggests that attention should be paid to crystal fines (< 10 μm) rather than crystals of 10-60 μm in order to improve their recoverability.

Chapter 9. Discussion.

The batch crystallisation of a fungal lipase from an industrial process solution has been characterised. Under similar conditions the resulting crystals were either diamond, rod-shaped or a mixture of the two. Industrially the diamond crystal form is preferred due to its superior filtration characteristics.

The batch operation of the crystallisation of diamond-shaped crystals at high initial supersaturation (2-5) gave a large number of small crystals (0-40 μm). Nucleation and growth were estimated from series of crystal size distributions using s-plane analysis. Crystals were found to form at a maximum rate of 50-60 1/(s·μL) and grew with velocities of up to 20 nm/s. The degrees of supersaturation (as calculated from a mass balance) were combined with nucleation and growth rates using conventional models to obtain the crystallisation kinetics. High orders of dependency on the supersaturation were found for both nucleation (8) and growth (6). A narrow metastable zone (approximately 0.3-0.4 supersaturation units) combined with the high order of supersaturation dependencies were thought to be the main reasons for the small terminal size of the crystals. The observations are probably identical to those which are termed "growth cessation" in the literature. That is the protein crystals (almost) stop growing in supersaturated solutions (Pusey *et al.*, 1988; Hirsch *et al.*, 1986; Durbin and Feher, 1986). None of the traditional explanations for growth cessation could account for observations in this work. Besides these unusual crystallisation kinetics, the shape of the crystal size distributions was unexpected. This will be attempted explained below in the context of the interplay between the two crystal forms.

Of the two crystal forms the diamond-shaped is favoured at low pH and higher levels of surfactant while the rod-shaped are favoured at higher pH and low levels of surfactant. At intermediate levels of pH and surfactant concentration, mixtures of the two crystals are formed.

The understanding developed in Chapter 7 will be further clarified using Figures 58-61. A diagrammatic phase equilibrium diagram for a batch of material yielding only diamond-shaped crystals is shown in Figure 58. Two operating lines are shown. First the pH is adjusted down to 4.3, the end point being indicated with a black circle. At point (a) the operating line splits into two. One line represents the bulk conditions and the other represents the conditions near the crystal surface. At the black circle the crystallisation can either be left to start spontaneously or seed crystals can be added.

Figure 59 shows four stages of crystal growth which relate to the various stages in Figure 58. Initially the crystal surfaces are "naked". With the incorporation of molecules in the crystal lattice hydrogen ions are released (Monaco and Rosenberger, 1993) making the environment near the crystal surface more acidic (Figure 59b) and thus of a lower degree of supersaturation. The more acidic the surface environment the lower the degree of supersaturation in the micro-environment. Hence the growth rate will drop. The operating point of the micro-environment will move close to, but never across, the solubility limit ((b) in Figure 58).

In the bulk solution the protein has a net-charge (z) of zero but in the environment near the crystal surface the protein molecule will carry a net positive charge. Diffusion of charged molecules at low salt concentration is controlled by coupled diffusion (Nernst-Planck diffusion). This is similar to Fick's law diffusion but also includes the zero current constraint, i.e. when a charged molecule diffuses it has either to co-diffuse with molecules of the opposite charge or counter-diffuse with molecules of the same charge. In the system studied the pH and the salt concentration are low, meaning that the counter-diffusion of hydrogen ions is more likely. Such counter-diffusion will deplete the zone near the crystal surface of hydrogen ions. The exact balance between the number of hydrogen ions released per molecule incorporating the crystal lattice and the number required for counter-diffusion will determine the pH of the micro-environment. In this work pH is believed to increase and only until reaching the other solubility limit ((c) Figure 58). During this shift in pH a temporary increase in supersaturation happens leading to a short period of rapid nucleation before reaching the other solubility curve where both the nucleation and growth rates drop to a low level. This pH change means that there are now two zones around the growing crystal (see Figure 59c) and further explained in Figure 60). Nearest to the crystal pH, is high and the net-charge of the protein is negative leading to co-diffusion of hydrogen ions to the surface. Since there is an overall production of hydrogen ions at the interface these will diffuse to the bulk solution. A second zone of lower pH is therefore situated outside the first in which the protein carries a positive charge and hydrogen ions are counter-diffusing. In this situation the growth of the protein is self-stopping and preventing the operating point from reaching the solubility curve within the 24 h of the experiments. Higher diffusion rates of protein molecules and/or their incorporation both lead to a lower degree of supersaturation near the crystal surface. Slow growth will

however take place maintaining the micro-environment. This explains the unusual nucleation and growth kinetics observed in the experiments.

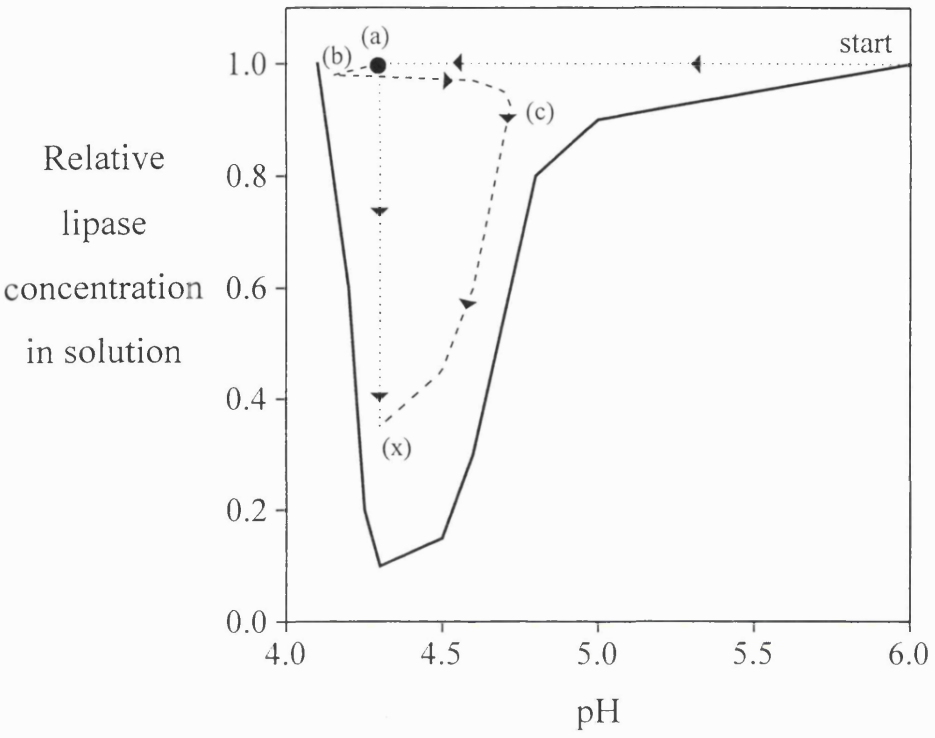

Figure 58. Diagrammatic phase equilibrium diagram for a batch forming only diamond-shaped crystals. The solid line is the solubility curve, the dotted line represents the bulk conditions and the dashed line represents the surface micro-environment. Letters (a) to (c) refer to the various growth stages in Figure 59. (x) is the completion of the crystallisation.

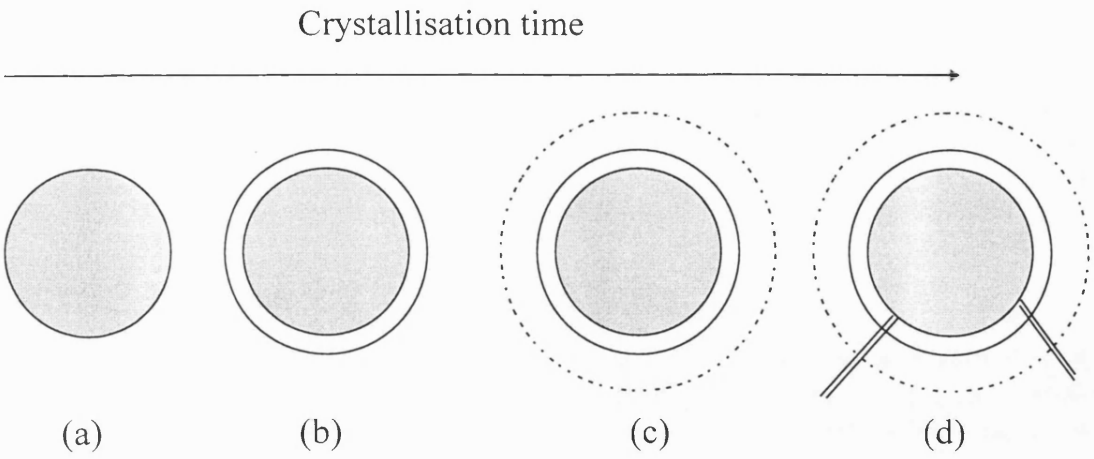

Figure 59. Schematic diagram for the different states of the protein crystal. Letters refer to Figure 58. (a) is the initial (seed) crystal, (b) low-pH environment formed due to early crystal growth, (c) show the establishment of the Nernst-Planck diffusion zone outside a high-pH zone and (d) shows the growth of crystals in the concentration gradient near the surface of the growing crystal.

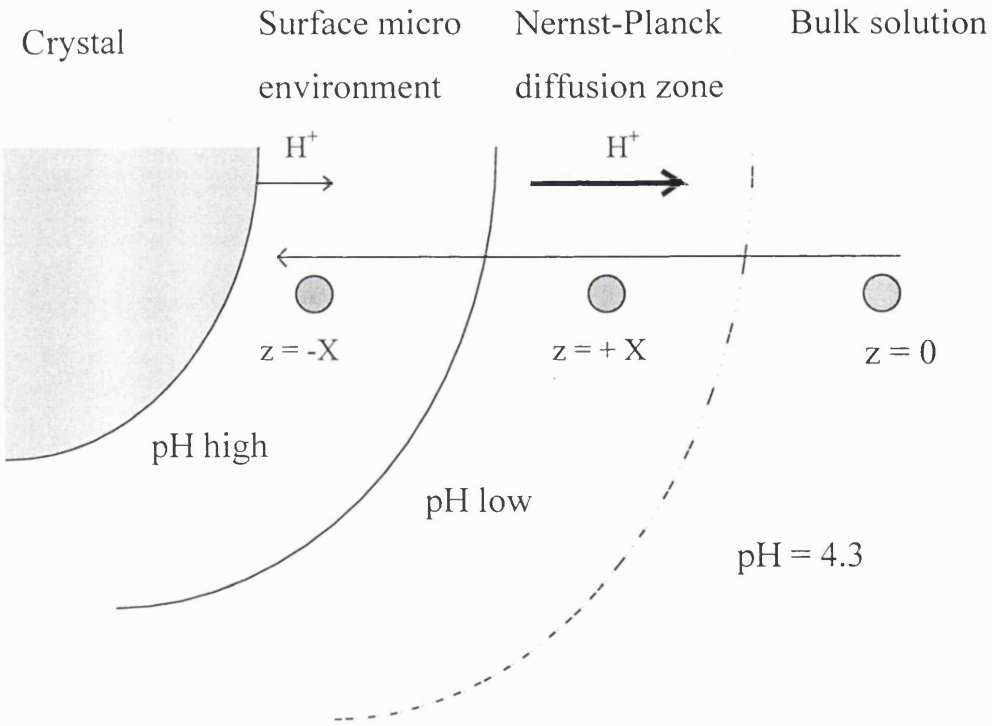

Figure 60. Schematic diagram for the two zones developing around a growing crystal. Z is the net-charge of the protein.

So far, the discussion has only been concerned with batches yielding diamond-shaped crystals. A phase equilibrium diagram for batches forming both diamond and rod-shaped crystals is shown in Figure 61. The scenario is almost the same as it was in Figure 58. However the lower level of surfactant for the batches forming both crystal form, means that convection will disturb the diffusion layer sufficiently to allow the growth of dendrites from the surface of the diamond-shaped crystals ((d), Figure 59). It is difficult to say whether the rod-shaped crystals formed in the presence of diamond-shaped crystals are dendrites or rod-shaped crystals nucleated at the surface of the diamond-shaped crystal. As can be seen by comparing Figure 58 and Figure 61 more protein comes out of solution if the second crystal form is present. This is because the growth of the diamond-shaped crystals has almost stopped in low but supersaturated solution while the dendrite growth can bypasses this limitation of the diamond-shaped crystals.

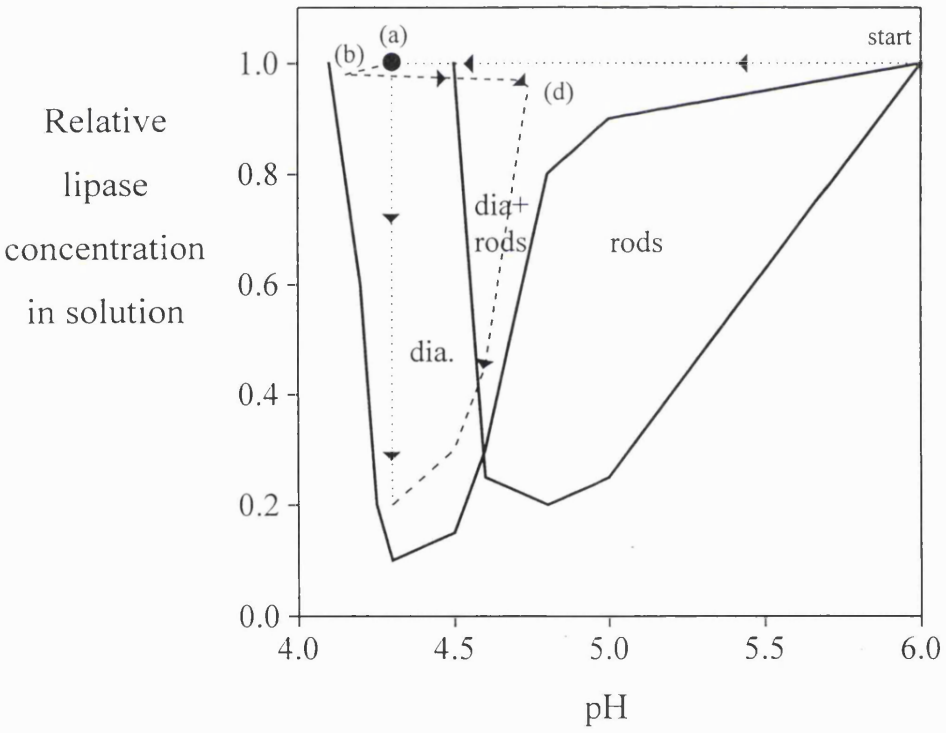

Figure 61. Diagrammatic phase equilibrium diagram for a batch forming both diamond and rod-shaped crystals. The solid line is the solubility curve, the dotted line represents the bulk conditions and the dashed line represents the surface micro-environment.

This way of understanding the crystallisation is supported by a number of experimental observations. Size dependent growth indicates the presence of a diffusion layer. The formation of dendrite shaped crystals is another indication of the presence of

surface gradients in supersaturation. The release of hydrogen ions during crystal growth has been detected. Unsteady nucleation rates resulting from the pH instability have been observed in the form of multimodal crystal size distribution. The high dependencies of nucleation and growth on supersaturation can also support the understanding. This is in particular the case when realising that crystals, which practically had stopped growing in supersaturated solution, were found, when seeded, to grow with a speed similar to that of the newly nucleated crystals.

A system closely resembling the above is ion exchange chromatography. The similarities are that charged molecules are diffusing to, and bind to, a highly charged surface. The difference being that the crystal surface is moving while the chromatographic surface is stationary. For ion exchange chromatography initial pH instabilities and surface micro-environments are well-known (Hu *et al.,* 1992). The highly charged protein crystal surface could explain how protein molecules can bind as rapidly as observed. For example when lysozyme (M_w = 14 kDa) grows at 4 nm/s this correspond to 2-3 layers per second (Skori *et al.,* 1995). This is very similar to what is expected for the system studied because the larger lipase molecules (M_w = 35 kDa) make the lipase crystals grow faster than lysozyme crystals. Such high growth rates are difficult to imagine considering that the protein molecule will have to diffuse and reorientate before binding. If a such strong electric field is radiating from the crystal surface this may correctly orientate the protein molecule well before the actual attachment. Uniformly distributed crystals grown in space also suggests that high surface charges are present (McPherson, 1992).

The presented model has been used qualitatively on data from the literature. Generally speaking the observed effect will be expected in solutions of low conductivity. However, the effect may also be observed in high salt solutions when crystallising far from the isoelectrical point of the crystallising protein. For lysozyme more hydrogen ions are expected to be released at low pH but this alone will probably not cause changes in pH since it is linked to a higher rate of counter-diffusion required by the diffusion of the more charged protein molecules. The lower the bulk pH the lower the Fick's law gradient for hydrogen ion transport to the bulk solution. This could be the interpretation of high growth rate dependencies on supersaturation reported by Forsythe *et al.* (1994), Monaco and Rosenberger (1993), Ewing *et al.* (1996) and Durbin and Feher (1986) all crystallising lysozyme at low pH and high salt concentration (pI for lysozyme being 11.2). Crystallising proteins near their isoelectrical point at high salt

concentration, resulted in low crystal growth rate dependencies on supersaturation for concanavalin A (Moré and Saenger, 1995) and ovalbumin (Judge *et al.*, 1995).

As pointed out by Fiddis *et al.* (1979) the high power dependencies of the nucleation and growth processes on the degree of supersaturation means that equilibrium will be approached very slowly. If it is assumed that equilibrium has not been achieved then the Nernst-Planck diffusion theory can be used to explain the published *apparent* solubility data. In such a case, the solubility would be expected to be lower near to pI and at high ionic strength. These trends were indeed observed by Ewing *et al.* (1994), Howard *et al.* (1988) and Ataka and Tanaka (1986).

In conclusion much more focus on the effect of charges on the protein crystallisation may benefit its understanding.

The kinetics of the crystallisation suggest that the nucleation and growth processes should be decoupled in order to grow large crystals. As described below, this can be achieved by seeding at low supersaturation followed by slow generation of supersaturation.

The practical focus of this research was to improve the filterability of the final crystal suspension, while keeping the overall yield high. Two methods were identified which could shift the balance between the two crystal forms so to obtain only the easy-filtering diamond-shaped crystals. Addition of non-ionic surfactants ('Tween' 80 or Brij-35) proved efficient in obtaining just diamond-shaped crystals from batches which otherwise would have given either a mixture of the two or just rod-shaped crystals. Also coating of metal surfaces delayed the formation of rod-shaped. Both methods gave 20 % lower yield of crystals.

The effect of surfactant is probably that they will be localised near the surface of slow growing diamond-shaped crystals and sterically hinder the growth of dendrites/rod-shaped crystals. Stabilisation of the supersaturation gradient is also expected to reduce both dendrite growth and the growth of rod-shaped crystals from the diamond-crystal surface.

This interplay between the two crystal forms makes it difficult to shift the balance toward the formation of diamond-shaped crystals if low conductivity is essential for the protein to come out of solution. Speculations on how to overcome this are given in Chapter 11, Future work.

The work was concluded with a study of the use of seeding combined with slow generation of supersaturation for decoupling of the nucleation from the growth process.

Using a seed suspension volume of 12.5 % of the reactor working volume and a ramping time of 700-1000 mins for taking pH from 5.1 to 4.3 was successful in growing the seed crystals 50 % larger. If a shorter ramping time was chosen, the conditions will be supersaturated enough to allow nucleation.

The non-seeded experiment at the large scale yielded broad crystal size distributions probably while at the small scale a more narrow and multimodal size distributions were found. The crystallisation at the large scale may have reached the induction time with crystallisation starting in several places in the reactor within a few minutes. The broad size distribution is then an average of many pulses that is out of tune. In the small scale experiments, such broad size distributions were rarely observed and only in runs with extra long induction times. The induction time seemed longer on the small scale probably due to the smaller reactor volume (the statistical event of nucleation less likely) and that the small reactor was made of glass providing less potential nucleation points. The most common and premature start of the crystallisation was probably caused by a single particles of external origin causing the multimodal crystal size distributions.

Finally the pH ramping experiments were evaluated by filtration of the crystal suspension. Although the ramping experiments produced larger crystals these did not filter better than those produced by seeded or non-seeded experiments. This could be due to the bimodal character of the crystal size distribution as suggested by Jones *et al.*, (1987) doing similar work on potassium sulphate.

Chapter 10. Conclusion.

The batch crystallisation of a lipase from an impure solution has been characterised. Two crystal forms, diamond and rod, have been observed and parameters which affect their formation identified. The level of supersaturation, surfactant concentration, pH and materials in contact with the crystallisation were all found to be important. Series of crystal size distributions were used to estimate nucleation and growth rates during crystallisation. Strong dependencies upon the supersaturation were found both for nucleation (diamond: 8, rod: 5) and growth (diamond: 6, rod: 3), making the approach to equilibrium slow. The crystals produced were generally 10-30 μm. Seeding and slow generation of supersaturation were found to increase the size of the seed crystals up to 50 %. These larger crystals were not found to have improved filterability compared to the simple batch operated crystallisation, probably due to the presence of fines.

A range of observations including the high dependencies of nucleation and growth on supersaturation contributed to an overall understanding of the crystallising system. A crystal surface micro-environment caused by Nernst-Planck diffusion seems able to fully explain the observations.

Chapter 11. Future work.

11.1 Affecting the crystal morphology.

From the proposed understanding of the crystallisation (Chapter 9) comes a number of ideas on how the process could be manipulated to produce crystal suspensions of higher filterability.

The aim is to only obtain diamond-shaped crystals at high yields. Addition of surfactants can slow down the formation of the rod-shaped crystals, but due to the formation of the micro-environment, the processing time to obtain the full yield as diamond-shaped crystals would be prohibitively long. It could be interesting to test other surfactants, for example those having acid groups with pKa near pH 4.3. These may take up some of the excess hydrogen ions, allowing the growth of the diamond-shaped crystals to continue at a higher rate. Also, the effect of the physical size of the surfactant on the crystal growth is relevant. In the spirit of process integration, the antifoam agent (= surfactants) used during fermentation should therefore not only be selected on the basis of its suitability for the fermentation step but also its effect on the crystallisation.

Adding salt to the system would be another way of limiting the effect of the Nernst-Planck diffusion layer and hence allowing more rapid crystal growth. However this has been found to increase the solubility of the lipase and is thus unacceptable in industry. A solution could be to replace any remaining salt in the crystallisation solution with a strong buffer that could maintain the pH of the micro-environment near 4.3.

The suggestions above are under the assumption that the proposed understanding truly represents the system studied. Further attempts to find experimental support for the understanding could be to conduct the crystallisation in the presence of a pH indicator which changes color at pH 4.4-4.6. Since the volume of the micro-environment is expected to be small, a strongly colored pH indicator is required. Variations agitation should also be tested to provide further support for the existence of a diffusion layer. Finally, crystallisation of a pure lipase preparation could eliminate any possible effects of the impurities present in the system.

11.2 Improved process design and operation.

The result of Chapter 8 suggests that seed preparation techniques should be explored further. The focus should be on particles smaller than 10 μm. Freezing or freeze-drying could be ways of preserving the seed crystal stock. Chemical stabilisation of the mother liquor may also be considered so that the seed crystals could be stored at room temperature or 4°C.

Instead of using pH as control parameter, temperature can perhaps be used. The benefit of starting at low temperatures would be the higher stability of the process solution. As the protein system studied here does not show significant temperature dependence on solubility down to 15 °C, extra costs for lowering the temperature would be expected. If the growth is limited by a Nernst-Planck diffusion layer, it could be interesting to use salt removal (by dialysis for example) as control parameter. Initial high levels of salt would allow rapid crystal growth while low salt concentration towards the end of the crystallisation would allow a high yield to be achieved.

Also the fill and draw operation for which results are briefly reported in the appendix could prove advantageous for less stable protein products. For such system a modified reactor design is required and ways of limiting the effect of contamination should also be considered.

Finally, it seems that the reactor environments particular for the crystallisation of the rod-shaped crystals can have a significant effect. Providing a gentle environment for crystal growth could reduce the extent of crystal breakage. This could be achieved by using smoother construction materials and minimising agitation both of which should improve the filterability of the final crystal suspension.

Chapter 12. References.

Abergel, C., Nesa, M. P. and Fontecilla-Camps, C. (1991) The effect of protein contaminants on the crystallisation of turkey egg white lysozyme. *J. Cryst. Growth,* **110**, 11-19

Aires-Barros, M. R., Taipa, M. A. and Cabral, M. S. (1994) Isolation and purification of lipases. In:. Lipases- their structure, biochemistry and application. Ed. Woolley, P. and Petersen, S. B Cambridge University Press (1994), Cambridge.

Allen, T. Particle Size Measurement. Chapman and Hall, London, 1981,1997.

Ataka, M. and Tanaka, S. (1986) The Growth of Large Single Crystals of Lysozyme. *Biopolymers*, **25**, 337-350.

Azuma, T., Tsukamoto, K. and Sunagawa, I. (1989) Clustering phenomenon and growth units in lysozyme aqueous solution as revealed by laser light scattering method. *J. Cryst. Growth*, **98**, 371-376.

Bailey, J. E. and Ollis, D. F. (1986) Biochemical engineering fundamentals. 2.Ed. McGraw-Hill International Editions, Singapore.

Baker, E. N. and Dodson, G. (1970) X-ray Diffraction Data on Some Crystalline Varieties of Insulin. *J. Mol. Biol.*, **54**, 605-609.

Bates, R. L., Fondy, P. L. and Corpstein, R. R. (1963) An examination of some geometric parameters of impeller power. *Ind. Engng. Chem. Process Des. and Dev.*, **2**, 310-314.

Berne, B. J. and Pecora, R. (1976) Dynamic light scattering. John Wiley & Sons, Inc. (New York).

Bishop, J. B., Fredericks, W. J., Howard, S. B. and Sawada, T. (1992) Dynamic light scattering analysis of solutions from which lysozyme crystals grow. *J. Cryst. Growth*, **122**, 41-49.

Bishop, J. B., Martin, J. C. and Rosenblum, W. M. (1991) A light scattering method for qualitatively monitoring aggregation rates in macromolecular systems. *J. Cryst. Growth*, **110**, 164-170.

Bohach, G. A., Chi, Y.-I. and Stauffacher, C. V. (1992) Crystallization and Preliminar X-Ray Diffraction Analysis of Staphyllococcal Enterotoxin Type C. *Proteins Struct. Funct. Genet.*, **13**, 152-157.

Boistelle, R., Astier, J. P., Marchis-Mouren, G., Desseaux, V. and Haser, R. (1992) Solubility, phase transtion, kinetic ripening and growth rates of porcine pancreatic α-amalyse isoenzymes. *J. Cryst. Growth*, **123**, 109-120.

Boistelle, R. and Astier, J. P. (1988) Crystallization mechanisms in solution. *J. Cryst. Growth*, **90**, 14-30.

Bonnerjea, J., Ob, S., Hoare, M. and Dunnill, P. (1986) Protein purification: the right step at the right time. *Biotechnol.*, **4**, 954-957.

Bourne, J. R. (1992) Mixing in single-phase chemical reactors. In: Mixing in the process industry. 2. Ed. Harnby, N., Edwards, M. F. and Nienow, A. W. Butterworth-Heinemann, Oxford.

Brange, J. (1987) Galenics of Insulin. Springer-Verlag, Berlin.

Brockerhoff, H. and Jensen, R. G. (1974) Lipolytic Enzymes. Academic Press, NewYork.

Buurman, C., Resoort, G. and Plaschkes, A. (1986) Scalling-up rules for solid suspension in stirred vessels. *Chem. Engng. Science.*, **41**(11), 2865-2871.

Carter, Jr., C. W. (1990) Efficient Factorial Designs and the Analysis of Macromolecular Crystal Growth Conditions. *METHODS: A Companion to Methods in Enzymology*, **1**, 12-24.

Chudacek, M. W. (1986) Relationships between Solid Suspension Criteria, Mechanism of Suspension, Tank Geometry, and Scale-Up Parameters in Stirred Tanks. *Ind. Eng. Chem. Fundamentals.*, **25**, 391-401.

Conroy, M. J. and Lovrien, R. E. (1992) Matrix coprecipitation and cocrystallizing ligands (MCC ligands) for bioseparations. *J. Cryst. Growth*, **122**, 213-222.

DeMattei, R. C. and Feigelson, R. S. (1989) Growth rate study of single crystals. *J. Cryst. Growth*, **97**, 333-336.

Diepen, P. J., Bruinsma, O. S. L. and van Rosmalen, G. M. (1997) Crystal size engineering in melt suspension crystallization. *Trans. Inst. Chem. Engrs.*, **75A**, 171-175.

Doshi, M. R. and Trettin, D. R. (1981) Ultrafiltration of Colloidal Suspensions and Macromolecular Solutions in an Unstirred Batch Cell. *Ind. Eng. Chem. Fundamantals.* **20**, 221-229.

Ducruix, A. F. and Ries-Kautt, M. M. (1990) Solubility Diagram Analysis and the Relative Effectiveness of Different Ions on Protein Crystal Growth. *METHODS: A Companion to Methods in Enzymology*, **1**, 25-30.

Durbin, S. D. and Feher, G. (1986) Crystal growth studies of lysozyme as a model for the protein crystallization. *J. Cryst. Growth*, **76**, 583-592.

Eberstein, W., Georgalis, Y. and Saenger, W. (1994) Molecular interactions in crystallizing solutions studied by photon correlation spectroscopy. *J. Cryst. Growth*, **143**, 71-78.

Edwards, M. F., Baker, M. R. and Godfrey, J. C. (1992) Mixing of liquids in stirred tanks. In: Mixing in the process industry. 2. Ed. Harnby, N., Edwards, M. F. and Nienow, A. W. Butterworth-Heinemann, Oxford.

Erwing, F., Forsythe, E., van der Woerd, M. and Pusey, M. (1996) Effects of purification on the crystallization of lysozyme. *J. Cryst. Growth*, **160**, 389-397.

Erwing, F., Forsythe, E. and Pusey, M. (1994) Orthorhombic Lysozyme Solubility. *Acta Cryst.*, **D50**, 424-428.

Fiddis, R. W., Longman, R. A. and Calvert, P. D. (1979) Crystal Growth Kinetics of Globular Proteins. *Trans. Faraday Soc.*, **75**, 2753-2761.

Feigelson, R. S. (1988) The relevance of small molecule crystal growth theories and techniques to the growth of biological macromolecules. *J. Cryst. Growth*, **90**, 1-13.

Forsythe, E., Ewing, F. and Pusey, M. (1994) Studies on Tetragonal Lysozyme Crystal Growth Rates. *Acta Cryst.*, **D50**, 614-619.

Garavito, R. M. and Rosenbusch, J. P. (1980) Three-dimensional Crystals of an Integral Membrane Protein: An Initial X-ray Analysis. *J. Cell. Biol.*, **86**, 327-329.

George, A. and Wilson, W. (1994) Predicting Protein Crystallization from a Dilute Solution Property. *Acta Cryst.*, **D50**, 361-365.

Garavito, R. M. and Picot, D. (1991) The Art of Crystallizing Membrane Proteins. *METHODS: A Companion to Methods in Enzymology*, **1**, 57-69.

Garti, N. and Zour, H. (1997) The effect of surfactants on the crystallization and polymorphic transformation of glutamic acid. *J. Cryst. Growth*, **172**, 486-498.

George, A. and Wilson, W. (1994) Predicting Protein Crystallization from a Dilute Solution Property. *Acta Cryst.*, **D50**, 361-365.

Gernert, K. M., Smith, R. and Carter, D. C. (1988) A Simple Apparatus fo Controlling Nucleation and Size in Protein Crystal Growth. *Analyt. Biochem.*, **168**, 141-147.

Giegé, R., Dock, A. C., Kern, D., Lorber, B., Thierry, J. C. and Moras, D. (1986) The role of purification in the crystallization of proteins and nucleic acids. *J. Cryst. Growth*, **76**, 544-561.

Gilliland, G. L. and Bickmam, D. M. (1990) The Biological Macromolecule Crystallization Database: A Tool for Developing Crystallization Strategies. *METHODS: A Companion to Methods in Enzymology*, **1**, 6-11.

Gilliland, G. L. (1988) A biological macromolecule crystallization database: a basis for a crystallization strategy. *J. Cryst. Growth*, **90**, 51-59.

Grant, M. L. and Saville, D. A. (1991) The role of transport phenomena in protein crystal growth. *J. Cryst. Growth*, **108**, 8-18.

Gray, J. B. (1986) Flow patterns, fluid velocities, and mixing in agitated vessels. In: Mixing, theory and practice, vol 3, Uhl, V. W. and Gray, J. B. Academic Press, Orlando.

Hames, B. D. and Rickwood, D. (1990) Gel Electrophoresis of Protein. 2.Ed. IRL Press, Oxford.

Hirsch, R. E., Lin, M. J. and Nagel, R. L. (1988) The Inhibition of Hemoglobin C Crystallization by Hemoglobin F. *J. Biol. Chem.*, **263(12),** 5936-5939.

Hermia, J. (1982) Constant pressure blocking filtration laws-application to power-law non-newtonian fluids. *Trans IChemE.*, **60**, 183-187.

Hirschler, J., Charon, M. and Fontecilla-Camps, J. C. (1995) The effect of filtration on the protein nucleation in different media. *Protein Science*, **4**, 2573-2577.

Howard, S. B., Twigg, P. J., Baird, J. K. and Meehan, E. J. (1988) The solubility of hen egg-white lysozyme. *J. Cryst. Growth*, **90**, 94-104.

Hu, X., Do, D. D. and Yu, Q. (1992) Effect of supporting and buffer electrolytes (NaCl, CHCOOH and NH_4OH) on the diffusion of BSA in porous media. *Chem. Engng. Science*, **47**(1), 151-164.

Jones, A. G. and Teodossiev, N. M. (1988) Microcomputer Programming of Dosage Rate during Batch Precitation. *Cryst. Res. Technol.*, **23**, 957-966.

Jones, A. G., Budz, J. and Mullin, J. W. (1987) Batch crystallization and solid-liquid separation of Potassium Sulphate. *Chem. Engng. Science*, **42**, 619-629.

Jones, A. G., Akers, S. R. G. and Budz, J. (1986) Microcomputer Programming of Temperature in Batch Cooling Crystalliser. *Cryst. Res. Technol.*, **21** (11), 1383-1390.

Judge, R. A., Johns, M. R. and White, E.T. (1995) Protein Purification: The Recovery of Ovalbumin. *Biotech. Bioeng.*, **48**, 316-323.

Kabasci, S., Althaus, W. and Weinspach, P.-M. (1996) Batch-precipitation of calcium carbonate from highly supersaturated solutions. *Trans. Inst. Chem. Engrs.*, **74A**, 765-772.

Kadima, W., McPherson, A., Dunn, M. F. and Jurnak, F. (1991) Precrystallisation aggregation of insulin by dynamic light scattering and comparison with canavalin. *J. Cryst. Growth*, **110**, 188-194.

Kadima, W., McPherson, A., Dunn, M. F. and Jurnak, F. (1990) Characterisation of precrystallisation aggregation of canavalin by dynamic light scattering. *Biophys. J.*, **57**, 125-132.

Kam, F., Shore, H. B. and Feher, G. (1978) On the Crystallization of Proteins. *J. Mol. Biol.*, **123**, 539-555.

Kordel, M., Hofmann, B., Schomburg, D. and Schmid, R. D. (1991) Extracelluar Lipase of *Pseudomonas* sp. Strain ATCC 21808: Purification, Characterisation, Crystallisation, and Preliminar X-Ray Diffraction Data. *J. Bacteriol.*, **173**, 4836-4841.

Kouyama, T., Yamamoto, M., Kamiya, N., Iwasaki, H., Ueki, T. and Sakurai, I. (1994) Polyhedral Assembly of a Membrane Protein in its Three-dimensional Crystal. *J. Mol. Biol.*, **236**, 990-994.

Lang, D., Haalck, L., Hofman, B., Hecht, H.-J., Spener, F., Schmid, R. D. and Schomburg, D. (1994) Crystallisation and Preliminary X-ray Analysis of a Lipase from *Chromobacterium viscosum. Acta Cryst.*, **D50**, 225-227.

Larson, S., Day, J., Greenwood, A., Oliver, J., Rubingh, D. and McPherson, A. (1991) Preliminary Investigations of Crystals of the Neutral Lipase from *Pseudomonas fluorescens. J. Mol. Biol.*, **222**, 21-22.

Lee, Y-K. and Choo, C-K. (1988) The Kinetics and Mechanism of Shear Inactivation of Lipase from Candida cylindracea. *Biotech. Bioeng.*, **33**, 183-190.

Leedom, R. P. and Parker, N. H. (1967) Mechanical design of impeller-type liquid mixing equiment. In: Mixing, theory and practice, vol 2, Uhl, V. W. and Gray, J. B. Academic Press, London.

Lines, R. W. (1992) The Electrical Sensing Zone Method (The Coulter Principle). In: Particle Size Analysis. Ed. Stanley-Wood, N. G. and Lines, R. W. Royal Soc. of Chemistry

Liu, X. Y., Boek, E. S., Briels, W. J. and Bennema, P. (1995) Prediction of crystal growth morphology based on structural analysis of the solid-fluid interface. *Nature*, **374**, 23 March 1995.

Lorber, B., Skouri, M., Munch, J. and Giegè, R. (1993) The influence of impurities on protein crystallisation; the case of lysozyme. *J. Cryst. Growth*, **128**, 1203-1211.

Mahajan, A. and Kirwan, D. J. (1994) Nucleation and growth kinetics of biochemicals measured at high supersaturation. *J. Cryst. Growth*, **144**, 281-290.

Mahajan, A., Orella, C. J. and Kirwan, D. J. (1991) Analysis of size distributions and growth kinetics during the batch crystallization of L-aspargine. *AIChE Symp. Ser.*, **No. 284, 87**, 143-153.

Malkin, A. J., Kuznetsov, Y. G., Land, T. A., DeYoreo, J. J. and McPherson, A. (1995) Mechanisms of growth for protein and virus crystals. *Nature*, **2** (11.nov), 956-959.

Malkin, A. J., Cheung, J. and McPherson, A. (1993) Crystallization of satellite tobacco mosaic virus I. Nucleation phenomena. *J. Cryst. Growth*, **126**, 544-554.

Malkin, A. J. and McPherson, A. (1993a) Crystallization of satellite tobacco mosaic virus II. Postnucleation events. *J. Cryst. Growth*, **126**, 555-564.

Malkin, A. J. and McPherson, A. (1993b) Light scattering investigations of protein and virus crystals growth: ferritin, apoferritin and satellite tobacco mosaic virus. *J. Cryst. Growth*, **128**, 1232-1235.

Martinelle, M. and Hult, K. (1994) Kinetics of triglyceride lipases. In: Lipses -their structure and application. Ed. Woolley, P. and Petersen, S. B. Cambridge University Press, Cambridge.

Matthews, B. W. (1974) Determination of Molecular Weight from Protein Crystals. *J. Mol. Biol.*, **82**, 513-526.

McPherson, A. (1992) Effects of a microgravitational environment on the crystallization of biological macromolecules. *Proceedings VIll European Symposium in Materials and Fluid Science in Microgravity*, Brussels, Belgium, 12-16 April 1992, ESA SP-333 (August 1992)

McPherson, A. (1990) Reveiw: Current approaches to macromolecular crystallization. *Eur. J. Biochem.*, **189**, 1-23.

McPherson, A. and Schlichta, P. (1987) Facilitation of growth of proteins crystals by heterogeneous / epitaxial nucleation. *J. Cryst. Growth*, **85**, 206-214.

McPherson, A., Koszelak, S., Axelrod, H.,Day, J., Robinson, L., McGrath, M., Williams, R. and Cascio, D. (1986) The effect of neutral dertergents on the crystallization of soluble proteins. *J. Cryst. Growth*, **76**, 547-553.

McPherson, A. (1985a) Crystallisation of Macromolecules: General Principles. *Methods Enzymol.*, **114**, 112-120.

McPherson, A. (1985b) use of Polyethylene Glycol in Crystallisation of Macromolecules. *Methods Enzymol.*, **114**, 120-125.

McPherson, A. (1985c) Crystallisation of Proteins by Variation of pH or Temperature. *Methods in Enzymology*, **114**, 125-135.

Mikol, V., Hirsch, E. and Giegé, R. (1990) Diagnostic of Precipitant for Biomacromolecule Crystallization by Quasi-elastic Light-scattering. *J. Mol. Biol.*, **213**, 187-195.

Mikol, V., Vincendon, P., Eriani, G., Hirsch, E. and Giegé, R. (1991) Diagnostic of protein crystallization by dynamic light scattering; an application to an aminoacyl-tRNA synthetase. *J. Cryst. Growth*, **110**, 195-200.

Miyashita, S., Komatsu, H., Suzuki, Y. and Nakada, T. (1994) Observation of the concentration distribution around a growing lysozyme crystal. *J. Cryst. Growth*, **141**, 419-424.

Monaco, L. A. and Rosenberger, F. (1993) Growth and etching kinetics of tetragonal lysozyme. *J. Cryst. Growth*, **129**, 465-484.

Moré, S. and Saenger, W. (1995) Growth mechanism of concanavalin A crystals. *J. Cryst. Growth*, **153**, 35-41.

Mullin, J. W. and Nyvlt, J. (1971) Programmed cooling of batch crystallisers. *Chem. Engng. Science*, **26**, 369-377.

Mullin, J. W. (1993) Crystallization, Third Edition. Butterworth Heinemann, Oxford.

Narendranathan, T. J. and Dunnill, P. (1982) The Effect of Shear on Globular Proteins during Ultrafiltration: Studies of Alcohol Dehydrogenase. *Biotech. Bioeng.*, **24**, 2103-2107.

Navia, M. A., Clair, N. L. and Griffith, J. P. (1992) Crosslinked enzyme crystals (CLECs™) as immobilized enzyme particles. In: Stability and Stabilization of Enzymes, Proceedings of an International Symposium held in Maastricht, The Netherlands, 22-25 November 1992, Eds.van den Tweel, W. J. J., Harder, A. and Buitelaar, R. M. Elsevier Science Publisher B.V.

Nielsen, A. E. and Toft, J. M. (1984) Electrolyte crystal growth kinetics. *J. Cryst. Growth*, **67**, 278-288.

Nienow, A. W. (1992) The mixer as a reactor: liquid/solid systems. In: Mixing in the process industry. 2. Ed. N. Harnby, M. F. Edwards and A. W. Nienow. Butterworth-Heinemann, Oxford.

Nilsson, B., Laustsen, M. A. and Pahle, C. (1994) Separation of proteins. International Patent Appplication number WO 94/22903.

Paetzel, M., Chernaia, M., Strynadka, N., Tschantz, W., Cao, G., Dalbey, R. E. and James, M. N. G. (1995) Crystallization of a Soluble, Catalytically Active Form of *Escherichia coli* Leader Peptidase. *Proteins Struct. Funct. Genet.*, **23**, 122-125.

Pellegrini, M., Wukovitz, S. W. and Yeates, T. O. (1997) Simulation of Protein Crystal Nucleation. *Proteins Struct. Funct. Genet*, **28**, 515-521.

Peterson, G. L. (1983) Determination of Total Protein. In: Enzyme Structure. Ed. C. H. W. Hirs and S. N. Timasheff. Academic Press Inc., USA.

Porter, M. R. (1994) Handbook of Surfactants. Blackie Academic & Professional, printed at Chapman & Hall, Glasgow.

Pusey, M. L. (1991) Estimation of the initial equilibrium constants in the formation of tetragonal lysozyme nuclei. *J. Cryst. Growth*, **110**, 60-65.

Pusey, M., Witherow, W. and Naumann, R. (1988) Preliminary investigation into solutal flow about growing tetragonal lysozyme crystals. *J. Cryst. Growth*, **90**, 105-111.

Pusey, M. and Naumann, R. (1986) Growth kinetics of tetragonal lysozyme crystals. *J. Cryst. Growth*, **76**, 593-599.

Randolph, A. D. and Larson, M. A. (1988) Theory of particulate processes: analysis and techniques of continuous crystallization. 2nd. ed. Academic Press, San Diego.

Ransac, S., Blaauw, M., Lesuisse, E., Schanck, K., Colson, C. and Dijkstra, W. (1994) Crystallisation and Preliminary X-ray Analysis of a Lipase from *Bacillus subtilis*. *J. Mol. Biol.*, **238**, 857-859.

Rieger, F. and Ditl, P. (1994) Suspension of solid particles. *Chem. Engng. Science*, **49**(14), 2219-2227.

Ries-Kraut, M. and Ducruix, A. (1992) In: Crystallisation of Nucleic Acids and Proteins. Ed. Ducruix, A. and Giegé, R. IRL. Press, Oxford.

Rosenberger, F. (1986) Inorganic and protein crystal growth - similarities and differences. *J. Cryst. Growth*, **76**, 618-636.

Rosenberger, F. and Meehan, J. (1988) Control of nucleation and growth in protein crystal growth. *J. Cryst. Growth*, **90**, 74-78.

Rosenberger, F., Howard, S. B., Sowers, J. W. and Nyce, T. A. (1993) Temperature dependence of protein solubility - determination and application to crystallization in X-ray capillaries. *J. Cryst. Growth*, **129**, 1-12.

Sazaki, G., Aoki, S., Ooshima, H. and Kato, J. (1994) Effect of self-degradation products on crystallisation of protease thermolysin. *J. Cryst. Growth*, **139**, 95-103.

Sazaki, G., Ooshima, H., Kato, J., Harano, Y. and Hirokawa, N. (1993) Mechanism of crystallisation of enzyme protein thermolysin. *J. Cryst. Growth*, **130**, 357-367.

Schlichtkrull, J. (1957a) Insulin Crystals. 4. The Preparation of Nuclei, Seeds and Monodisperse Insulin Suspensions. *Acta Chem. Scand.*, **11**, 299-302.

Schlichtkrull, J. (1957b) Insulin Crystals. 5. *Acta Chem. Scand.*, **11**, 439-460.

Schlichtkrull, J. (1957c) Insulin Crystals. 6. The Anisotropic Growth of Insulin Crystals. *Acta Chem. Scand.*, **11**, 484-486.

Schlichtkrull, J. (1957d) Insulin Crystals. 7. The Growth of Insulin Crystals. *Acta Chem. Scand.*, **11**, 1248-1256.

Schrag, J. D., Li, Y., Wu, S. and Cygler, M. (1991) Multiple Crystal Forms of Lipases from *Geotrichum candidum*. *J. Mol. Biol.*, **220**, 541-543.

Selim, M. S., Kothari, A. C. and Turian (1983) Sedimentation of Multisized Particles in Concentrated Suspensions. *Trans. Inst. Chem. Engrs.*, **29 (6),** 1029-1038.

Shamlou, P. A. and Koutsakos, E. (1989) Solid suspension and distribution in liquids under turbulent agitation. *Chem. Engng. Sci.*, **44** (3), 543-558.

Simon, B. and Boistelle, R. (1981) Crystal growth from low temperature solutions. *J. Cryst. Growth*, **52**, 779-788

Skouri, M., Lorber, B., Giegé, R. Munch, J. and Candau, S. (1995) Effect of macromolecular impurities on the lysozyme solubility and crystallizability: dynamic light scattering, phase diagram, and crystal growth studies. *J. Cryst. Growth*, **152**, 209-220.

Sousa, R. and Lafer, E. M. (1990) The Use of Glycerol in Crystallization of T17 RNA Polymerase: Implications for the Use of Cosolvents in Crystallising Flexible Proteins. *METHODS: A Companion to Methods in Enzymology*, **1**, 50-56.

St. Clair, N. L. and Navia, M. A. Cross-linked Enzyme Crystal as Robust Biocatalysts. *Am. Chem. Soc. J.*, **114** (18), 7314-7316.

Stura, E. A. and Wilson, I. A. (1990) Analytical and Production Seeding Techniques. *METHODS: A Companion to Methods in Enzymology*, **1**, 38-49.

Synowiec, P., Jones, A. G. and Shamlou, A. (1993) Crystal break-up in diluted turbulently agitated suspensions. *Chem. Engng. Sci.*, **48**, 3485-3495.

Taksen, K. G. (1984) Industrial approaches to fermentation recovery R&D. In: Bioactive # Microbial Products 3. Ed. Stowell, J. D., Bailey, P. J. and Winstanley, D. J., Academic Press, Great Britain.

Takano, K. J., Harigae, H., Kawamura, Y. and Ataka, M. (1997) Effect of hydrostatic pressure on the crystallization of lysozyme based on in situ observations. *J. Cryst. Growth*, **171**, 554-558.

Tavare, N. S. (1995) Industrial crystallization: process simulation, analysis and design. Plenum, New York.

Tavare, N. S. (1991) Batch Crystallisers. *Rev. Chem. En.*, **7(3-4).**

Tavare, N. S. and Garside, J. (1986) Simultaneous estimation of crystal nucleation and growth kinetics from batch experiments. *Chem. Engng. Res. Des.*, **64**, 22-30.

Thibault, F., Langowski, J. and Leberman, R. (1992) Optimizing protein crystallization by aggregate size distribution analysis using dynamic light scattering. *J. Cryst. Growth*, **122**, 50-59.

Thaller, C., Eichele, G., Weaver, L. H., Wilson, E., Karlson, R. and Jansonius, J. N. (1985) Seed Enlargement and Repeated Seeding. *Methods Enzymol.*, **114**, 132-135.

Thaller, C., Weaver, L. H., Eichele, G., Wilson, E., Karlson, R. and Jansonius, J. N. (1980) Repeated Seeding Technique for Growing Large Single Crystals of Proteins. *J. Mol. Biol.*, **147**, 465-469

Vecht-Lifshitz, S. E. and Ison, A. P. (1992) Biotechnological applications for image analysis: present and future prospects (review). *J. Biotechnol.*, **23**, 1-18.

Veesler, S. Marco, S. Lafont, S., Astier, J. P. and Boistelle, R. (1994) Influence of Polydispersity on Protein Crystallization: a Quasi-Elastic Light-Scattering Study Applied to α-Amylase. *Acta Cryst.*, **D50**, 355-360.

Vekilov, P. G., Ataka, M. and Katsura, T. (1993) Laser Michelson interferometry investigation of protein crystal growth. *J. Cryst. Growth*, **130**, 317-59

Virkar, P. D., Narendranathan, T. J., Hoare, M. and Dunnill, P. (1980) Studies of the Effects of Shear on Globular Proteins: Extension to High Shear Fields and to Pumps. *Biotech. Bioeng.*, **23**, 425-429.

Visuri, K., Kaipainen, E., Kivimäki, J., Niemi, H., Leisola, M. and Palosaari, S. (1990) A new method for protein crystallization using high pressure. *Biotechnol.*, **8**, 547-549.

Visuri, K. (1989) Industrial scale crystallisation of glucose isomerase. Enzyme Engineering X, International Conference, September 24-29, 1989, Kashikojima, Japan.

Weber, P. C. (1991) Physical principles of protein crystallization. *Adv. Protein Chem.*, **41**, 1-36.

Wilson, L. J., Adcock, L. D. ans Pusey, M. L. (1993) A dialysis technique for determining aggregate concentration in crystallising protein solutions. *J. Phys. D: Appl. Phys.*, **26**, B113-B117.

Wilson, W. W. (1990) Monitoring Crystallization Experiments Using Dynamic Light Scattering: Assaying and Monitoring Crystallization in Solution. *METHODS: A Companion to Methods in Enzymology*, **1**, 110-117.

Wozniak, J. A., Faber, H. R., Dao-pin, S., Zhang, X-J. and Matthews, B. W. (1990) Crystallization of Designed Protein Variants. *METHODS: A Companion to Methods in Enzymology*, **1**, 100-104.

Yoshikawa, S., Shinzawa, K., Tsukihara, T., Abe, T. and Caughey, W. S. (1991) Crystallization of beef heart cytochrome c oxidase. *J. Cryst. Growth*, **110**, 247-251.

Young, C. C., De Mattei, R. C., Feigelson, R. S. and Tiller, W. A. (1988) Some implications of colloid stability theory for protein crystallization. *J. Cryst. Growth*, **90**, 79-85.

Appendix 1. Measuring crystal size distributions.

Four methods of particle sizing have been tested on the protein crystals studied in this work. These include the electrical sensing zone method, light microscopy, focused beam reflectance measurement and low angle light scattering. Sieving was not considered due to the small size of the protein crystals. Sedimentation was attempted briefly but slow sedimentation rates combined with a low stability of the crystals in the medium made the method unattractive. Finally image analysis was also tested. However poor contrast was found even when using polarized light and crystal breakage occurred.

The crystal size distributions have been normalized such that the number of crystals in the measuring range were similar.

1.1 Diamond-shaped crystals.

Figures 62-64 compare size distributions for crystals of diamond morphology. The scatter on the microscopic analysis is due to the difficulty of measuring a significant number of particles. The particles are shown to be of the same size range using the 4 methods. The shape of the crystal size distributions are also similar though a narrow sub-population was not detected by FBRM method in Figure 63. Low angle light scattering and the electrical sensing zone method are compared in Figure 64. Detection of the narrow sub-population of crystals has been successful.

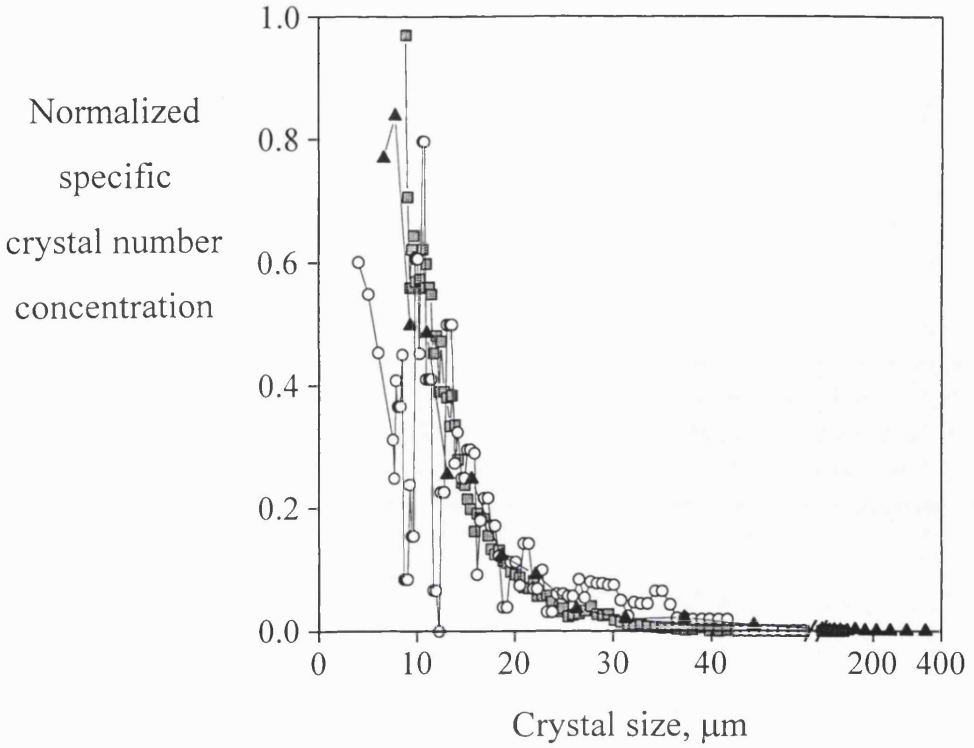

Figure 62. Comparison between crystal size distributions measured using a light microscope at 400 times magnification (❍), the electrical sensing zone method with a 210 μm orifice (■) and the FBRM method (▲). Crystals were diamond-shaped.

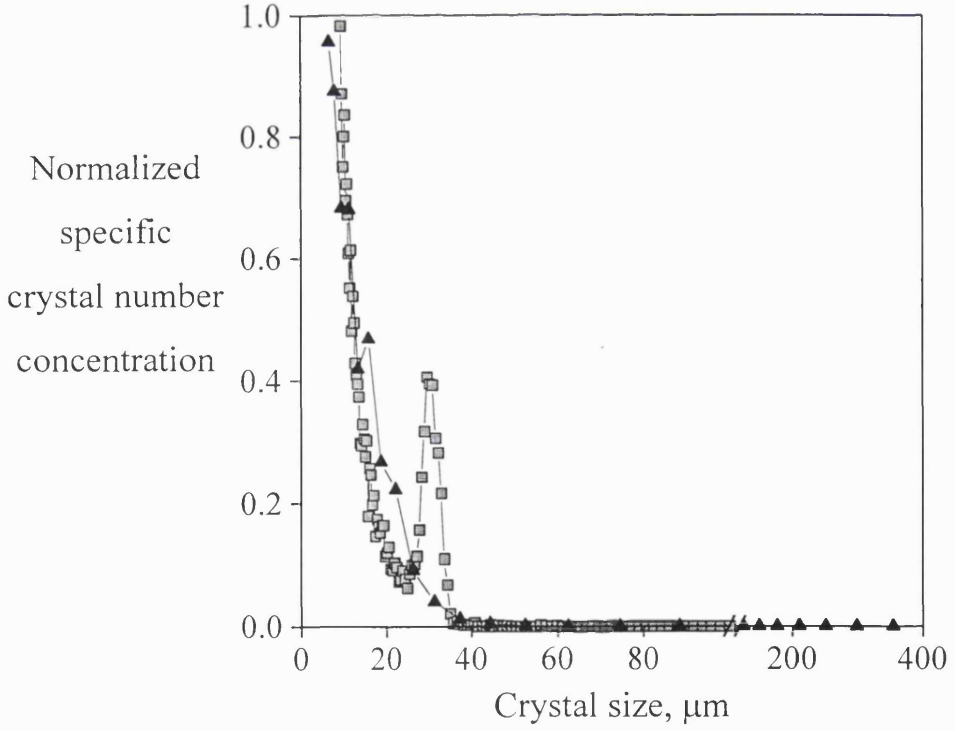

Figure 63. Comparison between crystal size distributions measured using the electrical sensing zone method with a 210 μm orifice (■) and the FBRM method (▲). Crystals were diamond-shaped.

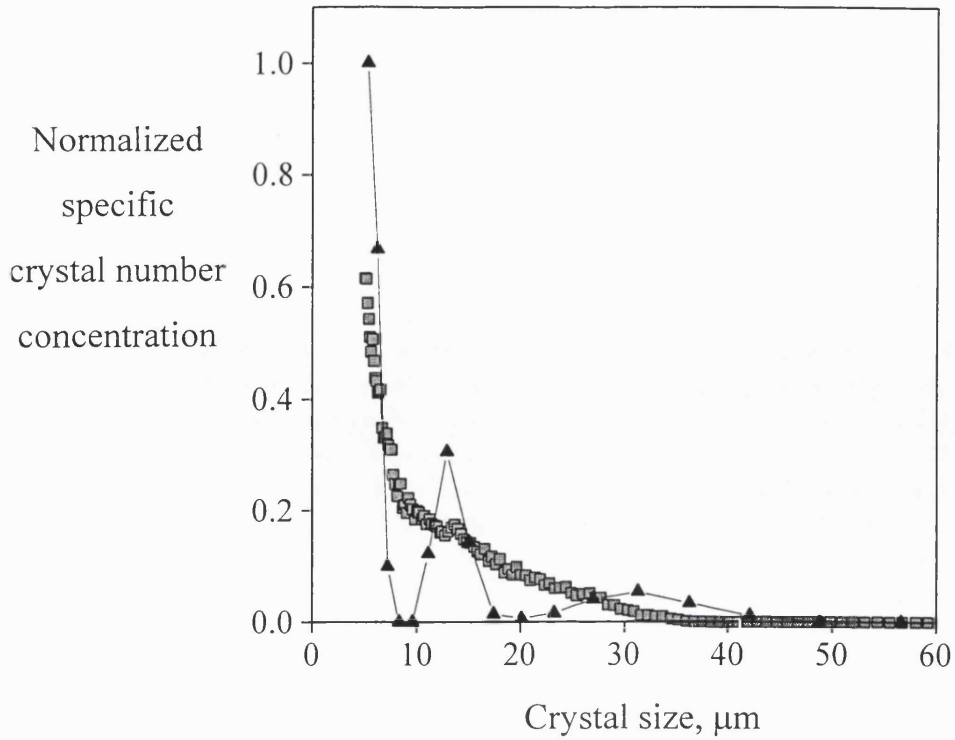

Figure 64. Comparison between crystal size distributions measured using the electrical sensing zone method (■) and the low angle light scattering method (▲). Crystals were diamond-shaped.

1.2 Rod-shaped crystals.

Sizing of irregular shaped particles such as the rod-shaped crystals in this study is difficult. With a length to width ratio ranging from 2- 26 and a thickness to width ratio ranging from around 0.1- 1, it is difficult to give the size of the rod-shaped crystals with just one parameter. Hence, the data comparison in this section is highly empirical. The electrical sensing zone method provides a size equivalent to a sphere with the same volume as the particle sized. The light microscopy method gives only width and length and generally no thickness. Thus comparison to the electrical sensing zone method is difficult. Here the crystal sizes measured with the microscope are given as crystal length giving over-estimation of the size as seen in Figure 65. Finally the FBRM method measures chord lengths giving a wider size distribution than would be expected from the electrical sensing zone method and this is seen in Figure 65. In Figure 66 the low angle light scattering method is compared with the electrical sensing zone method giving rather similar crystal size distributions.

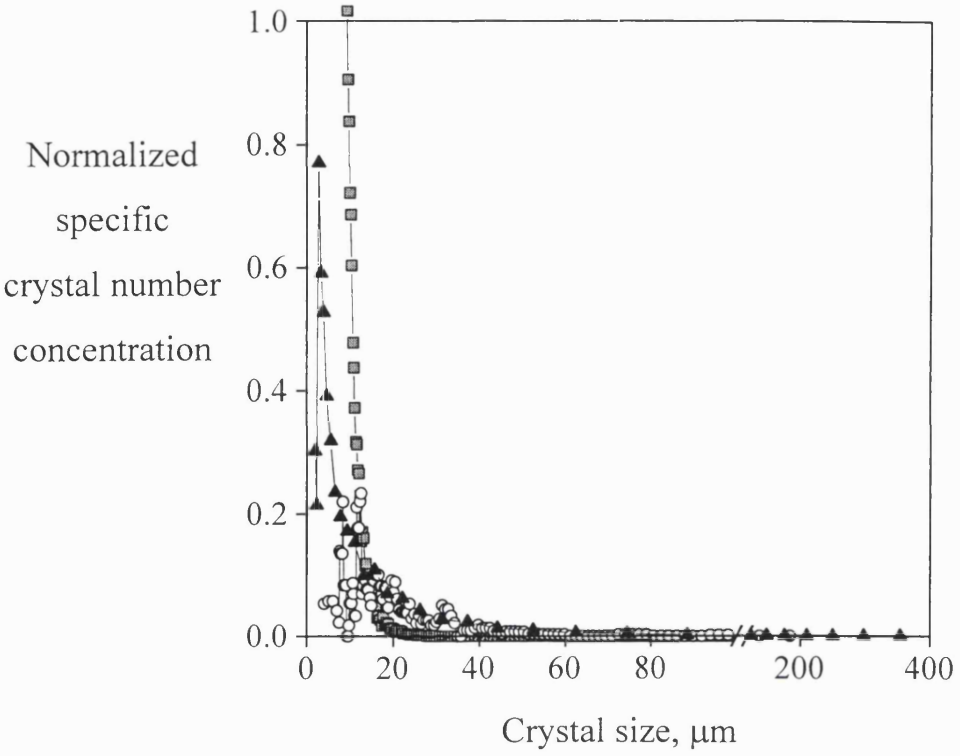

Figure 65. Comparison between crystal size distributions measured using light microscopy (400 times magnification) and given as crystal length (❍), the electrical sensing zone method (210 μm orifice), given as equivalent spherical size (■) and the FBRM method given as chord length (▲). The crystals were rod-shaped.

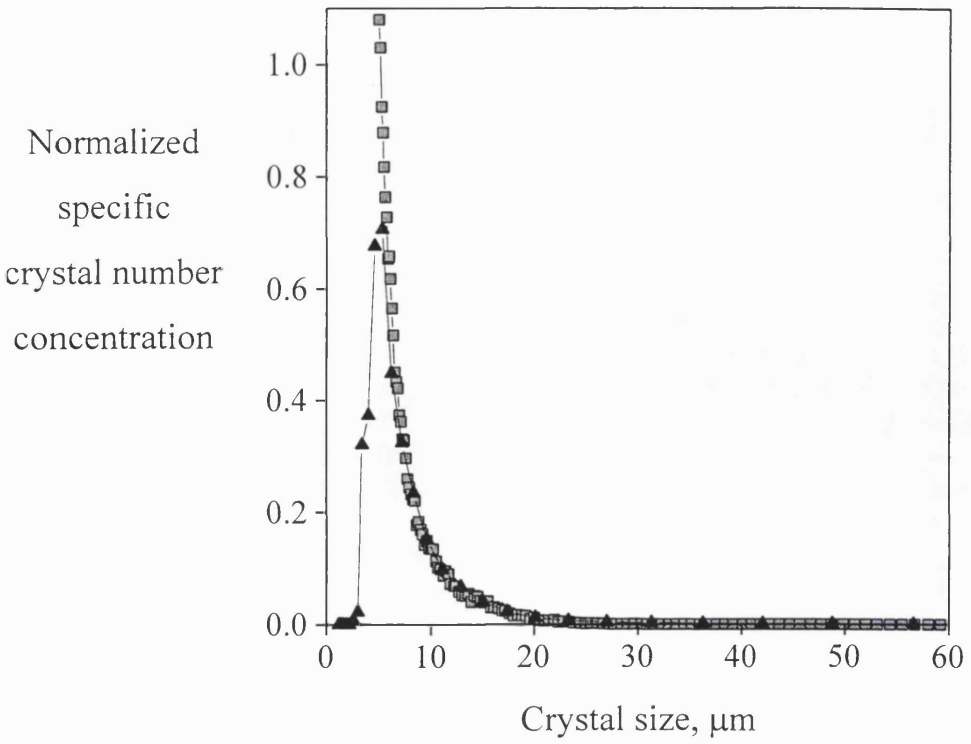

Figure 66. Comparison between crystal size distributions measured using the electrical sensing zone method (210 μm orifice) (■) and the low angle light scattering method (▲). The crystals were rod-shaped.

Appendix 2. Measuring progress of crystallisation.

A range of very different simple analytical methods have briefly been evaluated for their ability of describing the progress of a crystallisation. Here the meaning of "progress" is the volume of crystals formed as measured by the electrical sensing zone method. The agreement between the methods was determined by linear plots using the correlation coefficient and the relative ordinate intercept of the regression for evaluation. In the case of the Lasentec method the crystals number was compared due to difficulty in converting the chord length to crystal volume.

	$Y(0)/Y_{max}$	R^2	comments
sludge height	7 %	0.93	the sludge height levels off at the end of crystallisation
OD (680 nm)	2 %	0.97	the OD (680 nm) levels off at the end of crystallisation
OD (280 nm)	20 (19) %	0.17 (0.73)	scatter
lipase activity	20 %	0.69	scatter
Lasentec no.	39 %	0.72	steep increase early followed by plateau

Table 10. Progress of a pH ramp crystallisation for a mixed morphology batch. Exp 12, chapter 7. Only rod-shaped crystals were present except for the last hour where a few diamond-shaped crystals formed. Correlation to the total crystal volume as detected by the electrical sensing zone method is given except in the comparison to the Lasentec method where crystal numbers are compared.

	$Y(0)/Y_{max}$	R^2	comments
sludge height	13 %	0.93	good
OD (680 nm)	1 %	0.86	seems to corr. better to crystal no.
OD (280 nm)	2 %	0.77	scattered
lipase activity	23 (13) %	0.73 (0.91)	good when outlier removed
Lasentec no.	10 %	0.88	good corr. during diamond crystal, steep increase when rod start to form followed by plateau.

Table 11. Progress of a batch crystallisation for a mixed morphology batch. Exp 11, chapter 7. Diamond-shaped crystals formed first followed by rod-shaped crystals. Correlation to the total crystal volume as detected by the electrical sensing zone method is given except in the comparison to the Lasentec method where crystal numbers are compared.

For both experiments the sludge height method correlated well with the electrical sensing zone method. This is at least partly because the method is very simple leaving little data scatter due to experimental errors. Special tall and narrow spin tubes should be used to allow accurate readings.

The Lasentec method is also very simple to operate being on-line and in-situ. Good correlation was found when only diamond-shaped crystals were present. In the early part of the crystallisation of rod-shaped crystals the Lasentec counts increases well above that of the electrical sensing zone method. This was expected since some of the particles detected by the Lasentec method have chord lengths longer than 7.8 μm even though the spherical equivalent volume sizes (the "size" detected by the electrical sensing zone method) were smaller than 7.8 μm chosen as the lower limit here.

The optical density of the supernatant at OD (280 nm) and of the crystal suspension at OD (680 nm) are sensitive to dilution errors making the data points scatter above and below the linear regression curve. However, in particular the OD measurement at 680 nm correlates well to the total crystal volume determined by the electrical sensing zone method and even better correlation would be found is compared to the crystal number.

The method used to determine the lipase activity of the supernatant did not correlate well. The experimental procedure should probably be further improved.

Appendix 3. Fill and draw operation of crystallisation.

Control of crystal nucleation and growth by keeping the supersaturation low can be achieved in ways other than the slow addition of reagent described in chapter 8. In this section preliminary results on the so-called "fill and draw" operation mode are reported. The aims are twofold: 1) to grow larger crystals and 2) affect the balance between the two crystal forms. This has been done on two systems:

a) diamond-crystallisation-substrate added to a suspension of diamond-shaped crystals.

b) mixed-morphology-substrate added to a solely diamond-shaped crystal suspension

The substrate feed rate profile determines the supersaturation. Of particular interest is the feed rate required to maintain a certain degree of supersaturation. This can be found from a mass balance for the product protein in solution in the reactor working volume V(t) and over the time Δt:

$$\text{in} - \text{out} = \text{accummulation} - \text{generation}$$

no product protein is generated.

$$C_0 Q\Delta t - F\rho_c GA\Delta t = C(V_0 + Q\Delta t) - C_S V_0$$

where $\mathbf{C_0}$ is the concentration of product protein in the feed stream, **Q** is the volumetric feed rate, **F** is the protein mass fraction of the crystal, ρ_C is the crystal density, **G** is the linear crystal growth rate, **A** is the total surface area of the crystals present, **C** is the concentration of product protein in solution, $\mathbf{V_0}$ is the suspension starting volume of $\mathbf{C_S}$ protein concentration .

$$C_0 Q - F\rho_c GA = V\frac{dC}{dt} + QC$$

and Δc and Δt→ 0

The aim is to maintain the protein product concentration as high as possible without generating new nuclei. If the system is maintained at the optimal supersaturation, dC/dt = 0 can be assumed.

$$Q_{opt} = \frac{F\rho_c GA}{C_0 - C_{opt}}$$

eq. 52

the surface area of the sphere is given by:

$$A = 4\pi R^2$$

when a sphere grows from size R_0 to R the area changes:

$$\Delta A = 4\pi R^2 - 4\pi R_0^2 \Leftrightarrow$$

$$\Delta A = 4\pi (R^2 - R_0^2) \Leftrightarrow$$

$$\Delta A = 4\pi (R + R_0)(R - R_0) \Leftrightarrow$$

$$\Delta A = 4\pi (R_0 + Gt + R_0)\Delta R \text{, since}$$

$$\frac{dR}{dt} = G \Leftrightarrow R = R_0 + Gt$$

$$A = A_0 + 4\pi (2R_0 + G \cdot t)Gt \Leftrightarrow$$

$$A = A_0 + 8\pi R_0 Gt + 4\pi G^2 t^2 \Leftrightarrow$$

if this expression is used with eq. 52 for the optimal feed rate becomes:

$$Q_{opt} = \frac{F\rho_c G A_0}{C_0 - C_{opt}} + \frac{F\rho_c G^2 \pi 8 R_0}{C_0 - C_{opt}} \cdot t + \frac{F\rho_c \pi 4 G^3}{C_0 - C_{opt}} \cdot t^2$$

eq. 53

The optimal feed rate profile is a polynomial of second order in time but the last contribution can be neglected (when $t < 24$ h). Hence the feed rate profile necessary to maintain constant supersaturation should be a linear function of time. In the experiments presented below, such linear time dependent feed rate profile was used in the first experiment while in the second constant feed rate was used.

3.1 Fill and draw operation for control of crystal size.

To an initial suspension of diamond-shaped crystals, a fresh protein solution containing surfactant was added resulting in the exclusive formation of diamond-shaped crystals.

As can be seen from Figure 67, a fill and draw crystallisation consist of two phases. In the first dilution is dominant, making the initial peak in Figure 67 smaller. This is best seen between 0-4 h. In the second phase crystal growth shifts the peak toward the right and increasing its height (4-23 h). If the experiment has been successful then no crystals should be smaller than 10-15 μm which is the size increase of the starting crystals during the run. It is difficult to judge from Figure 67 if the experiment was successful because this is below the limit of detection. However, a new peak seems to have grown partly into the measuring range indicating that perhaps the fresh material

was added too fast, increasing the degree of supersaturation to levels where nucleation occurs. Another possibility is that fines carried with the starting material have grown large enough to be detected. The degree of supersaturation is directly linked to the total crystal volume. In Figure 68 the total crystal volume and number are plotted as a function of time.

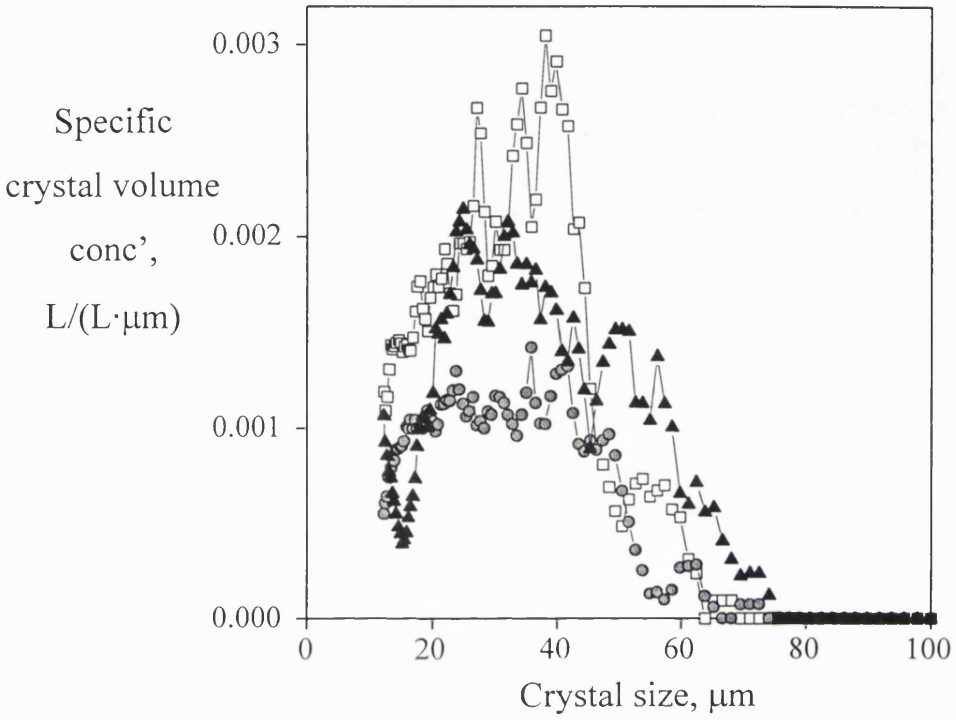

Figure 67. Specific crystal volume size distributions for a fill and draw operated crystallisation forming diamond-shaped crystals. Samples were taken at time 0 h (□), 4 h (●) and 23 h (▲). pH = 4.3, 28.0°C and the data was obtained using the electrical sensing zone method.

The substrate addition profile used in this experiment ensures an almost constant degree of supersaturation between 3 and 8 hours crystallisation. From Figure 69 it can be seen that this was achieved by first adding sufficient material to bring the supersaturation to a level of reasonable high growth rate (0-3 h) after which the addition rate was reduced to maintain the achieved level. Slowly over the next 5 h the addition rate was increased to maintain this level of supersaturation. After the addition ended crystal growth again reduced the level of supersaturation to near one over the next 17 h. Unfortunately the total number of crystals in the measuring range increases during this period. The maximum degree of supersaturation found in this experiment was 2.9. In the corresponding batch operated crystallisation new crystals were produced by nucleation

at this supersaturation and that by a rate of approximately 10 % of the maximum observed in the batch experiment. Taking the ratio of the total crystal volume to the total crystal number should indicate the general degree of enlargement of the crystals in the measuring range and as can be seen in Figure 69. A 15 % improvement was achieved compared to the starting material.

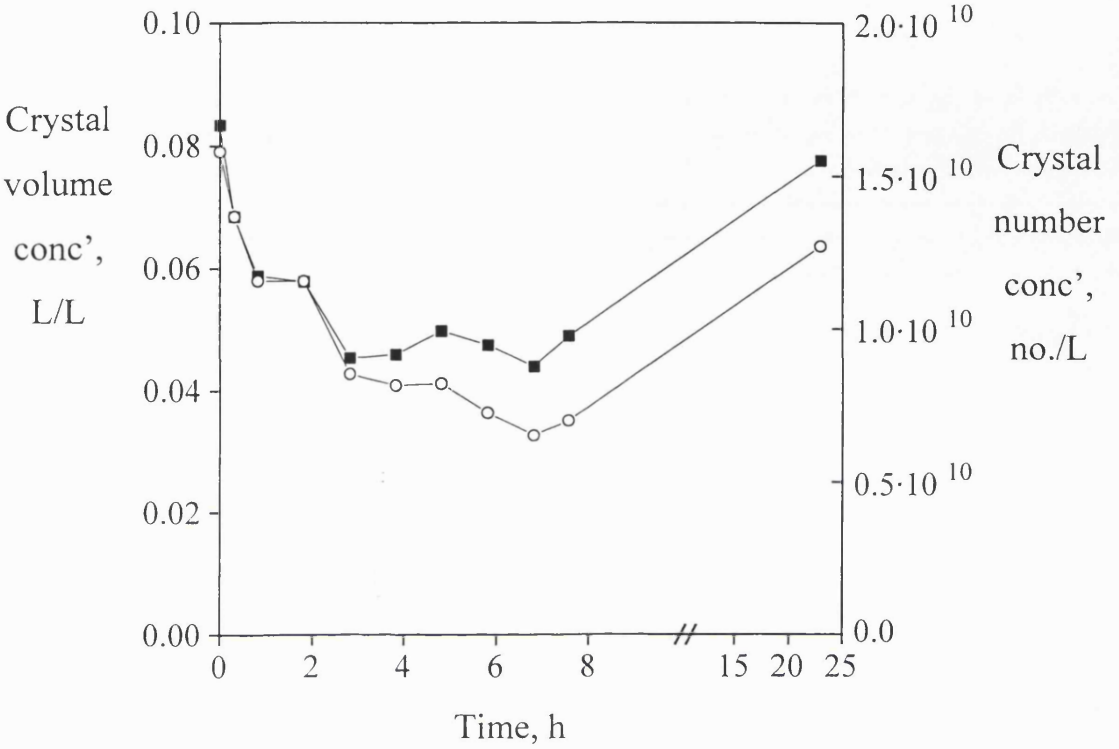

Figure 68. Crystal volume (■) and number (O) concentration given as a function of crystallisation time for a fill and draw operated crystallisation forming only diamond-shaped crystals. pH 4.3, 28.0°C and the data was obtained using the electrical sensing zone method.

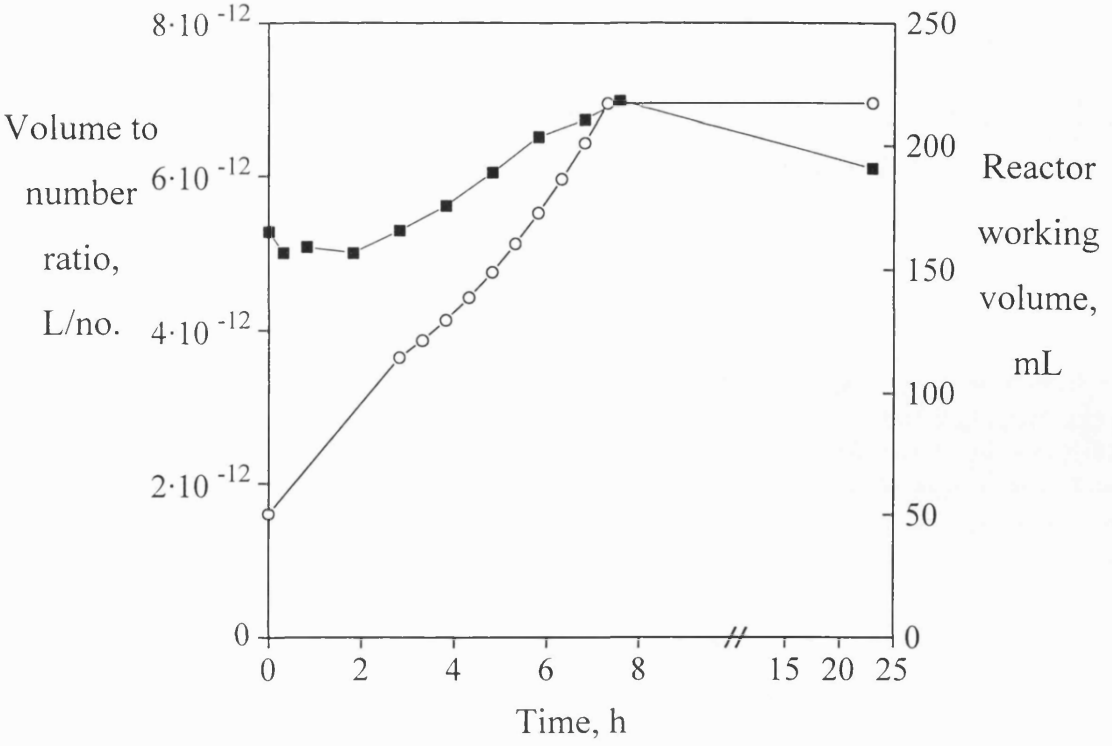

Figure 69. Crystal volume to number ratio (■) and reactor working volume (O) plotted as a function of time. pH 4.3, 28.0°C.

3.2 Fill and draw operation for control of crystal shape.

The idea was to use diamond-shaped crystals as starting material for a fill and draw crystallisation where the added material under batch conditions would form both rod and diamond-shaped crystals. It was hoped that the product protein would incorporate onto the large excess of diamond-shaped crystal surface rather than form rod-shaped crystals. This strategy would be expected to be successful if it is possible to keep the operation point below the supersaturation at which the rod-shaped crystals start to nucleate.

It is clear from Figure 70 that the diamond-shaped crystals did grow some 15 μm during the experiment but nevertheless late in the experiment rod-shaped crystals formed. The maximum degree of supersaturation observed was 2.3 (between 5-8 h) below which rod-shaped crystals have been found to nucleate in batch operated crystallisation. It should be pointed out that the final volume to number ratio was improved 30 % compared to the non-seeded batch operated crystallisation forming both rod and diamond-shaped crystals.

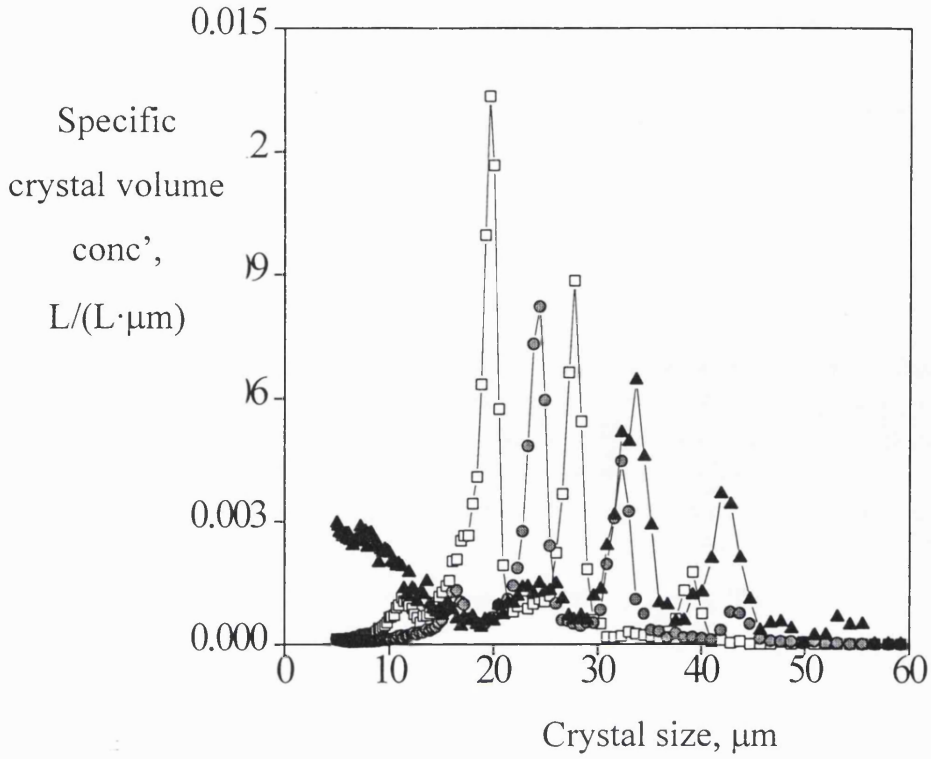

Figure 70. Specific crystal volume size distributions for a fill and draw operated crystallisation started with a suspension diamond-shaped crystals and forming both diamond and rod-shaped crystals. Sample times 0 h (□), 4 h (●) and 23 h (▲). pH 4.3, 28.0°C and constant substrate addition of 6.2 μL/s and the data was obtained using the electrical sensing zone method.

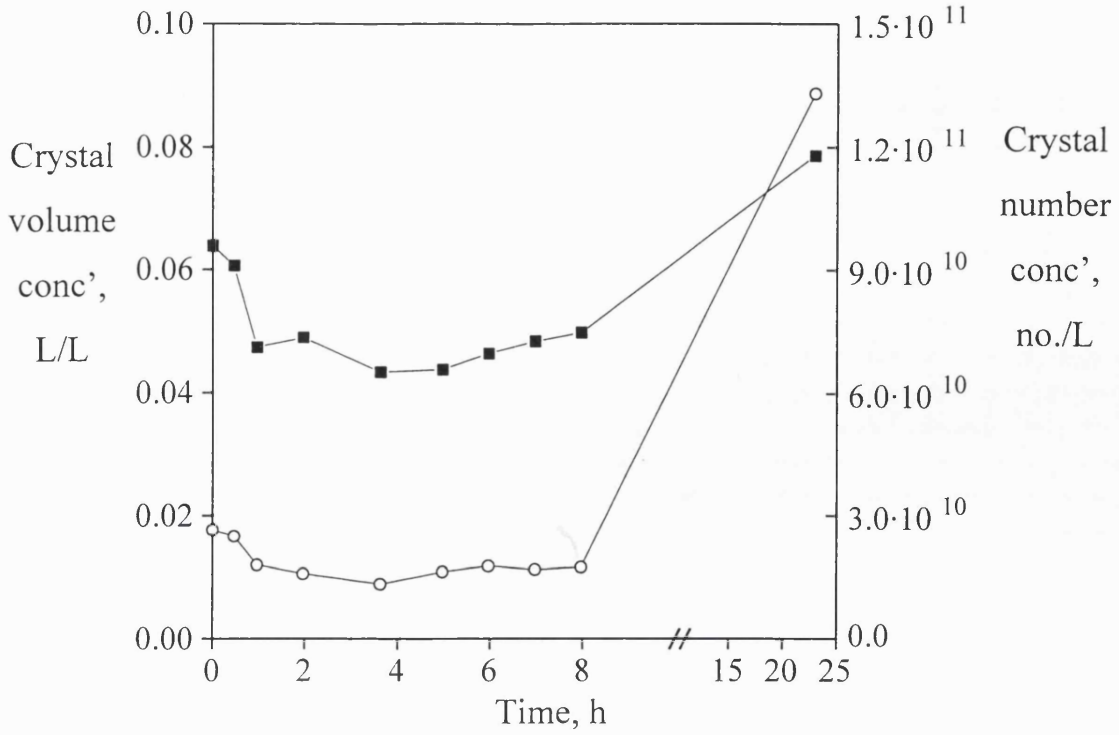

Figure 71. Crystal volume (■) and number (O) concentration given as a function of crystallisation time for a fill and draw operated crystallisation started with only diamond-shaped crystals but forming both diamond and rod-shaped crystals. pH 4.3, 28.0°C and constant substrate addition rate of 6.2 μL/s. The data was obtained using the electrical sensing zone method.

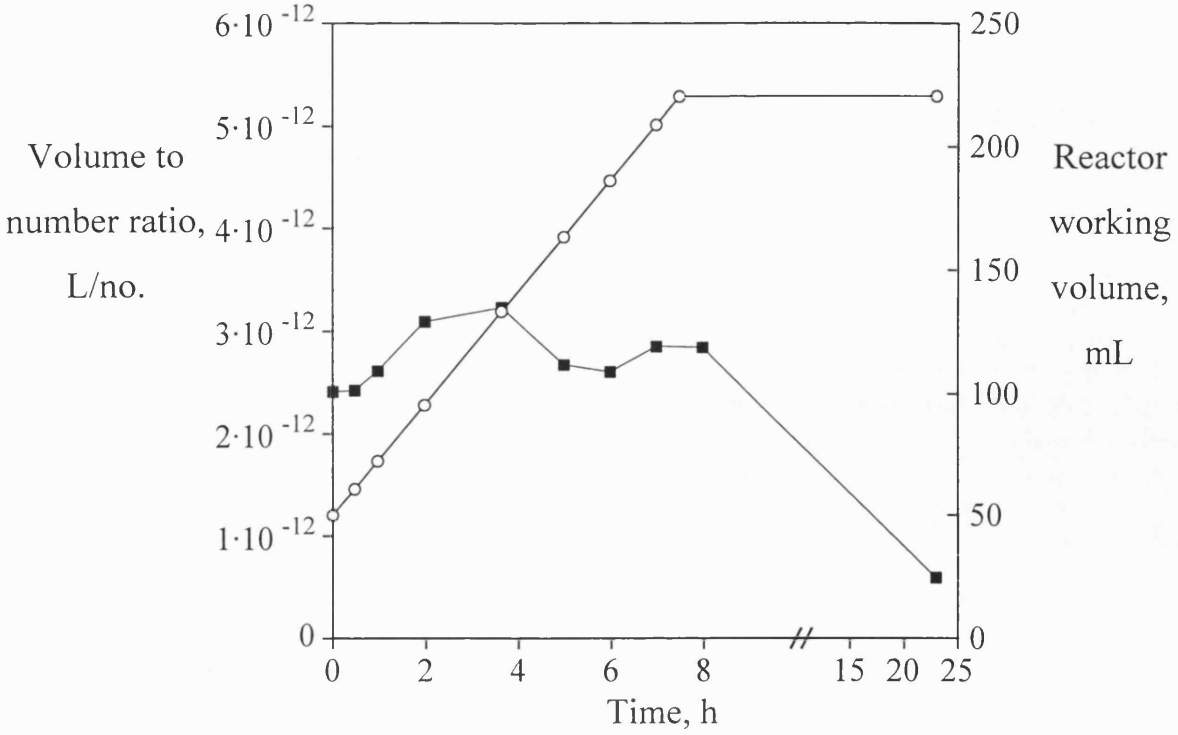

Figure 72. Crystal volume to number ratio (■) and reactor working volume (O) plotted as a function of time. pH 4.3, 28.0°C and constant substrate addition rate 6.2 μL/s.

3.3 Discussion.

Fill and draw operation can reduce nucleation compared to the corresponding batch operated crystallisation. Larger crystals resulted and the balance was shifted towards the diamond-shaped crystals. The real benefit of fill and draw operation is not obvious from the experiments shown here mainly due the growth kinetics of the diamond-shaped crystals. The high dependency of the growth rate on the degree of supersaturation makes it necessary to operate at semi-high degrees of supersaturation to achieve a reasonably fast process. At such degrees of supersaturation nucleation is likely to take place. Moreover, the width of the metastable zone does not seem very wide (see Chapter 5) making fill and draw operated crystallisation more difficult to operate.

Appendix 4. Experimental procedures.

BIOINDUSTRIAL GROUP

ANALYTICAL METHOD

AUTHOR/TRANSL. BY	NUMBER	NO. OF PAGES
OG	AF 95/6-GB	5
	SUPERSEDES NUMBER AF 95/5-GB	
APPROVED BY HMa	DATE 1991.02.07	

Novo Nordisk A/S

Novo Allé
2880 Bagsvaerd
Denmark

Tel. +45 4449 0033
Fax. +45 4449 0555
Telex 37173

A/S Reg. No. 16201

Lipase/Esterase - pH-stat Method on a Tributyrin Substrate (LU).

Principle

The method is based on the hydrolysis of tributyrin by the enzyme, and the alkali consumption in a pH-stat is determined as a function of time.

Unit Definition

1 LU (Lipase Unit) is the amount of enzyme which liberates 1 µmol titratable butyric acid per minute under the given reaction conditions.

Due to variations in the quality of avalable tributyrine batches, the activity for a specific lipase may also be determined relative to an enzyme standard with an activity based on a particular substrate batch.

Reaction Conditions

pH	: 7.0
Substrate concentration	: 4.8 % (m/V) =0.159 M Tributyrine
Temperature	: 30.0°C (+-0.5°C)
Emulsifier	: Gum Arabic (0.094 % (m/V))
Reaction time	: 5 minutes
Enzyme concentration	: Aprox. 0.063 LU/ml

Method specifity and -sensitivity

Specific lipases may need special pretreatment to obtain full activity.
Special agreements have to be arranged for samples containing less than 0.3 LU/g - and for all samples containing detergents (separate method AF 95.5-GB).

Apparatus

pH-stat system (from Radiometer) including:

Autoburette 2.50 ml
pH-meter
Titrator
Recorder
Timer
Titration set-up with stirring

Blender (Silverson L4R laboratory mixer with axial flow head).
Thermostate Water bath 30.0°C

Reagents

1. 0.05 N NaOH Reagent

Empty a 0.1 N NaOH ampoule (Merck Titrisol no 9959) quantitatively into a 2000 ml volumetric flask.
Add demineralized water to the 2000 ml mark and stir under cover.
Store in a glassflask protected from air contact.
Maximum advisable storage time: 2 month.
Check the normality every week.

2. Emulsification Reagent

Sodium chloride, NaCl (Merck art. 6404)	17.9	g
Potassium di-hydrogene phosphate KH_2PO_4 (Merck art. 4873)	0.41	g
Demineralized water	400	ml
Glycerol(Merck art. 4094)	540	ml
Gum Arabic (Sigma no. G-9752)	6.0	g

Weigh out the Sodium chloride and Potassium di-hydrogene phosphate into a 1000 ml beaker.
Add 400 ml demineralized water and 540 ml glycerol and under vigorous stirring sprinkle the Gum Arabic into the solution. Stir until all has dissolved.
Transfer to a 1000 ml measuring flask and add demineralized water to the mark.
Maximum advisable storage time: 1 months at room temperature.

3. Substrate Emulsion

Tributyrine (Merck art. 1958).....15.0 ml
Demineralized water.....235 ml
Emulsification reagent (no. 2).....50 ml

Pipet 15 ml tributyrine into a 1/2 l measuring glass (diameter approx. 60 mm)..
Add 235 ml demineralised water.
Add 50 ml Emulsification Reagent (no.2).

Use a Silverson L4R blender with axial flow head.
Lower the head of the blender until it is 1 cm from the bottom of the measuring glass.

Set the timer to 2 1/2 min.
Start from zero and increase the speed to between the fourth and the fifth line on the scale (11000-13000 rpm) as fast as possible without losing the emulsion.
The blending time is 2 1/2 min including the startup.

Transfer the Substrate Emulsion to a brown glass bottle with a dispenser set on 15 ml.
Stir for 30 min before starting the procdure in the "Enzyme control"-section.
Stir for the rest of the day.

The emulsion is made fresh every day.

Be extremely carefull not to contaminate the Substrate Emulsion with dust (or dirth) contaning Lipolase protein.

3. Benzoic Acid Reagent

Benzoic acid (Merck art. 136).....240 mg

Weigh out the Benzoic acid in a 200 ml volumetric flask.
Add demineralized water to the mark, and dissolve by stirring and heating to 30-40°C.

Apparatus control (to be done every day)

a) The electrode is kept in the substrate for "conditioning" for approx. 5 minutes before start up.
b) 15 ml substrate that has been temperature equilibriated is titrated to pH = 7.00.
c) Set the counter of the burette to zero.
d) Add 1.000 ml benzoic acid.
e) When the pH-value is back to 7.00, read the amount of added titrant (the form of the titrationcurve may give information about the condition of the electrode. It has to be linear).
f) The normality of the titrant (0.05 N NaOH) shall be 0.050 ± 0.001 N. Repeat from b) until 3 following titrations makes the limits (see the calculation under g)).

g) Calculate the normality of the titrant:

Normality of titrant =

$$\frac{\text{Weighing (mg)}}{200} \times \frac{1}{122.1\ (\text{mg/mmol})} \times \frac{1}{\text{Used titrant (ml)}}$$

$$= \frac{\text{Weighing (mg)}}{24420\ (\text{mg/mmol}) \times \text{Used titrant (ml)}}$$

where 122.1 is the molecular mass of benzoic acid.
200 is the dilution of the benzoic acid.

Enzyme Solutions

The enzyme preparations are diluted in demineralized water to a concentration of approx. 1.0 LU/ml. Acceptable dilution is 0.50 -1.5 LU/ml.

Liquid and powders :At the first dilution step stir for 20 minutes before the final dilution to ensure that the total activity has been released.

Granules: Using Glycine buffer (see the analytical method for the specific enzyme) in the first dilution step can release the activity in approx. 20 min.
Using demineralised water makes the dissolution much slower.

To make sure that a representative sample is taken - weigh out minimum 1 g for granulates and blended powders.

When using only a small amount of enzyme, 1.0 LU can be weighed out directly into the titration vessel.

Level check

Analyze a known lipase as the first sample to check the level of the day.

Procedure

I :Pipet 15 ml substrate into the reaction vessel

II :Preheat the substrate for at least 3 minutes at 30°C in the ther mostat, before placing the reaction vessel in the titrationset-up. The stirring in the vessel should be vigorous without whipping air into the substrate.

III:Add 1.000 ml enzyme dilution (if the sample has a low activity up to 5 ml can be added) to the substrate.

IV :Adjust pH with 0.1 N NaOH or 0.1 N HCl to 6.8 - 6.9 (or on the auto burette with 0.05 N NaOH). Start the pH-stat titration.

V :After 1-3 minutes when the titrant addition is stable rezero the burette.

VI :Stop the titration after 5 minutes with a constant (linear) rate of alkali addition and read the titrant consumption.

Reagent Blank Correction

For accurate determination 1 ml of the reagent, that is used for the lipase dilution, is analysed as a sample - and this titration value is subtracted from the titration value of the lipase before the activity of the lipase is calculated.

Calculation

$$LU/g = \frac{\text{Titrant consumption (µlNaOH)} * \text{Dilution (ml)}}{100 * \text{Weighing(g)}}$$

Example 1

Weighing out: 0.640 g(enzyme in 25.0 ml demineralized water).

Titrant consumption: 85 µl in 5 minutes.

$$LU/g = \frac{85 \times 25}{100 \times 0.64} = 33.2 \text{ LU/g}$$

Example 2

Dilution: 1 ml enzyme in 100 ml demineralized water.

Titrant consumption: 85 µl in 5 minutes.

$$LU/ml = \frac{85 \times 100}{100} = 85.0 \text{ LU/ml}$$

A-6491

F9602745

Sequential Injection Analysis (SIA) for fast at-line process analysis of enzyme activity

Lars Hallgren, Jan Eriksen and Anette Rasmussen
Novo Nordisk A/S, DK-2880 Bagsvaerd, Denmark

Summary

A Sequential Injection Analysis (SIA) instrument was developed. The Instrument is aimed at fast at-line enzyme activity quantification in the Production and in R&D. The in-house designed SIA instrument, which is robust and user friendly, contains advanced hardware and software that facilitate rapid assay development directly from a computer keyboard.

Principle of SIA

SIA is a new liquid handle concept based on the well-known Flow Injection Analysis (FIA) principle. In SIA, however, there is no fixed size sample loop. All reagents, which are conveniently clustered around a multiposition valve, can be injected in various volumes via a precision pump (**Fig. 1**). The same instrument can therefore be used for different methods without changes in hardware configuration.

Sample and substrate are sequentially drawn from different ports of a mutiposition valve (MV) stacking the zones in a holding coil (HC). Then the flow is reversed and the zones mixed in a coil (MC) prior to entering the flow-through cell (FC) of the detector. Here the time-course kinetics of the mixing zone is studied during a stop-flow period and the catalytic activity determined from the increase in absorbance of a give wavelength interval.

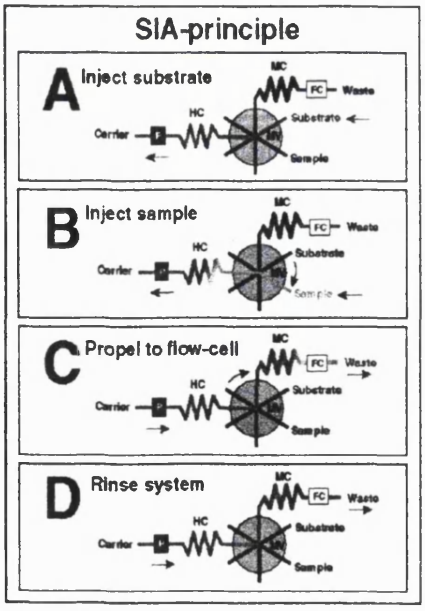

Figure 1. Principle of an enzyme assay employing SIA. A-B. Substrate and sample are sequentially injected into a holding coil (HC). C: Sample/substrate plug is propelled via a mixing coil (MC) to the flow-cell (FC). D: The SIA system is finally rinsed prior to next cycle.

Hardware

The instrument (**Fig. 2**) is equipped with two high-precision linear syringe pumps (P1 and P2), a multiposition valve (MV), a temperature regulated flow-through cell (FC), a fiber lamp (L) and an optical fiber based CCD-detector (D). The temperature of the flow-cell is controlled by two Peltier elements (range: 10-60°C ± 0.1°C). The temperature controller (TC), the pumps and valves are controlled by a serial PC port (RS-232/485) and data from the detector are acquired via a high speed PC data board.

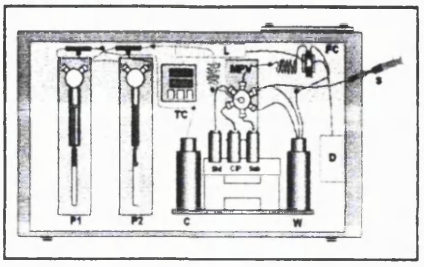

Figure 2. In-house build instrument for Sequential Injection Analysis. Calibration is done by automatic dilution of a single standard connected to the multi-position valve.

Software

A Microsoft® Windows 95™ based software program was developed in order to control the hardware and perform the data acquisition. The software control program consists of an expert part where methods are designed and a user part where ready-to-use methods can be executed (**Fig. 3**). Presently, methods are available for proteases, lipases, laccases and α-amylases running at-line on the SIA instrument.

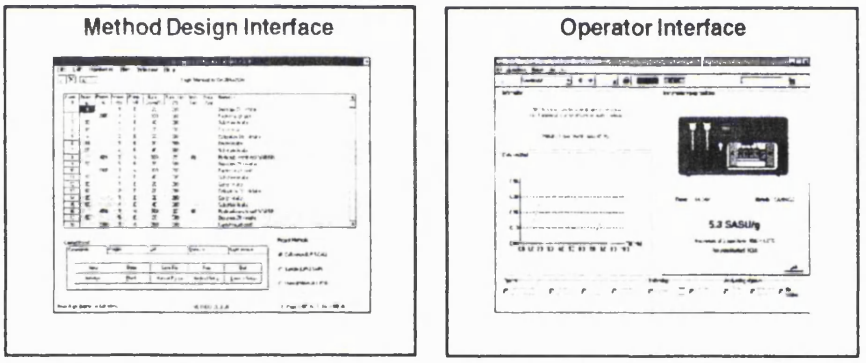

Figure 3. SIA control software. Left: The 'Design mode' screen where methods are developed and tested by the knowledgeable chemist or technicians. Right: The 'User mode' screen where ready-to-use methods are selected by the process operator.

Results

Enzyme samples of a detergent lipase, Lipolase®, were analyzed in parallel on both SIA and a conventional pH-stat laboratory method. A high correlation was found between results from the SIA method and results from the pH-stat reference method (see example **Fig. 4**).

Figure 4. Comparison between results from a lipase assay obtained by SIA and by the conventional off-line laboratory method (pH-stat titration).

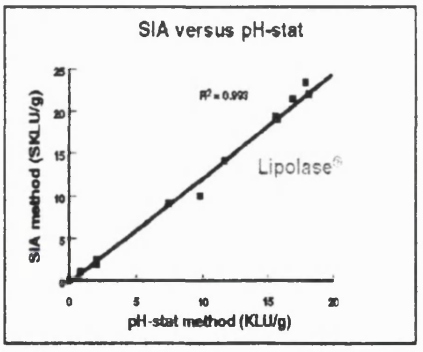

Conclusions

An at-line process analyzer, based on the Sequential Injection Analysis (SIA) principle, was developed. It is an easy-to-use instrument and it produces reliable results within minutes with minimal consumption of reagents. Several important at-line enzyme assays (lipases, proteases, laccases and α-amylases) are now implemented on the SIA-instrument. The SIA instrument will provide better process control for Production and faster product development for R&D.

Appendix 5. MATLAB script.

The nucleation and growth rates in this work were estimated using the following program.

Main program:

```
%function [Z] =Laplace
Aname=zeros(118,1);
t=[];
n=[];
scale=[];

i2=input('How many samples have been taken?')

Ax=input('what is the file name of the size axis used? ')
filename=(['c:\matlab\toolbox\matlab\' Ax '.txt']);
eval(['load ' filename]);
Aname=eval(Ax);

filename=(['c:\matlab\toolbox\matlab\factors.txt']);
eval(['load ' filename]);
scale=eval('factors');

filename=(['c:\matlab\toolbox\matlab\time.txt']);
eval(['load ' filename]);
t=eval('time');

filename=(['c:\matlab\toolbox\matlab\nsamples.txt']);
eval(['load ' filename]);
n=eval('nsamples');

N=zeros(1,1);
for i=1:i2
        N=N+n(i);
end
```

```
f1=input('What is the number of the first file to be imported? ')
f2=input('What is the number of the last file to be imported? ')
dir=input('In which directory and on what drive is the files stored? ')
X=import(f1,f2,dir);
V=importv(f1,f2,dir);

dL=zeros(117,1);
for i=1:117
        dL(i,1)=Aname(i+1,1)-Aname(i,1);
end
for i=1:N;
        for j=1:117;
        Y(j,i)=X((j+10),i)/(dL(j,1));
        end
end
for i=1:N;
        for j=1:117;
        W(j,i)=V((j+10),i)/(dL(j,1));
        end
end
V=average(W,scale,n,i2);
Z=average(Y,scale,n,i2);
sf=zeros(1,i2);
u0=zeros(1,1);
u1=zeros(1,1);
for i=1:i2
        for j=1:117
                u0=u0+Z(j,i)*dL(j,1);
                u1=u1+Z(j,i)*dL(j,1)*Aname(j,1);
        end
sf(1,i)=0.01*u0/u1;
u0=zeros(1,1);
u1=zeros(1,1);
```

```
end
x1=zeros(50,1);
y1=zeros(50,1);
x2=zeros(50,(i2-1));
y2=zeros(50,(i2-1));

for i=1:(i2-1)
sff=sf(1,(i+1));
[p(i,:),x1,y1]=gronucl(Z(:,(i+1)),Z(:,i),t,Aname,i2,dL,sff,i,x1,y1);
        for j=1:50;
                x2(j,i)=x1(j,1);
                y2(j,i)=y1(j,1);
        end
end
for i=1:(i2-1)
                T(i,1)=(t(1,(i+1))-t(1,i))/2+t(1,i);
end
sx=zeros(i2,1);
sv=zeros(i2,1);
for i=1:i2
        for j=1:117
                sx(i,1)=sx(i,1)+Z(j,i)*dL(j,1);
                sv(i,1)=sv(i,1)+V(j,i)*dL(j,1);
        end
end
```

Sub-programs:

```
function [Z] =average(X,scale,n,i2)
position=0;
[m1,m2]=size(X);
Y=zeros(m1,1);
m1
Z=zeros(m1,i2);
for j=1:i2;
```

```
        position=position+n(j);
                for k=(position+1-n(j)):position;
                        Y=Y+X(:,k);
                        Z(:,j)=(Y*scale(j))/n(j);
                end
        Y=zeros(m1,1);
end

function [X] = import(l1      ,l2      , dir      )
X=[];
for l=l1:l2
        s=dir;
        t=['c' int2str(l)];
        filename=[s   t   '.txt'];
        eval(['load    '  filename ]);
        r=eval(t);
        X=[X r(:,2)];
end

function [V] = import(l1      ,l2      , dir      )
V=[];
for l=l1:l2
        s=dir;
        t=['v' int2str(l)];
        filename=[s   t   '.txt'];
        eval(['load    '  filename ]);
        r=eval(t);
        V=[V r(:,2)];
end

function [p,x,y] =gronuc(n2,n1,t,Aname,i2,dL,sff,f,x1,y1)
dt=zeros(1,(i2-1));
for i=1:(i2-1)
        dt(1,i)=(t(1,(i+1))-t(1,i));
```

```
end
s=zeros(50,1);
for i=1:51
s(i)=0+(i-1)*(sff/50);
end
for i=1:50
N1=zeros(1,1);
N2=zeros(1,1);
        for j=1:117
                N1=N1+n1(j,1)*exp(-s(i,1)*Aname(j,1))*dL(j,1);
                N2=N2+n2(j,1)*exp(-s(i,1)*Aname(j,1))*dL(j,1);
        end
y(i,1)=(N2-N1)/dt(1,f);
x(i,1)=s(i,1)*(N1+N2)/2;
y1(i,f)=y(i,1);
x1(i,f)=x(i,1);
end
p=polyfit(x,y,1)
```

Appendix 6. Mass balance.

The degree of supersaturation was defined as:

$$S(t) = \frac{C}{C_S}$$

where **C(t)** is the product protein concentration in solution (g/L), and C_S is the product protein concentration at phase equilibrium (assumed achieved after 24 h)

A mass balance for product protein gives:

$$(C(t) - C_S) = (V_S - V(t))\rho_C F$$

$$S(t) = 1 + \frac{(V_S - V(t))\rho_C F}{C_S}$$

$$S(t) = 1 + K(V_S - V(t)), K = \frac{\rho_C F}{C_S}$$

where **V(t)** is the volume of crystal measured using the electrical sensing zone method (L crystals/L suspension), $\mathbf{V_S(t)}$ is the phase equilibrium volume of crystals formed (assumed achieved after 24 h), ρ_C is the crystal density (measured with Nycodenz®) (g crystal/L crystal), **F** is the protein mass fraction of the crystal (g protein/g crystal).

The crystal density (ρ_C) was found to 1250 g/L. The equilibrium concentration of protein in solution, C_S, was found from activity measurements by first determining the reduction of lipase activity in the supernatant during the experiment (activity loss believed to be minor) the knowledge that the solution from start contained 80 g/L product protein. This was however only done for 4 experiments (with a similar result) due to the labour intensive activity assay. Instead the measured crystal volume could accurately be used to determine the yield of a given crystallisation run due to the high structural homogeneity of crystalline material. The protein mass fraction of the crystal, F, was found by dividing the mass of protein remove from the supernatant (as determined from the activity reduction) with the mass of crystals formed (as found from the product of the crystal volume and the crystal density). F = 0.57 was calculated for experiments of 55-60 % yield and 0.065 L crystals/L suspension.

Appendix 7. Calculation example for the s-plane analysis.

In this section the estimation of nucleation and growth rates by the s-plane analysis is explained a using simple model data set. The size distributions measured at time t_1 and t_2 are given in colon 2 and 3 in the table while the corresponding size axis is given in the first colon. The justification for the modified axis is given in Chapter 5, p112.

Channel, μm	no. conc. at t_1	no. conc. at t_2	Modi. axis, μm	L, μm
5-10	10	50	0-5	2.5
10-15	5	40	5-10	7.5
15-20	2	20	10-15	12.5
20-25	0	8	15-20	17.5
25-30	0	0	20-25	22.5

To find the range of the Laplace variable, s, the zero'th and first moment of the distribution are first calculated (see Chapter 2 and 5):

$\mu_1(t_2) = 2.5 \times 50 + 7.5 \times 40 + 12.5 \times 20 + 17.5 \times 8 = 815$ μm·no/L

$\mu_0(t_2) = 50 + 40 + 20 + 8 = 118$ no./L

$\mu_1/\mu_0 = 6.9$ μm

Defining the range of the Laplace vaiable, s:

$s = \{0, , , , s_F\}$

The number of s values can be between 0 and s_F has to be decided (see chapter 5, p112)

$s_F = k \cdot \mu_0/\mu_1$ and if k =0.01 then:

$s = \{0, 0.0007, 0.0014\}\mu m^{-1}$ if only three values of s are used.

$$\bar{n}(t,s) = \sum n(t,L) \cdot \exp(-s \cdot L)$$

s, μm^{-1}	$n(t_1,s)$, no./L	$n(t_2,s)$, no./L
0	17.0	118.00
0.0007	16.94	117.43
0.0014	16.88	116.87

for $t_1 = 60$ s and $t_2 = 120$ s (these being the time at which the samples for CSD determination has taken)

s = 0.0000:

Y = 101/60 = 1.68 no./(L·s) (see Chapter 1, eq. 5, p24)

X = 0·(118.00 + 17.0)/2 = 0 no./(L·μm) (see Chapter 1, p)

s = 0.0007:

Y = 100.5/60 = 1.675 no./(L·s)

X = 0.0007· (16.94 + 117.43)/2 = 0.047 no./(L·μm)

s = 0.0014:

Y = 99.96/60 = 1.666 no./(L·s)

X = 0.0014· (116.87 + 16.88)/2 = 0.094 no./(L·μm)

and linear regression gives:

Y = -0.15·X + 1.68

meaning G = 0.15 μm/s and B = 1.68 no./(L·s)